ACTIVATION OF DIHYDROGEN BY RUTHENIUM COMPLEXES
CONTAINING CHELATING PHOSPHINES

By

AJEY MADHAV JOSHI

B.Sc. (Hons.), University of Poona, 1980

M.Sc., Indian Institute of Technology, Bombay, 1983

M.Sc., University of British Columbia, Vancouver, 1986

A THESIS SUBMITTED IN PARTIAL FULFILMENT OF

THE REQUIREMENTS FOR THE DEGREE OF

DOCTOR OF PHILOSOPHY

in

THE FACULTY OF GRADUATE STUDIES

DEPARTMENT OF CHEMISTRY

We accept this thesis as conforming

to the required standard

THE UNIVERSITY OF BRITISH COLUMBIA

November 1990

© Ajey M. Joshi, 1990

In presenting this thesis in partial fulfilment of the requirements for an advanced degree at the University of British Columbia, I agree that the Library shall make it freely available for reference and study. I further agree that permission for extensive copying of this thesis for scholarly purposes may be granted by the head of my department or by his or her representatives. It is understood that copying or publication of this thesis for financial gain shall not be allowed without my written permission.

Department of CHEMISTRY

The University of British Columbia
Vancouver, Canada

Date DECEMBER 27th, 1990

ABSTRACT

The previously reported synthesis of dinuclear mixed-valence ruthenium complexes of general formula $Ru_2Cl_5(P-P)_2$, P–P = DPPP, DPPB, S,S-CHIRAPHOS, or R,R-DIOP, has been extended to include other diphosphines: P–P = DPPN, DPPH, *rac*-DPPCP, *rac*-DPCYCP, S,S-BDPP, R- and S-BINAP, or S-PHENOP. The complexes are prepared by the reaction of $RuCl_3P_2(DMA)\cdot DMA$, P = PPh_3 or P(p-tolyl)$_3$, with one equivalent of the appropriate diphosphine. The H_2-reduction of $Ru_2Cl_5(P-P)_2$ complexes in DMA, or in toluene in the presence of an added base, affords the corresponding dimeric Ru(II) complexes $[RuCl(P-P)(\mu-Cl)]_2$, P–P = DPPN, R- or S-BINAP, or S,S-BDPP, which have been characterised by NMR spectroscopy.

The $[RuCl(P-P)(\mu-Cl)]_2$ complexes (Structure I) show a great propensity to form trichloro-bridged dinuclear species (Structure II) in the presence of neutral coordinating ligands (L). A series of trichloro-bridged complexes of the type $[(L)(P-P)Ru-(\mu-Cl)_3RuCl(P-P)]$ (e.g. P–P = DPPB; L = NEt_3, $NHBu_2$, CO, DMA, PhCN, MeI) have been isolated or studied *in situ* and characterised spectroscopically. The molecular structure of the DMSO analogue shows an S-bonded DMSO ligand with an unsymmetrical arrangement of the chelating DPPB ligand (*cf.* Structure II).

I

II
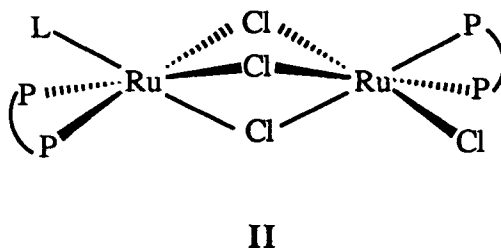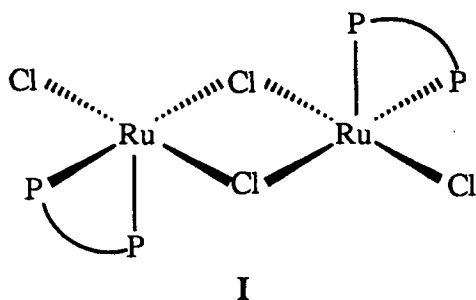
The reaction of $[RuCl(DPPB)(\mu-Cl)]_2$ with H_2 has been investigated. In benzene or toluene, in the absence of an added base, dihydrogen adds reversibly to the ruthenium

dimer to give the remarkably simple molecular hydrogen complex (L = η^2-H$_2$; Structure II); the η^2-H$_2$ ligand (with an H–H distance of 0.86 Å as estimated by ^{1}H NMR variable temperature spin-lattice relaxation data; $T_1(min)$ = 12 ms at 300 MHz) is replaceable by N$_2$.

The reaction of [RuCl(P–P)(μ-Cl)]$_2$, P–P = DPPB or *S,S*-CHIRAPHOS, with H$_2$ in the presence of NEt$_3$ as the added base yields the corresponding trinuclear Ru(II) hydride complex, [RuHCl(P–P)]$_3$, along with [(NEt$_3$)(P–P)Ru(μ-Cl)$_3$RuCl(P–P)]. The hydride complexes had been synthesised previously, albeit in low yields (<10%), and the crystal structure of the CHIRAPHOS derivative obtained. During the present work the original synthetic procedure has been modified to obtain the desired [RuHCl(P–P)]$_3$ complexes in ~50% yield. In addition, these species have been characterised completely by NMR spectroscopy. The conversion of [RuCl(P–P)-(μ-Cl)]$_2$ to the corresponding hydride derivative likely proceeds via deprotonation by NEt$_3$ of the initially formed molecular hydrogen species. Under hydrogen atmosphere, [RuHCl(DPPB)]$_3$ breaks down to form the dinuclear derivative [(η^2-H$_2$)(DPPB)Ru(μ-H)(μ-Cl)$_2$RuH(DPPB)] containing a molecular hydrogen ligand, which has been identified by ^{1}H NMR T_1 measurements; similar complexes, but with a nitrile ligand (MeCN or PhCN) in place of the η^2-H$_2$, have also been observed.

Alternative routes to ruthenium complexes containing only one diphosphine per Ru ("Ru^{II}(P–P)") have been investigated. Some of the trichloro-bridged derivatives (e.g. L = amine, CO; Structure II, see above) are also accessible through reactions of the mixed-phosphine complex RuCl$_2$(DPPB)(PPh$_3$) with amines and aldehydes, respectively. Studies on the reactions of RuCl$_2$(DMSO)$_4$ or [RuCl(*p*-cymene)-(μ-Cl)]$_2$ with one equivalent of diphosphines show that the nature and the distribution of product(s) (i.e. RuCl$_2$(P–P)$_2$ *vs.* "RuCl$_2$(P–P)") are greatly influenced by the chelate size of the diphosphine. The "RuCl$_2$(P–P)" species is observed only for those phosphines which form at least a six-membered ring upon coordination to the metal.

Solid-state ^{31}P NMR studies indicate that the structure of $RuCl_2(DPPB)(PPh_3)$ is similar to that of $RuCl_2(PPh_3)_3$, which has been characterised previously by X-ray crystallography. Reactions of $RuCl_2(DPPB)(PPh_3)$ with chelating ligands afford six-coordinate complexes of the type $RuCl_2(DPPB)(L-L)$, L–L = PPh_2Py, DPPM, or norbornadiene; the corresponding hydridochloro derivatives are obtained when the reactions are conducted under an atmosphere of H_2 in the presence of Proton Sponge®.

The dimeric $[RuCl(P-P)(\mu-Cl)]_2$ and the trinuclear $[RuHCl(P-P)]_3$ complexes described in this study are effective catalyst precursors for the hydrogenation of various alkene, ketone, imine, and nitrile substrates under relatively mild conditions (30–100 °C, 1–12 atm of H_2). A detailed kinetic study on the hydrogenation of styrene catalysed by $[RuCl(DPPB)(\mu-Cl)]_2$ shows a first-order dependence of the maximum rate on catalyst concentration, a first- to zero-order dependence on styrene concentration and a zero- to first-order dependence on the H_2 pressure. A mechanism involving formation of the molecular hydrogen (η^2-H_2) complex (see above) followed by hydrogen transfer to the substrate is proposed to account for the observations, and the rate constants at 30 °C for the various steps have been determined. Preliminary data on acetophenone and benzonitrile hydrogenation shows that the trinuclear hydride complexes are an order of magnitude more effective than the corresponding dimeric precursors.

iv

TABLE OF CONTENTS

LIST OF TABLES

LIST OF FIGURES

LIST OF ABBREVIATIONS

The following list of abbreviations, most of which are commonly used in the chemical literature, will be employed in this thesis:

A_t	absorbance at time t (UV-Vis)
Å	angstrom, 10^{-8} centimeter
APT	attached proton test (NMR)
atm	atmosphere; 1 atm = 760 mm Hg
(S,S)-BDPP	(2S,4S)-bis(diphenylphosphino)pentane; also called Skewphos
BINAP	(R)- or (S)-2,2'-bis(diphenylphosphino)-1,1'-binaphthyl
bipy	2,2'-bipyridine
BMPP	(R)-(+)-benzylmethylphenylphosphine
BPPFA	1,1'-bis(diphenylphosphino)-2'-(1-N,N-α-dimethylaminoethyl) ferrocene
BPPM	(2S,4S)-N-(t-butoxycarbonyl)-4-diphenylphosphino-2-diphenylphosphinomethylpyrolidine
br	broad
Bu	butyl, $CH_2(CH_2)_2CH_3$
c	concentration (in g/100 mL)
^{13}C	carbon-13
°C	degree Celsius
cat.	catalyst
CD	circular dichroism
S,S-CHIRAPHOS	(2S,3S)-bis(diphenylphosphino)butane
cm	centimeter

cod	cyclooctadiene
CP	cross polarisation (NMR)
Cp	cyclopentadienyl, η^5-C_5H_5
COSY	homonuclear correlation spectroscopy
Cp*	pentamethylcyclopentadienyl, η^5-C_5Me_5
CYCPHOS	1-cyclohexyl-1,2-bis(diphenylphosphino)ethane
D	configuration relative to D-glyceraldehyde
°C	degree Celsius
d	doublet (NMR)
d	dextrorotatory
DBU	1,8-diazabicyclo[5.4.0]undec-7-ene
DIOP	(2*R*,3*R*) or (2*S*,3*S*)-*O*-isopropylidene-2,3-dihydroxy-1,4-bis(diphenylphosphino)butane
DIPAMP	1,2-bis(*ortho*-anisylphenylphosphino)ethane
DMA	N,N-dimethylacetamide, $CH_3C(=O)N(CH_3)_2$
DMSO	dimethylsulphoxide
DPCYCP	*rac*-(±)-1,2-bis(dicyclohexylphosphino)cyclopentane
DPPB	1,4-bis(diphenylphosphino)butane
DPPCP	*rac*-(±)-1,2-bis(diphenylphosphino)cyclopentane
DPPE	1,2-bis(diphenylphosphino)ethane
DPPH	1,6-bis(diphenylphosphino)hexane
DPPM	1,1-bis(diphenylphosphino)methane
DPPN	1,5-bis(diphenylphosphino)pentane
DPPP	1,3-bis(diphenylphosphino)propane
EAC	ethyl-(Z)-α-acetamidocinnamate
e.e.	enantiomeric excess
fac	facial

FID	flame-ionisation detector
GC	gas chromatography
gem	geminal
^{1}H	proton-1
Hz	Hertz, cycles per second
HETCOR	heteronuclear correlation (NMR)
IR	infra-red
^{i}Pr	iso-propyl, $(CH_3)_2CH$
J	coupling constant, in Hz
k	rate constant
L	ligand
	litre
L	configuration relative to L-glyceraldehyde
l	path length
l	levorotatory
M	central metal atom in a complex
	molarity, moles L^{-1}
m	multiplet (NMR)
	moderate intensity (IR)
$[M]_D^T$	molar rotation, $[M]_D^T = [\alpha]_D^T$ x molecular weight / 100
MA	magic angle (NMR)
MAC	methyl-(Z)-α-acetamidocinnamate
Me	methyl, CH_3
mer	meridional
min	minute(s)
mL	millilitre
mmol	millimole(s)

mol	mole(s)
nm	nanometer(s)
nbd	2,5-norbornadiene
NMR	nuclear magnetic resonance
NOEDIFF	nuclear Overhauser effect difference
o	*ortho*
obs	observed
o.y.	optical yield
p	*para*
^{31}P	phosphorus-31
P–P	ditertiary phosphine
Ph	phenyl, C_6H_5
phen	1,10-phenanthroline
PHENOP	the chiral aminophosphinephosphinite ligand: $Ph_2PN(Et)CH(CH_2Ph)CH_2OPPh_2$
PPh$_2$Py	diphenyl(2-pyridyl)phosphine
ppm	parts per million
PROPHOS	1,2-bis(diphenylphosphino)propane
py	pyridine
q	quartet
(*R*)-	absolute configuration (latin: *rectus*; right)
RT	room temperature
S	solvent or substrate
(*S*)-	absolute configuration (latin: *sinister*; left)
s	singlet (NMR), strong (IR)
T_1	spin-lattice (or longitudinal) relaxation time (NMR)
t	triplet

TCD	thermal-conductivity detector
tert	tertiary
TMS	tetramethylsilane
tol	tolyl, $-C_6H_4CH_3$
UV-vis	ultraviolet-visible
w	weak intensity (IR)
$w_{1/2}$	linewidth at half height
α	observed rotation
$[\alpha]_D^T$	specific or absolute rotation (measured as the sodium D line) at temperature T
Δ	heat
ε	extinction coefficient (in M^{-1} cm^{-1})
λ	wave length
δ	chemical shift (in ppm downfield from TMS)
ν	frequency (cm^{-1})
η	descriptor for hapticity
μ	descriptor for bridging
*	chiral centre

ACKNOWLEDGEMENTS

CHAPTER 1

Introduction

1.1 General Introduction

The past three decades have witnessed enormous advances in the field of homogeneous catalysis. The use of soluble organometallic complexes, particularly those containing transition metals, is fast becoming an important tool in effecting a variety of stoichiometric and catalytic organic reactions. The ever-increasing demand for synthetic specialty fine chemicals, including pharmaceuticals, food additives, and pesticides, whose syntheses often consist of highly specific and selective organic transformations, has provided impetus for further development in this area.[1] Transition metal complexes catalyse a wide range of important chemical reactions (e.g. references 1–6); these include hydrogenation, hydrosilylation, and hydrocyanation of unsaturated organic substrates, olefin isomerisation, dehydration of tertiary alcohols, and various hydroformylation, epoxidation, and polymerisation reactions.

The relative advantages and disadvantages of homogeneous and heterogeneous catalysts, particularly from an industrial point of view, have been widely discussed.[7-9] The generally higher activity of homogeneous catalysts compared to the industrially more prevalent heterogeneous catalysts allows for the use of relatively mild reaction conditions. Greater specificity, selectivity and reproducibility exhibited by the homogeneous systems, and the ability to vary systematically their catalytic properties by simply changing the ligand environment around the metal centre, are strongly desirable for industrial processes.

Moreover the ease of monitoring homogeneous catalytic reactions by conventional spectroscopic and other kinetic techniques makes them amenable to detailed mechanistic investigations.[2]

The difficulty in separating the often expensive soluble catalysts from reaction products and, to a lesser extent, the oxygen- and moisture-sensitivity and low thermal stability of the catalysts, remain the principal hurdles toward a more widespread use of homogeneous systems in large scale industrial processes.[7] Considerable efforts have been made to circumvent the separation problem by anchoring homogeneous catalysts on insoluble inorganic supports (e.g. silica, alumina and zeolites), or on organic cross-linked (e.g. polystyrene-divinylbenzene)[7, 8, 10] as well as noncross-linked (e.g. polyamides)[11] polymer supports. Phase-transfer catalysis offers another promising approach.[12] The Wacker and the Oxo processes, methanol carbonylation, oligomerisation of dienes, some Ziegler-Natta systems, and the adiponitrile synthesis, are some notable examples from the forty-odd industrial processes[5b] currently using homogeneous catalysts.[3, 5]

In recent years, a major thrust in research on homogeneous catalysis has been directed at designing catalysts containing chiral ligands for asymmetric synthesis of optically active compounds, whereby enantiomeric products are obtained in unequal amounts. A number of comprehensive reviews have been published.[13-19] Because specific biological activity of organic compounds is often associated with only one of the enantiomers or diastereomers, it is highly desirable and in some cases even necessary to obtain such compounds in pure form.[1a, 20, 21] Asymmetric synthesis through enantioselective catalysis offers the most plausible alternative to the costly and tedious process of resolution of a racemic mixture. Biosynthetic pathways, while highly specific and efficient, may not always be available or suitable for such transformations.[14, 21, 22]

Monsanto's introduction of a Wilkinson-type rhodium(I) catalyst with a chiral diphosphine ligand (P*—*P) for large scale commercial production of the amino acid drug

2

S-Dopa (Equation 1.1), which is used for treating Parkinson's disease, was one of the most significant developments.[15]

$$\underset{\substack{\text{HO} \quad \text{OH}}}{\overset{\substack{\text{H} \diagdown \quad \diagup \text{CO}_2\text{R} \\ \text{C}=\text{C} \\ \diagup \quad \diagdown \text{NHCOR}}}{\bigcirc}} \quad \xrightarrow[\substack{\text{H}_2, \text{ S} = \text{MeOH} \\ 2)\ \text{H}_3\text{O}^+}]{1)\ [\text{Rh}(\text{P*}\!-\!\text{*P})(\text{S})_2]^+} \quad \underset{\substack{\text{OH}}}{\overset{\substack{\text{CO}_2^- \\ \text{H}_3\overset{+}{\text{N}} - \overset{*}{\text{C}} - \text{H} \\ \text{CH}_2}}{\bigcirc_{\text{OH}}}} \qquad (1.1)$$

S–Dopa
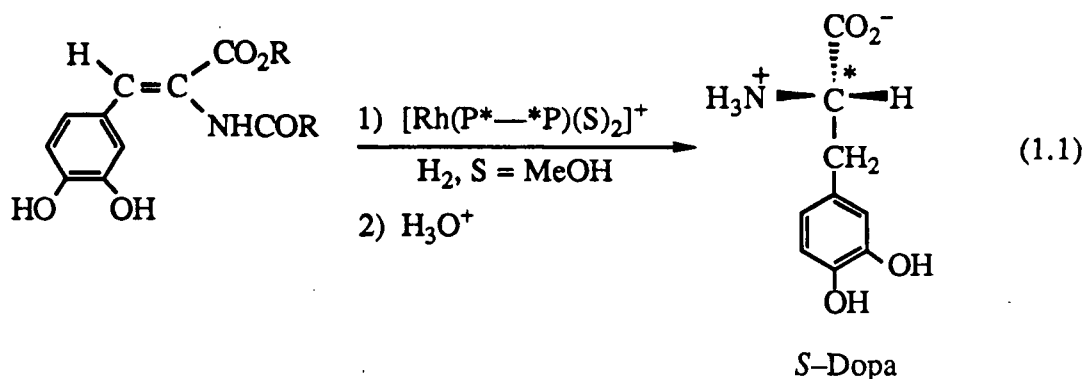
Similar chiral catalyst systems are being employed elsewhere for the asymmetric synthesis of other amino acids,[13-15] for example, in the production of constituents of the popular sugar substitute aspartame (Nutrasweet™) which is a methyl ester of the dipeptide *S*-aspartyl-*S*-phenylalanine.[23] Of note, none of the other three diastereomers of aspartame is sweet.

1.2   Homogeneous Hydrogenation

Hydrogenation of unsaturated organic substrates is by far the most extensively studied area of homogeneous catalysis, as evidenced by the vast amount of literature available on this topic. A number of excellent comprehensive reviews,[8, 24-27] specialised texts and books have been published.[28-31] Partly because of historical reasons and partly because of obvious potential commercial applications, a major portion of the literature on homogeneous hydrogenation deals with the more easily reduced and more commonly available substrates containing carbon-carbon multiple bonds.[32] A number of systems have been studied in considerable detail and their mechanisms deduced. However, work

on the reduction of carbon-nitrogen and carbon-oxygen double bonds has gained momentum in recent years.[13, 31-34]

Based on the mechanistic studies, hydrogenation of alkenes mediated by a transition metal complex may be seen generally as consisting of four fundamental processes:[25, 29]

a) activation of molecular hydrogen

b) substrate activation

c) hydrogen transfer to the substrate

d) release of the product and, in case of a catalytic reaction, regeneration of the catalyst.

1.2.1   Asymmetric Homogeneous Hydrogenation

The earliest attempts at asymmetric hydrogenation of organic substrates, in fact, employed a heterogeneous palladium catalyst absorbed on silk, but gave poor results.[35] Attention soon turned to the use of transition metal complexes modified with chiral auxiliary ligands. Chiral monophosphines of the type $P^*PhR^1R^2$, which have a centre of asymmetry at the phosphorus atom, were first reported in 1968.[36] Kagan's group reported the synthesis of the first chiral diphosphine *viz*. DIOP (Figure 1.1), from naturally occurring tartaric acid;[37] in DIOP the chirality resides in the carbon skeleton joining the two phosphorus atoms. Successful use of transition metal complexes with these phosphines as catalysts for asymmetric hydrogenation of several prochiral alkenes triggered a rapid development. The progress in asymmetric homogeneous hydrogenation of organic substrates is well-documented.[13-19, 33, 38-40]

A quantitative measure of the effectiveness of chiral induction via enantioselective catalysis is provided by the enantiomeric excess (e.e.) or the optical yield (o.y.), which are usually considered to be equivalent (Equations 1.2 and 1.3).

$$\text{o.y.(\%)} = \frac{\text{observed specific rotation } [\alpha]_D^T}{\text{specific rotation of pure enantiomer } [\alpha]_D^T} \times 100 \quad (1.2)$$

$$\text{e.e.(\%)} = \frac{|[R] - [S]|}{[R] + [S]} \times 100 \quad (1.3)$$

Catalyst systems incorporating rhodium and chiral diphosphines were first proved to be the most effective for asymmetric hydrogenation of a variety of olefinic acids and related derivatives, under relatively mild conditions (20–100 °C, 1–10 atm of H_2).[41] Until recently, chiral catalyst systems consisting of group 8–10 transition metals other than rhodium remained largely underdeveloped. In the last few years, however, some ruthenium-chiral diphosphine systems have emerged as effective enantioselective hydrogenation catalysts for a much wider range of organic substrates, including the olefinic acids, allylic alcohols, dienes, and functionalised ketones.[13, 33, 42]

At best, only moderate optical yields (~50%) have been obtained using non-phosphine chiral ligands such as Schiff bases, amines, amides, and sulphoxides.[26, 33] A large number of chiral phosphines have been synthesised and tested as ligands in the past fifteen years.[14, 16b] Some prominent representative examples of such phosphines are: PROPHOS and BPPM, derived from lactic acid and the amino acid proline, respectively; CHIRAPHOS, which contains two asymmetric centres in the carbon backbone; ferrocene-based BPPFA, which exhibits planar as well as carbon chirality; and DiPAMP, which is used in the Monsanto S-DOPA process[15, 43] (Figure 1.1).
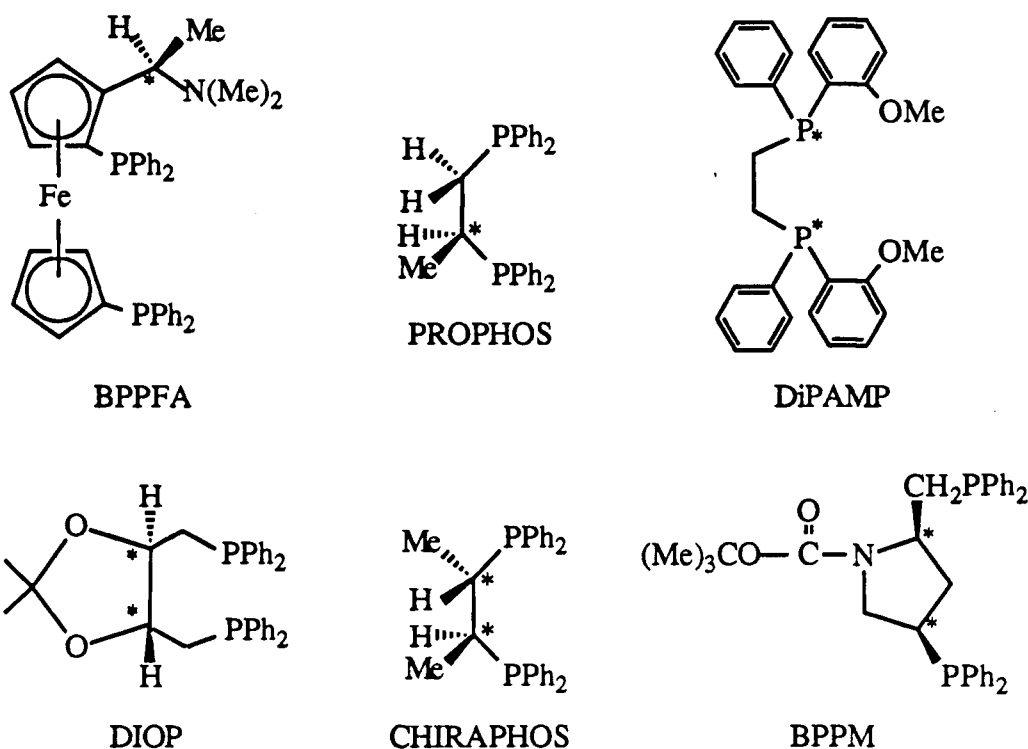
Figure 1.1: Selected chiral diphosphines used in asymmetric catalysis.

Of particular interest is the diphosphine BINAP (Figure 1.2) which exhibits solely a planar or axial chirality.[13, 44] The steric bulk of the naphthyl rings and the attached diphenylphosphine substituents prevents free rotation about the carbon-carbon single bond joining the naphthyl groups, essentially locking the ligand in one of the two configurations.
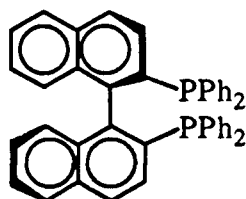
Figure 1.2: The chiral diphosphine BINAP.

Rhodium- and ruthenium-BINAP systems have been reported to give consistently high optical yields (90-100%) for hydrogenation of not only dehydroamino acids and dicarboxylic acids,[13, 44, 45] but perhaps more significantly, for reduction of a variety of

functionalised carbonyl substrates[13, 42, 46] (e.g. β-ketoesters and substituted aceto-phenones).

A large amount of e.e. data has accumulated over the years on hydrogenation of a wide range of substrates using various chiral ligand-metal combinations as catalyst precursors. Enantiomeric excesses of close to 100% have been achieved for hydrogenation of several alkenes.[16b, 41] Attempts to correlate the observed e.e. with the nature of the ligand, the metal, the substrate, and also with the absolute configurations of the ligand and the metal compound, highlight the complexity of the enantioselection process.[17, 41, 47]. While no general correlations are forthcoming, some useful trends have emerged. Chelating ligands are more effective than monodentate ones.[14, 17, 41] Ligands such as CHIRAPHOS that form rigid five-membered chelates are more likely to show higher enantioselectivity than those which form more flexible, six- or seven-membered rings. A rigid chiral array of phenyl rings in the five-membered chelates presumably helps discriminate the enantiotopic faces of the prochiral substrate in the binding step.[17] Nature of the substrate also plays an important role in determining the extent of asymmetric induction. High optical yields are often realised for functionalised substrates with the ability to bind the metal in a bidentate fashion which presumably provides a degree of rigidity in the configuration determining step. For example, enamides such as methyl-(Z)-α-acetamido-cinnamate (MAC) consistently give high e.e. (up to 100%) compared to simple prochiral alkenes such as α-ethylstyrene (< 20%).[16b]

Using an ingenious combination of kinetic, X-ray, and NMR studies, Halpern and coworkers have elucidated a possible mechanism for asymmetric hydrogenation of prochiral alkenes catalysed by the extremely effective Rh-CHIRAPHOS and Rh-DiPAMP systems (Figure 1.3).[48] Addition of methyl- or ethyl-(Z)-α-acetamidocinnamate (R = methyl, MAC; R = ethyl, EAC; see Figure 1.3) substrate to the catalyst precursor [Rh(P–P)(MeOH)$_n$]$^+$, generated *in situ* (P–P = CHIRAPHOS, DiPAMP), affords two diastereomers (A' and A") which differ only in the olefinic faces coordinated. The two

diastereomers could be distinguished in solution by ^{31}P NMR spectroscopy. Examination of the major diastereomer (A') of [Rh(S,S–CHIRAPHOS)(EAC)]$^+$ClO$_4^-$, which was isolated and characterised by X-ray crystallography, revealed that the major diastereomer was *not* the one expected to lead to the principal product. Earlier, the enantioselectivity of the reduction was thought to be governed by the initial diastereomeric ratio (A'/A") of the catalyst-substrate adduct. However, detailed kinetic studies showed that it was the relative reactivity of the diastereomers with H$_2$ that determined the observed optical yield. For example, in the related [Rh(R,R-DiPAMP)]$^+$ system using MAC as the substrate, the minor species, A", reacted with H$_2$ ~580 times faster than did the major diastereomer, A' (k" = 6.4 x 10^2 and k' = 1.1 M^{-1}s^{-1}, respectively, at 25 °C, 1 atm H$_2$), yielding the corresponding S-enantiomer in over 95% e.e.

The mechanism illustrated in Figure 1.3 also explains the observed decrease in e.e. with increasing H$_2$ pressure. Increase in H$_2$ pressure increases rates of both the pathways (k' and k"). This can lead to depletion of the minor diastereomer A" faster than the equilibrium between A' and A" can be re-established, consequently producing more of the R-isomer, and hence lower optical yields.

1.2.2 Hydrogenation of Carbonyl Compounds

As mentioned in Section 1.2, work on reduction of substrates other than alkenes has lagged behind considerably. This is evident from the relatively few literature reports on homogeneous hydrogenation of aldehydes, ketones, esters, imines, nitriles, anhydrides, and nitro compounds.[29, 31, 32] There appears to be a certain degree of correlation between the ease of reduction of these substrates and the volume of work done on them. Amongst the non-olefinic substrates, those containing a carbonyl functionality are the most easily reduced and have probably received the most attention.
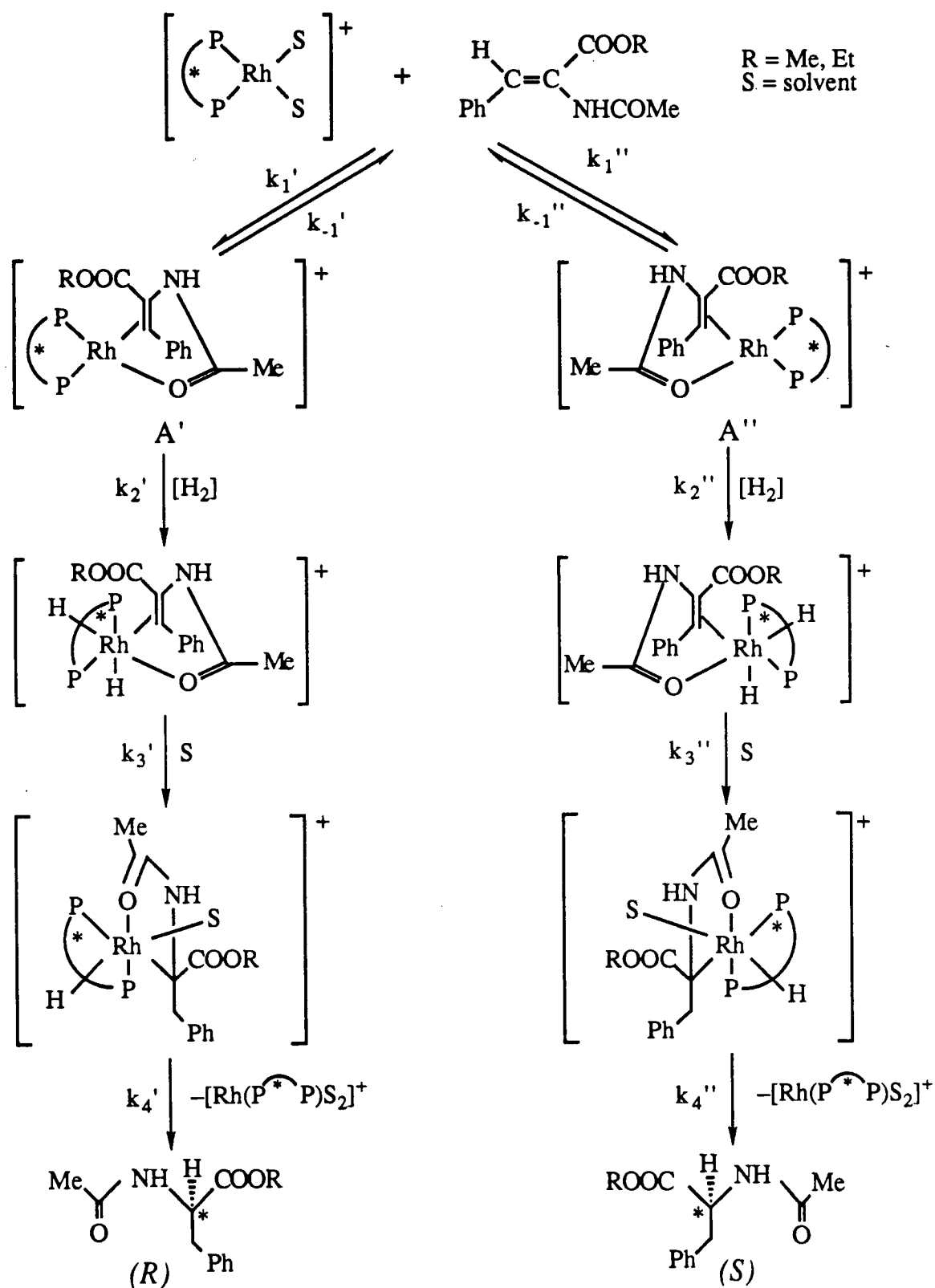
Figure 1.3: A possible mechanism for the chiral diphosphine rhodium-catalysed asymmetric hydrogenation of prochiral olefins.

9

Except in a limited number of documented systems,[25] substrate activation by coordination to the metal centre is usually essential for a metal-catalysed transformation to take place. Carbonyl groups exhibit a much lower binding ability (compared to alkenes) toward transition metals, and very few late transition metal coordination complexes containing carbonyl compounds are known.[49, 50] Also, unlike in the case of olefin substrates and their reduction product alkanes, the non-olefinic substrates and their hydrogenation products show very similar affinity toward the metal catalyst (for example, carbonyl compounds and the corresponding product alcohols).[32] In many cases the hydrogenation products of non-olefinic substrates exhibit even higher affinity toward the metal catalyst when compared to that of the parent substrates (for example, amines vs. imines). Such product coordination can result in a competitive inhibition of further reduction.

Aldehydes are the most easily reduced of the carbonyl compounds (followed by ketones and esters); however, aldehydes are prone to facile and usually irreversible decarbonylation by the hydrogenation catalysts. This in turn results in a progressive loss of catalytic activity by CO poisoning of the catalyst;[31b, 32] the presence of a CO ligand is known to lessen the catalytic hydrogenation activity of most group 8 and 9 transition metal catalysts.[51] The anionic hydrido(phosphine)ruthenate complexes reported by Grey *et al.* are perhaps the only effective catalysts known for H_2–hydrogenation of esters to the corresponding alcohols (Equation 1.4) under relatively mild conditions.[52, 53] Stoichiometric reduction by hydride reagents such as $NaBH_4$ and $LiAlH_4$ is still the method of choice for reduction of ester substrates.[32]

$$CH_3\overset{\displaystyle O}{\overset{\|}{C}}-OCH_3 \quad \xrightarrow[\substack{[K(diglyme)]^+[RuH_2(PPh_3)_2(PPh_2C_6H_4)]^-}]{10 \text{ atm } H_2, 90\text{ °C, toluene}} \quad CH_3CH_2OH + CH_3OH + CH_3\overset{\displaystyle O}{\overset{\|}{C}}-OCH_2CH_3 \qquad (1.4)$$
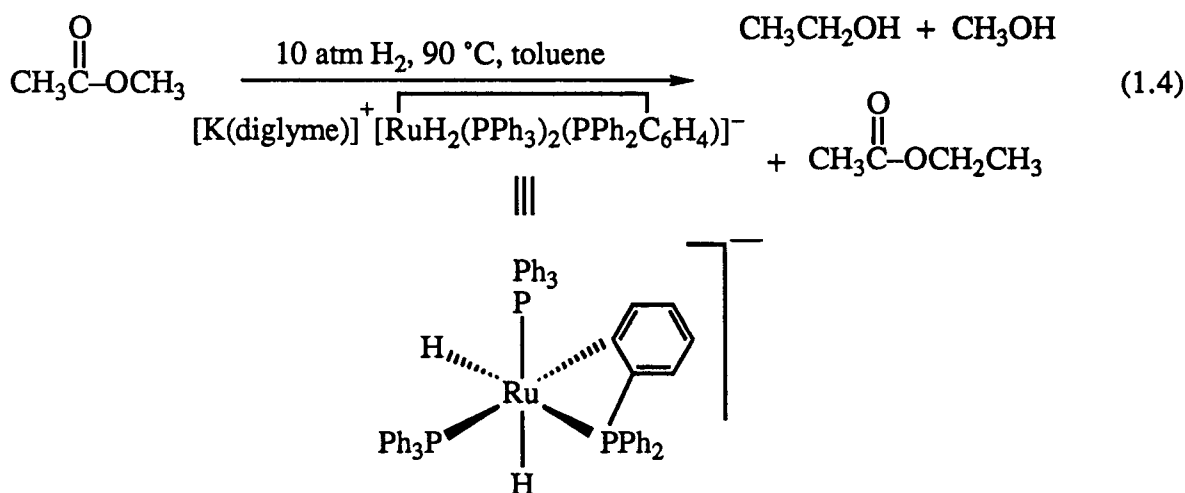
Work on hydrogenation of ketones has gathered momentum in recent years, and a number of reviews have appeared.[31b, 32, 33, 49] The increase in activity in this area stems mainly from the interest in asymmetric synthesis of chiral alcohols. The chiral secondary alcohols, obtained by hydrogenation of prochiral ketones (R^1COR^2), are important intermediates in the fine chemicals and pharmaceutical industries and in natural product synthesis.[54] Stoichiometric borohydride and organoborane reagents modified by chiral auxiliaries have been shown to hydrogenate simple prochiral ketones in high e.e. (up to 100%).[55] In one interesting case, propiophenone was reduced with 78% e.e. by achiral $NaBH_4$ in the presence of bovine serum albumin as the chiral template.[56] However, these reagents lack diversity and are often much less effective for reduction of functionalised ketones, such as aryl diketones and α-dicarbonyl compounds.

As in the case of olefin hydrogenation, phosphine complexes of group 8 and 9 metals constitute the largest and the most effective class of homogeneous catalysts for ketone hydrogenation. Schrock and Osborn[57] investigated H_2-hydrogenation of simple ketones (e.g. acetone, acetophenone) under relatively mild conditions catalysed by cationic rhodium catalysts (Equation 1.5) of the type $[RhH_2(PR_3)_2(solv)_2]^+$ which are easily prepared in situ from $[Rh(diene)(PR_3)_2]^+X^-$ precursors.[32] Use of relatively more basic

phosphines, such as PBu$_3$, resulted in turnovers of *ca.* 1000 or more, notably in the presence of added water (~ 1%), at 60–80 °C and ~ 7 atm H$_2$.[58]

$$\underset{\substack{\\ {}^1R \quad R^2}}{C}\overset{O}{\|} \; + \; H_2 \quad \xrightarrow[\text{1\% H}_2\text{O}]{[\text{Rh(diene)P}_2]^+\,X^-} \quad \underset{\substack{\\ {}^1R \quad R^2}}{\overset{OH}{\underset{|}{CH}}} \hspace{2cm} (1.5)$$

$$P = PAr_xR_{3-x}$$

$$X = PCl_6, \; BF_4, \; ClO_4$$
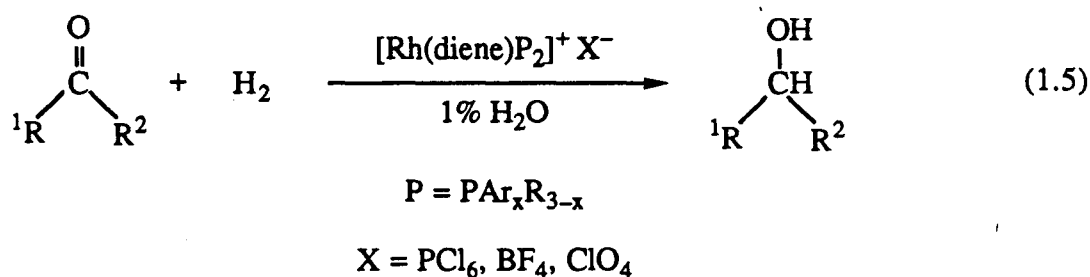
Based on their studies, Schrock and Osborn proposed the following mechanism (Figure 1.4) for the hydrogenation of ketones.

$$P = PAr_xR_{3-x}$$
$$S = \text{solvent}$$
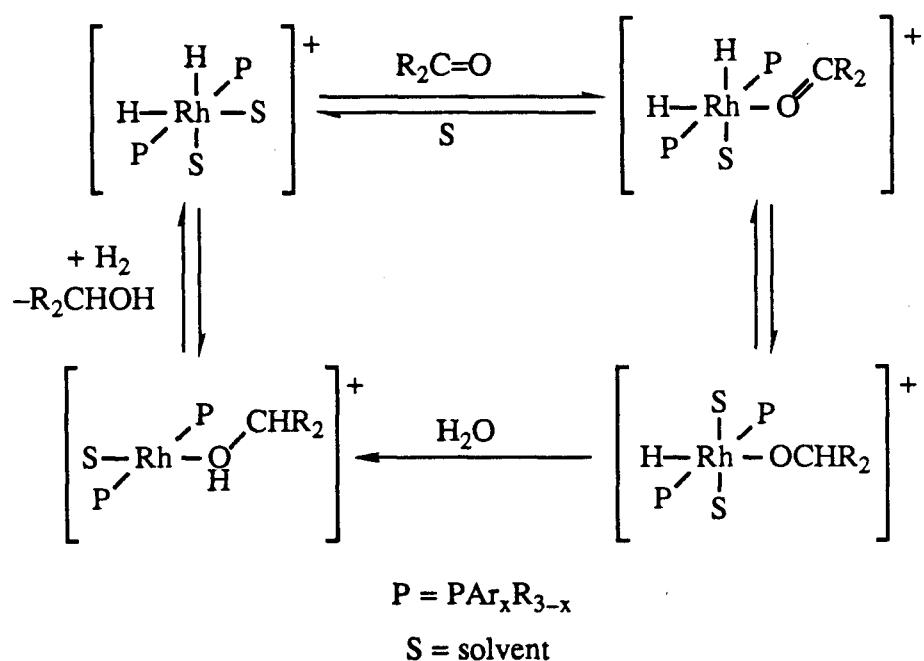
Figure 1.4: Mechanism proposed by Schrock and Osborn[57] for the rhodium-phosphine catalysed homogeneous hydrogenation of ketones.

The initial *cis*-hydride migration to the carbonyl carbon of the bound ketone is followed by a water-promoted proton transfer to the carbonyl oxygen. Dissociation of the product

alcohol and subsequent oxidative addition of H_2 then regenerate the catalyst. The observed incorporation of deuterium exclusively at the carbonyl carbon of acetone, when D_2 is used for the reduction, supports the above mechanism and also rules out participation of the enol tautomer in the catalytic cycle.[57]

The proposed role of water in the proton transfer step is illustrated below (Figure 1.5). There is no clear evidence as to whether the proton abstraction by OH$^-$ from the rhodium dihydride, and the proton transfer from a water molecule to the bound alkoxy moiety, occur in a concerted fashion or in a stepwise manner.
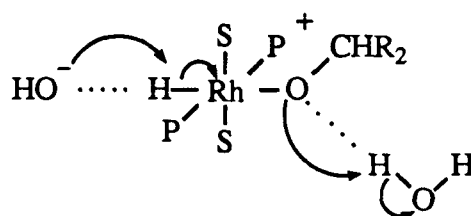
Figure 1.5: Suggested role of water in rhodium-phosphine catalysed homogeneous hydrogenation of ketones (also see Figure 1.4).

As in the case of alkene hydrogenation, phosphine complexes of group 8 and 9 metals have proved to be the most effective for ketone hydrogenation. Recently, however, rhodium and iridium complexes containing nitrogen-based donor ligands such as 2,2'-bipyridine (bipy), 1,10-phenanthroline (phen) and related ligands have been reported to be highly active for H_2- and transfer hydrogenation (Section 1.2.4) of ketones.[59, 60] The use of such non-phosphine catalyst systems may become important in light of the problems of degradation and ligand loss sometimes associated with phosphine ligands (under hydrogenation conditions).[61]

The asymmetric hydrogenation of prochiral ketones is not as well understood as that of alkenes.[33] Attempts at using heterogeneous catalysts, notably Raney nickel, modified by chiral auxiliaries have been only moderately successful at best.[35b, c]

13

However, 3-hydroxybutanoate has been obtained in ~85% e.e. by hydrogenation of methyl acetoacetate using a Raney nickel catalyst modified by tartaric acid and NaBr.[14] High optical yields have been obtained for hydrogenation of acetylacetone to 2,4-pentanediol, using a similar catalyst system.[62]

Asymmetric homogeneous hydrogenation of unsubstituted ketones under mild conditions (30 °C, 1 atm H_2), using the Schrock–Osborn type cationic $[RhH_2P_2(solvent)_2]^+$ systems containing chiral phosphines, gave poor optical yields (e.g. < 10% for acetophenone) at low rates.[63] Of the several chiral phosphines studied only a few exhibit good activity and enantioselectivity. Higher e.e.'s are generally observed for aryl alkyl ketones than for dialkyl ketones. Addition of small amounts of triethylamine to the neutral [Rh(nbd)Cl]$_2$/DIOP catalyst system resulted in a dramatic increase in the observed e.e. (from 51% to ~ 80%) for hydrogenation of acetophenone at 50 °C and 70 atm H_2 pressure (Equation 1.6).[54, 64]

$$
\underset{\underset{Ph}{\overset{Me}{\diagup}}{\diagdown}}{\overset{O}{\overset{\|}{C}}} + H_2 \xrightarrow[\substack{NEt_3,\ benzene \\ 50°C,\ 70\ atm}]{1/2\ [Rh(nbd)Cl]_2,\ (+)\text{-DIOP}} \underset{\underset{H}{|}}{\overset{\overset{OH}{|}}{Me-\underset{*}{C}-Ph}} \qquad (1.6)
$$

$$80\%\ e.e.$$
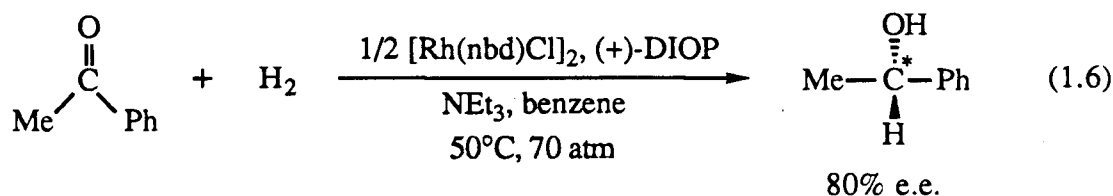
Results of H_2-reduction of functionalised ketones have been generally more encouraging. Improved optical yields have been attributed to the increased rigidity of the catalyst-substrate adduct due to the chelating effect of the secondary functional group (hydroxy, alkoxy, carboxy, halo etc.).[17, 46, 54] Close to 100% optical (and chemical) yields have been realised for the reduction of a wide range of substituted ketones using Ru-chiral phosphine systems, particularly with BINAP.[13, 46]

Hydrosilylation of prochiral ketones in the presence of appropriate chiral transition metal catalysts, followed by hydrolysis, provides an indirect alternative route to enantioselective synthesis of chiral secondary alcohols.[14, 16, 17, 38, 65] Optical yields of up

to 85% with rhodium chiral phosphine catalysts have been reported.[49, 65] Non-phosphine chiral ligands have also proved effective in asymmetric synthesis of chiral secondary alcohols *via* ketone hydrosilylation. Acetophenone is converted to 1-phenylethanol in 98% e.e. and quantitative yield using a rhodium catalyst prepared *in situ* from [Rh(cod)Cl]$_2$ and a pyridine thiazolidine derivative (shown in Equation 1.7);[14] the thiazolidine ligand can be synthesised by a one-step condensation of 2-pyridinealdehyde with an L-cysteine ester.

$$ (1.7) $$
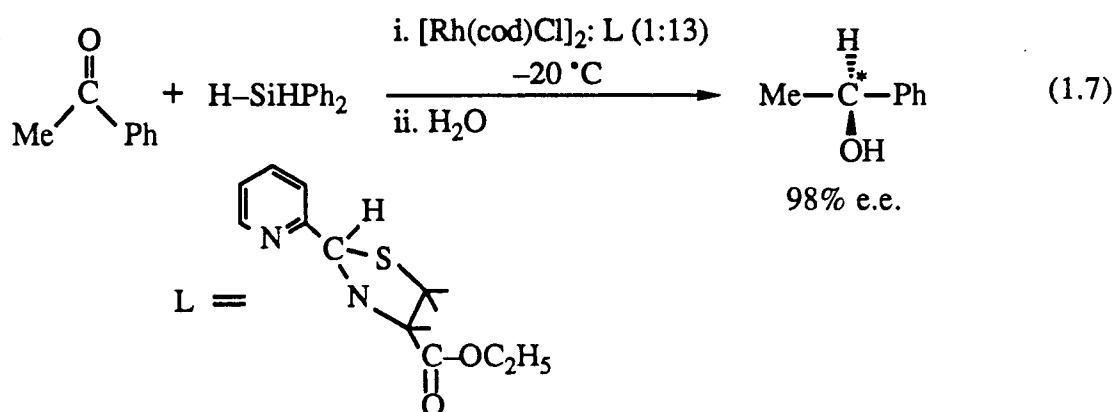
Asymmetric reduction of prochiral ketones can also be achieved by hydrogen transfer from an appropriate donor (e.g. alcohols, amines) in a chiral environment. Transfer hydrogenation is discussed in Section 1.2.4.

1.2.3 Homogeneous Hydrogenation of Nitriles and Imines

There are very few reports in the literature dealing with transition metal catalysed hydrogenation of carbon-nitrogen multiple bonds (C≡N, C=N).[31, 33, 49] Relatively severe temperatures (100–200 °C) and pressures (40–200 atm H$_2$) are generally required in order to obtain reasonably fast rates.[32] Catalytic hydrogenation (both homogeneous and heterogeneous) of nitriles often results in the formation of a mixture of primary, secondary and tertiary amines as well as ammonia (Equation 1.8). Selectivity for only one product is usually the prime consideration in the choice of a catalyst. For example, the complex

15

RuHCl(PPh3)3 catalyses hydrogenation of acetonitrile in toluene at 90 °C and 7 atm H_2; at 15% conversion (20 h) of the nitrile, a mixture of ethylamine (34%), diethylamine (58%), triethylamine (8%) and ammonia was obtained (Equation 1.8).[52]

$$CH_3CN \xrightarrow[\text{RuHCl(PPh}_3)_3]{\text{7 atm H}_2,\ 90\ °C,\ \text{toluene}} \begin{array}{c} CH_3CH_2NH_2\ +\ (CH_3CH_2)_2NH \\ 34\% \qquad\qquad 58\% \\[4pt] +\ (CH_3CH_2)_3N\ +\ NH_3 \\ 8\% \end{array} \qquad (1.8)$$
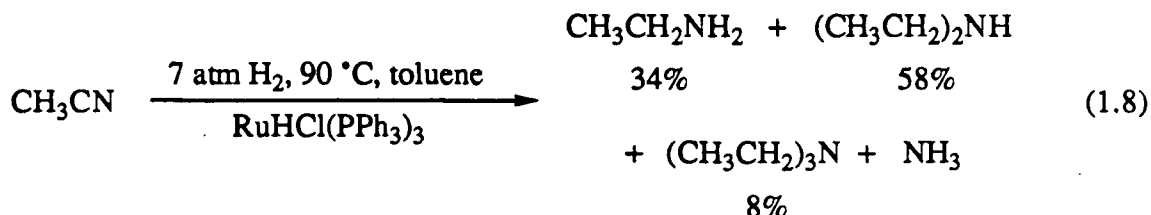
Interestingly, under the same reaction conditions the anionic hydrido(phosphine)ruthenate complex (shown in Equation 1.4), which is derived from the neutral RuHCl(PPh3)3 precursor, hydrogenated acetonitrile to ethylamine with 98% selectivity and at a faster rate (38% conversion); the rate of hydrogenation could be further increased by addition of 18-crown-6 to this system (60% conversion in 20 h).[52]

The rhodium hydride complex RhH(PPr^{i}3)3 is an extremely effective nitrile hydrogenation catalyst; a number of alkyl and aryl nitriles have been reduced selectively to the corresponding primary amines (Equation 1.9) under very mild conditions (20 °C, 1 atm H_2).[31, 66] Of note, this rhodium complex also catalyses the reverse reaction, viz. dehydrogenation of primary amines (Equation 1.10), in the absence of H_2 and at high temperatures (110 °C).

$$^1R–C{\equiv}N \xrightarrow[\text{RhH(PPr}^i_3)_3]{\text{1 atm H}_2,\ 20\ °C,\ \text{THF}} {}^1R–CH_2NH_2 \qquad (1.9)$$

$$^1R = Bu^n,\ Bu^t,\ Pr^i,\ Bz,\ CH_2{=}CHCH_2,\ Ph$$

$$PhCH_2NH_2 \xrightarrow[\text{RhH(PPr}^i_3)_3]{110\ °C,\ 0.05\ torr} PhC{\equiv}N\ +\ 2\,H_2 \qquad (1.10)$$
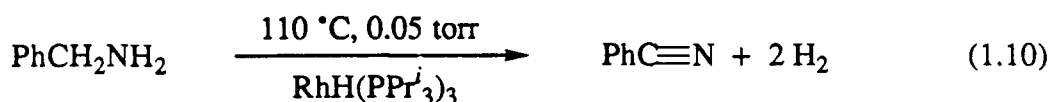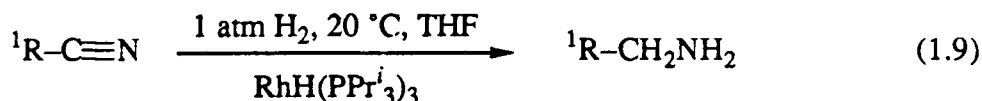
Imines are intermediates in the reduction of nitriles to amines. They are also easily accessible synthetically *via* simple condensation reactions of carbonyl compounds such as aldehydes and ketones with primary amines (Equation 1.11).[67] Several rhodium and ruthenium phosphine complexes are active catalysts for the reduction of imines using molecular hydrogen;[31-33, 49, 63] relatively severe conditions are often required. Moreover, catalyst poisoning by the amine products sometimes results in reduced catalytic activity.

$$
\begin{array}{c}
{}^{1}R \\
{}^{2}R
\end{array}\!\!\!C{=}O \;+\; {}^{3}R{-}NH_2 \;\; \underset{}{\overset{cat.}{\rightleftharpoons}} \;\; \begin{array}{c} {}^{1}R \\ {}^{2}R \end{array}\!\!\!C{=}N{\sim}\!R^3 \;+\; H_2O \qquad (1.11)
$$
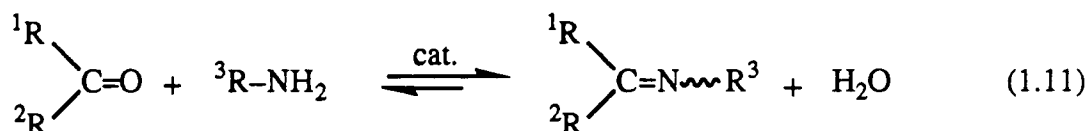
Reduction of imines provides an easy route to substituted amines; in particular, there is considerable interest in the asymmetric synthesis of chiral amines (Equation 1.12).[33, 68, 69] For example, some chiral amine derivatives are used as herbicides,[68, 69] in which one enantiomer is found to be far more potent than the other. Asymmetric synthesis of the more active enantiomer in high e.e. is desirable for environmental reasons because it would allow for the use of smaller doses of these herbicides.

$$
\begin{array}{c}
{}^{1}R \\
{}^{2}R
\end{array}\!\!\!C{=}N{\sim}\!R^3 \;\; \xrightarrow[cat^*.]{H_2} \;\; \begin{array}{c} {}^{1}R \\ {}^{2}R \end{array}\!\!\!H{=\!\!=\!}\overset{*}{C}{-}N{\sim}\!R^3 \qquad (1.12)
$$
$$
({}^{1}R \neq {}^{2}R)
$$
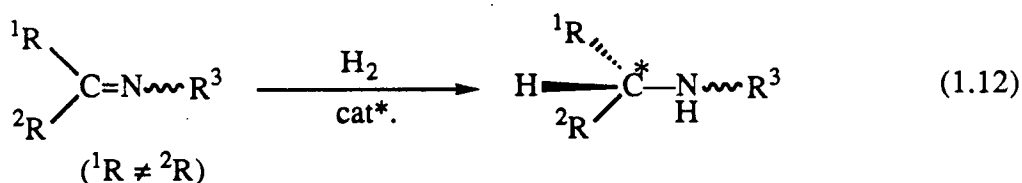
Attempts at asymmetric hydrogenation of prochiral imines, until recently,[68, 69] have been generally much less successful (typical e.e.'s < 40%) when compared to the relatively high e.e.'s (90–100%) achieved for enantioselective hydrogenation of several functionalised alkene and ketone substrates.[33] However, the recently reported rhodium catalyst generated *in situ* from [Rh(nbd)Cl]₂ and (*R*)-(+)-CYCPHOS (Figure 1.6) gives

high e.e.'s for hydrogenation of several prochiral imines in the presence of added iodide cocatalyst at low temperatures ($\leq 25\ °C$) and high H_2 pressures (70 atm).[68, 69]
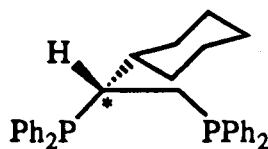
Figure 1.6: Structure of the chiral diphosphine CYCPHOS.

For example, the imine shown in Figure 1.7 was hydrogenated with 91% e.e.; interestingly, in the absence of iodide only 71% e.e. was observed.[68, 69] Other workers[70] have also reported increased optical yields upon the addition of halide cocatalysts, iodide being the most effective of Cl^-, Br^- and I^-.
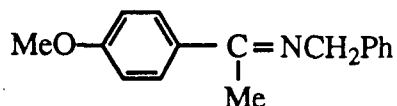
Figure 1.7: Structure of the imine substrate.

Recently, Sinou and coworkers[71] have reported > 95% e.e. for hydrogenation (70 atm H_2, 20 °C) of the imine obtained from acetophenone and benzylamine, using as catalysts water-soluble rhodium complexes containing poly-*m*-sulphonated derivatives of the chiral chelating phosphine 2,4-bis(diphenylphosphino)pentane (Figure 1.8). The reductions were carried out in an aqueous/organic two-phase solvent system (e.g. H_2O/AcOEt). Interestingly, the best optical yields were obtained when a mixture of mono-, di- and tri-sulphonated phosphines was used as opposed to the pure tetra-sulphonated phosphine.
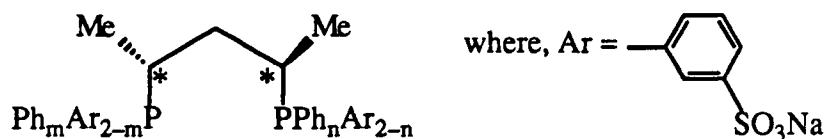
Figure 1.8: Poly-*m*- sulphonated derivatives of the bidentate chiral phosphine 2,4-bis-(diphenylphosphino)pentane.

The mechanism for the H_2-hydrogenation of imines is thought to be very similar to that of ketone hydrogenation, although few kinetic and mechanistic studies are available. Several workers have noted the requirement for an alcohol co-solvent for effective imine hydrogenation,[68, 69, 72] and hydrogen-bonding between the alcohol –OH proton and the imine nitrogen during the substrate binding step has been invoked as a possible explanation.[68, 72] Based on the limited literature data available for asymmetric hydrogenation of imines, neutral and anionic (*in situ*) catalysts appear to be relatively more enantioselective than cationic ones, at least for the rhodium-based systems.[69, 70] The nature of the chiral induction step(s) remains unclear.

1.2.4 Transfer Hydrogenation

Catalytic hydrogen transfer from an appropriate donor organic molecule (DH_2) to an unsaturated acceptor substrate (A) provides an alternative to direct H_2-hydrogenation (Equation 1.13). Transfer hydrogenation reactions can be carried out under mild conditions (1 atm pressure) usually at the boiling point of the solvent; also, the use of relatively expensive H_2 and the high pressure equipment often required for H_2-hydrogenation reactions is avoided.

$$DH_2 \; + \; A \; \underset{}{\overset{cat.}{\rightleftharpoons}} \; D \; + \; AH_2 \qquad\qquad (1.13)$$

19
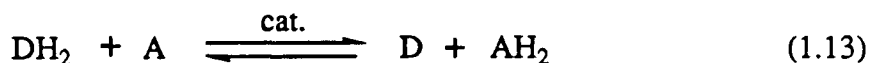
The extensive literature on transfer hydrogenation has been reviewed periodically.[73, 74] Alcohols, glycols, aldehydes, amides, amines, ethers and alkylbenzenes are some of the compounds which have been used as a source of hydrogen.[26] Alcohols are the most commonly used donors, 2-propanol being the prime choice. 2-Propanol is inexpensive, and its dehydrogenation product, acetone, can be easily distilled off from the reaction mixture. Secondary alcohols are more reactive than primary, but the latter are generally more selective.[31b]

Complexes of cobalt, rhodium, iridium and ruthenium are sometimes efficient catalysts for hydrogen transfer reactions;[26, 75] a variety of ligands including phosphines, phosphites, sulphoxides, Schiff bases and other nitrogenous compounds (e.g. bipy, substituted phenanthrolines, and alkaloids) has been employed successfully.[26, 32] The presence of a base cocatalyst such as KOH or NEt_3 is often essential.[76, 77] Small amounts of added water (~0.1% by volume) is also known to improve the catalytic activity of many systems.[77, 78] The roles of the base and the added water are not well understood. It should be noted that base by itself is capable of catalysing the hydrogen transfer by a different mechanism,[76, 77] albeit rather slowly compared to the transition metal-mediated reaction.[76]

Generally speaking, the best catalytic activity for the reduction of ketones and imines is achieved by transfer hydrogenation. For example, under the same conditions (82 °C), the time required for complete $RhCl(PPh_3)_3$-catalysed hydrogenation of benzylidene aniline ($C_6H_5CH=NC_6H_5$) is reduced from 6 h to a few minutes when 2-propanol is used instead of H_2 (70 atm).[32]

As depicted in Equations 1.13 and 1.14, transfer hydrogenation reactions are often reversible. The reduction products of carbonyl and imine substrates (*viz.* alcohols and amines, respectively) themselves can act as hydrogen donors toward the concomitantly formed oxidation product of the original donor (e.g. acetone formed from 2-propanol).[49] The extent of transfer hydrogenation is therefore determined by thermodynamic parameters.

20

The equilibrium can be shifted to the right by continual distillation of the dehydrogenated product, R^3COR^4, from the reaction mixture (Equation 1.14).

$$\underset{R^1}{\overset{X}{\underset{}{\overset{\|}{C}}}}\underset{R^2}{} \; + \; \underset{R^3-\overset{OH}{\underset{}{\overset{|}{CH}}}-R^4}{} \; \xrightleftharpoons{\text{cat.}} \; \underset{R^1-\overset{X-H}{\underset{}{\overset{|}{CH}}}-R^2}{} \; + \; \underset{R^3}{\overset{O}{\underset{}{\overset{\|}{C}}}}\underset{R^4}{} \qquad (1.14)$$

$$X = O \text{ or } N\text{-}\!\text{-}\!\text{-}R$$
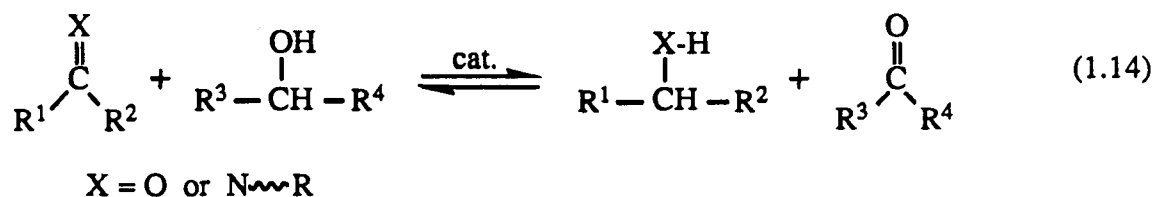
Of particular interest are the unusual selectivities sometimes observed for reduction by transfer hydrogenation as opposed to direct H_2-hydrogenation. For example, the $IrHCl_2(DMSO)_3$-catalysed transfer hydrogenation of α,β-unsaturated aldehydes in 2-propanol selectively affords the corresponding α,β-unsaturated alcohols (Equation 1.15), whereas H_2-hydrogenation invariably results in the formation of saturated aldehydes and, under more severe conditions, the saturated alcohols.[79]

$$\underset{R}{\overset{H}{\underset{}{}}}C=C\underset{H}{\overset{CHO}{\underset{}{}}} \xrightarrow[\text{(CH}_3)_2\text{CH(OH)}]{IrHCl_2(DMSO)_3} \underset{R}{\overset{H}{\underset{}{}}}C=C\underset{H}{\overset{CH_2OH}{\underset{}{}}} \qquad (1.15)$$

$$R = C_6H_5, CH_3$$
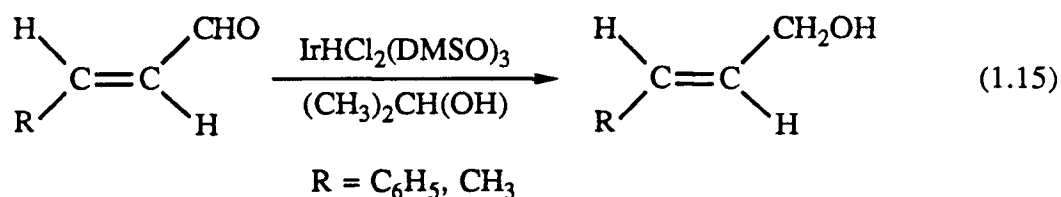
Only low to moderate optical yields have been observed for the asymmetric transfer hydrogenation of simple aryl alkyl ketones.[80] The best e.e.'s to date (~50%) have been realised for the reduction of t-butyl phenyl ketone and benzyl phenyl ketone by hydrogen transfer from 2-propanol using $[Ir(cod)(PPEI)]^+ClO_4^-$ as catalyst, where PPEI is a chiral Schiff base (Figure 1.9).[81] Propiophenone is reduced with 33% e.e. using the same system.[81] Optical yields of 30-50% have been achieved for hydrogen transfer to acetophenone and propiophenone using chiral sulphoxide complexes of rhodium as catalyst precursors.[33, 78, 82-84]

21
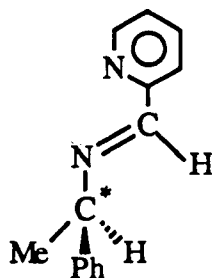
Figure 1.9: The chiral Schiff base PPEI.

Kinetic and mechanistic investigation of transfer hydrogenation reactions is made difficult by the complex nature of these systems; a large number of species is often present in solution during the course of the reaction.[31b] Two pathways, which are formally equivalent to the saturate and the unsaturate routes encountered in H_2-hydrogenation, have been suggested.[25] Transfer of the β-hydrogen from the alkoxide is thought to be the rate determining step in both these mechanisms (see below).

The unsaturate route (Figure 1.10) involves initial coordination of the substrate, then that of the alcohol donor. Formation of an alkoxide, which may be base-assisted, is followed by transfer of the β-hydrogen of the alkoxide to the bound substrate. Finally, protonolysis liberates the product and regenerates the catalyst.[25]

$$M \; + \; substrate(S) \; \rightleftharpoons \; M(S) \; \xrightarrow[-H^+]{R^1R^2CH(OH)} \; \begin{array}{c} M(S) \\ | \\ OCHR^1R^2 \end{array}$$

$$\underset{R^1 \quad R^2}{\overset{O}{\underset{}{\|}}C} \; + \; SH_2 \; + \; M \; \xleftarrow{H^+} \; \begin{array}{c} M-SH \\ | \\ O = CR^1R^2 \end{array}$$
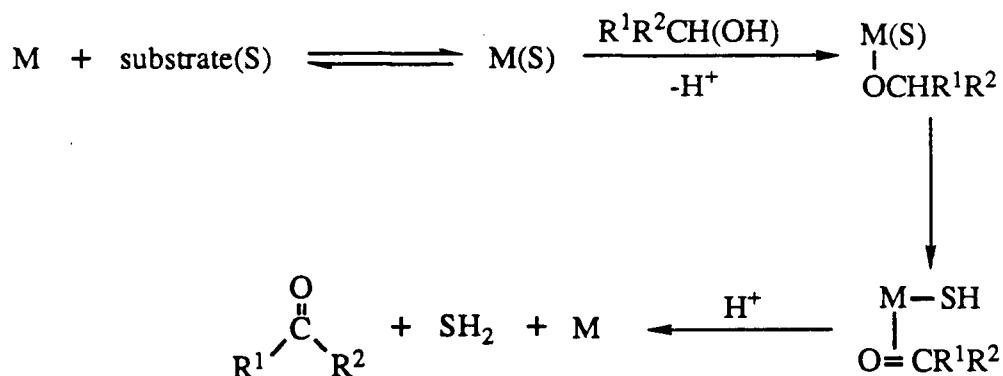
Figure 1.10: The unsaturate route in transfer hydrogenation from an alcohol donor.

In the saturate (hydride) route (Figure 1.11), initial reaction of the metal complex and the alcohol donor yields a hydridoalkoxide species.[25] β-Hydrogen transfer from the alkoxide and coordination of the substrate result in a dihydride species which can transfer both hydrides to the substrate either in a single step or in a stepwise, hydride transfer – protonolysis sequence.[25]

$$MHClP_n \xrightarrow[-HCl]{R^1R^2CHOH} MHP_n(OCHR^1R^2)$$
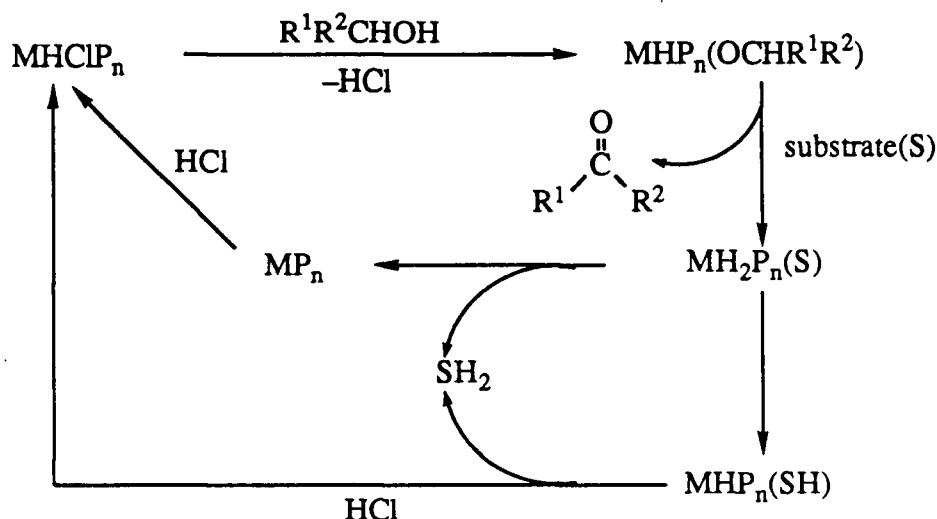
Figure 1.11: The saturate route for transition metal hydride-catalysed hydrogen transfer from an alcohol donor.

1.3 Dihydrogen Activation

As mentioned earlier (Section 1.2), activation of dihydrogen by a metal complex is a key step in both stoichiometric and catalytic hydrogenation. For a metal complex to be able to activate hydrogen (or the substrate), coordinative unsaturation at the metal centre is usually essential.[25, 29, 85, 86] Coordinatively saturated complexes, which are generally unreactive toward hydrogen for lack of a vacant site, may become active in solution through dissociation of a labile ligand. Not surprisingly, group 8–10 metal complexes, which are often coordinatively unsaturated, or which can easily become so by loss of a ligand, constitute the largest group of hydrogenation catalysts. The nature of the interaction

between molecular hydrogen and a metal complex is also dictated by the electronic and steric properties of the surrounding ligands.[85, 86]

The energetics of hydrogen activation have important consequences for the catalytic activity of the metal complex. While too strong a metal-hydrogen (M–H) bond may retard or even prevent hydrogen transfer to the coordinated substrate, too weak an interaction may result in a concentration of the M–H species too small to achieve an appreciable reaction rate.

As summarised by Halpern,[87] activation of dihydrogen may involve (a) base-promoted overall heterolytic splitting of the H–H bond to form a hydride and a proton (Equation 1.16), or (b) oxidative addition resulting in homolytic cleavage of the H–H bond (Equations 1.17a–c). Further, hydrogenolysis of a metal-metalloid bond[25, 88] such as M–Ge, M–Si, but most commonly M–C (Equation 1.18), can be considered a special case of heterolytic activation, wherein the leaving group itself plays the role of a base (denoted by B in Equation 1.16). These different processes of H_2-activation have been discussed in detail in a number of review articles on hydrogenation.[25, 26, 86a]

$$M^n + H_2 + B \longrightarrow H^-M^n + BH^+ \qquad \text{Heterolytic splitting} \qquad (1.16)$$

$$2\,M^n + H_2 \longrightarrow 2\,HM^{n+1} \qquad \text{Homolytic splitting} \qquad (1.17a)$$

$$M_2^n + H_2 \longrightarrow 2\,HM^{n+1} \qquad -''- \qquad (1.17b)$$

$$M^n + H_2 \longrightarrow (H)_2M^{n+2} \qquad -''- \qquad (1.17c)$$

$$R–M^n + H_2 \longrightarrow H^-M^n + R–H \qquad \text{Hydrogenolysis} \qquad (1.18)$$
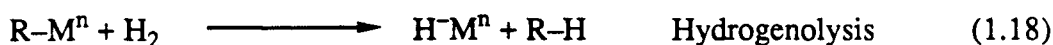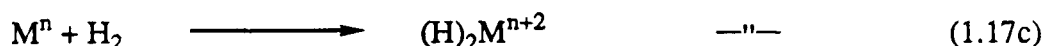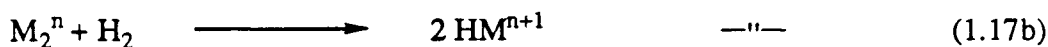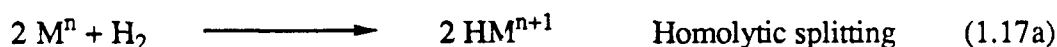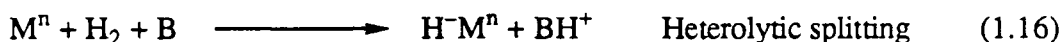
Heterolytic splitting of H_2 (Equation 1.16) is thought to involve a four-centre transition state (Figure 1.12a). Oxidative addition of H_2 at a metal centre (Equation 1.17c) is thought to proceed *via* initial coordination of the dihydrogen molecule; a subsequently formed three-centre, two-electron transition state is often invoked (Figure 1.12b).

a   **b**
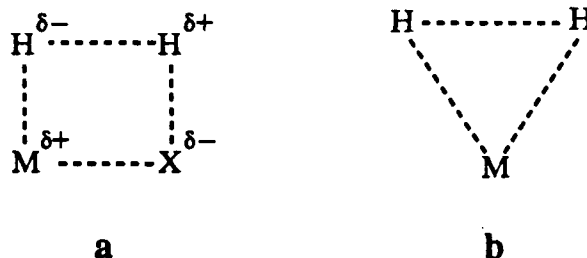
Figure 1.12: Proposed transition states during a) heterolytic and, b) homolytic activation of dihydrogen by transition metal complexes.

The latest development concerning the various modes of H_2-activation came with Kubas' discovery in 1984 of the first isolable molecular hydrogen complexes[89] $M(CO)_3(PPr^i_3)_2(\eta^2\text{-}H_2)$, M = Mo or W, which contain an H_2 ligand bonded side-on (Figure 1.13) as in the transition state shown in Figure 1.12b.

M = Mo, W

R = Pr^i, Cy
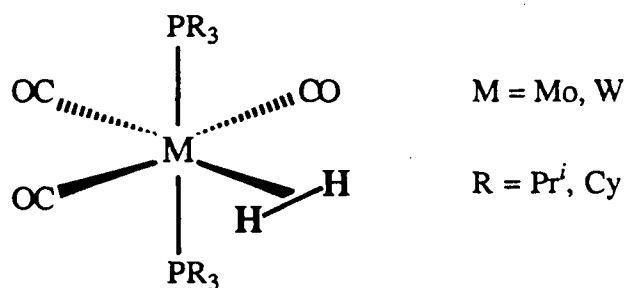
Figure 1.13: First reported examples of complexes containing the bound molecular hydrogen ($\eta^2\text{-}H_2$) ligand.[89]

A growing number of new complexes containing one or more bound molecular hydrogen ($\eta^2\text{-}H_2$) ligands has been reported since in the literature.[90, 91] The formation of molecular hydrogen complexes, and their role in catalytic processes, are of particular relevance to the topic of this thesis. More detailed background information encompassing various aspects of these novel complexes is given in a later chapter (Chapter 5).

1.4 Scope of This Thesis

Much effort has been directed at developing chiral rhodium catalysts for asymmetric hydrogenation. Chiral hydrogenation catalysts involving metals other than rhodium have received relatively little attention. The recent success of the chiral Ru-BINAP catalysts in asymmetric hydrogenation of several functionalised prochiral substrates has highlighted the potential of non-rhodium catalyst systems.[13, 42]

Previous work from this laboratory on RuHCl(DIOP)$_2$-catalysed asymmetric hydrogenation of alkenes revealed that the active species contained one DIOP per Ru(II) centre ["RuHCl(DIOP)"].[83, 92, 93] This provided the impetus for devising a general synthetic approach toward complexes containing a single bidentate phosphine (P–P) per Ru. Thorburn *et al.* in 1985 successfully developed such a synthetic strategy and isolated several such derivatives as dichloro-bridged, dimeric complexes of the type Ru$_2$Cl$_4$(P-P)$_2$.[33, 94-96] While the development of other potential synthetic routes to such complexes remained one of the objectives, the main objective of the current work was to investigate in detail the interaction of the Ru$_2$Cl$_4$(P–P)$_2$ species with H$_2$. Because of the high cost of chiral phosphines, much of the general chemistry was performed on complexes containing the nonchiral bidentate phosphine analogues, Ph$_2$P(CH$_2$)$_n$PPh$_2$ (n = 1–6). The nonchiral ligand 1,4-bis(diphenylphosphino)butane, (DPPB, n = 4), which forms a seven-membered chelate similar to the chiral DIOP and BINAP ligands (see Figures 1.1 and 1.2), was used extensively.

Chapter 3 deals with alternative synthetic routes to dichloro-bridged ruthenium(II)-diphosphine complexes of the type Ru$_2$Cl$_4$(P–P)$_2$. These complexes readily coordinate simple organic ligands (L) to give trichloro-bridged species of the general formula Ru$_2$Cl$_4$(P–P)$_2$(L). The previously known ruthenium complexes RuCl$_2$(DPPB)(PPh$_3$)[97] and *cis*-RuCl$_2$(Me$_2$SO)$_4$[98] were found to be useful as precursors to such trichloro-bridged

dinuclear species. Phosphorus-31 and proton-1 NMR spectral studies in solution were used to characterise the trichloro-bridged complexes. An X-ray diffraction study of $[(Me_2SO)(DPPB)Ru(\mu\text{-}Cl)_3RuCl(DPPB)]$ confirmed the trichloro-bridged dinuclear structure.

Attempts to use the mixed-phosphine complex, $RuCl_2(DPPB)(PPh_3)$, as a precursor to $Ru_2Cl_4(DPPB)_2$ and related derivatives led to the study of its reactivity with a variety of ligands. Reactions of $RuCl_2(DPPB)(PPh_3)$ with chelating ligands (L–L) gave six-coordinate complexes of the type $RuCl_2(DPPB)(L–L)$ by a simple substitution of the PPh_3 ligand. Characterisation of such complexes and their reactivity with H_2, as well as a solid-state CP/MAS ^{31}P NMR spectral study of the complexes $RuCl_2(DPPB)(PPh_3)$ and $RuCl_2(PPh_3)_3$, are presented in Chapter 4.

Reactivity of the chloro-bridged, dinuclear Ru(II) complexes with H_2 was investigated as a means of preparing hydride complexes (Chapter 5). Solution NMR studies (^1H, ^{31}P and T_1-measurements) on the DPPB complex in the presence of H_2, without and with an added base, established the *in situ* formation of a molecular hydrogen complex, $[(\eta^2\text{-}H_2)(DPPB)Ru(\mu\text{-}Cl)_3RuCl(DPPB)]$,[99] *en route* to the trinuclear ruthenium(II)-hydride cluster, $[RuHCl(DPPB)]_3$.[33, 96] The corresponding CHIRAPHOS trimer had been characterised earlier by X-ray crystallography.[33, 96] The temperature dependence of the ^1H NMR longitudinal relaxation times (T_1) of the $\eta^2\text{-}H_2$ moiety was used to estimate the H–H internuclear distance. Interestingly, the trinuclear hydridochloro complex, $[RuHCl(DPPB)]_3$, breaks down under hydrogen atmosphere to give dinuclear complexes of the type $[(\eta^2\text{-}H_2)(P–P)ClRu(\mu\text{-}Cl)_2(\mu\text{-}H)RuH(P–P)]$.

Hydridodiene complexes containing bidentate phosphines were of interest as potential precursors to "RuHCl(P–P)" species (by hydrogenation of the diene moiety) and to acyl complexes "Ru(COR)Cl(P–P)" (by carbonylation). Chapter 6 describes the synthesis and properties of RuHCl(nbd)(DPPB) (nbd = 2,5-norbornadiene) and its reactivity with H_2 and CO.[100]

The dinuclear $Ru_2Cl_4(P-P)_2$ complexes and their trinuclear hydride derivatives, $[RuHCl(P-P)]_3$, were found to be effective catalysts for hydrogenation of a variety of substrates including alkenes, ketones, imines and nitriles (Chapter 7). Results of preliminary investigations into certain alkene-, ketone- and nitrile-hydrogenations are presented.

1.5 References – Chapter 1

1. Sheldon, R. *Chemistry and Industry* **1990**, 212.

2. Collman, J. P.; Hegedus, L. S.; Norton, J. R.; Finke, R. G. *Principles and Applications of Organotransition Metal Chemistry*; University Science Books: Mill Valley, CA, 1987.

3. Jennings, J. R. *Selected Developments in Catalysis*; Blackwell Scientific Publications: Oxford, Vol. 12, 1985.

4. Masters, C. *Homogeneous Transition-metal Catalysis- a Gentle Art*; Chapman and Hall: London, 1981.

5. (a) Parshall, G. W. *Homogeneous Catalysis*; Wiley-Interscience: New York, 1980.
    (b) *ibid.*; 2nd Edn., *in press*.

6. Nakamura, A.; Tsutsui, M. *Principles and Applications of Homogeneous Catalysis*; Wiley-Interscience: New York, 1980.

7. (a) Hartley, F. R. in *Supported Metal Complexes, Catalysis by Metal Complexes Ser.*; James, B. R., Ugo, R., Eds.; D. Reidel Publishing Co.: Boston, 1985.
    (b) Iwasawa, Y., Ed.; *Tailored Metal Catalysts, Catalysis by Metal Complexes Ser.*; D. Reidel Publishing Co.: Boston, 1986.

8. Dolcetti, G.; Hoffman, N. W. *Inorg. Chim. Acta* **1974**, *9*, 269; and references therein.

9. (a) Bayer, E.; Shurig, V. *Chemtech.* **1976**, 212.
    (b) Skinner, K. J. *Chem. & Eng. News* **1977**, Feb. 7, 18.

10. (a) Hartley, F. R.; Vezey, P. N. *Adv. Organomet. Chem.* **1977**, *15*, 189.
    (b) Haggin, J. *Chem. & Eng. News* **1982**, Nov. 15, 11.
    (c) Manassen, J. *Plat. Met. Rev.* **1971**, *15*, 142; and references therein.

11.	Michalska, Z. M.; Ostaszewski, B. *J. Organomet. Chem.* **1986**, *299*, 259.

12.	Alper, H. *Adv. Organomet. Chem.* **1981**, *19*, 183.

13.	(a) Noyori, R. *Science* **1990**, *248*, 1194; and references therein.
	(b) Noyori, R.; Kitamura, M. in *Modern Synthetic Methods*, Scheffold R., Ed.;
	Springer-Verlag: Berlin, 1989; p 115.

14.	(a) Brunner, H. *Synthesis* **1988**, 645.
	(b) Brunner, H. *J. Organomet. Chem.* **1986**, *300*, 39.

15.	Knowles, W. S. *Acc. Chem. Res.* **1983**, *16*, 106.

16.	(a) Kagan, H. B. in *Comprehensive Organometallic Chemistry*; Wilkinson, G.,
	Ed.; Pergamon Press: Oxford, 1982; Vol. 8, Chapter 53.
	(b) Caplar, V.; Comisso, G.; Sunjic, V. *Synthesis* **1981**, 85.

17.	Bosnich, B.; Fryzuk, M. D. in *Topics in Inorganic and Organometallic Stereo-
	chemistry*; Geoffrey, G. L., Ed.; Wiley-Interscience: New York, 1981, p 119.

18.	(a) Pino, P.; Consiglio, G. in *Fundamental Research in Homogeneous Catalysis*;
	Tsutsui, M., Ed.; Plenum: New York, 1979; Vol. 3, p 519.
	(b) *ibid.*; Tsutsui, M., Ugo, R., Eds.; 1977; Vol. 1, p 147.

19.	(a) Blystone, S. L. *Chem. Rev.* **1989**, *89*, 1663.
	(b) Brown, J. M.; Chaloner, P. A.; Murrer, B. A.; Parker, D. *ACS Symposium
	Series*, **1980**, *119*, 169.
	(c) Valentine, D.; Scott, J. W. *Synthesis* **1978**, 329.

20.	For example, (a) Emsley, J. *New Scientist* **1990**, March 31, 32.
	(b) Larsen, R. D.; Corley, E. G.; Davis, P.; Reider, P. J.; Grabowski, E. J. J.
	J. Am. Chem. Soc. **1990**, *111*, 7650.

21.	Lehninger, A. L. *Principles of Biochemistry*; Worth Publishers: New York, 1982;
	Chapters 3 and 30.

22. (a) Bednarski, M. D. in *Catalysis of Organic Reactions*; Blackwell, D. W., Ed.; Marcel Dekker: New York, 1990; Vol. 40, Chapter 5; and references therein.
(b) Yamada, K.; Kinoshita, S.; Tsunoda, T.; Aida, K. *The Microbial Production of Amino Acids*; Wiley: New York, 1972.

23. Hatada, M.; Jancarik, J.; Graves, B.; Kim, S. *J. Am. Chem. Soc.* **1985**, *107*, 4279.

24. Brown, J. M. *Angew. Chem., Int. Ed. Engl.* **1987**, *26*, 190.

25. James, B. R. in *Comprehensive Organometallic Chemistry*; Wilkinson, G., Ed.; Pergamon Press: Oxford, 1982; Vol. 8, Chapter 51.

26. James, B. R. *Adv. Organomet. Chem.* **1979**, *17*, 319.

27. Crabtree, R. H. *Acc. Chem. Res.* **1979**, *12*, 331.

28. Rylander, P. N. *Catalytic Hydrogenation in Organic Syntheses*; Academic Press: New York, 1979.

29. James, B. R. *Homogeneous Hydrogenation*; Wiley: New York, 1973.

30. Freifelder, M. *Practical Catalytic Hydrogenation*; Wiley-Interscience: New York, 1971.

31. (a) Ref. 2, Chapter 10.
(b) Chaloner, P. *Handbook of Coordination Catalysis in Organic Chemistry*; Butterworths: Toronto, 1986: Chapter 2.
(c) Cotton, F. A.; Wilkinson, G. *Advanced Inorganic Chemistry*; Wiley-Interscience: New York, 4th Edn., 1980; Chapter 30.

32. Mestroni, G.; Camus, A.; Zassinovich, G. in *Aspects of Homogeneous Catalysis*; Ugo, R., Ed.; D. Reidel Publishing Co.: Dordrecht, 1981; Vol. 4, p 71.

33.   James, B. R.; Joshi, A. M.; Kvintovics, P.; Morris, R. H.; Thorburn, I. S. in *Catalysis of Organic Reactions*; Blackburn, D. W., Ed.; Marcel Dekker: New York, 1990; Chapter 2; and references therein.

34.   (a) Eleveld, M. B.; Hogeveen, H.; Schudde, E. P. *J. Org. Chem.* **1986**, *51*, 3635.
        (b) Sanchez-Delgado, R. A.; Valencia, N.; Marquez-Silva, R.; Andriollo, A.; Medina, M. *Inorg. Chem.* **1986**, *25*, 1106.
        (c) Chan, Y. N. C.; Meyer, D.; Osborn, J. A. *J. Chem. Soc., Chem. Commun.* **1990**, 869.

35.   (a) Akabori, S.; Sakurai, S.; Izumi, Y.; Fujii, Y. *Nature* **1956**, *178*, 323.
        (b) Izumi, Y. *Angew. Chem., Int. Ed. Engl.* **1971**, *10*, 871.
        (c) Wittmann, Gy. in *Stereochemistry of Heterogeneous Metal Catalysis*; Bartok, M., Ed.; Wiley-Interscience: New York, 1985; Chapter 11.

36.   (a) Horner, L.; Siegel, H.; Buthe, H. *Angew. Chem., Int. Ed. Engl.* **1968**, *7*, 942.
        (b) Knowles, W. S.; Sabacky, M. J. *J. Chem. Soc., Chem. Commun.* **1968**, 1445.

37.   (a) Dang, T. P.; Kagan, H. B. *J. Chem. Soc., Chem. Commun.* **1971**, 481.
        (b) Kagan, H. B.; Dang, T. P. *J. Am. Chem. Soc.* **1972**, *94*, 6429.

38.   Bosnich, B., Ed.; *Asymmetric Catalysis*, Martinus Nijhoff: Dordrecht, 1986.

39.   Morrison, J. D., Ed.; *Asymmetric Synthesis*, Academic Press: New York, 1985; Vol. 5.

40.   (a) Andrade, J. G.; Prescher, G.; Schaefer, A.; Nagel, U. in *Catalysis of Organic Reactions*; Blackburn, D. W., Ed.; Marcel Dekker: New York, 1990; Chapter 3.
        (b) Noyori, R.; Takaya, H. *Acc. Chem. Res.* **1990**, *23*, 345.

41.   (a) Koenig, K. E. in *Catalysis of Organic Reactions*; Kosak, J. R., Ed.; Marcel
        Dekker: New York, 1984; Chapter 3.
        (b) Marko, L.; Bakos, J. in *Aspects of Homogeneous Catalysis*; Ugo, R., Ed.;
        D. Reidel Publishing Co.: Dordrecht, 1981; Vol. 4, p 145.

42.   Noyori, R. *Chem. Soc. Rev.* **1989**, *18*, 187; and references therein.

43.   Vineyard, B. D.; Knowles, W. S.; Sabacky, M. J.; Bachman, G. L.;
        Weinkauff, D. J. *J. Am. Chem. Soc.* **1977**, *99*, 5946.

44.   (a) Miyashita, A.; Yasuda, A.; Takaya, H.; Toriumi, K.; Ito, T.; Souchi, T.;
        Noyori, R. *J. Am. Chem. Soc.* **1980**, *102*, 7932.
        (b) Miyashita, A.; Takaya, H.; Souchi, T.; Noyori, R. *Tetrahedron* **1984**, *40*,
        1245.
        (c) Takaya, H.; Mashima, K.; Koyano, K.; Yagi, M.; Kumobayashi, H.;
        Taketomi, T.; Akutagawa, S.; Noyori, R. *J. Org. Chem.* **1986**, *51*, 629.

45.   (a) Kawano, H.; Ishii, Y.; Ikariya, T.; Saburi, M.; Yoshikawa, S.; Uchida, Y.;
        Kumobayashi, H. *Tetrahedron Lett.* **1987**, *28*, 1905.
        (b) Ikariya, T.; Ishii, Y.; Kawano, H.; Arai, T.; Saburi, M.; Yoshikawa, S.;
        Akutagawa, S. *J. Chem. Soc., Chem. Commun.* **1985**, 922.

46.   (a) Mashima, K.; Kusano, K.; Ohta, T.; Noyori, R.; Takaya, H. *J. Chem.
        Soc., Chem. Commun.* **1989**, 1208.
        (b) Kitamura, M.; Ohkuma, T.; Inoue, S.; Sayo, N.; Kumobayashi, H.;
        Akutagawa, S.; Ohta, T.; Takaya, H.; Noyori, R. *J. Am. Chem. Soc.* **1988**,
        110, 629.
        (c) Noyori, R.; Ohkuma, T.; Kitamura, M.; Takaya, H.; Sayo, N.;
        Kumobayashi, H.; Akutagawa, S. *J. Am. Chem. Soc.* **1988**, *109*, 5856.

47.   (a) Slack, D. A.; Greveling, J.; Baird, M. C. *Inorg. Chem.* **1979**, *18*, 3125.
        (b) Bosnich, B.; Roberts, N. K. *Adv. Chem. Ser.* **1982**, *196*, 337.
        (c) Knowles, W. S.; Christophel, W. C.; Koenig, K. E.; Hobbs, C. F. *Adv.
        Chem. Ser.* **1982**, *196*, 325.

48. (a) Chan, A. S. C.; Pluth, J. J.; Halpern, J. *J. Am. Chem. Soc.* **1980**, *102*, 5952.
    (b) Halpern, J. *Science* **1982**, *217*, 401.
    (c) Halpern, J. in Ref. 39, Chapter 2.

49. Heil, B.; Marko, L.; Toros, S. in *Homogeneous Catalysis with Metal Phosphine Complexes*; Pignolet, L. H., Ed.; Plenum Press: New York, 1983; p. 317.

50. Huang, Y-H.; Gladysz, J. A. *J. Chem. Ed.* **1988**, *65*, 298.

51. James, B. R. *Inorg. Chim. Acta Rev.* **1970**, *4*, 73.

52. (a) Pez, G. P.; Grey, R. A.; Corsi, J. *J. Am. Chem. Soc.* **1981**, *103*, 7528.
    (b) Grey, R. A.; Pez, G. P.; Wallo, A. *J. Am. Chem. Soc.* **1981**, *103*, 7536.

53. Pez, G. P.; Grey, R. A. in *Fundamental Research in Homogeneous Catalysis*; Graziani, M. and Giongo, M., Eds.; Plenum: New York, 1982; Vol. 4, p. 97.

54. Chan, A. S. C.; Landis, C. R. *J. Mol. Catal.* **1989**, *49*, 165.

55. (a) Midland, M. M. *Chem. Rev.* **1989**, *89*, 1553.
    (b) *Aldrichimica Acta*, **1987**, *20(1)*; and references therein.

56. Sugimoto, T.; Matsumura, Y.; Tanimoto, S.; Okano, M. *J. Chem. Soc., Chem. Commun.* **1978**, 926.

57. Schrock, R. R.; Osborn, J. A. *J. Chem. Soc., Chem. Commun.* **1970**, 567.

58. Solodar, J. *Chemtech.* **1975**, 421.

59. Mestroni, G.; Spogliarich, R.; Camus, A.; Martinelli, F.; Zassinovich, G. *J. Organomet. Chem.* **1978**, *157*, 345.

60. (a) Mestroni, G.; Zassinovich, G.; Alessio, E.; Tornatore, M. *J. Mol. Catal.* **1989**, *49*, 175.
(b) Zassinovich, G.; Mestroni, G. *J. Mol. Catal.* **1987**, *42*, 81.
(c) Mestroni, G.; Zassinovich, G.; Camus, A.; Martinelli, F. *J. Organomet. Chem.* **1980**, *198*, 87.

61. Garrou, P. E. *Chem. Rev.* **1985**, *85*, 171.

62. (a) Ito, K.; Harada, T.; Tai, A.; Izumi, Y. *Chem. Lett.* **1979**, 1049.
(b) Bakos, J.; Toth, I.; Marko, L. *J. Org. Chem.* **1981**, *46*, 5427.

63. Levi, A.; Modena, G.; Scorrano, G. *J. Chem. Soc., Chem. Commun.* **1975**, 6.

64. Heil, B.; Toros, S.; Bakos, J.; Marko, L. *J. Organomet. Chem.* **1979**, *175*, 229.

65. (a) Brunner, H. in *Catalysis of Organic Reactions*; Blackburn, D. W. , Ed.; Marcel Dekker: New York, 1990; Chapter 1.
(b) Ojima, I.; Yamamoto, K.; Kumada, M. in *Aspects of Homogeneous Catalysis*; Ugo, R., Ed.; Reidel: Dordrecht, 1977; Vol. 3, p. 185.
(c) Karim, A.; Mortreux, A.; Petit, F.; Buono, G.; Peiffer, G.; Siv, C. *J. Organomet. Chem.* **1986**, *317*, 93.
(d) in Reference 39, Chapter 3.

66. Yoshida, T.; Okano, T.; Otsuka, S. *J. Chem. Soc., Chem. Commun.* **1979**, 870.

67. Dayagi, S.; Degani, Y. in *The Chemistry of Carbon-Nitrogen Double Bond*; Patai, S., Ed.; Interscience: New York, 1970; Chapter 2.

68. Kang, G.; Cullen, W. R.; Fryzuk, M. D.; James, B. R.; Kutney, J. P. *J. Chem. Soc., Chem. Commun.* **1988**, 1466.

69. Cullen, W. R.; Fryzuk, M. D.; James, B. R.; Kutney, J. P.; Kang, G.-J.; Herb, G.; Thorburn, I. S.; Spogliarch, R. *J. Mol. Catal.* **1990**; *in press.*

70.   Vastag, S.; Bakos, J.; Toros, S.; Takach, N. E.; King, R. B.; Heil, B.; Marko, L. *J. Mol. Catal.* **1984**, *22*, 283.

71.   (a) Bakos, J.; Heil, B.; Lecompte, L.; Sinou, D. 5th IUPAC Symposium on Organometallic Chemistry directed towards Organic Synthesis (OMCOS-V), Florence, Italy, October 1989; Abstract # PS1-36.[71b]
(b) Amrani, Y.; Lecompte, L.; Sinou, D.; Bakos, J.; Toth, I.; Heil, B. *Organometallics* **1989**, *8*, 542.

72.   Longley, C. J.; Goodwin, T. J.; Wilkinson, G. *Polyhedron* **1986**, *5*, 1625.

73.   Brieger, G.; Nestrick, T. J. *Chem. Rev.* **1974**, *74*, 567.

74.   Kolomnikov, I. S.; Kukolev, V. P.; Volpin, M. E. *Russ. Chem. Rev. (Engl. Transl.)* **1974**, *43*, 399.

75.   Imai, H.; Nishiguchi, T.; Fukuzumi, K. *J. Org. Chem.* **1976**, *41*, 665.

76.   Spogliarich, R.; Kaspar, J.; Graziani, M. *J. Catal.* **1985**, *94*, 292.

77.   Sasson, Y.; Blum, J. *J. Org. Chem.* **1975**, *40*, 1887.

78.   Kvintovics, P.; James, B. R.; Heil, B. *J. Chem. Soc., Chem. Commun.* **1986**, 1810.

79.   James, B. R.; Morris, R. H. *J. Chem. Soc., Chem. Commun.* **1978**, 929.

80.   Toros, S.; Heil, B.; Kollar, L.; Marko, L. *J. Organomet. Chem.* **1980**, *197*, 85.

81.   Zassinovich, G.; Bianco, C. D.; Mestroni, G. *J. Organomet. Chem.* **1981**, *222*, 323.

82.   Morris, R. H., Ph.D. Dissertation, The University of British Columbia, Vancouver, Canada, 1978.

83. James, B. R.; McMillan, R. S.; Morris, R. H.; Wang, D. K. W. *Adv. Chem. Ser.* **1978**, *167*, 122.

84. MacFarlane, K. S., M.Sc. Dissertation, The University of British Columbia, Vancouver, Canada, 1989.

85. Halpern, J. *Adv. Chem. Ser.* **1968**, *70*, 1.

86. (a) Harmon, R. E.; Gupta, S. K.; Brown, D. J. *Chem. Rev.* **1973**, *73*, 21.
    (b) Henrici-Olive, G.; Olive, S. *Angew. Chem. Int. Ed. Engl.* **1971**, *10*, 105.

87. Halpern, J. *Disc. Faraday Soc.* **1968**, *46*, 7.

88. Tkatchenko, I. in *Comprehensive Organometallic Chemistry*; Wilkinson, G., Ed.; Pergamon Press: Oxford, 1981; Vol. 8, Chapter 50-3.

89. Kubas, G. J.; Ryan, R. R.; Swanson, B. I.; Vergamini, P. J.; Wasserman, H. J. *J. Am. Chem. Soc.* **1984**, *106*, 451.

90. Kubas, G. J. *Acc. Chem. Res.* **1988**, *21*, 120; and references therein.

91. (a) Crabtree, R. H.; Hamilton, D. F. *Adv. Oraganomet. Chem.* **1988**, *28*, 299; and references therein.
    (b) Crabtree, R. H. *Acc. Chem. Res.* **1990**, *23*, 95; and references therein.

92. James, B. R.; Wang, D. K. W. *Can. J. Chem.* **1980**, *58*, 245.

93. Wang, D. K. W., Ph.D. Dissertation, The University of British Columbia, Vancouver, Canada, 1978.

94. Thorburn, I. S., Ph.D. Dissertation, The University of British Columbia, Vancouver, Canada, 1985.

95. Thorburn, I. S.; Rettig, S. J.; James, B. R. *Inorg. Chem.* **1986**, *25*, 234.

96. James, B. R.; Pacheco, A.; Rettig, S. J.; Thorburn, I. S.; Ball, R. G.; Ibers, J. A. *J. Mol. Catal.* **1987**, *41*, 147.

97. Jung, C. W.; Garrou, P. E.; Hoffman, P. R.; Caulton, K. G. *Inorg. Chem.* **1984**, *23*, 726.

98. (a) James, B. R.; Ochiai, E.; Rempel, G. I. *Inorg. Nucl. Chem. Lett.* **1971**, *7*, 781.
     (b) Evans, I. P.; Spencer, A.; Wilkinson, G. *J. Chem. Soc., Dalton Trans.* **1973**, 204.

99. Joshi, A. M.; James, B. R. *J. Chem. Soc., Chem. Commun.* **1989**, 1785.

100. Dekleva, T. W.; Joshi, A. M.; Thorburn, I. S.; James, B. R.; Evans, S. V.; Trotter, J. *Isr. J. Chem.* **1990**, *30(4)*; *in press.*

CHAPTER 2

Experimental Procedures

2.1 Materials

2.1.1 Solvents

Spectral or reagent grade solvents were obtained from MCB, BDH, Mallinckrodt, Fisher, Eastman or Aldrich Chemical Co. Benzene, toluene, hexanes, tetrahydrofuran (THF) and diethyl ether were refluxed with, and distilled from, sodium metal/benzophenone under a nitrogen atmosphere. N,N–dimethylacetamide (DMA) was stirred with CaH_2 for at least 24 h, vacuum distilled at 35–40 °C, and stored under argon in the dark. Dichloromethane, acetone, methanol, ethanol and 2-propanol were distilled after refluxing with the appropriate drying agents (P_2O_5 for CH_2Cl_2, anhydrous K_2CO_3 for acetone, and Mg/I_2 for the alcohols).[1] All solvents were deoxygenated by freeze-pump-thaw cycles prior to use.

The deuterated solvents ($CDCl_3$, CD_2Cl_2, C_6D_6, toluene-d_8, acetone-d_6, CD_3CN, DMSO-d_6, methanol-d_4, 2-propanol-d_8 and D_2O), used in NMR spectroscopy, were obtained from Merck Frosst Canada Ltd. and Aldrich Chemical Co. All deuterated solvents (with the exception of D_2O!) were dried if necessary over activated molecular sieves (Fisher: Type 4 Å, 4–8 mesh), and stored under argon.

2.1.2 Gases

Purified argon (H.P.), nitrogen (U.S.P.), carbon monoxide (C.P.) and hydrogen (U.S.P.) were obtained from Union Carbide Canada Ltd.; all except hydrogen were used without further purification. Hydrogen was passed through an Engelhard Deoxo catalytic hydrogen purifier to remove traces of oxygen.

2.1.3 Phosphines

Reagent grade triphenylphosphine (PPh$_3$), tri(p-tolyl)phosphine (P(p-tol)$_3$), methyltriphenylphosphonium iodide (MePh$_3$P$^+$I$^-$), and the chelating phosphines Ph$_2$P(CH$_2$)$_n$PPh$_2$ (n = 1, DPPM; 2, DPPE; 3, DPPP; 4, DPPB; 5, DPPN; 6, DPPH) were used as supplied (all from Strem Chemicals, Inc.). The chiral phosphines: (2S,3S)-bis(diphenylphosphino)butane (S,S–CHIRAPHOS), (2S,4S)-bis(diphenylphosphino)-pentane (S,S–BDPP), (2R,3R)-2,3,-O-isopropylidene-2,3-dihydroxy-1,4-bis(diphenyl-phosphino)butane (R,R–DIOP), and (R)- and (S)-2,2'-bis-(diphenylphosphino)-1,1'-binaphthyl (R– and S–BINAP, respectively), were also obtained from Strem Chemicals and used as received. The chiral aminophosphinephosphinite ligand, S-Ph$_2$PN(Et)CH(CH$_2$Ph)CH$_2$OPPh$_2$ (S-PHENOP), was prepared from S–phenylalanine using a literature method.[2] The phosphines, rac-(±)-1,2-bis(diphenylphosphino)-cyclopentane (DPPCP) and rac-(±)-1,2-bis(dicyclohexylphosphino)cyclopentane (DPCYCP), were synthesised by a reported method and used as such without resolution.[3] Diphenyl(2-pyridyl)phosphine (PPh$_2$Py) was prepared by L. Xie in this laboratory using a published procedure.[4] Purity of all the phosphines was ascertained by ^{31}P{^{1}H} and ^{1}H NMR spectroscopy.

40

2.1.4   Substrates

The alkene substrates: 1-hexene, styrene, α-methylstyrene, 2,5-norbornadiene, 1,3-cyclohexadiene and 1,4-cyclohexadiene (all Eastman or Aldrich) were purified prior to use by passing through a column of activated alumina (Fisher, A-950 neutral chromatographic grade, 80–200 mesh). Itaconic acid (Eastman), (Z)-α-acetamidocinnamic and (Z)-α-methylcinnamic acids (Aldrich) were recrystallised from hot ethanol to yield colourless crystals.

The ketone substrates acetophenone and propiophenone (Aldrich) were dried over anhydrous $CaSO_4$, purified by vacuum distillation, and stored under argon. The nitrile substrates acetonitrile and benzonitrile (BDH) were distilled from CaH_2, and then stored under argon. *N*–Benzylideneaniline and *N*–benzylidenebenzylamine were synthesised by P. Kvintovics and G. Kang of this department; both imines were used without further purification. The imine, $(C_6H_3(CH_3)_2N=C(CH_3)(CH_2OCH_3))$, formed by condensation of 1-methoxyacetone and 2,6-dimethylaniline, was used as supplied by Ciba-Geigy. Purity of all the substrates used in this study was confirmed by ^1H NMR spectroscopy.

Authentic samples of the hydrogenation products corresponding to the above mentioned substrates were purchased from appropriate sources (mostly Aldrich), and used as supplied for comparison.

2.1.5   Other Materials

Triethylamine, di-*n*-butylamine and tri-*n*-butylamine (all from MCB) were stirred over KOH and purified by distillation. Polyvinylpyridine (PVP) and the non-nucleophilic base, 1,8-diazabicyclo-[5.4.0]-undec-7-ene (DBU), were used as supplied by Aldrich. Proton Sponge®, 1,8-bis(dimethylamino)naphthalene, from Aldrich, was purified by passing an *n*-pentane solution of the base through an alumina column. Concentration of the

solution yielded Proton Sponge as a white solid. The reagents $LiAlH_4$, $NaBH_4$, and KO^tBu were used as received.

The ruthenium, supplied on loan by Johnson Matthey Ltd., was obtained as hydrated $RuCl_3$; depending upon the batch, the ruthenium content varied from 38 to 42%.

2.2   Instrumentation

Infrared spectra were recorded on a Nicolet 5DX FT-IR spectrophotometer as KBr pellets, or Nujol mulls between CsI plates, unless specified otherwise. UV-visible spectra were recorded on a Perkin Elmer 552A spectrophotometer with thermostatted cell compartments, using spectral cells (path length = 0.1 or 1.0 cm) attached to Schlenk flasks.[5]

The solution nuclear magnetic resonance (NMR) spectra were recorded on a Bruker AC200 (200.1 MHz for ^{1}H, 50.3 MHz for ^{13}C, 81.0 MHz for ^{31}P), a Varian XL300 (300.0 MHz for ^{1}H, 75.0 MHz for ^{13}C, 121.4 MHz for ^{31}P), or a Bruker WH400 (400.0 MHz for ^{1}H) FT-NMR spectrometers, using tetramethylsilane (TMS) and PPh_3 (*ca.* −6 ppm w.r.t. 85% H_3PO_4)[6] as external standards. All ^{31}P NMR shifts are reported relative to 85% H_3PO_4, with downfield shifts taken as positive.

Variable temperature NMR spectral studies and various *1D*- and *2D*-NMR experiments (e.g. selective decoupling studies, *NOEDIFF*, and *COSY* experiments) were conducted on the Varian XL300, the Bruker WH400 or the Bruker AMX500 spectrometer. ^{1}H NMR longitudinal relaxation time (T_1) measurements were performed on the Varian XL300 spectrometer, using a standard (180°–t–90°) pulse sequence. The ^{31}P NMR spectral simulations were performed on a Varian ADS4000 work station using Varian NMR spectral spin simulation software.

The [31]P{[1]H} solid state cross polarization, magic angle spinning (CP/MAS) FT-NMR spectra were recorded (with kind help from Dr. Andy Root of this department) on a

Bruker MSL400 or a Bruker CXP200 instrument (161.97 and 80.99 MHz for ^{31}P, respectively).

Optical rotation values were measured on a Perkin Elmer 141 polarimeter at the sodium–D line (589 nm) at ambient temperature, using a thermostatted glass optical cell (~1.0 mL capacity) with a pathlength of 1.000 dm (also see Section 2.4.2).

Gas chromatographic analyses (also see Sections 2.4.1 and 2.4.3) were performed on a temperature programmable Hewlett Packard 5890A instrument equipped with a thermal conductivity detector (TCD) and a flame ionisation detector (FID), using helium as the carrier gas (flow rate ~40 mL/min). Carbowax 20M on Chromosorb W 80/100 (3 m, packed), or HP1 (15 m, 0.2 mm I.D. capillary, crosslinked methyl silicone) columns were used for qualitative and quantitative analyses of alkene/alkane, ketone/alcohol, and nitrile/ imine/amine mixtures. A 25 m x 0.25 mm I.D. capillary chiral column, Chirasil–Val III (Alltech), was used for separating enantiomers of chiral alcohol and amine products (Section 2.4.3).

Gas uptakes for stoichiometric or kinetic studies and gas solubility measurements were performed on a conventional constant-pressure, constant-temperature gas-uptake apparatus. The general procedure employed for gas-uptake measurements is described elsewhere.[5, 7]

Elemental analyses were performed by Mr. Peter Borda of this department. Single crystal X-ray diffraction studies were carried out by Dr. Steven Rettig of the departmental crystallographic service.

2.3 Catalytic Hydrogenation of Unsaturated Organic Substrates

Catalytic hydrogenation of various alkene, ketone, nitrile and imine substrates (0.05 to 2.0 M) was typically carried out in 5–10 mL solvent, using 0.5–5.0 mM catalyst (precursor), in the temperature range 20–100 °C. The gas-uptake apparatus was used to

monitor the course of catalytic hydrogenation at ≤ 1 atm H_2 pressure. Specially designed, thick walled Schlenk tubes (~60 mL capacity) fitted with Kontes valves were used for hydrogenation reactions between 1–12 atm H_2 pressures, and also for transfer hydrogenation experiments. Reactions at up to 80 atm H_2 pressures were conducted in glass-lined, high-pressure steel vessels.

2.3.1 Work-up of Reaction Mixtures

At the end of each hydrogenation run, the reaction mixture was transferred with a syringe to a Kugelrohr type apparatus (Figure 2.1) under a stream of argon. A typical procedure used for isolation of substrate and product(s) is described below.
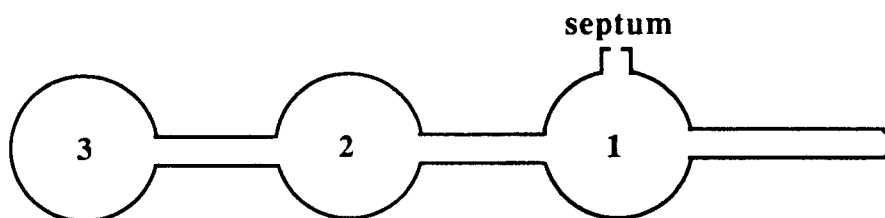
Figure 2.1: Kugelrohr type apparatus.

The reaction mixture was frozen in bulb 3 by immersing this bulb in a Dewar of liquid nitrogen. The Kugelrohr apparatus was then removed from liquid N_2. Whenever the solvent used was relatively low boiling compared to both substrate and product(s), for example, toluene solution containing acetophenone and 1-phenylethanol, the solvent was pumped off under vacuum until the third bulb had returned to room temperature. At this point, most of the solvent had been removed. The mixture of substrate and product(s), and also the solvent, in case of relatively high boiling solvents such as DMA, was then isolated by bulb-to-bulb vacuum distillation in the Kugelrohr apparatus, leaving behind the metal complex residue and any solid products (see below). This was achieved by gradually

heating under vacuum the second and third bulbs of the apparatus up to ~100 °C in a small oven, while the first bulb was cooled with liquid N_2 in order to collect the product-substrate (and solvent) mixture.

Solid products resulting from the hydrogenation experiments were isolated from the residue as follows:

Typically the residue was dissolved in dichloromethane, or an appropriate solvent (5–10 mL), and the solution was passed through a ~5 cm long column of neutral alumina in a Pasteur pipet to remove the metal complex and any insoluble material. The column was further eluted with ~5 mL of the solvent. The mixture of solid substrate/product(s) was then isolated from the eluate by evaporating the solvent. The product(s) could be further purified, if necessary, by recrystallisation or sublimation and analysed by ^{1}H NMR spectroscopy or GLC and, in case of chiral products, also by optical rotation measurements.

2.4   Analysis of the Hydrogenation Products

The separated product mixture was analysed by gas chromatography (Section 2.4.1), or examined by ^{1}H NMR spectroscopy, to determine the conversion (%) of the substrate to product(s). The optical purity of a chiral product (% e.e.) was determined either by: (a) measuring the optical rotation of the solution using a polarimeter (Section 2.4.2); or (b) injecting a derivative of the product onto a chiral column (Section 2.4.3). Finally, the catalyst residue in bulb 3 (Section 2.3) was dissolved in an appropriate deuterated solvent and transferred under a stream of argon for examination by NMR spectroscopy.

2.4.1 Gas Chromatographic Analysis

The extent of hydrogenation was determined by gas chromatographic analysis of the product mixture using an HP1 capillary column (for alkenes/alkanes, nitriles, imines/amines), or a Carbowax 20M packed column (ketones/alcohols). Benzonitrile hydrogenation products (benzonitrile/benzyl amine/dibenzylidene aniline/dibenzylamine mixtures) were analysed in the temperature programme mode (80 °C, 5 min–30 °C/min–230 °C, 10 min), with injector and detector (FID) temperatures of 325 °C. Analyses of the undiluted and the diluted (10 μL of product mixture in 1.0 mL of 2-propanol, diethyl ether or hexane) ketone/alcohol product mixtures, e.g. acetophenone/1-phenylethanol, were performed isothermally at 150 °C with injector and detector (TCD) temperatures of 250 °C. The conversion of substrate to product was taken as an average value obtained from 3-4 injections of each substrate-product solution.

Retention times (min) and the relative detector response factors (peak area per unit volume or unit weight) of all components under the conditions used were determined by injection of authentic samples. The response factors were then used to calculate the product concentration (g/mL). As an illustration, the retention times and normalised response factors under the conditions specified above for the substrate (acetophenone), the corresponding hydrogenated product (1-phenylethanol) and the 2-propanol solvent are shown in Table 2.1.

The concentration of the product alcohol was determined by dividing the areas obtained from the GC integrator by the appropriate response factor and using the density (g/mL) of the alcohol. Determination of the concentration was necessary for calculation of the specific rotation from the observed rotation (Equation 2.1, see below).

46

<u>Table 2.1</u>: Retention Times and Response Factors.

Compound	Retention time (min)	Response factor
2-propanol	0.7	1.0
acetophenone	5.8	4.0
1-phenylethanol	9.6	4.0

2.4.2 Optical Rotation Measurements

Optical rotations were measured on mixtures of the chiral products and substrates (e.g. 1-phenylethanol and acetophenone). The rotations were corrected for the presence of substrate using calibration curves (see Appendix A-1), knowing the amount of substrate present from GC analysis. The corrected observed rotation, α, was used to calculate the specific rotation $[\alpha]_D^T$ according to the equation:

$$[\alpha]_D^T = \frac{\alpha}{1 \times C} \qquad (2.1)$$

where $[\alpha]_D^T$ = specific rotation at temperature T, measured at the sodium–D line;

α = observed rotation;

l = pathlength of the cell in decimeters; and

C = concentration of solution in g/mL.

The optical purity of a reaction product in terms of the enantiomeric excess (% e.e.) can be determined knowing the specific rotation of a pure enantiomer (Eqs. 1.2 and 1.3, see Section 1.2.1).

2.4.3 Gas Chromatographic Separation of Enantiomers of Chiral Alcohol and Amine Products Using a Chiral Column

In order to separate effectively the enantiomers of chiral alcohols it is essential to first derivatise the alcohol.[8,9] Enantiomer separation of alcohols was achieved using their isopropyl urethane derivatives (Equation 2.2) which were conveniently prepared by dissolving the product alcohol mixture (1–20 µL, depending on the conversion of the substrate to the product) in dichloromethane (200 µL), followed by addition of isopropyl isocyanate (~100 µL, ≤100 fold excess). The mixture was heated in a screw-capped vial at 100 °C for 20 min. The solvent and excess isopropyl isocyanate were removed with a stream of nitrogen, and the urethane derivatives were dissolved in diethyl ether (~0.5 mL) for injection onto the chiral column, Chirasil-Val III.

$$
\begin{array}{c}
\overset{\text{OH}}{\underset{R}{\overset{|}{\underset{\diagdown}{\overset{*}{C}}}} \text{H}} \\
\end{array}
\;+\;
\begin{array}{c}
\text{H}_3\text{C} \\
\diagdown \\
\text{H}_3\text{C} \diagup
\end{array}
\text{CH-N=C=O}
\;\xrightarrow[100°C]{\text{CH}_2\text{Cl}_2}\;
\text{H}-\overset{\overset{\text{R}}{|}}{\underset{\underset{\text{R'}}{|}}{\overset{*}{C}}}\text{-O-}\overset{\overset{\text{O}}{||}}{C}\text{-NH-CH}\begin{array}{c}\diagup \text{CH}_3 \\ \diagdown \text{CH}_3\end{array}
\qquad (2.2)
$$
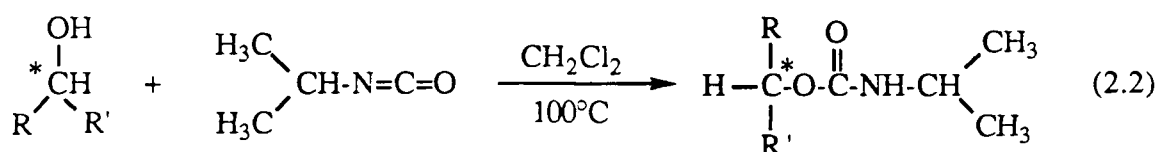
Gas chromatographic analysis was performed isothermally at 145 °C with injector and detector (FID) temperatures of 250 and 300 °C, respectively. The e.e. was taken as the average of 3-4 injections. Enantiomers of chiral amines can also be separated using this isocyanate method.[10] No racemisation was observed when this procedure was performed on pure enantiomers, consistent with previous reports.[11] Injection of derivatives of known enantiomeric composition showed a good correlation with the observed e.e., with an estimated error of ± 1%.[12]

2.5 Synthesis and Characterisation of Ruthenium Complexes

All synthetic reactions, unless specified otherwise, were carried out under an atmosphere of argon, employing Schlenk techniques,[13] as most of the ruthenium complexes prepared in the course of this work were susceptible to oxidation by air, at least in solution. The yields reported for synthetic reactions are generally the average of several preparations.

2.5.1 Ruthenium Precursors

The following ruthenium complexes, used as starting materials for the synthesis of ruthenium- chelating ditertiary phosphine complexes described in this study, were prepared by literature methods: cis-RuCl$_2$(DMSO)$_4$;[14, 15] [RuCl(η^6-p-cymene)(μ-Cl)]$_2$;[16] RuCl$_3$(PAr$_3$)$_2$(DMA)·DMA solvate (Ar = phenyl or p-tolyl);[17–19] RuCl$_2$(PPh$_3$)$_3$;[19–21] RuHCl(PPh$_3$)$_3$·C$_6$H$_6$ solvate;[22, 23] and $trans$-RuHCl(nbd)(PPh$_3$)$_2$.[23] All these complexes were analytically pure (see below); the spectroscopic data (NMR, IR, UV-VIS) agreed with those reported previously in the literature.[14–23]

2.5.1.1 Cis-RuCl$_2$(DMSO)$_4$:[14]

The complex was prepared by refluxing a DMSO solution (10 mL) of RuCl$_3$·3H$_2$O (2.0 g, 7.65 mmol) under N$_2$ atmosphere followed by precipitation with acetone (~40 mL), according to the procedure described by Wilkinson and coworkers.[14b] This method is sensitive to the reaction conditions (temperature, duration of heating, quality of DMSO used– it works better with 'bad' DMSO), and often gives inconsistent results, sometimes leading to other undesired products.[15, 24a] Yield of this bright yellow complex varied from 50–90%. The method reported by our group (using H$_2$ to reduce the Ru to the divalent state[14a]), or simply refluxing the RuCl$_3$·3H$_2$O/DMSO solution in air instead of under

49

nitrogen,[24b] gives more consistent, albeit lower, yields (50–60%). Anal. Calcd for $C_8H_{24}O_4S_4Cl_2Ru$: C, 19.83; H, 4.99; S, 26.47. Found: C, 19.8; H, 4.9; S, 26.5. IR (Nujol, cm^{-1}): $\nu_{(S=O)}$ at 1115, 1089 (s, $\underline{S}$-bonded DMSO; reported: 1125 and 1095 cm^{-1}); $\nu_{(S=O)}$ at 932 (s, $\underline{O}$-bonded DMSO; reported: 925 cm^{-1}).

2.5.1.2   [RuCl(η^6-p-cymene)(μ–Cl)]$_2$:[16]

The Ru(II)-η^6-p-cymene complex was prepared by refluxing an ethanolic solution (100 mL) of RuCl$_3$·3H$_2$O (2.0 g, 7.65 mmol) with 5-isopropyl-2-methylcyclohexa-1,3-diene (10 mL), according to the procedure reported by Bennett and Smith.[16] Yield of the dark red-brown solid: 1.45 g (62%). Anal. Calcd for $C_{20}H_{28}Cl_4Ru_2$: C, 39.23; H, 4.61. Found: C, 39.4; H, 4.6.

2.5.1.3   RuCl$_3$(PPh$_3$)$_2$(DMA)·DMA solvate:[17–19]

This Ru(III) complex was synthesised by stirring a DMA solution (30 mL) of RuCl$_3$.3H$_2$O (2.0 g, 7.65 mmol) with two equivalents of PPh$_3$ (4.0 g, 15.3 mmol) for 24 h at room temperature.[17, 18] The green product was filtered, washed with DMA (2 x 5 mL) and hexane (10 mL), and vacuum dried. Yield: 5.2 g (75%). Anal. Calcd for $C_{44}H_{48}N_2O_2Cl_3P_2Ru$: C, 58.32; H, 5.34; N, 3.09; Cl, 11.74. Found: C, 58.3; H, 5.3; N, 3.0; Cl, 12.0. IR (Nujol, cm^{-1}): $\nu_{(C=O)}$ at 1632 (m, uncoordinated DMA); $\nu_{(C=O)}$ at 1598 (m, coordinated DMA).

A small amount of a previously unknown, crystalline dark red complex (~0.5 g) was isolated from the DMA filtrate after ~4 weeks. A single crystal X-ray diffraction study by Dr. S. Rettig of this department established the identity of the new compound to be the related Ru(III) complex, mer-RuCl$_3$(PPh$_3$)(DMA)$_2$·DMA solvate, in which one of the PPh$_3$ ligands has been replaced by DMA. Attempts to make this complex on purpose by stirring only one equivalent PPh$_3$ (0.546 g, 2.1 mmol) with RuCl$_3$·3H$_2$O (0.5 g, 2.1 mmol) in DMA (5 mL) were not successful; a dark red-brown solution was obtained after

~24 h but no solid could be isolated on work-up. Anal. Calcd for $C_{30}H_{42}N_3O_3Cl_3PRu$: C, 49.29; H, 5.79; N, 5.75. Found: C, 49.1; H, 5.9; N, 5.8. IR (Nujol, cm^{-1}): $\nu_{(C=O)}$ at 1635 (m, uncoordinated DMA); $\nu_{(C=O)}$ at 1593, 1572 (m, coordinated DMA). The crystal structure data, including tables of bond lengths and bond angles, and the ORTEP stereoview of the molecular structure, are presented in the Appendix (A-2.1).

2.5.1.4 RuCl$_3$(P(p-tolyl)$_3$)$_2$(DMA)·DMA solvate:[17b, 18]

The title complex was prepared in exactly the same manner as its PPh$_3$ analogue, but using two equivalents of P(p–tolyl)$_3$ (4.7 g, 15.3 mmol).[17b, 18] Yield of the bright green solid: 4.47 g (59%). Anal. Calcd for $C_{50}H_{60}N_2O_2Cl_3P_2Ru$: C, 60.64; H, 6.11; N, 2.83; Cl, 10.74. Found: C, 60.4; H, 6.1; N, 2.6; Cl, 10.6. IR (Nujol, cm^{-1}): $\nu_{(C=O)}$ at 1646 (m, uncoordinated DMA); $\nu_{(C=O)}$ at 1598 (m, coordinated DMA).

2.5.1.5 RuCl$_2$(PPh$_3$)$_3$:[19–21]

The Ru(II) complex was prepared by refluxing a methanol solution (300 mL) of RuCl$_3$·3H$_2$O (2.0 g, 7.65 mmol) and PPh$_3$ (12.1 g, 46.1 mmol) under N$_2$.[19, 20] Yield of the dark brown product: 7.2 g (98%). Anal. Calcd for $C_{54}H_{45}Cl_2P_3Ru$: C, 67.64; H, 4.73; Cl, 7.39. Found: C, 67.6; H, 4.7; Cl, 7.4.

2.5.1.6 RuHCl(PPh$_3$)$_3$·C$_6$H$_6$ solvate:[22, 23]

This complex was synthesised by stirring a benzene suspension (200 mL) of RuCl$_2$(PPh$_3$)$_3$ (4.5 g, 4.7 mmol) with triethylamine (0.07 mL, 5 mmol) under 1 atm H$_2$ at room temperature.[22, 23] Yield of the dark violet solid: 4.1 g (87%). Anal. Calcd for $C_{60}H_{52}ClP_3Ru$: C, 71.89; H, 5.23; Cl, 3.54. Found: C, 71.9; H, 5.2; Cl, 3.4. IR (Nujol, cm^{-1}): $\nu_{(Ru-H)}$ at 2028 (w). ^{1}H NMR (CDCl$_3$, 20 °C): δ −17.75 ppm (q, $^2J_{P-H}$ = 26 Hz, Ru–H).

2.5.1.7   *Trans*–RuHCl(nbd)(PPh$_3$)$_2$, 34:[23]

The hydridochloro derivative was prepared by stirring a benzene suspension (50 mL) of RuHCl(PPh$_3$)$_3$·C$_6$H$_6$ solvate (1.9 g, 1.9 mmol) with 2,5-norbornadiene (2 mL) at room temperature.[23]   Yield of the pale brown solid: 1.0 g (70%). Anal. Calcd for C$_{43}$H$_{38}$ClP$_2$Ru: C, 68.57; H, 5.08; Cl, 4.71. Found: C, 68.4; H, 5.2; Cl, 4.6. IR (Nujol, cm^{-1}): $\nu_{(Ru–H)}$ at 2082 (w). ^{1}H NMR (CD$_2$Cl$_2$, 20 °C): δ –8.90 ppm (t, $^2J_{PH}$ = 24 Hz, Ru–H).

2.5.2   Mixed-Phosphine Complexes, RuCl$_2$(P–P)(PPh$_3$)

2.5.2.1   Dichloro(1,4-bis(diphenylphosphino)butane)(triphenylphosphine)- ruthenium(II), RuCl$_2$(DPPB)(PPh$_3$), <u>23</u>

The title complex was prepared according to the method reported by Caulton and coworkers.[25] DPPB (0.445 g, 1.04 mmol) was added to a CH$_2$Cl$_2$ (20 mL) solution of RuCl$_2$(PPh$_3$)$_3$ (1.0 g, 1.04 mmol) at room temperature; the dark brown solution turned green immediately. The solution was stirred under argon for 2 h, and concentrated to ~5 mL by pumping off the solvent under vacuum. Addition of dry ethanol (40 mL) caused precipitation of the green product, which was filtered, washed with ethanol (2 x 10 mL) and hexanes (2 x 10 mL), and dried *in vacuo*. The concentration step prior to the addition of ethanol (not reported in the original procedure[25]) improved the yield of the complex dramatically, to essentially quantitative as compared to the ~66% reported by Caulton *et al.* Yield: 0.86 g (96%); Anal. Calcd for RuCl$_2$(DPPB)(PPh$_3$), C$_{46}$H$_{43}$Cl$_2$P$_3$Ru: C, 64.19; H, 5.04. Found: C, 63.6; H, 5.0. The complex sometimes contained small amounts (<2–3%) of the known dinuclear Ru(II) complex with a bridging DPPB ligand, (DPPB)Cl$_2$Ru(μ-DPPB)RuCl$_2$(DPPB),[26] as evidenced by ^{31}P NMR spectroscopy and elemental analysis (see Section 2.5.11.1); this CH$_2$Cl$_2$–insoluble impurity can be removed

by filtration of the CH$_2$Cl$_2$ solution of RuCl$_2$(DPPB)(PPh$_3$) at the pre-concentration stage. Details of further characterisation of the mixed-phosphine complex are described in Chapter 4, Section 4.2.

2.5.2.2 Dichloro((*R*)-2,2'-bis-(diphenylphosphino)-1,1'-binaphthyl)-(triphenylphosphine)ruthenium(II), RuCl$_2$(*R*-BINAP)(PPh$_3$), 21

The *R*-BINAP analogue was prepared by stirring RuCl$_2$(PPh$_3$)$_3$ (0.12 g, 0.125 mmol) with one equivalent of the diphosphine in dichloromethane solution (15 mL) for 10 h under argon. There was no perceptible change in the initial brown colour of the solution. Addition of diethyl ether (15 mL) following concentration of the solution to ~2 mL resulted in precipitation of an orange-brown solid. The mixture was stirred for 4 h, and the product was separated by filtration, washed with diethyl ether and hexane (5 mL each), and dried under vacuum. Yield: 0.13 g (81%); Anal. Calcd for RuCl$_2$(BINAP)(PPh$_3$), C$_{62}$H$_{47}$Cl$_2$P$_3$Ru: C, 70.46; H, 4.48; Cl, 6.71. Found: C, 70.2; H, 4.6; Cl, 6.5. Spectroscopic characterisation of this complex is presented in Section 4.6.

2.5.3 *Trans*-Chlorohydrido(η^2,η^2-norbornadiene)[(1,4-bis(diphenylphos-phino)butane)]ruthenium(II), RuHCl(nbd)(DPPB),[27] 36

(a) One equivalent of DPPB (0.227 g, 0.53 mmol) was added to a benzene solution (25 mL) of RuHCl(nbd)(PPh$_3$)$_2$, (0.40 g, 0.53 mmol), and the solution stirred at 20 °C for 20 h under argon. The resulting yellow solution was concentrated to ~10 mL, hexane (30 mL) added, and the mixture stirred for 2 h. The yellow-brown solid that precipitated was filtered, washed with hexane (2 x 10 mL), and dried under vacuum (yield: 0.10 g); this solid contained substantial amount of unreacted starting complex, RuHCl(nbd)(PPh$_3$)$_2$, along with the desired product (^{31}P NMR evidence, see below).

Concentration of the filtrate to *ca.* 10 mL followed by stirring for 10 h precipitated the pure RuHCl(nbd)(DPPB) complex as an off-white solid. Yield: 0.14 g (40%).

(b) A benzene (30 mL) solution of $RuCl_2(DPPB)(PPh_3)$ (0.40 g, 0.47 mmol) was stirred with 2,5-norbornadiene (3.5 mL, 34 mmol) at 60 °C for 18 h under argon; the initially green solution turned into a greenish yellow suspension. Proton Sponge (0.234 g, 1.1 mmol) was added and the mixture stirred under 1 atm H_2 for 24 h. The resulting yellow suspension was then allowed to cool to 20 °C and filtered to remove the white Proton Sponge hydrochloride (PSH^+Cl^-; confirmed by ^1H NMR, quantitative yield). The yellow filtrate was concentrated to 10 mL; addition of hexane (50 mL) precipitated the off-white product which was filtered, washed with hexane (2 x 10 mL) to remove any traces of PPh_3 and Proton Sponge, and dried *in vacuo*. Yield: 0.19 g (62%). Anal. Calcd for RuHCl(nbd)(DPPB), $C_{35}H_{37}ClP_2Ru$: C, 64.05; H, 5.68; Cl, 5.41. Found: C, 64.2; H, 5.8; Cl, 5.6. IR (Nujol, cm^{-1}): $v_{(Ru-H)}$ 2045 (w). ^1H NMR (C_6D_6, 20 °C), ppm: δ 8.25, 7.33 (4 H each, m, *ortho*-phenyl, DPPB), δ 7.3–6.9 (12 H, br m, *meta-*, *para-* phenyl, DPPB), δ 3.89, 2.84 (2 H each, br m, olefinic, nbd), δ 3.75, 2.07, 1.22 and 0.98 (2 H each, br m, methylene, DPPB), δ 3.67, 3.36 (1 H each, br m, methine, nbd), δ 0.90 (2 H, s, bridgehead methylene, nbd); δ –9.69 (–10.38 in $CDCl_3$; 1 H, t, Ru-H, $^2J_{PH}$ = 20.7 Hz); $^{31}P\{^1H\}$ NMR: 43.2 ppm, s.

2.5.4 Dichloro-tri-μ-chloro-bis(bidentate phosphine)diruthenium(II,III) Complexes, [(P–P)ClRu(μ-Cl)₃RuCl(P–P)] or Ru₂Cl₅(P–P)₂

P–P = DPPP, DPPB, *R,R*-DIOP, *S,S*-CHIRAPHOS, DPPN, DPPH, *rac*-DPPCP, *rac*-DPCYCP, *S,S*-BDPP, *R*-BINAP, and *S*-BINAP, *S*-PHENOP:

The procedure described by Thorburn *et al.* for the preparation of Ru₂Cl₅(P–P)₂ complexes, containing P–P = DPPP, DPPB, DIOP, CHIRAPHOS and NORPHOS,[28, 29]

was employed for the preparation of similar complexes containing other bidentate phosphines.

A suspension of $RuCl_3(PAr_3)_2(DMA) \cdot DMA$ solvate (1.0 g) in hexanes (150 mL) was refluxed under a N_2 atmosphere with an equimolar amount of the appropriate bidentate phosphine (Ar = phenyl, for P–P = DPPB, DPPN, DPPH, or DIOP, 1.1 mmol; Ar = p-tolyl, for all other chelating phosphines, 1.0 mmol). The brown products were filtered, rinsed well with hexanes (4 x 20 mL) and vacuum dried. The crude product was washed down the filter as a solution with CH_2Cl_2 (~30–60 mL) leaving behind some insoluble impurities. Analytically pure products were obtained from the filtrate after concentration to ~10 mL followed by addition of diethyl ether (~40 mL).

The complexes were characterised by elemental analysis, IR and UV-visible spectroscopy, and magnetic susceptibility measurements where possible (see Chapter 3, Section 3.3.1). The Ru–Cl stretch in the IR spectra of $Ru_2Cl_5(P-P)_2$ complexes was found in 320–340 cm^{-1} (w) range.

2.5.4.1   P–P = DPPP: $Ru_2Cl_5(DPPP)_2$, **1**[29]

Yield: 0.45 g (74%). Anal. Calcd for $Ru_2Cl_5(DPPP)_2$, $C_{54}H_{52}Cl_5P_4Ru_2$: C, 53.86; H, 4.35; Cl, 14.72. Found: C, 53.7; H, 4.5; Cl, 14.6.

2.5.4.2   P–P = DPPB: $Ru_2Cl_5(DPPB)_2$, **2**[29]

Yield: 0.54 g (80%). Anal. Calcd for $Ru_2Cl_5(DPPB)_2$, $C_{56}H_{56}Cl_5P_4Ru_2$: C, 54.58; H, 4.58; Cl, 14.38. Found: C, 55.0; H, 4.5; Cl, 13.7.

2.5.4.3   P–P = R,R-DIOP: $Ru_2Cl_5(DIOP)_2$, **3**[29]

Yield: 0.51 g (70%). Anal. Calcd for $Ru_2Cl_5(DIOP)_2$, $C_{62}H_{64}O_4Cl_5P_4Ru_2$: C, 54.10; H, 4.69; Cl, 12.88. Found: C, 54.1; H, 4.8; Cl, 12.8.

2.5.4.4 P–P = *S,S*-CHIRAPHOS: $Ru_2Cl_5(CHIRAPHOS)_2$, 4[29]

Yield: 0.55 g (81%). Anal. Calcd for $Ru_2Cl_5(CHIRAPHOS)_2$, $C_{56}H_{56}Cl_5P_4Ru_2$: C, 54.58; H, 4.58; Cl, 14.38. Found: C, 54.5; H, 4.8; Cl, 14.3.

2.5.4.5 P–P = DPPN: $Ru_2Cl_5(DPPN)_2$, 5

Yield: 0.40 g (58%). Anal. Calcd for $Ru_2Cl_5(DPPN)_2$, $C_{58}H_{60}Cl_5P_4Ru_2$: C, 55.27; H, 4.80. Found: C, 55.7; H, 4.5.

2.5.4.6 P–P = DPPH: $Ru_2Cl_5(DPPH)_2$, 6

Yield: 0.42 g (59%). Anal. Calcd for $Ru_2Cl_5(DPPH)_2$, $C_{60}H_{64}Cl_5P_4Ru_2$: C, 55.93; H, 5.01. Found: C, 55.5; H, 5.0.

2.5.4.7 P–P = *rac*-DPPCP: $Ru_2Cl_5(DPPCP)_2$, 7

Yield: 0.44 g (69%). Anal. Calcd for $Ru_2Cl_5(DPPCP)_2$, $C_{58}H_{56}Cl_5P_4Ru_2$: C, 55.45; H, 4.49. Found: C, 55.1; H, 4.5.

2.5.4.8 P–P = *rac*-DPCYCP: $Ru_2Cl_5(DPCYCP)_2$, 8

Yield: 0.175 g (27%). Anal. Calcd for $Ru_2Cl_5(DPCYCP)_2$, $C_{58}H_{104}Cl_5P_4Ru_2$: C, 53.39; H, 8.03; Cl, 13.59. Found: C, 53.5; H, 8.0; Cl, 16.2[§] (14.0).

[§] The higher than expected chloride content found for complex 8 (elemental analysis) is likely due to interference by PO_4^{3-} (produced as a result of combustion of the sample prior to halide-determination), which coprecipitates with AgCl during the Cl-analysis ($AgNO_3$ method). The interference was removed by a) maintaining a high acidic *p*H (<2) during halide-determination, or b) by pretreating the solution with $La(NO_3)_3$ to remove the PO_4^{3-}. The new values (given in brackets) of the Cl-content obtained by one of these modified methods are in reasonable agreement with those expected. A higher than expected Cl-content was also found for the analogous mixed-valence dinuclear complexes 10 and 11, (see the next page).

2.5.4.9   P–P = *S,S*-BDPP: Ru$_2$Cl$_5$(BDPP)$_2$, 9

Yield: 0.50 g (78%). Anal. Calcd for Ru$_2$Cl$_5$(BDPP)$_2$, C$_{58}$H$_{60}$Cl$_5$P$_4$Ru$_2$: C, 55.27; H, 4.80. Found: C, 52.0; H, 4.7.

2.5.4.10   P–P = *R*-BINAP: Ru$_2$Cl$_5$(*R*-BINAP)$_2$, 10   (half scale)

Yield: 0.26 g (64%). Anal. Calcd for Ru$_2$Cl$_5$(*R*-BINAP)$_2$, C$_{88}$H$_{64}$Cl$_5$P$_4$Ru$_2$: C, 65.05; H, 3.97; Cl, 10.91; Calcd for C$_{88}$H$_{64}$Cl$_5$P$_4$Ru$_2$·H$_2$O: C, 64.34; H, 4.05; Cl, 10.79. Found: C, 64.3; H, 4.2; Cl, 17.0[§]. The presence of water was confirmed from the IR spectrum.

2.5.4.11   P–P = *S*-BINAP: Ru$_2$Cl$_5$(*S*-BINAP)$_2$, 11

Yield: 0.70 g (85%). Anal. Calcd for Ru$_2$Cl$_5$(*S*-BINAP)$_2$, C$_{88}$H$_{64}$Cl$_5$P$_4$Ru$_2$: C, 65.05; H, 3.97; Cl, 10.91; Calcd for C$_{88}$H$_{64}$Cl$_5$P$_4$Ru$_2$·H$_2$O: C, 64.34; H, 4.05; Cl, 10.79. Found: C, 64.6; H, 4.3; Cl, 16.9[§] (10.6).

2.5.4.12   P–P = *S*-PHENOP: Ru$_2$Cl$_5$(PHENOP)$_2$, 12

The *S*-PHENOP is insoluble in hexane, therefore, some benzene (~30 mL) was added to the hexane suspension in order to solubilise the ligand and facilitate the reaction. Yield: 0.41 g (56%). Anal. Calcd for Ru$_2$Cl$_5$(PHENOP)$_2$, C$_{70}$H$_{70}$N$_2$O$_2$Cl$_5$P$_4$Ru$_2$: C, 57.02; H, 4.78; N, 1.90. Found: C, 57.5; H, 5.0; N, 1.6.

2.5.5   Dichloro-di-μ-chloro-bis(bidentate phosphine)diruthenium(II) Complexes, [RuCl(P–P)(μ-Cl)]$_2$

The dinuclear complexes, [RuCl(P–P)(μ-Cl)]$_2$, were prepared by the H$_2$-reduction of the respective Ru(II,III)-bidentate phosphine complexes, Ru$_2$Cl$_5$(P–P)$_2$ (Section 2.5.4), in the presence of an appropriate base (DMA or polyvinylpyridine), following the general

strategy developed by Thorburn from this laboratory.[29, 30] The complexes were stored under argon, because they are air-sensitive to varying degrees, the initially orange-brown colour turning greenish black on exposure to air (within a few minutes in solution and in a few hours to days in the solid state). The spectroscopic characterisation (NMR, UV-visible) of the new complexes is presented in Chapter 3, Section 3.3.2.

(a) P–P = DPPP, DPPB, DPPN:

Typically, $Ru_2Cl_5(P–P)_2$ (1.0 g) was stirred in 20 mL DMA under 1 atm H_2 for 24 h. The resulting dark brown solution was concentrated to 5 mL, dry methanol (40 mL) added, and the mixture stirred overnight under H_2. The orange yellow product was filtered, washed with methanol (2 x 5 mL) and diethyl ether (10 mL) and vacuum dried.

2.5.5.1   P–P = DPPP: $Ru_2Cl_4(DPPP)_2$, 13 [29]

Yield: 0.45 g (74%). Anal. Calcd for $Ru_2Cl_4(DPPP)_2 \cdot H_2O$, $C_{54}H_{52}Cl_4P_4Ru_2 \cdot H_2O$: C, 54.65; H, 4.59; Cl, 11.95. Found: C, 54.7; H, 4.8; Cl, 11.9.

2.5.5.2   P–P = DPPB: $Ru_2Cl_4(DPPB)_2$, 14 [29]

The complex is hygroscopic even in the solid state (IR and ^{1}H NMR evidence). Yield: 0.88 g (89%). Anal. Calcd for $Ru_2Cl_4(DPPB)_2.H_2O$, $C_{56}H_{56}Cl_4P_4Ru_2.H_2O$: C, 55.36; H, 4.81. Found: C, 55.4; H, 5.0.

The DPPB complex was also obtained as its more stable acetone adduct, $Ru_2Cl_4(DPPB)_2(acetone) \cdot acetone$ solvate,[29, 30] by dissolution of the product in acetone/dichloromethane (1:1, 10 mL) and reprecipitation by addition of 40 mL of diethyl ether (~70% yield). Anal. Calcd for $Ru_2Cl_4(DPPB)_2(acetone)$ ·acetone solvate, $C_{62}H_{68}O_2Cl_4P_4Ru_2$: C, 56.71; H, 5.22; O, 2.44; Cl, 10.82. Found: C, 56.5; H, 5.1; O, 2.6; Cl, 10.6. IR (Nujol, cm^{-1}): $v_{(C=O)}$ at 1705 (m, uncoordinated acetone); $v_{(C=O)}$ at 1645 (m, coordinated acetone).

2.5.5.3 P–P = DPPN: Ru$_2$Cl$_4$(DPPN)$_2$, 17 (half scale)

Yield: 0.38 g (79%). Anal. Calcd for Ru$_2$Cl$_4$(DPPN)$_2$, C$_{58}$H$_{60}$Cl$_4$P$_4$Ru$_2$: C, 56.87; H, 4.94. Found: C, 57.5; H, 5.2.

(b) P–P = *R,R*–DIOP, *S,S*–CHIRAPHOS, *R*-BINAP, *S*-BINAP, and *S,S*–BDPP:

The Ru$_2$Cl$_5$(P–P)$_2$ (1.0 g) was added to a rigorously deoxygenated benzene or toluene suspension (30 mL) of polyvinylpyridine (PVP, 2.5 g) and the mixture stirred under 1 atm H$_2$ for 24 h. The orange-brown solution obtained after separation of the insoluble polymer by filtration was concentrated to ~5 mL. Addition of dry hexanes (40 mL) followed by stirring for a few hours yielded the respective Ru$_2$Cl$_4$(P–P)$_2$ products as brown solids which were filtered, washed with hexanes (20 mL) and vacuum dried.

2.5.5.4 P–P = *R,R*-DIOP: Ru$_2$Cl$_4$(DIOP)$_2$, 15 [29]

Yield: 0.81 g (83%). Anal. Calcd for Ru$_2$Cl$_4$(DIOP)$_2$, C$_{62}$H$_{64}$O$_4$Cl$_4$P$_4$Ru$_2$: C, 55.53; H, 4.81; Cl, 10.57. Found: C, 55.7; H, 5.0; Cl, 10.8.

2.5.5.5 P–P = *S,S*-CHIRAPHOS: Ru$_2$Cl$_4$(CHIRAPHOS)$_2$, 16 [29]

Yield: 0.80 g (82%). Anal. Calcd for Ru$_2$Cl$_4$(CHIRAPHOS)$_2$, C$_{56}$H$_{56}$Cl$_4$P$_4$Ru$_2$: C, 56.20; H, 4.72; Cl, 11.85. Found: C, 56.2; H, 4.9; Cl, 11.6.

2.5.5.6 P–P = *R*-BINAP: Ru$_2$Cl$_4$(*R*-BINAP)$_2$, 18 (1/5th scale)

Yield: 0.16 g (81%). Anal. Calcd for Ru$_2$Cl$_4$(*R*-BINAP)$_2$, C$_{88}$H$_{64}$Cl$_4$P$_4$Ru$_2$: C, 66.50; H, 4.06. Found: C, 65.9; H, 4.5.

2.5.5.7 P–P = *S*-BINAP: Ru$_2$Cl$_4$(*S*-BINAP)$_2$, 19 (1/5th scale)

Yield: 0.17 g (87%). Anal. Calcd for Ru$_2$Cl$_4$(*R*-BINAP)$_2$, C$_{88}$H$_{64}$Cl$_4$P$_4$Ru$_2$: C, 66.50; H, 4.06; Cl, 8.92. Found: C, 66.2; H, 4.2; Cl, 8.8.

2.5.5.8   P–P = *S,S*-BDPP: Ru₂Cl₄(BDPP)₂, 20

No reaction could be observed, even after heating the mixture at 60 °C for 4 days under 1 atm of H_2, as the toluene solution remained essentially colourless and the mixed-valence precursor **9** remained undissolved in the toluene solvent. After two months, the toluene solution had become yellow-orange, although much of the starting complex was still present in suspension. The mixture was filtered to separate the solids and the filtrate evaporated to dryness. The resultant orange residue was dissolved in ~2 mL of CH_2Cl_2 addition of Et_2O (10 mL) precipitated an orange solid which was filtered, washed with a small amount of Et_2O (2 mL), and dried under vacuum. Yield: 0.08 g (8%). Anal. Calcd for Ru₂Cl₄(*S,S*-BDPP)₂, $C_{58}H_{60}Cl_4P_4Ru_2$: C, 56.87; H, 4.94. Found: C, 56.0; H, 5.2.

2.5.6   Chloro-tri-μ-chloro-(ligand)bis(1,4-bis(diphenylphosphino)butane)-diruthenium(II) Complexes, [(L)(DPPB)Ru(μ-Cl)₃RuCl(DPPB)]

Properties and characterisation of these complexes are discussed in Chapter 3, Sections 3.6 and 3.7.

2.5.6.1   L = NEt₃: [(NEt₃)(DPPB)Ru(μ-Cl)₃RuCl(DPPB)], 14b [30]

The triethylamine adduct was prepared by stirring [RuCl(DPPB)(μ-Cl)]₂ (0.20 g, 0.17 mmol Ru₂) with excess NEt₃ (0.5 mL, 3.6 mmol) in benzene or toluene (10 mL) for 6 h. Some orange solid precipitated; further precipitation was induced by adding hexanes (20 mL). The product was washed with ethanol and hexanes and dried under vacuum. Yield: 0.18 g (84%). Alternatively, this complex can be prepared starting with RuCl₂(DPPB)(PPh₃) and NEt₃, in the same manner (~90% yield). Anal. Calcd for [(NEt₃)(DPPB)Ru(μ-Cl)₃RuCl(DPPB)], $C_{62}H_{71}NCl_4P_4Ru_2$: C, 57.37; H, 5.51; N, 1.08; Cl, 10.92. Found: C, 57.3; H, 5.6; N, 1.0; Cl, 10.7. ¹H NMR (CDCl₃, 20 °C),

ppm: δ 3.20 (broad m, 6H, -NCH$_2$CH$_3$ of bound NEt$_3$), 1.08 (9H, broad m, -NCH$_2$CH$_3$ of bound NEt$_3$). ^{31}P{^{1}H} NMR: 48.3 ppm, s.

This complex is also a byproduct in the synthesis of the hydridochloro-Ru(II) complex, [RuHCl(DPPB)]$_3$ (see Section 2.5.10).[30]

2.5.6.2   L = NHBu^n$_2$: [(NHBu^n$_2$)(DPPB)Ru(μ-Cl)$_3$RuCl(DPPB)], 14c

The complex, [(NHBu^n$_2$)(DPPB)Ru(μ-Cl)$_3$RuCl(DPPB)], was prepared (a) from [RuCl(DPPB)(μ-Cl)]$_2$ in exactly the same manner as its NEt$_3$ analogue, but using NHBu^n$_2$; or (b) by refluxing a benzene/hexane (1:4, 20 mL) suspension of RuCl$_2$(DPPB)(PPh$_3$), (0.20 g, 0.23 mmol) with either NHBu^n$_2$ or NBu^n$_3$ (2 mL) for 3 h under N$_2$. In each case, the orange-brown product was filtered after concentration of the solution to ~5 mL followed by addition of hexanes (40 mL), washed with ethanol and hexanes and dried under vacuum.   Yield: 0.11 g (71%).   Anal. Calcd for [(NHBu^n$_2$)(DPPB)Ru(μ-Cl)$_3$RuCl(DPPB)], C$_{64}$H$_{75}$NCl$_4$P$_4$Ru$_2$: C, 57.97; H, 5.70; N, 1.06. Found: C, 57.7; H, 5.5; N, 1.0. IR (Nujol, cm^{-1}): 1572 (m, N–H bending). ^{1}H NMR (CDCl$_3$, 20 °C), ppm: δ 2.87 (4H, br m, -NCH$_2$ of bound NHBu$_2$), 1.62 (4H, m, -NCH$_2$CH$_2$), 1.34 (4H, m, -CH$_2$CH$_3$ of NHBu$_2$), and 0.97 (6H, t, -CH$_2$CH$_3$). ^{31}P{^{1}H} NMR: 48.2 ppm, s.

2.5.6.3   L = CO: [(CO)(DPPB)Ru(μ-Cl)$_3$RuCl(DPPB)], 14d [31]

The title complex was synthesised from [RuCl(DPPB)(μ-Cl)]$_2$ by decarbonylation of aldehydes such as formaldehyde, acetaldehyde, or benzaldehyde. Gaseous formaldehyde, generated by heating paraformaldehyde at 180 °C under a slow stream of argon, was bubbled through a CH$_2$Cl$_2$ solution (30 mL) of [RuCl(DPPB)(μ-Cl)]$_2$ (0.50 g, 0.42 mmol). After 10 min, the solution was concentrated to a red oil to which 30 mL of benzene were added; the solution was stirred for 16 h under argon and filtered through Celite® to remove some "polymeric" material. Concentration of the filtrate to *ca.* 10 mL

precipitated the orange product which was filtered, washed with hexanes and dried under vacuum. Yield: 0.29 g (57%). The carbonyl adduct can also be prepared by stirring a benzene solution of [RuCl(DPPB)(μ-Cl)]$_2$, **14** (0.25 g, 0.21 mmol), with excess acetaldehyde or benzaldehyde (0.5 mL) at 50 °C for 24 h; concentration of the solution to ~5 mL, followed by addition of hexanes (30 mL), gives the product in high yield.

Alternatively, this complex is obtained by heating to 50 °C a benzene solution (20 mL) of RuCl$_2$(DPPB)(PPh$_3$), (0.20 g, 0.23 mmol), with an equimolar amount of Mo(CO)$_6$ for 24 h under argon. Concentration of the resultant greenish yellow solution to ~5 mL followed by addition of hexane (30 mL) precipitates the orange-brown product (90% yield). Anal. Calcd for [(CO)(DPPB)Ru(μ-Cl)$_3$RuCl(DPPB)], C$_{57}$H$_{56}$OCl$_4$P$_4$Ru$_2$: C, 55.89; H, 4.61; Cl, 11.58. Found: C, 56.2; H, 4.8; Cl, 11.4. IR (Nujol, cm^{-1}): $\nu_{(CO)}$ at 1977 (s). ^{31}P{^{1}H}NMR (C$_6$D$_6$, 20 °C): $\delta_A = 53.8$, $\delta_B = 53.3$ ppm, $^2J_{AB} = 45.2$ Hz; $\delta_C = 46.9$, $\delta_D = 33.1$ ppm, $^2J_{CD} = 29.6$ Hz (see Chapter 3, Table 3.6).

Direct carbonylation with CO of either precursor (**14** or **23**) resulted in the formation of a different set of products. Details of the carbonylation reaction are discussed in Chapter 3, Section 3.6.2.

2.5.6.4   L = Me$_2$SO (DMSO): [(DMSO)(DPPB)Ru(μ-Cl)$_3$RuCl(DPPB)], 14e [31]

Some DPPB (0.15 g, 0.35 mmol) was added to a solution of *cis*–RuCl$_2$(DMSO)$_4$ (0.17 g, 0.35 mmol) in dichloromethane:acetone (1:1, 20 mL) and the mixture stirred for 8 h under argon. The original yellow solution instantly turned orange and further changed slowly to a greenish brown suspension. The bright green solid was filtered (Ru$_2$Cl$_4$(DPPB)$_3$,[26] ~7 mg) and washed with dichloromethane (5 mL). The orange-yellow filtrate was reduced to ~5 mL, diethyl ether (25 mL) added and the mixture stirred for 8 h. The resulting orange suspension was filtered to remove small amounts of RuCl$_2$(DPPB)$_2$ (~8 mg). The bright orange filtrate was refridgerated for a week to afford dark orange-red crystals of [(DMSO)(DPPB)Ru(μ-Cl)$_3$RuCl(DPPB)]. Yield: 0.17 g (76%). Anal. Calcd

for [(DMSO)(DPPB)Ru(μ-Cl)$_3$RuCl(DPPB)], $C_{58}H_{62}SOCl_4P_4Ru_2$: C, 54.63; H, 4.90; Cl, 11.12. Found: C, 54.7; H, 5.1; Cl, 11.0. The complex was characterised crystallographically (Sections 3.6.3, 3.6.4, and Appendix A-2.2). IR (Nujol, cm^{-1}): $\nu_{(S=O)}$ at 1090 (s, $\underline{S}$-bonded DMSO). $^{31}P\{^1H\}$NMR (C_6D_6, 20 °C): δ_A = 53.6, δ_B = 50.6 ppm, $^2J_{AB}$ = 43.8 Hz; δ_C = 41.6, δ_D = 28.9 ppm, $^2J_{CD}$ = 32.1 Hz (see Chapter 3, Table 3.6).

2.5.7 Reactions of *Cis*–RuCl$_2$(DMSO)$_4$ with Other Bidentate Phosphines

P–P = DPPM, DPPE, and *S,S*-BDPP:

Reactions of *cis*–RuCl$_2$(DMSO)$_4$ (0.17 g, 0.35 mmol) with one equivalent of the appropriate chelating phosphine were carried out in dichloromethane:acetone solution (1:1, 20 mL) employing the procedure described for the reaction with DPPB (previous section). Characterisation of the products by NMR spectroscopy is discussed in Section 3.8 of Chapter 3.

2.5.8 Chloro(*p*–cymene)(bidentate phosphine)ruthenium(II) chloride, [RuCl(*p*-cymene)(P–P)]Cl

Recently, Takaya and coworkers have reported on the synthesis of a series of complexes of general formula [RuX(arene)(*S*-BINAP)]$^+$X$^-$ (X = Cl, Br or I; arene = benzene, toluene, or *p*-cymene).[32] The procedure used for preparation of the complexes described below is similar to that reported.[32] The reactions are discussed in more detail in Chapter 3, Section 3.9.

A solution of [RuCl(*p*–cymene)(μ-Cl)]$_2$ (0.10 g, 0.33 mmol) in methanol/CH$_2$Cl$_2$ (3:1, 20 mL) was stirred with an equimolar amount of the appropriate bidentate phosphine, for 24 h under argon. The resultant orange-yellow solution was reduced to ~3 mL, diethyl ether (20 mL) added to precipitate the orange-yellow product, and the mixture stirred for

2 h. The solid was isolated by filtration, washed with diethyl ether (5 mL) and dried under vacuum.

2.5.8.1   P–P = *R*–BINAP: [RuCl(*p*-cymene)(*R*–BINAP)]Cl

Yield: 0.27 g (90%). Anal. Calcd for [RuCl(*p*-cymene)(BINAP)]Cl·0.5H$_2$O, C$_{54}$H$_{46}$Cl$_2$P$_2$Ru·0.5H$_2$O: C, 69.15; H, 5.05; Cl, 7.56. Found: C, 69.1; H, 5.1; Cl, 7.5. The presence of water was confirmed by IR and ^{1}H NMR spectroscopy. ^{31}P{^{1}H} NMR (CDCl$_3$, 20 °C): δ$_A$ = 40.0, δ$_B$ = 23.5 ppm, $^2J_{AB}$ = 62.5 Hz.

2.5.8.2   P–P = *S*–BINAP: [RuCl(*p*-cymene)(*S*–BINAP)]Cl [32]

Yield: 0.25 g (83%). Anal. Calcd for [RuCl(*p*-cymene)(BINAP)]Cl·0.5H$_2$O, C$_{54}$H$_{46}$Cl$_2$P$_2$Ru·0.5H$_2$O: C, 69.15; H, 5.05. Found: C, 69.2; H, 5.4. ^{31}P{^{1}H} NMR (CDCl$_3$, 20 °C): δ$_A$ = 41.2, δ$_B$ = 24.5 ppm, $^2J_{AB}$ = 62.6 Hz.

2.5.8.3   P–P = *S,S*–BDPP: [RuCl(*p*-cymene)(*S,S*–BDPP)]Cl

Reaction of [RuCl(*p*–cymene)(μ-Cl)]$_2$ with *S,S*-BDPP gave a mixture of products, including the desired arene derivative (NMR spectroscopic evidence, see below); details of this reaction are given in Chapter 3, Section 3.9. One of the products, isolated as bright red crystals from the CH$_2$Cl$_2$/Et$_2$O filtrate and identified as *trans*-RuCl$_2$(*S,S*-BDPP)$_2$ by NMR spectroscopy (^{31}P{^{1}H} NMR, CDCl$_3$, 20 °C: 8.7 ppm, s), has also been characterised by X-ray diffraction analysis. The molecular structure (ORTEP view), along with the various structural parameters including tables of selected bond lengths/angles are given in Appendix A-2.3. ^{31}P{^{1}H} NMR data (CDCl$_3$, 20 °C) for [RuCl(*p*-cymene)(*S,S*-BDPP)]Cl: δ$_A$ = 39.2, δ$_B$ = 29.1, $^2J_{AB}$ = 60.7 Hz.

2.5.9 Reactions of RuCl₂(DPPB)(PPh₃) with Chelating Ligands (L–L); Formation of RuCl₂(DPPB)(L–L)

A benzene solution (20 mL) of the mixed phosphine complex, $RuCl_2(DPPB)(PPh_3)$ (0.10 g, 0.12 mmol), was stirred under argon with the appropriate chelating ligand (0.12 mmol). The original green solution which changed to yellow within minutes was stirred for 16 h and concentrated to ~5 mL. Addition of hexanes (30 mL) followed by stirring for 2 h precipitated the product which was filtered, washed with hexanes and vacuum dried. The spectroscopic characterisation of the $RuCl_2(DPPB)(L–L)$ complexes is presented in Chapter 4, Sections 4.4 and 4.5.

2.5.9.1 L–L = PPh₂(2-Py): RuCl₂(DPPB)(PPh₂(2-Py))

The pyridylphosphine ligand, $PPh_2(2\text{-}Py)$, will be referred to as PPh_2Py for the sake of convenience.

(a) *Trans*–RuCl₂(DPPB)(PPh₂Py), **24**

Orange-yellow solid. Yield: 0.08 g (80%). Anal. Calcd for *trans*–$RuCl_2(DPPB)(PPh_2Py)$, $C_{45}H_{42}NCl_2P_3Ru$: C, 62.72; H, 4.91; N, 1.63; Cl, 8.23. Found: C, 62.7; H, 4.9; N, 1.8; Cl, 8.1.

(b) *Cis*–RuCl₂(DPPB)(PPh₂Py), **25**

The complex, *cis*–$RuCl_2(DPPB)(PPh_2Py)$, was obtained by heating a benzene solution of the *trans* isomer at 80 °C for 8 h. The *cis* isomer, being relatively insoluble in benzene, precipitated from the solution; the solid was washed carefully with a small amount of benzene followed by hexanes and dried under vacuum. Anal. Calcd for *cis*–$RuCl_2(DPPB)(PPh_2Py)$, $C_{45}H_{42}NCl_2P_3Ru$: C, 62.72; H, 4.91; N, 1.63; (for $C_{45}H_{42}NCl_2P_3Ru \cdot 0.5H_2O$: C, 62.07; H, 4.98; N, 1.61). Found: C, 62.0; H, 5.2; N, 1.6. The presence of water was confirmed by IR and ^1H NMR spectroscopy.

2.5.9.2 L–L = DPPM: *Trans*–RuCl₂(DPPB)(DPPM), 27

Pale brownish yellow solid. Yield: 0.10 g (87%). Anal. Calcd for *trans*–RuCl₂(DPPB)(DPPM), $C_{52}H_{48}Cl_2P_4Ru$: C, 64.47; H, 4.99; Cl, 7.33. Found: C, 64.2; H, 5.0; Cl, 7.0.

2.5.10 Synthesis of Chlorohydrido(bidentate phosphine)ruthenium(II) Trimers, [RuHCl(P–P)]₃

The title trinuclear ruthenium-hydride complexes containing DPPB and *S,S*-CHIRAPHOS were first isolated in ~5–10% yield by Thorburn in this laboratory.[30] The synthetic procedure described by Thorburn[30] has been modified during the present study, and the isolated yields of the trimeric Ru hydrides improved dramatically (~40–50%, see Chapter 5, Section 5.4 for details).

2.5.10.1 P–P = DPPB: [RuHCl(DPPB)]₃, 29.[30]

A benzene or toluene (60 mL) suspension/solution of the dichloro(DPPB)-ruthenium(II) dimer, [RuCl(P–P)(μ-Cl)]₂ (1.0 g, 1.67 mmol monomer), was stirred under 1 atm H₂ for 1 h at room temperature. The yellow-brown suspension turned lighter brown, and deoxygenated triethylamine (0.235 mL, 1.69 mmol) was then added carefully under a blanket of hydrogen. The supension turned into a deep red solution within a couple of hours; the mixture was left stirring under H₂ for 36 h, replenishing the H₂ once after 18 h. The resulting red-brown suspension/solution was reduced to 20 mL. The precipitated NEt₃·HCl salt and an orange complex, identified as the NEt₃ adduct [(NEt₃)(DPPB)Ru(μ-Cl)₃RuCl(DPPB)] (see Section 2.5.6.1), were filtered off. The clear deep wine-red filtrate was pumped to a viscous oil. Addition of hexane (10 mL) precipitated more of the NEt₃ adduct along with some of the desired Ru-hydride product. The solids were filtered and rinsed first with hexane (5 mL), followed with a 1:1

toluene/hexane mixture (15 mL) to wash down any precipitated hydride product. Concentration of the filtrate to ~10 mL afforded the hydride complex [RuHCl(DPPB)]$_3$ as a brown solid (darker brown when microcrystalline) which was filtered and vacuum dried.

The NEt$_3$·HCl salt, a shiny white solid, could be separated from the NEt$_3$ adduct by washing the mixture with ethanol and then stripping the solvent from the filtrate. The salt was identified by ^{1}H NMR spectroscopy (CDCl$_3$, 20 °C, ppm: δ 3.09, 6H, AB q of d, -NCH_2; δ 1.6, 1H, br m, -NH^+Cl$^-$; δ 1.41, 9H, t, CH$_2$CH_3. Yield of NEt$_3$·HCl salt: 0.14 g (60%).

Yield of [(NEt$_3$)(DPPB)Ru(μ-Cl)$_3$RuCl(DPPB)]: 0.40 g (40%). Characterisation of this complex is described earlier in Section 2.5.6.1.

Yield of [RuHCl(DPPB)]$_3$: 0.50 g (53%). Anal. Calcd for (C$_{28}$H$_{29}$ClP$_2$Ru)$_3$: C, 59.63; H, 5.18. Found: C, 61.0; H, 5.5. Small amounts of the triethylamine adduct (see above) are sometimes present, which is evidenced by the presence of nitrogen in elemental analysis and a singlet at 48.3 ppm in the ^{31}P NMR spectrum. IR (Nujol, cm^{-1}): $\nu_{(Ru-H)}$ at 2010 and 1995 (w). ^{1}H NMR, hydride region (C$_6$D$_6$, 20 °C), δ ppm: −17.65, t, $^2J_{PH}$ = 31.7 Hz, terminal Ru–H; −21.1, m with $^2J_{PH}$ ~13–18 Hz, terminal Ru–H; −21.9 ppm, t, $^2J_{PH}$ = 33.2 Hz, terminal Ru–H. The phosphorus NMR data are given in Chapter 5, Section 5.5.2.

2.5.10.2 P–P = *S,S*–CHIRAPHOS: [RuHCl(*S,S*–CHIRAPHOS)]$_3$, 30 [30]

The CHIRAPHOS trimer analogue was prepared in exactly the same manner as the corresponding DPPB complex (see above), but using [RuCl(CHIRAPHOS)(μ-Cl)]$_2$ precursor on half the scale.

The NEt$_3$·HCl salt was again identified by ^{1}H NMR spectroscopy. The orange coloured NEt$_3$ adduct , [(NEt$_3$)(CHIRAPHOS)Ru(μ-Cl)$_3$RuCl(CHIRAPHOS)] similar to the corresponding DPPB complex, was isolated in ~40% yield. Anal. Calcd for C$_{62}$H$_{71}$NCl$_4$P$_4$Ru$_2$: C, 57.37; H, 5.51; N, 1.08; Cl, 10.92. Found: C, 57.3; H, 5.6;

N, 1.0; Cl, 10.7. $^{31}P\{^1H\}$ NMR (C_6D_6, 20 °C), AB q: δ_A = 87.3, δ_B = 80.2 ppm, $^2J_{AB}$ = 37.3 Hz.

The trimeric hydride complex [RuHCl(CHIRAPHOS)]₃, a dark red-brown solid, was recrystallised from CH_2Cl_2/Et_2O. Bright red crystals suitable for X-ray diffraction studies were isolated by Thorburn;[30] results of the X-ray analysis, carried out by Dr. R. G. Ball then at the University of Alberta, are discussed in Chapter 5 (Section 5.5.1). Yield (after recrystallisation): 0.23 g (46%). Anal. Calcd for [RuHCl(CHIRAPHOS)]₃, ($C_{28}H_{29}ClP_2Ru$)₃: C, 59.63; H, 5.18. Found: C, 60.1; H, 5.3. IR (Nujol, cm⁻¹): $\nu_{(Ru-H)}$ at 2025 and 2015 (w). ^1H NMR, hydride region (C_6D_6, 20 °C), ppm: −17.0, dd, $^2J_{PH}$ = 36.6 and 26.4 Hz, terminal Ru–H; −19.4, m with $^2J_{PH}$ in the 8–21 Hz range, bridging Ru–H; −24.8, $^2J_{PH}$ = 36.3 and 31.8 Hz, terminal Ru–H. The phosphorus NMR data are given in Chapter 5, Section 5.5.2.

2.5.11 Synthesis of Diphosphine-Bridged Dinuclear Ruthenium(II) Complexes, [(P–P)Cl₂Ru(μ₂-(P–P))RuCl₂(P–P)]

Reaction of $RuCl_2(PPh_3)_3$ with ~1.5 mole equivalents of the diphosphines DPPB[26] and DIOP[17a, 33] are known to give diphosphine-bridged complexes of the stoichiometry $RuCl_2(P–P)_{1.5}$. Analogous new complexes containing the chelating phosphines DPPN and DPPH were prepared by a similar route, and characterised by NMR spectroscopy and elemental analysis. In a typical procedure, $RuCl_2(PPh_3)_3$ (0.1 g, 0.10 mmol) was stirred with ~2 equivalents of the appropriate diphosphine in benzene (25 mL) solution for 1 h under argon. The resultant dark green solution was concentrated to ~5 mL and hexanes (20 mL) added to precipitate the green product, which was then separated by filtration, washed with hexanes (2 x 10 mL) and dried under vaccum. These diphosphine-bridged complexes are essentially insoluble in most common non-aromatic organic solvents, and only sparingly soluble in aromatic solvents.

2.5.11.1   P–P = DPPB[26]

Yield: 0.070 g (86%). Anal. Calcd for [RuCl$_2$(DPPB)$_{1.5}$]$_2$, C$_{84}$H$_{84}$Cl$_4$P$_6$Ru$_2$: C, 62.15; H, 5.22; Cl, 8.74. Found: C, 62.5; H, 5.2; Cl, 8.6.

2.5.11.2   P–P = DPPN

Yield: 0.075 g (90%). Anal. Calcd for [RuCl$_2$(DPPN)$_{1.5}$]$_2$, C$_{87}$H$_{90}$Cl$_4$P$_6$Ru$_2$: C, 62.74; H, 5.45; Cl, 8.51. Found: C, 62.9; H, 5.4; Cl, 7.3. ^{31}P{^{1}H} NMR (toluene-d_8, –60 °C): δ_A = 20.8, δ_B = 41.5, δ_X = 78.6 ppm; $^2J_{AB}$ = 306, $^2J_{AX}$ = 27.8, $^2J_{BX}$ = 31.3 Hz.

The product usually contained small amounts of a related mononuclear complex, RuCl$_2$(DPPN)(DPPN*), as evidenced by the presence of an additional ^{31}P NMR singlet resonance at –17.0 ppm due to the free end of the dangling DPPN ligand, DPPN* (*cf.* –15.6 ppm for free DPPN). The DIOP analogue of RuCl$_2$(DPPN)(DPPN*) has been characterised by a previous worker in this laboratory,[17a] and a ^{31}P NMR shift just high-field of the free phosphine shift has been noted for the corresponding dangling phosphine (–26.3 and –24.7 ppm, respectively).

2.5.11.3   P–P = DPPH

Yield: 0.075 g (84%). Anal. Calcd for [RuCl$_2$(DPPH)$_{1.5}$]$_2$, C$_{90}$H$_{96}$Cl$_4$P$_6$Ru$_2$: C, 63.31; H, 5.67; Cl, 8.30. Found: C, 64.4; H, 5.8; Cl, 7.3. ^{31}P{^{1}H} NMR (toluene-d_8, 20 °C): δ_A = 23.1, δ_B = 32.0, δ_X = 70.7 ppm; $^2J_{AB}$ = 301, $^2J_{AX}$ = 29.9, $^2J_{BX}$ = 32.2 Hz.

Again, the presence of some RuCl$_2$(DPPH)(DPPH*) impurity, where DPPH* represents a dangling phosphine, is apparent from a ^{31}P NMR singlet at –17.0 ppm (*cf.* –15.6 ppm for free DPPH), which is assigned to the dangling end of DPPH; the differences in the calculated and the found % C, H, and Cl are also explained by the

presence of $RuCl_2(DPPH)(DPPH^*)$ impurity (Calcd for $C_{60}H_{64}Cl_2P_4Ru$: C, 66.66; H, 5.97; Cl, 6.56).

2.5.12 Acetatohydrido(1,4-bis(diphenylphosphino)butane)(triphenyl-phosphine)ruthenium(II), $Ru(CO_2Me)(H)(DPPB)(PPh_3)$

A suspension of $RuCl_2(DPPB)(PPh_3)$ (0.20 g, 0.23 mmol) in dry methanol/toluene (4:1, 25 mL) was stirred with sodium acetate (0.05 g, 0.61 mmol) at 60 °C for 16 h under argon. The resultant dark yellow solution was concentrated to ~5 mL. The solid that precipitated was filtered, washed with toluene (5 mL) and dried under vacuum (yield of the white solid: 0.03 g, NaCl and excess NaOAc). The filtrate was further concentrated to ~2 mL and hexane (20 mL) added to precipitate the yellow product, which was filtered, washed with diethyl ether and vacuum dried. The complex is air-sensitive even in the solid state, turning green within a few hours. Yield of the yellow solid: 0.11 g (55%). Anal. Calcd for $C_{48}H_{47}O_2P_3Ru$: C, 67.84; H, 5.57. Found: C, 65.1; H, 5.2. IR (KBr, cm^{-1}): 2065 (w, $\nu_{(Ru-H)}$); 1538 (s, $\nu_{(OCO)}$, acetate, asymm.); 1481 (s, $\nu_{(OCO)}$, acetate, symm.). ^1H NMR (C_6D_6, 20 °C), ppm: δ 1.1, 3H, s, $-CO_2CH_3$; −18.8, 1H, dt, $^2J_{PH} = 30.6$ (d) and 24.6 (t) Hz. $^{31}P\{^1H\}$ NMR: $\delta_A = 43.5$, $\delta_B = 46.7$, $\delta_X = 78.9$ ppm; $^2J_{AB} = 292$, $^2J_{AX} = 35.9$, $^2J_{BX} = 25.7$ Hz.

2.6   References – Chapter 2

1.   Perrin, D. D.; Armarego, W. L. F.; Perrin, D. R. *Purification of Laboratory Chemicals*; Pergamon Press: Oxford, 2nd Edn., 1980.

2.   Karim, A.; Mortreux, A.; Petit, F.; Buono, G.; Peiffer, G.; Siv, C. *J. Organomet. Chem.* **1986**, *317*, 93.

3.   Allen, D. L.; Gibson, V. C.; Green, M. L. H.; Skinner, J. F.; Bashkin, J.; Grebenik, P. D. *J. Chem. Soc., Chem. Commun.* **1983**, 895.

4.   Maisonnet, A.; Farr, J. P.; Olmstead, M. M.; Hunt, C. T.; Balch, A. L. *Inorg. Chem.* **1982**, *21*, 3961.

5.   Joshi, A. M., M.Sc. Dissertation, The University of British Columbia, Vancouver, Canada, 1986; Chapter 2.

6.   (a) Kosolapoff, G. M.; Maier, L. *Organic Phosphorus Compounds* ; Wiley-Interscience: New York, 2nd Edn., 1972; Vol. 1, p. 130.
      (b) This was confirmed by recording $^{31}P\{^1H\}$ NMR spectra (300 MHz) of PPh3 in various solvents ($CDCl_3$, CD_2Cl_2, C_6D_6, and toluene-d_8, 20 °C) against 85% H_3PO_4, which was placed in a sealed inner capillary tube. The observed $^{31}P\{^1H\}$ chemical shift values for PPh3 ranged from –5 to –6 ppm w.r.t. 85% H_3PO_4.

7.   (a) James, B. R.; Rempel, G. L. *Discuss. Faraday Soc.* **1968**, *46*, 48.
      (b) *Can. J. Chem.* **1966**, *44*, 233.

8.   König, W. A.; Francke, W.; Benecke, I. *J. Chromatogr.* **1982**, *239*, 227.

9.   Slessor, K. N.; King, G. G. S.; Miller, D. R.; Winston, M. L.; Cutforth, T. L. *J. Chem. Ecol.*, **1985**, *18*, 1659.

10.   König, W. A.; Benecke, I.; Sievers, S. *J. Chromatogr.* **1982**, *238*, 427.

11.   Chan, A. S. C.; Landis, C. R. *J. Mol. Catal.* **1989**, *49*, 165.

12. MacFarlane, K. S., M.Sc. Dissertation, The University of British Columbia, Vancouver, Canada, 1989; Chapter 2.

13. Shriver, D. F.; Drezdon, M. A. *The Manipulation of Air-Sensitive Compounds*; Wiley: New York, 2nd Edn., 1986.

14. (a) James, B. R.; Ochiai, E.; Rempel, G. I. *Inorg. Nucl. Chem. Lett.* **1971**, 7, 781.
    (b) Evans, I. P.; Spencer, A.; Wilkinson, G. *J. Chem. Soc., Dalton Trans.* **1973**, 204.
    (c) Mercer, A.; Trotter, J. *J. Chem. Soc., Dalton Trans.* **1975**, 2480.

15. Bora, T.; Singh, M. M. *Transition Met. Chem.* **1978**, 3, 27; and references therein.

16. Bennett, M. A.; Smith, A. K. *J. Chem. Soc., Dalton Trans.* **1974**, 233.

17. (a) Wang, D. K. W., Ph.D. Dissertation, The University of British Columbia, Vancouver, Canada, 1978; Chapter 2.
    (b) Thorburn, I. S., M.Sc. Dissertation, The University of British Columbia, Vancouver, Canada, 1980; Chapter 2.

18. Dekleva, T. W.; Thorburn, I. S.; James, B. R. *Inorg. Chim. Acta* **1985**, *100*, 49.

19. Stephenson, T. A.; Wilkinson, G. *J. Inorg. Nucl. Chem.* **1966**, *28*, 945.

20. Hallman, P.S.; Stephenson, T. A.; Wilkinson, G. *Inorg. Syntheses* **1970**, *12*, 237.

21. Hoffman, P. R.; Caulton, K. G. *J. Am. Chem. Soc.* **1975**, *97*, 4221.

22. Schunn, R. A.; Wonchoba, E. R.; Wilkinson, G. *Inorg. Syntheses* **1972**, *13*, 131.

23. Hallman, P. S.; McGarvey, B. R.; Wilkinson, G. *J. Chem. Soc., A* **1968**, 3143.

24. (a) Jaswal, J.; Rettig, S. J.; James, B. R. *Can. J. Chem.* **1990**, *in press*.
    (b) Yapp, D. T. T., *personal communication*.

25. Jung, C. W.; Garrou, P. E.; Hoffman, P. R.; Caulton, K. G. *Inorg. Chem.* **1984**, *23*, 726.

26. Bressan, M.; Rigo, P. *Inorg. Chem.* **1975**, *14*, 2286.

27. Dekleva, T. W.; Joshi, A. M.; Thorburn, I. S.; James, B. R.; Evans, S. V.; Trotter, J. *Isr. J. Chem.* **1990**, *30(4)*; *in press*.

28. Thorburn, I. S.; Rettig, S. J.; James, B. R. *Inorg. Chem.* **1986**, *25*, 234.

29. Thorburn, I. S., Ph.D. Dissertation, The University of British Columbia, Vancouver, Canada, 1985.

30. James, B. R.; Pacheco, A.; Rettig, S. J.; Thorburn, I. S.; Ball, R. C.; Ibers, J. A. *J. Mol. Catal.* **1987**, *41*, 147.

31. Joshi A. M.; James, B. R. *J. Chem. Soc., Chem. Commun.* **1989**, 1785.

32. Mashima, K.; Kusano, K.; Ohta, T.; Noyori, R.; Takaya, H. *J. Chem. Soc., Chem. Commun.* **1989**, 1208.

33. James, B. R.; McMillan, R. S.; Morris, R. H.; Wang, D. K. W. *Adv. Chem. Ser.* **1978**, *167*, 122.

CHAPTER 3

Chloro-Bridged Diruthenium(II,II) Complexes Containing Chelating Ditertiary Phosphines

3.1   Introduction

The phenomenal success of chiral rhodium complexes, particularly those containing chiral bidentate phosphines, as homogeneous catalysts for the asymmetric hydrogenation of a variety of prochiral unsaturated substrates is evident from even a brief survey of the literature in this field (see Chapter 1). Rhodium-chiral phosphine systems have attracted much attention in the past twenty years. The high degree of enantioselectivity achieved using these catalysts (up to 100% e.e.) and their easy synthetic accessibility have played an important part in their development. Work on chiral diphosphine complexes of other transition metals which also exhibit catalytic activity, however, has been very limited.

Over the years, ruthenium has developed a rich coordination and organometallic chemistry.[1, 2] The literature on the synthesis, reactivity, properties and catalytic applications of tertiary phosphine complexes of ruthenium is extensive.[1-5] The ruthenium(II) hydrido phosphine complex RuHCl(PPh3)3 surpasses, or is comparable to, its well-known rhodium analogue, Wilkinson's catalyst RhCl(PPh3)3, in its activity for the hydrogenation of terminal alkenes.[6-8] In contrast with the chemistry of diphosphine analogues of the Wilkinson catalyst, however, the chemistry of chelating phosphine analogues of the ruthenium complex is much less established.

Since the early work on ruthenium(II) diphosphine complexes by Chatt and Hayter,[9] a series of coordinatively saturated complexes of general formula $RuX_2(P-P)_2$ and $RuXY(P-P)_2$ containing an extensive array of diphosphines (P–P) has been prepared.[1, 10-12] X and Y represent anionic ligands such as halides, pseudohalides, hydrides, or σ-bonded alkyl or aryl groups; the complexes are largely of the *trans* geometry. A simple displacement of monodentate phosphines by bidentate phosphines from $Ru^{II}XY(PR_3)_3$ precursors almost always yields the corresponding inherently stable six-coordinate complexes (Equation 3.1); even when only one equivalent of the diphosphine is used, ~50% conversion to the bis(diphosphine) derivatives is noted.[13, 14]

$$RuXY(PR_3)_3 + 2\,P-P \longrightarrow RuXY(P-P)_2 + 3\,PR_3 \qquad (3.1)$$

X and Y = anionic ligands
PR_3 = monodentate phosphine
P–P = bidentate phosphine

As a result, very few coordinatively unsaturated (C.N. <6) ruthenium-diphosphine compounds have been synthesised by this route.[13-16] Figure 3.1 summarises the five-coordinate Ru(II) complexes containing a bidentate phosphine ligand reported to date.
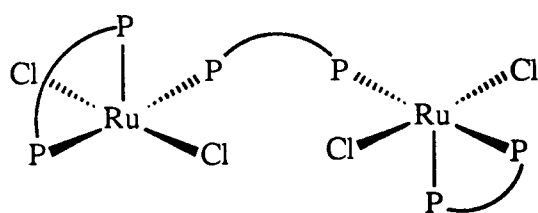
$P-P = DIOP^{15}$ or $Ph_2P(CH_2)_nPPh_2$

n = 4, DPPB;[16] 5, DPPN;[14] 6, DPPH;[14]
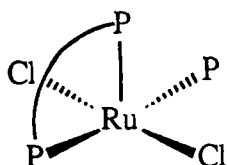
$P-P = DIOP^{15}$ or $DPPB^{13}$

$P = PPh_3$

Figure 3.1: Coordinatively unsaturated ruthenium(II)-diphosphine complexes prepared by phosphine displacement reactions.

Coordinative unsaturation at some stage in a catalytic cycle is usually essential for a transition metal complex to be catalytically active.[17] Previous work from this laboratory on Ru(II)-diphosphine complexes has clearly highlighted this unsaturation requirement. Mechanistic studies on the coordinatively saturated Ru(II)-hydride complex, *trans*–RuHCl(DIOP)$_2$, which was shown to catalyse asymmetric hydrogenation of prochiral alkenes under mild conditions, revealed that the active species contained only one DIOP per Ru(II) centre ["RuHCl(DIOP)"].[18, 19] Recent studies by Ikariya and coworkers[20] on the asymmetric hydrogenation of prochiral alkenes using *trans*–RuHCl(BINAP)$_2$ also point to "RuHCl(BINAP)", presumably produced *in situ* by phosphine dissociation, as the likely catalytically active species. Interestingly, RuHCl-(P–P)$_2$ complexes containing several other diphosphines (P–P), notably CHIRAPHOS and Ph$_2$P(CH$_2$)$_n$PPh$_2$ (n = 1–3), show little alkene hydrogenation activity,[15, 21] perhaps because the diphosphines are bound too strongly to undergo dissociation to the supposed catalytically active "Ru^{II}(P–P)" species.

Direct pathways to "RuX$_2$(P–P)" moieties (X = halide, hydride) are desirable in view of these observations; such catalysts would be analogous to the well-established Rh^I(P–P) systems.[22, 23] A major portion of this thesis deals with ways of accessing such "Ru^{II}(P–P)" species for the purpose of conducting an in-depth kinetic and mechanistic study into their catalytic behaviour. This chapter describes preparation of the dichloro species "RuCl$_2$(P–P)". Their role in activation of dihydrogen and the subsequent formation of hydridochloro complexes of the stoichiometry "[RuHCl(P–P)]" are discussed in Chapter 5.

3.2 Synthesis and Characterisation of [RuCl$_2$(P–P)]$_2$ Complexes – A Brief Review

The monodentate phosphine analogues of "RuCl$_2$(P–P)" complexes can be conveniently prepared as the dimeric [RuCl$_2$(PR$_3$)$_2$]$_2$ species by reduction of ruthenium(III) precursors such as RuCl$_3$(PR$_3$)$_2$.[24, 25] Attempts by Dr. Thorburn, previously of this laboratory, to prepare RuCl$_3$(P–P) complexes by phosphine displacement from RuCl$_3$(PR$_3$)$_2$ precursors led to the discovery of the formally mixed-valence dinuclear Ru$_2$[II, III] compounds of the type [(P–P)ClRu(μ-Cl)$_3$RuCl(P–P)] (Equation 3.2). Several such compounds were isolated (Equation 3.2) and characterised by various spectroscopic and analytical techniques.[26, 27] Thorburn's work which forms the basis of the present study is summarised in this section.

$$4\ RuCl_3(PR_3)_2\ +\ 4\ P\text{–}P\ \xrightarrow[\text{trace H}_2\text{O}]{\text{hexane, reflux}}\ \begin{array}{c} 2\ Ru_2Cl_5(P\text{–}P)_2\ +\ O{=}PR_3 \\ + \\ 7\ PR_3\ +\ 2\ HCl \end{array} \qquad (3.2)$$

R = phenyl, *p*–tolyl
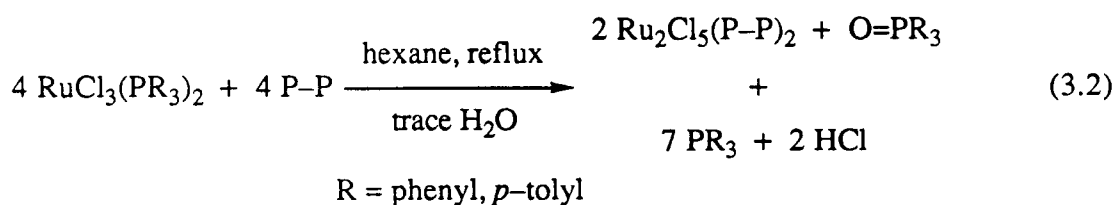
P–P = DPPP, DPPB, DIOP, CHIRAPHOS, NORPHOS

The X-ray diffraction analysis of the mixed-valence (*S,S*)-CHIRAPHOS complex showed the complex to be a highly symmetric trichloro-bridged species with irregular octahedral geometry about each ruthenium centre (Figure 3.2).[26, 27]
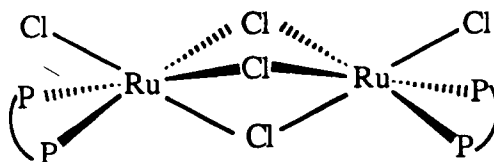
P—P = (*S,S*)-CHIRAPHOS

Figure 3.2: Geometry of Ru$_2$Cl$_5$(CHIRAPHOS)$_2$.

Reduction of the $Ru_2Cl_5(P-P)_2$ complexes with H_2 in the presence of an appropriate base then afforded the target "$Ru^{II}(P-P)$" compounds as dichloro-bridged dimers (Figure 3.3).[27, 28] The preparative chemistry leading to the synthesis of the $Ru_2^{II, II}$ diphosphine complexes, $[RuCl(P-P)(\mu-Cl)]_2$, starting from $RuCl_3\cdot3H_2O$ is summarised in Scheme 3-I; complexes containing DPPP, DPPB, CHIRAPHOS and DIOP were isolated and characterised. However, Thorburn noted that while the CHIRAPHOS complexes were successfully prepared by this route, similar complexes containing the nearest nonchiral analogue of CHIRAPHOS (viz. $Ru_2Cl_5(DPPE)_2$ and consequently $Ru_2Cl_4(DPPE)_2$, DPPE = $PPh_2CH_2CH_2PPh_2$) could not be synthesised.[26, 28] This was somewhat surprising because like CHIRAPHOS, DPPE forms a five-membered chelate ring on binding to a metal centre; DPPE differs from CHIRAPHOS only in having hydrogens in place of the methyl groups on the CHIRAPHOS backbone.

$$RuCl_3\cdot3H_2O \ + \ 2\,PR_3 \ \xrightarrow[\text{24 h, 25 °C}]{\text{DMA}} \ RuCl_3(PR_3)_2(DMA)\cdot DMA \text{ solvate}$$

DMA = N,N–dimethylacetamide

R = phenyl or p-tolyl

50–60%

P–P (1 eq./Ru^{III})

hexanes, reflux

24 h

$$[RuCl(P-P)(\mu-Cl)]_2 \xleftarrow[\text{Base.H}^+\text{Cl}^- \qquad \text{Base}]{\text{1 atm } H_2,\ 16\ h,\ 25\ °C} \ [(P-P)ClRu(\mu-Cl)_3RuCl(P-P)]$$

40–80%   45–80%

Base = DMA for P–P = DPPP and DPPB

Base = polyvinylpyridine for P–P = CHIRAPHOS and DIOP
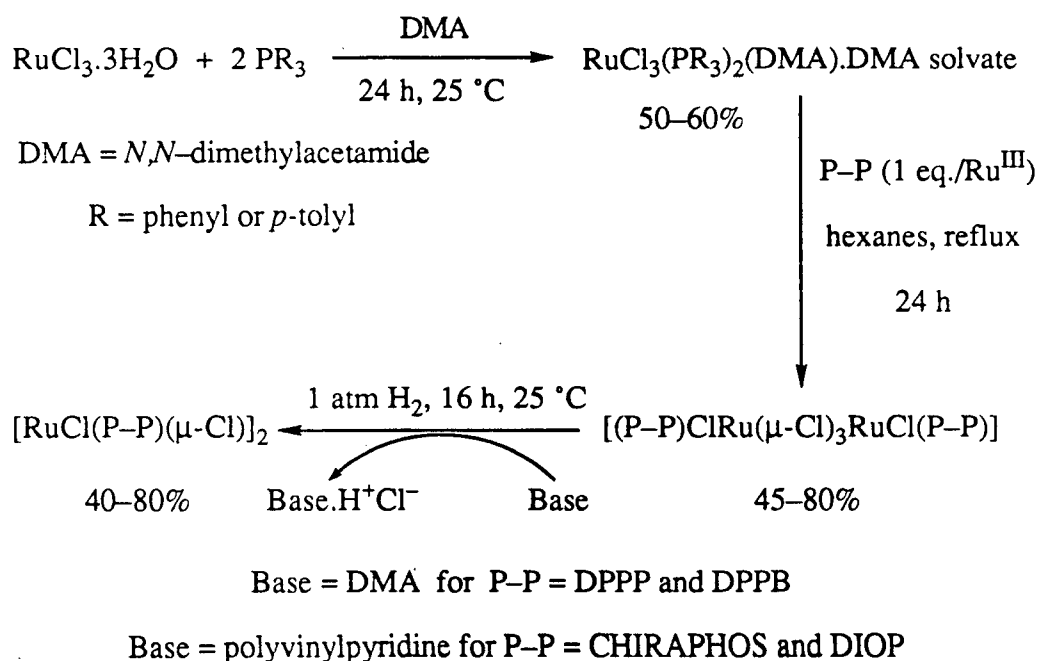
Scheme 3-I: Synthetic route to dinuclear ruthenium complexes containing only one chelating phosphine per Ru centre.

Molecular weight measurements in solution (Signer method[29]) on the CHIRAPHOS derivative indicated a dimeric structure for the "RuCl$_2$(P–P)" species; the phosphorus NMR spectroscopic observations (see below) supported the dimeric formulation [RuCl$_2$(P–P)]$_2$, which consists of two five-coordinate ruthenium(II) centres in square pyramidal geometry with two edge-bridging chlorides (Figure 3.3).[27, 28] A similar dichloro-bridged structure has been previously proposed for dimeric ruthenium(II) complexes containing monodentate phosphines such as PPh$_3$ and P(p-tolyl)$_3$.[4, 24, 25, 30]
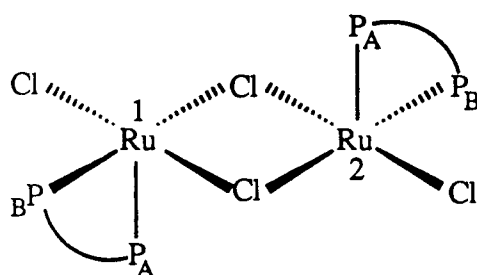
P–P = DPPP, DPPB, DIOP, CHIRAPHOS

Figure 3.3: Suggested geometry for [RuCl$_2$(P–P)]$_2$ complexes.

Phosphines provide an excellent NMR spectroscopic handle on the dimeric [RuCl(P–P)(μ-Cl)]$_2$ complexes. The ^{31}P{^{1}H} NMR spectra (32.4 MHz, CD$_2$Cl$_2$) of the nonchiral DPPP and DPPB derivatives and the chiral DIOP complex consisted of a single AB pattern while the CHIRAPHOS dimer showed two independent AB quartets of equal integrated intensity. The single AB pattern observed for the DPPP and DPPB species is consistent with the dimeric formulation (Figure 3.3) in which P$_A$(Ru^1) is chemically and magnetically equivalent to P$_A$(Ru^2), similarly for P$_B$, but P$_A$ is not equivalent to P$_B$. Chirality in the CHIRAPHOS backbone renders P$_A$(Ru^1) and P$_A$(Ru^2) inequivalent thus giving rise to two independent AB systems. The chiral [RuCl(DIOP)(μ-Cl)]$_2$ species, however, exhibited only one AB pattern, instead of the two expected by analogy with the CHIRAPHOS complex; this was suggested to be the result of coincidental degeneracy.

The $^{31}P\{^1H\}$ NMR spectroscopic data (121.42 MHz) for [RuCl(P–P)(μ-Cl)]$_2$ complexes including the ones prepared during the present study are listed in Table 3.3 (Section 3.3.2).

These Ru(II) complexes containing a single chelating phosphine per ruthenium did indeed prove to be efficient catalysts for the hydrogenation of a number of alkenes at 1 atm hydrogen pressure and 20–70 °C.[27, 28] Of particular interest, several functionalised prochiral alkenes were hydrogenated enantioselectively using as catalyst precursors [RuCl$_2$(P–P)]$_2$ complexes containing chiral phosphines. For example, the S,S-CHIRAPHOS complex catalysed the reduction of (Z)-α-acetamidocinnamic acid to the (S)-product with 97% e.e. (30 °C, 1 atm H$_2$) in N,N-dimethylacetamide (DMA) solvent.[27, 28] Surprisingly, no ruthenium hydrides were observed by ^1H NMR spectroscopy at the end of the catalytic runs.

Finally, Thorburn noted that in the presence of coordinating solvents such as acetone or DMA, the dichloro-bridged [RuCl(P–P)(μ-Cl)]$_2$ complexes showed a great propensity to form solvent-coordinated dinuclear species [Ru$_2$Cl$_4$(P–P)$_2$(solvent)] (Equation 3.3).[27] On the basis of a detailed NMR study, the acetone and the DMA adducts were assigned a trichloro-bridged dinuclear geometry as shown in Scheme 3-II. As will be discussed in later sections, formation of such complexes of the type [Ru$_2$Cl$_4$(P–P)$_2$(L)], where L is an incoming ligand, constitutes a prime mode of reactivity for the dichloro-bridged dimers.

$$[RuCl(P–P)(μ-Cl)]_2 \xrightleftharpoons{\text{solvent}} [Ru_2Cl_4(P–P)_2(\text{solvent})] \qquad (3.3)$$

solvent = acetone or DMA
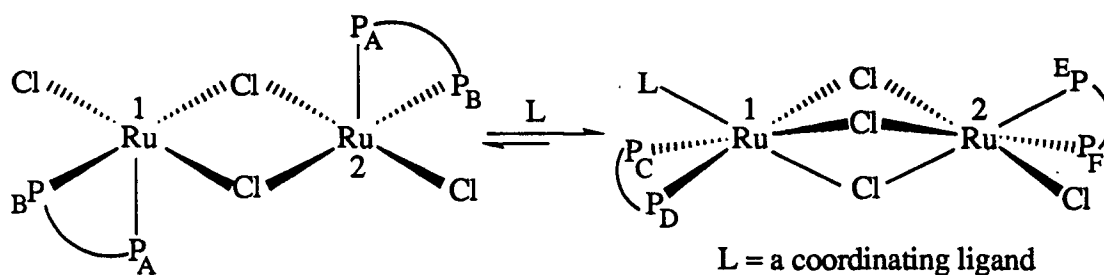
Scheme 3-II: Formation of trichloro-bridged species from [RuCl(P–P)(μ-Cl)]₂ in the presence of a coordinating ligand.

3.3 Present Work

The synthetic strategy used for the preparation of [RuCl(P–P)(μ-Cl)]$_2$ complexes, as elucidated in Section 3.2, has been extended to include more diphosphines; the ligands used are shown in Figure 3.4.

$$Ph_2P(CH_2)_nPPh_2 \quad n = 3, DPPP; \quad 4, DPPB; \quad 5, DPPN; \quad 6, DPPH$$

Ar = phenyl, DPPCP; cyclohexyl, DPCYCP

PHENOP

BDPP

DIOP

CHIRAPHOS

BINAP
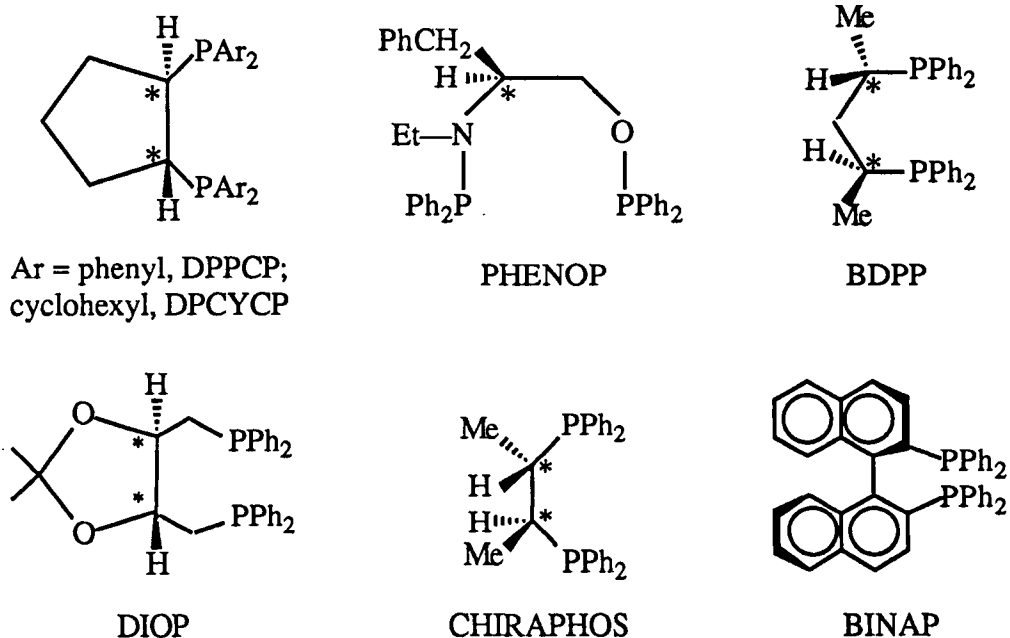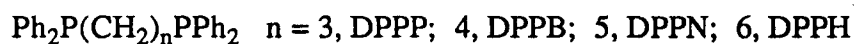
Figure 3.4: Diphosphines used in the preparation of Ru-(P–P) complexes.

81

3.3.1 $Ru_2Cl_5(P-P)_2$ Complexes

Refluxing a hexane suspension of $RuCl_3(PR_3)_2$ (R = phenyl or p–tolyl) with equimolar amounts of the appropriate diphosphines affords the corresponding formally mixed valence dinuclear complexes, $Ru_2Cl_5(P-P)_2$, as air-stable red-brown or yellow-brown powders. In addition to the complexes 1–4 reported by Thorburn,[26, 27] respectively containing DPPP, DPPB, R,R-DIOP and S,S-CHIRAPHOS, new analogous $Ru_2Cl_5(P-P)_2$ complexes incorporating the diphosphines DPPN (5), DPPH (6), rac-DPPCP (7), rac-DPCYCP (8), S,S-BDPP (9), R- and S-BINAP (10, 11), and the aminophosphinephosphinite ligand S-PHENOP (12), have been prepared. Details of their synthesis and characterisation (elemental analysis) are given in Section 2.5.4.

The very low solubility, in dichloromethane and most other common organic solvents, of the $Ru_2Cl_5(P-P)_2$ complexes 6 and 9 containing the diphosphines DPPH and BDPP, respectively, posed difficulties during recrystallisation/reprecipitation procedures. Relatively large volumes of CH_2Cl_2 had to be used and the products obtained were often analytically impure. The low solubility perhaps results from the increased alkyl chain length of the phosphine backbone.

The magnetic susceptibilities of the mixed-valence complexes were determined at 20 °C by the Evans' method[31] in $CDCl_3$ solutions containing ~2% (v/v) t-butanol. The solution magnetic moments, μ_{eff}, for the complexes 2, 5, 7, 10, 11 and 12, containing DPPB, DPPN, rac-DPPCP, R- and S-BINAP and S-PHENOP, respectively, are listed below (Table 3.1). The observed μ_{eff} values, which range from 1.8–2.2 B.M., are consistent with the presence of one unpaired electron per molecule ($\mu_{spin\ only}$ = 1.73 B.M.).[32, 33] The limited solubility of complexes 6, 8 and 9 prevented reliable solution magnetic susceptibility measurements. The μ_{eff} values for the complexes 3 (1.78 B.M.) and 4 (1.95 B.M.) have been determined previously.[27]

Table 3.1: Magnetic Moment Data for $Ru_2Cl_5(P-P)_2$ Complexes ($CDCl_3$, 20 °C).

$Ru_2Cl_5(P-P)_2$ Complex	Solution μ_{eff}, B.M.
$Ru_2Cl_5(DPPB)_2$, **2**	2.05
$Ru_2Cl_5(DPPN)_2$, **5**	2.20
$Ru_2Cl_5(rac\text{-}DPPCP)_2$, **7**	2.03
$Ru_2Cl_5(R\text{-}BINAP)_2$, **10**	1.82
$Ru_2Cl_5(S\text{-}BINAP)_2$, **11**	1.90
$Ru_2Cl_5(S\text{-}PHENOP)_2$, **12**	2.16

The UV-visible spectra of the mixed valence $Ru_2Cl_5(P-P)_2$ compounds in CH_2Cl_2 solution are shown in Figure 3.5 and the values of λ_{max}, ν_{max} and ε are given in Table 3.2. The DPPN, R-BINAP, S-BINAP, and S-PHENOP derivatives exhibit spectral features similar to those reported for the analogous complexes containing DPPP, DPPB, CHIRAPHOS, and DIOP ligands (**1–4**; λ_{max} ~370, 450, and 520 nm with ε values of *ca.* 4000, 2500, 1500 M^{-1} cm^{-1}, respectively).[26, 27] Thorburn has discussed the electronic spectra (UV-visible and near-IR) of $Ru_2Cl_5(P-P)_2$ complexes **1–4** in detail.[26, 27] Because of the analogous nature of the new complexes **5–12**, these aspects will not be dealt with in this thesis beyond noting their similarity. Some variations in intensities and absorption maxima are observed with changing phosphines.

The DMA solutions of $Ru_2Cl_5(P-P)_2$ complexes absorb half a mole equivalent of H_2 per Ru, at 1 atm of H_2 and 30 °C, in keeping with the behaviour noted previously for the analogous complexes **1–4**.[26-28] The H_2-uptake plots for the complexes **5, 7, 8, 10, 11**, and **12** are shown in Figure 3.6.
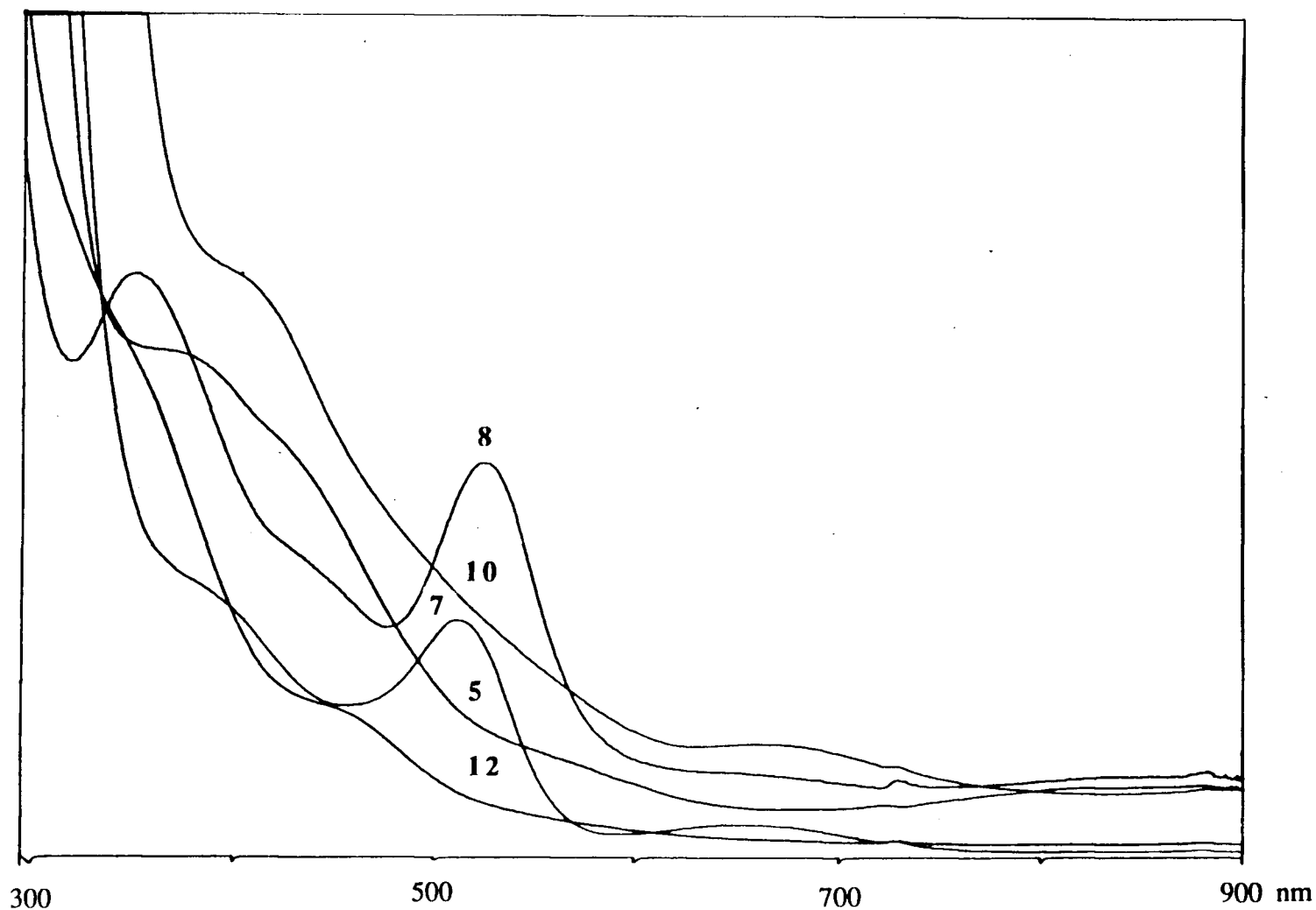
Figure 3.5: Visible spectra of the $Ru_2Cl_5(P–P)_2$ complexes in CH_2Cl_2 at 25 °C. P–P = (a) DPPN, **5**; (b) *rac*-DPPCP, **7**;
(c) *rac*-DPCYCP, **8**; (d) *R*-BINAP, **10**; and (e) *S*-PHENOP, **12**. [Ru2] = 2.0 ± 0.1 x 10^{-3} M for the complexes **5**, **7**,
10, and **12**; 0.80 x 10^{-3} M for **8**. The spectrum for the *S*-BINAP derivative **11** is essentially identical (not shown) to that
observed for the *R*-BINAP analogue.

Table 3.2: Visible Spectroscopic Data for the $Ru_2Cl_5(P–P)_2$ Complexes.

$Ru_2Cl_5(P–P)_2$ Complex[a] P–P =	Solvent	λ_{max}, nm	ϵ, $M^{-1}\,cm^{-1}$
DPPN, **5**	CH_2Cl_2	370	4415
		420	3810
		540	1170
rac-DPPCP, **7**	CH_2Cl_2	380	2550
		515	2210
		659	425
rac-DPCYCP, **8**	CH_2Cl_2	350	5225
		430	2840
		525	3590
R-BINAP, **10**	CH_2Cl_2	405	5215
		660	1135
S-BINAP, **11**	CH_2Cl_2	405	4978
		660	815
S-PHENOP, **12**	CH_2Cl_2	340	4950
		440	1485

[a] $[Ru_2] = 2.0 \pm 0.1 \times 10^{-3}$ M for complexes **5, 7, 10, 11**, and **12**; $[Ru_2] = 8.0 \times 10^{-4}$ M for complex **8**. The corresponding UV-visible spectra are shown in Figure 3.5.
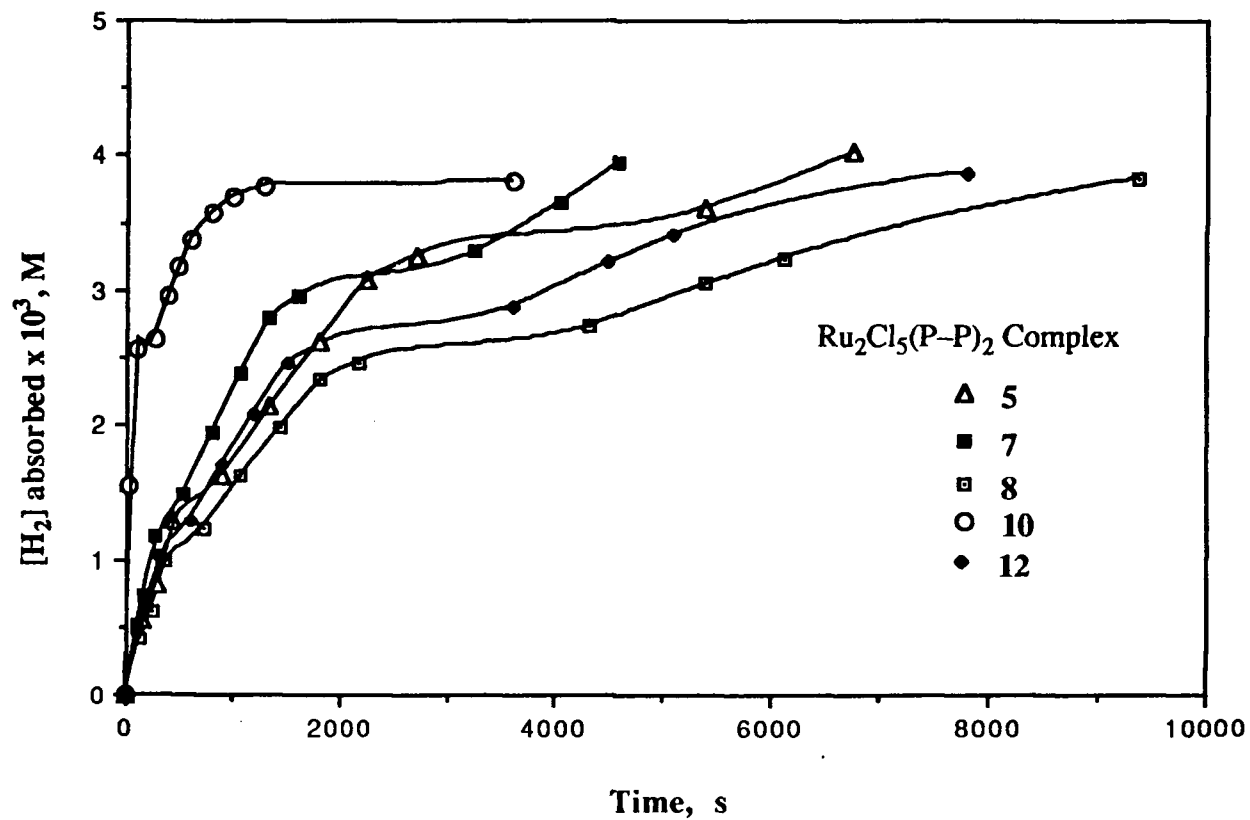
Figure 3.6: H_2-uptake plots for $Ru_2Cl_5(P-P)_2$ complexes in DMA at 30 °C under 1 atm H_2 pressure; $[Ru_2] = 4.0 \pm 0.1 \times 10^{-3}$ M. P–P = (a) DPPN, **5**; (b) *rac*-DPPCP, **7**; (c) *rac*-DPCYCP, **8**; (d) *R*-BINAP, **10**; and (e) *S*-PHENOP, **12**. The uptake plot for the *S*-BINAP derivative **11** is essentially identical to that shown for **10**.

The final stoichiometry of the H_2-reaction is consistent with reduction of the mixed-valence complexes to $Ru_2^{II,II}$ species in accordance with Equation 3.4.[26-28]

$$Ru_2Cl_5(P-P)_2 + 0.5\, H_2 \longrightarrow Ru_2Cl_4(P-P)_2 + H^+ + Cl^- \qquad (3.4)$$

3.3.2 [RuCl$_2$(P–P)]$_2$ Complexes

The reaction of $Ru_2Cl_5(P-P)_2$ complexes with hydrogen in DMA generates the ionic species $[Ru_2Cl_5(P-P)_2]^-DMAH^+$,[26-28] from which the corresponding neutral dimeric Ru(II) complexes [RuCl(P–P)(μ-Cl)]$_2$ are isolated (P–P = DPPP, **13**;[27, 28] DPPB, **14**;[27, 28] R,R-DIOP, **15**;[27, 28] S,S-CHIRAPHOS, **16**;[27, 28] DPPN, **17**; R-BINAP, **18**; S-BINAP, **19**; see Section 2.5.4). Alternatively, the dimeric complexes can be obtained by the H_2-reduction of $Ru_2Cl_5(P-P)_2$ in benzene or toluene suspension using polyvinylpyridine (PVP) as the base. The insoluble PVP and its HCl salt are easily removed by filtration, and the desired [RuCl(P–P)(μ-Cl)]$_2$ species isolated from the filtrate (Section 2.5.5).

The complexes are air-sensitive in solution, and hygroscopic in the solid state. The $^{31}P\{^1H\}$ NMR data for the [RuCl(P–P)(μ-Cl)]$_2$ complexes **13–19** are listed in Table 3.3. The data for the new complexes (P–P = DPPN, **17**; R-BINAP, **18**; S-BINAP, **19**) are consistent with a dichloro-bridged dimeric structure suggested previously for the DPPP, DPPB, DIOP, and CHIRAPHOS analogues (**13–16**, respectively; see Section 3.2, Figure 3.3).[27, 28]

The $^{31}P\{^1H\}$ NMR spectrum of [RuCl$_2$(S-BINAP)]$_2$, **19**, in C_6D_6 solution shows two AB quartets of equal integral intensity ($\delta_A = 75.6$, $\delta_B = 5.6$, $^2J_{AB} = 40.7$ Hz; $\delta_C = 58.7$, $\delta_D = 58.1$, $^2J_{CD} = 42.5$ Hz; see Figure 3.7 and Table 3.3). The corresponding spectrum of the R-BINAP analogue **18** is essentially identical. The same resonances are also observed in the ^{31}P spectrum of the related mixed-phosphine derivative
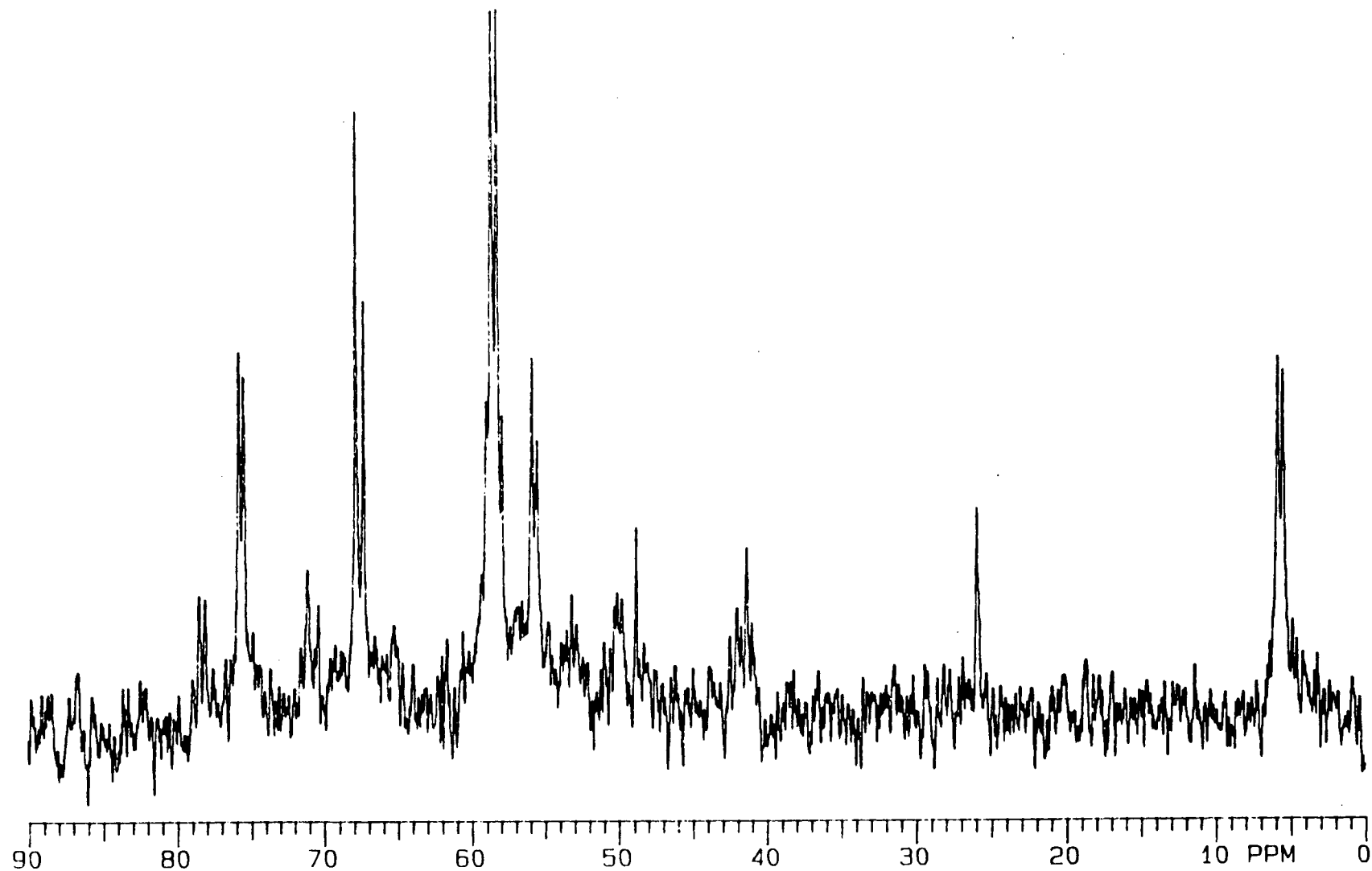
Figure 3.7: $^{31}P\{^1H\}$ NMR spectrum (121.42 MHz, 20 °C) of [RuCl$_2$(S-BINAP)]$_2$, **19**, in C$_6$D$_6$.

Table 3.3: $^{31}P\{^1H\}$ NMR Data (121.42 MHz, 20 °C) for [RuCl(P–P)(μ-Cl)]$_2$ Complexes.

[RuCl(P–P)(μ-Cl)]$_2$ Complex P–P =	Solvent	Chemical Shifts, δ (ppm)	$^2J_{PP}$, (Hz)
DPPP, **13**	C$_6$D$_6$	δ$_A$ = 59.0, δ$_B$ = 51.0	57.0
	CD$_2$Cl$_2$[a]	δ$_A$ = 58.0, δ$_B$ = 50.5	57.4
DPPB, **14**	C$_6$D$_6$	δ$_A$ = 64.0, δ$_B$ = 54.9	47.3
	CD$_2$Cl$_2$	δ$_A$ = 62.0, δ$_B$ = 53.8	46.6
R,R–DIOP, **15**	C$_6$D$_6$	δ$_A$ = 50.7, δ$_B$ = 47.5	46.1
	CD$_2$Cl$_2$[a]	δ$_A$ = 50.0, δ$_B$ = 47.1	46.4
S,S–CHIRAPHOS, **16**	C$_6$D$_6$	δ$_A$ = 88.0, δ$_B$ = 78.3	38.2
		δ$_C$ = 87.0, δ$_D$ = 75.7	39.2
	CD$_2$Cl$_2$[a]	δ$_A$ = 87.8, δ$_B$ = 77.9	39.1
		δ$_C$ = 87.1, δ$_D$ = 77.9	39.1
DPPN, **17**	C$_6$D$_6$	δ$_A$ = 55.8, δ$_B$ = 42.3	35.0
R-BINAP, **18**	C$_6$D$_6$	δ$_A$ = 75.8, δ$_B$ = 5.8	40.6
		δ$_C$ = 58.6, δ$_D$ = 58.2	43.2
S-BINAP, **19**	C$_6$D$_6$	δ$_A$ = 75.6, δ$_B$ = 5.6	40.7
		δ$_C$ = 58.7, δ$_D$ = 58.1	42.5
S,S-BDPP, **20**	C$_6$D$_6$	δ$_A$ = 64.5, δ$_B$ = 52.9	—[b]

[a] Spectrum recorded at 32.4 MHz; data taken from Ref. 26.

[b] Broad signals at ambient temperature with unresolved coupling.

RuCl$_2$(BINAP)(PPh$_3$), **21**, which, like the analogous DPPB and DIOP complexes, dissociates the PPh$_3$ ligand in solution to form the dimeric [RuCl$_2$(BINAP)]$_2$ species (see Equation 3.5 in Section 3.4.1, and Chapter 4, Section 4.6).

The resonances at 75.6 and 5.6 ppm are assigned to an apical/basal (P$_A$/P$_B$) pair of phosphorus nuclei by comparison with the reported chemical shifts and chemical shift differences observed for other square pyramidal ruthenium complexes containing similar apical/basal pairs of phosphines.[13, 30] The remaining two resonances are assigned to the BINAP ligand which occupies two *cis* positions in the basal plane. Thus, based on the ^{31}P NMR data, the BINAP complexes **18** and **19** are assigned a slightly different geometry (Figure 3.8) compared to that proposed for other dichloro-bridged complexes (*cf*. Figure 3.3).

P–P =*R*- or *S*-BINAP
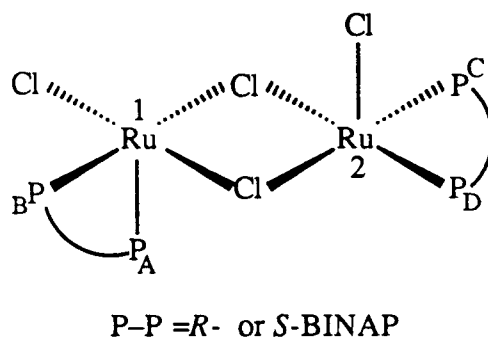
Figure 3.8: Suggested geometry of [RuCl(BINAP)(μ-Cl)]$_2$.

The additional peaks in the spectrum started growing in as the FID acquisition proceeded, and are due to unidentified impurities. In fact, a ^{31}P NMR spectrum of the same solution recorded after 48 h showed a large number of new peaks, with a corresponding decrease in the intensity of signals assigned to **19** (or **18**). The high reactivity of these complexes is perhaps consistent with the presence of two coordinatively unsaturated Ru centres as shown in the suggested dichloro-bridged dimeric structure (Figure 3.8). Ikariya *et al*. have reported the synthesis of the related

[Ru$_2$Cl$_4$(BINAP)$_2$(NEt$_3$)] species by a different route ([RuCl$_2$(COD)]$_n$ + 1 equiv BINAP, NEt$_3$).[33]

The S,S-BDPP analogue (20) was obtained in very low yields (<10%, see Section 2.5.5.8 for details) and only after leaving a suspension of the mixed-valence precursor under H$_2$ in the presence of PVP base for over two months. On the other hand, the complex Ru$_2$Cl$_5$(DPPH)$_2$ failed to undergo reduction by H$_2$ to the corresponding Ru$_2^{II, II}$ species (Equation 3.4). Relative insolubility of the respective precursor complexes in toluene (in fact, in most organic solvents) appears to have hampered the reductions.

The difficulties encountered in the synthesis of [RuCl(BDPP)(μ-Cl)]$_2$ via reduction of Ru$_2$Cl$_5$(BDPP)$_2$, and also the failure to obtain the DPPH analogue by the same route, led us to investigate other ways of getting to "Ru(II)-(P–P)" species.

3.4   Other Synthetic Routes to "Ru^{II}(P–P)" Complexes

One of the objectives of the current work was to develop alternative syntheses of "Ru^{II}(P–P)" species (for the reasons stated above) while continuing to utilise the strategy outlined in Scheme 3-I. This part of the chapter describes the synthesis of dinuclear Ru$_2^{II, II}$ complexes using routes other than that outlined in Scheme 3-I.

The choice of ruthenium starting material seems to play a crucial role in determining the results of the phosphine displacement reactions. For example, while the reaction in hexanes of one equivalent of a diphosphine P–P with the ruthenium(III) precursor RuCl$_3$(PPh$_3$)$_2$(DMA) gave the mixed valence Ru$_2$Cl$_5$(P–P)$_2$ complexes[26, 27] (see Section 3.3.1), that with the ruthenium(II) species [RuCl$_2$(PPh$_3$)$_2$]$_2$ generally yielded a mixture of the unreacted precursor, free PPh$_3$ and the $trans$-RuCl$_2$(P–P)$_2$ complexes (P–P = DPPM, DPPE, DPPP, CHIRAPHOS and BDPP). The $trans$-RuCl$_2$(P–P)$_2$ complexes were easily identified by comparison of their respective characteristic ^{31}P resonances, which appear as

singlets, with those of the authentic samples.[§] Reaction of the Ru(II) precursor with DPPB or DIOP resulted in an essentially complete conversion to the known mixed-phosphine species RuCl$_2$(P–P)(PPh$_3$)[13, 15] which were characterised by NMR spectroscopy and elemental analysis.

Of particular note, reaction of the Ru(III) complex RuCl$_3$(PPh$_3$)$_2$(DMA)·DMA solvate (0.1 g, 0.1 mmol) with one equivalent of DPPB in DMA solution instead of in hexanes afforded RuCl$_3$(DPPB)(DMA), **22**, as the initial product (reaction time 16–24 h), as characterised by elemental analysis and IR spectroscopy.[¶] Interestingly, the Ru(II) mixed-phosphine complex RuCl$_2$(DPPB)(PPh$_3$), **23**, (see Section 2.5.2.1) was obtained when the reaction mixture was left stirring for longer periods (4 days). It should be remembered that the mixed-valence Ru$_2$(II, III) dimer, Ru$_2$Cl$_5$(DPPB)$_2$, is the product obtained in the hexanes reaction (Section 3.3.1). The relatively high solubility in DMA of the initially formed Ru(III) product, RuCl$_3$(DPPB)(DMA), perhaps facilitates further reduction to the corresponding Ru$_2$(II, II) complex; triphenylphosphine in the presence of trace water is likely the reducing agent. The DPPB-derivative [RuCl(DPPB)(μ-Cl)]$_2$, **14**, thus formed could then react with free PPh$_3$ in the reaction mixture to generate RuCl$_2$(DPPB)(PPh$_3$). Addition of PPh$_3$ to a solution of **14** indeed results in the immediate formation of RuCl$_2$(DPPB)(PPh$_3$). Conversely, the essentially zero solubility of the Ru$_2$Cl$_5$(P–P)$_2$ complexes in hexanes perhaps slows down or even prevents a Ru$_2$(II, III) to Ru$_2$(II, II) reduction and therefore any further reaction.

---

§ ^{31}P{^{1}H} NMR data for *trans*-RuCl$_2$(P–P)$_2$ complexes; P–P, δ ppm in CDCl$_3$ at 20 °C: DPPM, –8.2;[13] DPPE, 44.5;[13] DPPP, –5.0;[13] *S,S*–CHIRAPHOS, 46.9;[21] *S,S*–BDPP, 8.7 (present work, see Section 2.5.8.4).

¶   Anal. Calcd for RuCl$_3$(DPPB)(DMA), C$_{32}$H$_{37}$NOCl$_3$P$_2$Ru: C, 53.31; H, 5.17; N, 1.94. Found: C, 53.2; H, 5.3; N, 2.2. IR (Nujol, cm^{-1}): ν$_{(CO)}$ at 1602 (m, coordinated DMA).

Two approaches were taken in search of new synthetic routes to "Ru^{II}(P–P)" complexes:

(a) modification within precursor complexes, such as RuCl$_2$(DPPB)(PPh$_3$), which already contain a single diphosphine ligand, and

(b) reactions of non-phosphine containing starting materials, such as *cis*–RuCl$_2$(DMSO)$_4$, with one equivalent of diphosphine ligand per Ru.

3.4.1 Reactions of RuCl$_2$(DPPB)(PPh$_3$), 23

The choice of the Ru(II) mixed-phosphine complex, RuCl$_2$(DPPB)(PPh$_3$), as a starting material for preparation of the dinuclear Ru^{II}-DPPB complex appeared particularly attractive, because the bright green precursor compound is known to dissociate in solution into free PPh$_3$ and the target dinuclear complex, [RuCl(DPPB)(μ-Cl)]$_2$, **14**, in accordance with Equation 3.5.[13] A more detailed description of the mixed-phosphine complex is provided in the next chapter (Section 4.2), while its reactions leading to the formation of dinuclear species containing the "RuCl$_2$(DPPB)" unit are presented in this chapter.
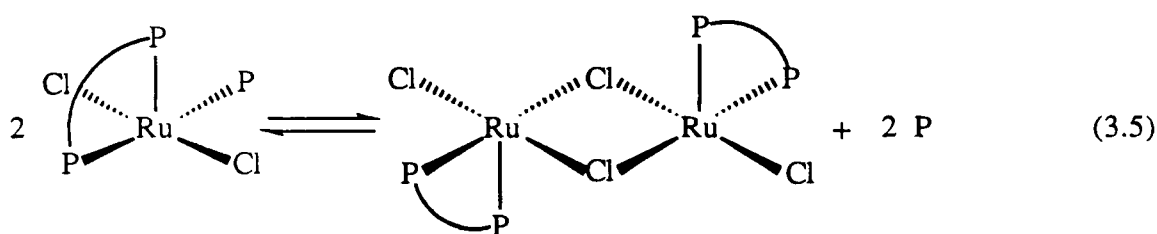
$$P = PPh_3; \quad P\text{---}P = DPPB \text{ (or DIOP)}$$

It should be noted that, like the nonchiral DPPB ligand, the chiral phosphines DIOP and BINAP also form a seven-membered ring upon coordination to the metal. In this respect, it is significant that both DPPB and DIOP form a mixed phosphine complex and a diphosphine-bridged species (RuCl$_2$(P–P)(PPh$_3$) and Ru$_2$Cl$_4$(P–P)$_3$, respectively, see

Figure 3.1). The DPPB and the DIOP analogues show identical solution behaviour (*cf.* Equation 3.5)[13, 15, 16] and the same reactivity with H_2 and CO (Equations 3.6–3.8).[15, 16]

$$Ru_2Cl_4(P-P)_3 + H_2 \longrightarrow RuHCl(P-P)_2 + RuCl_2(P-P) + HCl \quad (3.6)$$

$$Ru_2Cl_4(P-P)_3 + 2H_2 \xrightarrow{\quad P-P \quad} 2RuHCl(P-P)_2 + 2HCl \quad (3.7)$$

$$Ru_2Cl_4(P-P)_3 + 2CO \longrightarrow Ru_2Cl_4(P-P)_3(CO)_2 \quad (3.8)$$
(solid state)
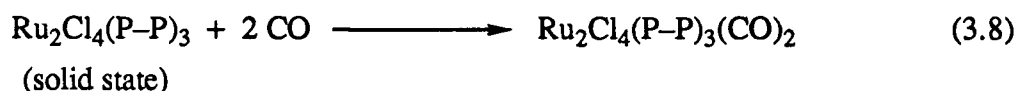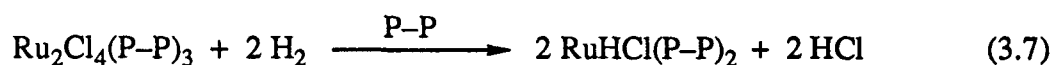
P–P = DPPB or DIOP

The chelate size of diphosphines within a metal complex has been suggested to play an important role in determining the reactivity properties of the complex,[13, 34] with ligands forming chelates of the same size often showing similar reactivity and selectivity in catalytic hydrogenation reactions. It is reasonable therefore to assume that the chemistry involving the DPPB (or DIOP) ligand may be extended to complexes containing the BINAP ligand. Indeed, the mixed-phosphine complex $RuCl_2(BINAP)(PPh_3)$ has been synthesised during the present work (Chapter 4, Section 4.6).

3.4.2 Reactions of Non-phosphine Precursors with One Equivalent of P–P

Several other ruthenium compounds were investigated as possible precursors to "$RuCl_2(P-P)$" species. The reactions summarised in Equations 3.9–3.12 show the expected products. Reactions of $RuCl_3$ and $[RuCl_2(nbd)]_n$ with diphosphines (Equations 3.9 and 3.12) were unsuccessful and gave complex mixtures of products; however, reactions of $RuCl_2(DMSO)_4$ and $[RuCl_2(p\text{-cymene})]_2$ (Equations 3.10 and 3.11) did produce isolable ruthenium-diphosphine complexes of the desired 1:1 stoichiometry, the results being influenced by the choice of the diphosphine ligand (Sections 3.7 and 3.8).

$$RuCl_3 \cdot xH_2O + P-P \longrightarrow RuCl_3(P-P) \qquad (3.9)$$

$$RuCl_2(DMSO)_4 + P-P \longrightarrow RuCl_2(DMSO)_y(P-P), \; _{y \, = \, 1, \, 2} \quad (3.10)$$

$$[RuCl_2(arene)]_2 + P-P \longrightarrow [RuCl(arene)(P-P)]Cl \qquad (3.11)$$

$$[RuCl_2(diene)]_n + P-P \longrightarrow RuCl_2(diene)(P-P) \qquad (3.12)$$

arene = *p*-cymene

diene = 2,5-norbornadiene

3.5 Attempted Removal of PPh₃ from RuCl₂(DPPB)(PPh₃), 23: Reaction of RuCl₂(DPPB)(PPh₃) with Methyl Iodide

The use of a "phosphine sponge" to remove a triphenylphosphine dissociated from RuCl₂(DPPB)(PPh₃) in solution could (Equation 3.5), in principle, yield [RuCl(DPPB)(μ-Cl)]₂. Such a "phosphine sponge" would have to form a stable, easily separable adduct with the dissociated phosphine. Alkyl halides, such as methyl iodide, are known to react with tertiary phosphines, R₃P, to give quaternary phosphonium salts of the type R₃PMe⁺I⁻.[35] These salts are generally insoluble in aromatic solvents and therefore easily removed by filtration.

In preliminary experiments, reactions of RuCl₂(PPh₃)₃ and RuHCl(PPh₃)₃ (0.10 g, 0.1 mmol) with *ca.* 10-fold excess of CH₃I in benzene solution (5 mL) gave encouraging results, wherein quantitative formation (isolated yield) of *only one* equivalent of Ph₃P(CH₃)⁺I⁻ was observed (Equation 3.13). The white precipitate was identified as Ph₃P(CH₃)⁺I⁻ by comparing its ^{31}P chemical shift (21.2 ppm, s, CH₂Cl₂ solution-C₆D₆ lock, 20 °C) with that of an authentic sample.

$$RuXCl(PPh_3)_3 + CH_3I \xrightarrow{\text{benzene, 20 °C}} \text{"RuXCl(PPh}_3)_2\text{"} \qquad (3.13)$$

$$X = Cl, H$$

$$Ph_3P(CH_3)^+I^-$$
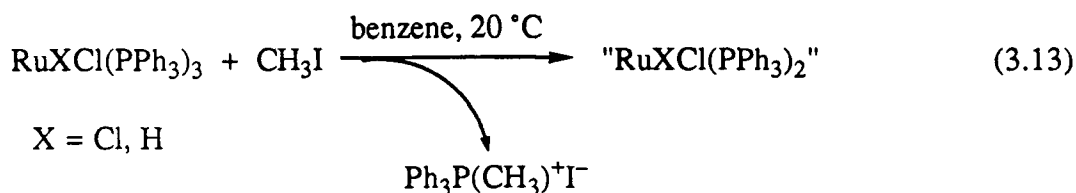
But surprisingly, the dark brown ruthenium products that were isolated from the reactions of the dichloro and the hydridochloro derivatives with MeI exhibited very similar ^{31}P NMR spectra. Two independent sets of ^{31}P NMR AB quartet patterns were observed, each likely indicative of a different, possibly dimeric species ($\delta_A = 56.9$, $\delta_B = 46.9$ ppm, $^2J_{AB} = 31.5$ Hz; $\delta_C = 47.8$, $\delta_D = 42.2$ ppm, $^2J_{CD} = 23.5$ Hz). Presumably, the Ru(II) precursors, or the "RuCl$_2$(PPh$_3$)$_2$" and "RuHCl(PPh$_3$)$_2$" fragments resulting from the PPh$_3$-abstraction (Equation 3.13) react further with the excess CH$_3$I to give the similar set of products which remain uncharacterised.

The reaction of RuCl$_2$(DPPB)(PPh$_3$), **23** (0.10 g, 0.12 mmol), with ~10 times excess methyl iodide was carried out in benzene solution under argon atmosphere. The initially green suspension turned dark brown over ~24 h. The white precipitate of Ph$_3$P(CH$_3$)$^+$I$^-$, tinted slightly pink presumably because of I$_2$ formed from CH$_3$I decomposition, was separated by filtration (65% isolated yield). The ^{31}P NMR spectrum (C$_6$D$_6$, 20 °C) of the brown solid obtained by work-up of the filtrate did exhibit an AB quartet pattern ($\delta_A = 71.1$, $\delta_B = 56.6$ ppm, $^2J_{AB} = 40.0$ Hz) indicating the presence of a possibly dimeric complex. However, these ^{31}P NMR parameters are quite different from the shifts for the known [RuCl(DPPB)(μ-Cl)]$_2$ complex ($\delta_A = 64.0$, $\delta_B = 54.9$ ppm, $^2J_{AB} = 47.3$ Hz). Again, the precursor complex **23**, or the chloro-bridged dimer [RuCl(DPPB)(μ-Cl)]$_2$ formed *in situ* by PPh$_3$-dissociation/abstraction from **23** (see Equations 3.5 and 3.13) likely reacts with the excess CH$_3$I to give the observed, as yet unidentified product. Of particular note, the reaction of pure [RuCl(DPPB)(μ-Cl)]$_2$, **14**, with ~100-fold excess of methyl iodide in CDCl$_3$ solution led to the *in situ* partial formation of a different product, as monitored by phosphorus NMR spectroscopy ($\delta_A = 52.6$, $\delta_B = 51.7$ ppm, $^2J_{AB} = 43.4$ Hz; $\delta_C = 48.6$, $\delta_D = 41.8$ ppm, $^2J_{CD} = 36.7$ Hz); the new complex is identified as a trichloro-bridged dinuclear ruthenium complex with a coordinated methyl iodide (see below, and Section 3.6.5 for details).

3.6 Synthesis of Trichloro-bridged Diruthenium(II,II) Complexes, [(L)(DPPB)Ru(μ-Cl)₃RuCl(DPPB)]

As mentioned in Section 3.2, the dimeric $[RuCl(P-P)(\mu-Cl)]_2$ complexes readily form solvent-coordinated adducts in coordinating solvents (Equation 3.3). In fact, the acetone adducts (P–P = DPPB, **14a**; CHIRAPHOS, **16a**) have been previously isolated and characterised by elemental analysis and IR spectroscopy ($\nu_{(C=O)}$, cm⁻¹, for coordinated acetone: 1645, **14a**; 1624, **16a**).[27, 28] Also, solutions of the acetone adducts were found to be relatively more stable to air-oxidation on account of the saturated coordination sphere about the ruthenium centres; however, the catalytic hydrogenation activity of **14a** and **16a** remained essentially same as that of the corresponding $[RuCl(DPPB)(\mu-Cl)]_2$ complexes.

Reactions of $RuCl_2(DPPB)(PPh_3)$, **23**, with a variety of ligands were investigated with the objective of trapping as a ligand adduct the $[RuCl(DPPB)(\mu-Cl)]_2$ species formed by PPh_3-dissociation (Equation 3.5). This would provide a convenient shorter route into the dimer chemistry. The synthesis and characterisation of some trichloro-bridged $[(L)(DPPB)Ru(\mu-Cl)_3RuCl(DPPB)]$ complexes are described in Sections 3.6.1 through 3.6.5, while the ^{31}P NMR spectra of these compounds are discussed in Section 3.7.

3.6.1 Synthesis of [(Amine)(DPPB)Ru(μ-Cl)₃RuCl(DPPB)], (Amine = NEt₃, 14b; NHBu₂, 14c)

In recent years Noyori, Takaya and coworkers have reported on the enantioselective hydrogenation catalysed by Ru(II)-BINAP complexes.[36, 37] They have noted that the dinuclear complex $Ru_2Cl_4(BINAP)_2(NEt_3)$ is a highly effective catalyst precursor for the asymmetric reduction of functionalised substrates including ketones.[38, 39]

The DPPB analogue, $Ru_2Cl_4(DPPB)_2(NEt_3)$, **14b**, can be easily obtained by addition of triethylamine to a solution of $[RuCl(DPPB)(\mu-Cl)]_2$, **14**. Moreover, the amine

appears to act as a base during an overall heterolytic activation of H_2, and help generate a Ru(II)-hydridochloride species (see Chapter 5).

Stirring a benzene or toluene solution of the mixed-phosphine complex $RuCl_2(DPPB)(PPh_3)$, **23**, with ~20-fold excess of triethylamine precipitates an orange solid. Filtration, followed by a washing of the solid with ethanol and hexanes to remove PPh_3 and excess NEt_3, yields the analytically pure $Ru_2Cl_4(DPPB)_2(NEt_3)$, **14b** (*cf.* Scheme 3-II). The methylene and the methyl ^1H NMR signals of the free NEt_3 ligand at 2.39 (q, 6H) and 0.95 (t, 9H) ppm, respectively, are shifted on coordination to 3.20 (broad m, 6H) and 1.08 (broad m, 9H) ppm.

Reaction of $RuCl_2(DPPB)(PPh_3)$, **23**, with tri-*n*-butylamine, in benzene:hexane (1:4) under reflux conditions, similarly yielded an orange-brown amine adduct, **14c**. Examination of the ^1H NMR spectrum of this product (Figure 3.9) revealed that the integral intensities for the amine protons, relative to those of the DPPB ligand protons, did not correspond to those expected for a bound $N[(CH_2)_3CH_3]_3$. For example, the triplet at 0.95 ppm assigned to the methyl protons of the butyl group integrates to ~6H instead of the expected 9H; the product actually contains a coordinated di-*n*-butylamine ligand, and indeed the IR spectrum of the complex shows a band at 1571 cm^{-1} (m) which is assigned to the N–H bending mode characteristic of secondary amines.[40] This band is absent in the IR spectrum of the NEt_3-analogue. Reactions of **14** or **23** with di-*n*-butylamine also yield $Ru_2Cl_4(DPPB)_2(NHBu_2)$, **14c**, as confirmed by NMR and IR spectroscopy and by elemental analysis. The ^{31}P NMR spectra of **14b** and **14c** in $CDCl_3$ showed a single resonance at 48.3 and 48.2 ppm, respectively, from 30 to –60 °C (see Section 3.7 for details).

Formation of $NHBu_2$ from NBu_3 in the presence of $RuCl_2(DPPB)(PPh_3)$ was unexpected; the reaction amounts to an overall de-alkenylation of tributylamine. Such conversion of tertiary amines to the secondary and even primary amines, in the presence of transition metal complexes, has been reported previously.[41, 42]
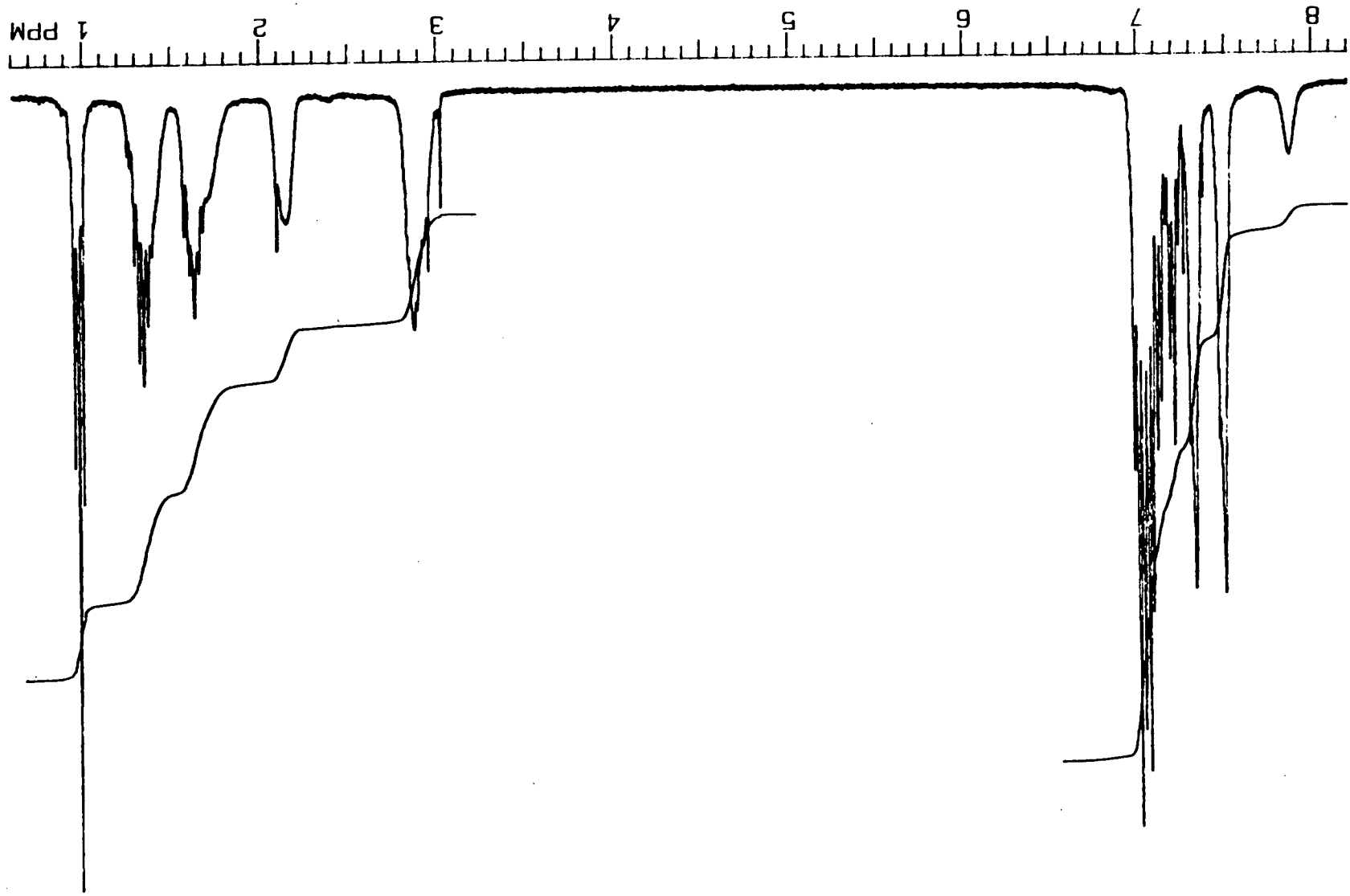
Figure 3.9: ^1H NMR spectrum of $(NHBu_2)(DPPB)Ru(\mu-Cl)_3RuCl(DPPB)$, 14c, in $CDCl_3$ (300 MHz, 20 °C).

3.6.2 Synthesis of [(CO)(DPPB)Ru(μ-Cl)$_3$RuCl(DPPB)], <u>**14d**</u>

Direct reaction of the complexes **14** or **23** with CO yields an isomeric mixture of RuCl$_2$(DPPB)(CO)$_2$ complexes, and some monocarbonyl species 'RuCl$_2$(DPPB)(CO)', and the observed stoichiometry of ~1.8 mole equivalents of CO per Ru (as determined by gas uptake measurements) for the carbonylation of **14** and **23** is consistent with this. The ^{31}P NMR spectrum of the off-white products shows a number of peaks in the 0–50 ppm region, while the infra-red spectrum of the same off-white solid reveals several bands in the 1900–2100 cm^{-1} region assignable to terminal CO ligands. However, the dinuclear carbonyl complex of interest, [(CO)(DPPB)Ru(μ-Cl)$_3$RuCl(DPPB)], **14d**, (see below), was successfully prepared by stoichiometric decarbonylation of aldehydes.

The reaction of **14** with gaseous formaldehyde, acetaldehyde or benzaldehyde in dichloromethane solution, followed by work-up of the reaction mixture as described in Section 2.5.6.3, affords an orange-coloured complex which is identified as [(CO)(DPPB)Ru(μ-Cl)$_3$RuCl(DPPB)], **14d**, by IR and NMR spectroscopy, and elemental analysis (Section 2.5.6.3). The terminal CO stretch in the IR spectrum is observed at 1977 cm^{-1} (s). The phosphorus NMR spectrum in C$_6$D$_6$ consists of two independent AB patterns (designated as AB and CD) centred at 53.55 ($^2J_{AB}$ = 45.2 Hz) and 40.0 ppm ($^2J_{CD}$ = 29.6 Hz), respectively (see Table 3.6 and Section 3.7 for further details).

Decarbonylation of organic carbonyl compounds, such as aldehydes and acid chlorides, by transition metal complexes is a well-known reaction;[43–46] several ruthenium and rhodium phosphine complexes are known to effect stoichiometric decarbonylation of aldehydes under mild conditions.

Of interest, the reaction of RuCl$_2$(DPPB)(PPh$_3$), **23**, with Mo(CO)$_6$ also yields the carbonyl adduct **14d** by decarbonylation of the hexacarbonyl species. Varshavsky *et al.* have reported on decarbonylation of metal carbonyls by rhodium complexes,[47–49] For example, the reaction of RhCl(PPh$_3$)$_3$ with the carbonyl complexes Mo(CO)$_6$, W(CO)$_6$,

Fe(CO)$_5$, or Ni(CO)$_4$ resulted in a rapid, partial decarbonylation to give phosphine-substituted metal carbonyls and [Rh(CO)$_2$Cl]$_2$ as outlined in Equation 3.14; a complete decarbonylation by [Rh(diene)Cl]$_2$ complexes was noted in the absence of ligands (such as PPh$_3$) capable of stabilizing partially decarbonylated species.[47] Ruthenium phosphine complexes, however, were found to be much less efficient in decarbonylating other metal carbonyl species.[49]

$$M(CO)_n + RhCl(PPh_3)_3 \longrightarrow M(CO)_{n-1}(PPh_3) + M(CO)_{n-2}(PPh_3)_2 \quad (3.14)$$

$$+ 1/2 \, [Rh(CO)_2Cl]_2$$
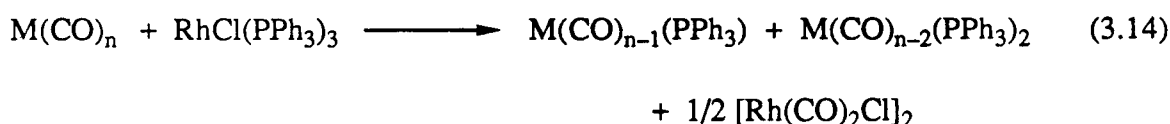
The reaction of RuCl$_2$(DPPB)(PPh$_3$), **23**, with Mo(CO)$_6$ presumably parallels the reaction elucidated in Equation 3.14, the dinuclear CO adduct **14d** being the ruthenium product.

3.6.3   Synthesis of [(DM<u>S</u>O)(DPPB)Ru(μ-Cl)$_3$Ru(Cl)(DPPB)], <u>14e</u>

Addition of one equivalent of DPPB to a dichloromethane:acetone (1:1) solution of *cis*–RuCl$_2$(DMSO)$_4$ causes a rapid change in the colour of the solution, the initially bright yellow solution turning bright orange. A small amount of a green precipitate (< 2%), that formed during the reaction, was identified as the known phosphine-bridged species [RuCl$_2$(DPPB)$_{1.5}$]$_2$ (see Figure 3.1 and Section 2.5.11.1).[16] Dark red crystals of the DMSO adduct [(DM<u>S</u>O)(DPPB)Ru(μ-Cl)$_3$Ru(Cl)(DPPB)], **14e**, were isolated from a concentrated orange filtrate as a Et$_2$O/CH$_2$Cl$_2$ solvate (0.67:0.33 per molecule, ^{1}H NMR spectral and X-ray crystallographic evidence, see below) by slow recrystallisation with diethyl ether at 0 °C. The intense IR absorption band at 1090 cm^{-1} assigned to the S=O stretch of the bound DMSO is within the range reported for an S-bonded sulphoxide ligand (1060–1130 cm^{-1}) in other ruthenium complexes;[50] the S=O stretch for an O-bonded

101

sulphoxide is observed generally in the range 920–980 cm^{-1}.[50] For example, the S=O

stretches for the S-bonded DMSO of cis–RuCl$_2$(DMSO)$_4$ appear at 1125 and 1095 cm^{-1},

while that for the O-bonded sulphoxide is observed at 925 cm^{-1}.[51, 52]

Phosphorus NMR spectrum of **14e** in C$_6$D$_6$ consists of two independent, equal

intensity AB patterns (designated as AB and CD; see Section 3.7 and Table 3.6) centred at

52.1 ($^2J_{AB}$ = 43.8 Hz) and 35.3 ppm ($^2J_{CD}$ = 32.1 Hz), respectively.

3.6.4.   Molecular Structure of [(DMSO)(DPPB)Ru(μ-Cl)$_3$Ru(Cl)(DPPB)]

The single crystal X-ray diffraction study of the DMSO adduct **14e**, carried out by

Dr. S. J. Rettig of this department, reveals the complex to be the dinuclear trichloro-

bridged species with the S-bonded dimethyl sulphoxide ligand as shown in Figure 3.10.

The various structural parameters are given in the Appendix (A-2.2), and some selected

bond lengths and bond angles are listed in Tables 3.4 and 3.5, respectively.

The geometry about each ruthenium in **14e** is irregular octahedral. The bond

distances Ru(1)–S (2.244 Å), S–O (1.474 Å), and Ru(1)–Cl(3) (2.429 Å) for the bridging

chloride *trans* to DMSO, are comparable to those found in *cis*–RuCl$_2$(DMSO)$_4$ (average

2.276, 1.485 and 2.435 Å, respectively)[53] and *fac*-[RuCl$_3$(DMSO)$_3$]$^-$ complexes (average

2.262, 1.477 and 2.426 Å, respectively),[54] which also contain S-bonded sulphoxides *trans*

to a chloride ligand. The slight shortening of the Ru–S bond of **14e** is likely because of

the reduced *trans* influence of the bridging chloride as compared to that of a terminal Cl.

While the respective Ru(1)–P(1, 2) and Ru(2)–P(3, 4) bond lengths of 2.305 and 2.26 Å

(average ~2.28 Å) are within normal range found for Ru(II) tertiary phosphine

complexes,[55–57] the difference between the two sets is indicative of the different

environments about the Ru(II) centres. The Ru–Cl bond length for the bridging chlorides

which are *trans* to phosphorus (average 2.493 Å) is longer than the Ru(2)–Cl(1) distance
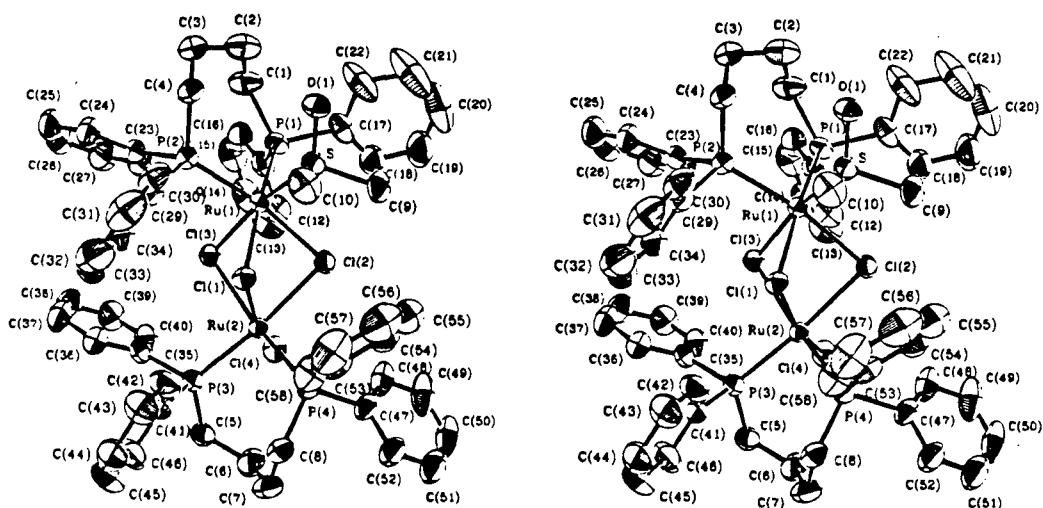
Figure 3.10: An ORTEP stereoview of [(DMSO)(DPPB)Ru(μ-Cl)₃Ru(Cl)(DPPB)] showing the atom numbering scheme used. The thermal ellipsoids for non-hydrogen atoms are drawn at 50% probability. See Appendix A2.2 (p. 296) for a larger view.

Table 3.4: Selected Bond Lengths (Å) for [(DMSO)(DPPB)Ru(μ-Cl)₃Ru(Cl)(DPPB)] with Estimated Standard Deviations in Parentheses.

Bond	Length (Å)	Bond	Length (Å)
Ru(1)—Cl(1)	2.469(1)	Ru(2)—Cl(1)	2.418(1)
Ru(1)—Cl(2)	2.495(1)	Ru(2)—Cl(2)	2.517(1)
Ru(1)—Cl(3)	2.429(1)	Ru(2)—Cl(3)	2.492(1)
Ru(1)—S(1)	2.244(1)	Ru(2)—Cl(4)	2.399(1)
Ru(1)—P(1)	2.305(1)	Ru(2)—P(3)	2.261(1)
Ru(1)—P(2)	2.305(1)	Ru(2)—P(4)	2.257(1)
P(1)—O(1)	3.433(3)	S(1)—C(9)	1.788(5)
S(1)—O(1)	1.474(3)	S(1)—C(10)	1.792(5)
Ru(1)—Ru(2)	3.3542(4)		

Table 3.5: Selected Bond Angles (deg) for [(DMSO)(DPPB)Ru(μ-Cl)₃Ru(Cl)(DPPB)] with Estimated Standard Deviations in Parentheses.

Bonds	Angle (deg)	Bonds	Angle (deg)
Cl(1)—Ru(1)—Cl(2)	78.25(3)	Cl(1)—Ru(2)—Cl(2)	78.78(3)
Cl(1)—Ru(1)—Cl(3)	78.46(3)	Cl(1)—Ru(2)—Cl(3)	78.23(3)
Cl(1)—Ru(1)—S(1)	91.86(4)	Cl(1)—Ru(2)—Cl(4)	163.48(4)
Cl(1)—Ru(1)—P(1)	172.23(4)	Cl(1)—Ru(2)—P(3)	102.24(4)
Cl(1)—Ru(1)—P(2)	93.62(4)	Cl(1)—Ru(2)—P(4)	94.23(4)
Cl(2)—Ru(1)—Cl(3)	80.80(3)	Cl(2)—Ru(2)—Cl(4)	79.18(3)
Cl(2)—Ru(1)—P(1)	94.73(4)	Cl(2)—Ru(2)—Cl(4)	88.45(4)
Cl(2)—Ru(1)—P(2)	169.35(4)	Cl(2)—Ru(2)—P(3)	172.71(4)
Cl(2)—Ru(1)—S(1)	91.94(4)	Cl(2)—Ru(2)—P(4)	95.12(4)
Cl(3)—Ru(1)—P(1)	97.29(4)	Cl(3)—Ru(2)—P(3)	93.92(4)
Cl(3)—Ru(1)—P(2)	90.90(4)	Cl(3)—Ru(2)—P(4)	171.26(4)
Cl(3)—Ru(1)—S(1)	168.87(4)	Cl(3)—Ru(2)—Cl(4)	89.18(4)
P(1)—Ru(1)—S(1)	91.68(4)	Cl(4)—Ru(2)—P(3)	93.92(4)
P(2)—Ru(1)—S(1)	95.23(4)	Cl(4)—Ru(2)—P(4)	89.13(4)
P(1)—Ru(1)—P(2)	92.93(4)	P(3)—Ru(2)—P(4)	92.00(4)
Ru(1)—S(1)—O(1)	120.8(1)	O(1)—S(1)—C(9)	105.6(2)
Ru(1)—S(1)—C(9)	112.6(2)	O(1)—S(1)—C(10)	104.9(2)
Ru(1)—S(1)—C(10)	112.7(2)	C(9)—S(1)—C(10)	97.5(3)
Ru(1)—Cl(1)—Ru(2)	86.69(3)	Ru(1)—Cl(2)—Ru(2)	85.01(3)
Ru(1)—Cl(3)—Ru(2)	85.93(3)		

104

(2.418 Å) where Cl(1) is *trans* to the terminal chloride Cl(4). The stronger trans influence of phosphine, compared to chloride, clearly results in a weaker and consequently longer bond.

Two regular octahedra sharing one face have a bridging angle $\emptyset$ of 70.5° (given by $\cos \emptyset/2 = 2/3$).[57] In this complex the average bridging angle ($\angle$ Ru–Cl–Ru) is 85.54°, implying that the two Ru atoms are further apart than they would be in a regular cofacial bioctahedron. Indeed, the distance between the ruthenium centres (3.35 Å) is well outside the range (2.28–2.95 Å) usually observed for a Ru–Ru bond.[25, 58, 59]

This is perhaps only the second crystal structure of a dinuclear Ru complex containing a chelating diphosphine, the first being the structure of the formally mixed valence Ru$_2$(II,III)-CHIRAPHOS derivative mentioned earlier (Section 3.2).[26, 27] The two structures are drawn schematically in Figure 3.11 for comparison.

P—P = DPPB   P—P = *S,S*-CHIRAPHOS

a   b
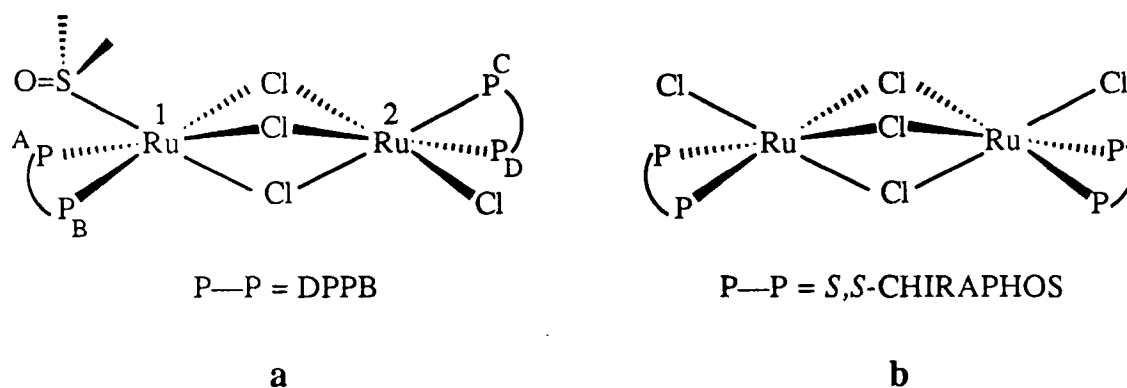
Figure 3.11: Geometry of a) [Ru$_2$Cl$_4$(DPPB)$_2$(DMSO)], **14e** and,
b) [Ru$_2$Cl$_5$(CHIRAPHOS)$_2$], **4**.[26, 27]

The various bond lengths and bond angles in the two complexes are very similar in spite of the different formal oxidation states (i.e. II, II *vs.* II, III) at the ruthenium centres. However, there is one striking difference in the geometries: unlike in the highly symmetrical CHIRAPHOS complex, the positioning of the diphosphines in the DPPB complex is unsymmetrical in that one of the octahedra has been rotated by ±120° about the

Ru–Ru vector. The analogous $Ru_2^{II, II}$ thiocarbonyl complex containing triphenyl-phosphines, $[(CS)(PPh_3)_2Ru(\mu\text{-}Cl)_3RuCl(PPh_3)_2]$, reported by Fraser and Gould[56b] also shows a similar unsymmetrical arrangement of the PPh_3 ligands (Figure 3.12).

$$P = PPh_3$$
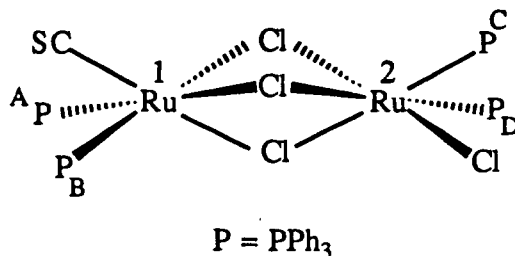
Figure 3.12: Geometry of $[(CS)(PPh_3)_2Ru(\mu\text{-}Cl)_3RuCl(PPh_3)_2]$.[56b]

3.6.5 Other $[(L)(DPPB)Ru(\mu\text{-}Cl)_3Ru(Cl)(DPPB)]$ Complexes

Several other trichloro-bridged dinuclear complexes of the general formula $[(L)(DPPB)Ru(\mu\text{-}Cl)_3Ru(Cl)(DPPB)]$ were prepared *in situ* by reaction of various coordinating ligands with the dimeric precursor $[RuCl(DPPB)(\mu\text{-}Cl)]_2$, **14**, or with the mixed-phosphine complex $RuCl_2(DPPB)(PPh_3)$, **23**, and characterised spectroscopically, chiefly using NMR and IR techniques.

Of particular interest is the *in situ* formation of trichloro-bridged dinuclear complexes incorporating molecular hydrogen and dinitrogen ligands ($L = \eta^2\text{-}H_2$ and $\eta^1\text{-}N_2$, respectively) from $[RuCl(DPPB)(\mu\text{-}Cl)]_2$, **14**, under 1 atm of the respective gases.[60] Detailed discussion of their characterisation has been deferred to Chapter 5 of this thesis.

The 'non-nucleophilic' bases Proton Sponge® (PS) and DBU (Figure 3.13) readily coordinate to the DPPB dimer **14**. The ^{31}P NMR AB quartet of **14** in $CDCl_3$ disappeared when either reagent was added, and singlets assigned to $[(PS)(DPPB)Ru(\mu\text{-}Cl)_3RuCl(DPPB)]$ and to the corresponding DBU analogue became apparent at δ 48.4 and at 44.8 ppm, respectively (see Section 3.7).

106
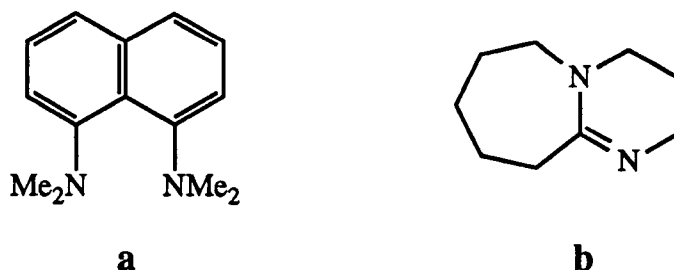
Figure 3.13: The 'non-nucleophilic' bases (a) Proton Sponge® and (b) DBU.

Notably, addition of ~100-fold excess of methyl iodide to a $CDCl_3$ solution of **14** resulted in the appearance in the ^{31}P NMR spectrum of two additional sets of AB patterns, centred at 52.2 and 45.2 ppm, which are assigned to [(MeI)(DPPB)Ru(μ-Cl)$_3$RuCl(DPPB)] (see Section 3.7). Oxidative addition reactions of MeI at a transition metal centre have been studied extensively,[61] but examples of MeI acting as a neutral ligand are rare. Recently, Crabtree and coworkers have reported the synthesis of a series of complexes of the type [Cp*M(L)$_2$(R^{1}I)]$^+$ where M = Ru or Fe; R^1 = Me, Et, p-tolyl, Cy; L = CO, PPh$_3$ or DPPE.[62]

Further, the reaction of **14** or **23** (0.1 mmol) with benzonitrile (2 mL) in CH_2Cl_2 (10 mL) followed by addition of Et$_2$O (20 mL) to the reaction mixture concentrated to 5 mL precipitated a yellow microcrystalline solid, which is identified as a bis(PhCN)-coordinated dinuclear species, [RuCl(DPPB)(PhCN)(μ-Cl)]$_2$. A single infra-red C≡N stretch for the two end-on coordinated benzonitrile ligands is observed at 2238 cm^{-1} (m). The principal resonance in the ^{31}P NMR spectrum ($CDCl_3$, 20 °C) of the bis(nitrile) derivative consists of a single AB pattern (δ_A = 48.8, δ_B = 45.2 ppm, $^2J_{AB}$ = 35.7 Hz; Figure 3.14). Examination of the proton NMR spectrum confirms the presence of only one PhCN ligand per Ru-DPPB unit based on proton integral intensities (Figure 3.15). The observed IR and NMR spectral data are consistent with the dinuclear bis(PhCN) formulation of structure **3-I**; a singlet phosphorus resonance would be expected for a complex of geometry **3-II**.

Analogous bis(nitrile)diruthenium complexes, containing monodentate phosphines in place of the bidentate DPPB, have been reported previously by Cole-Hamilton and Wilkinson.[63] Similar symmetric structures have been proposed to explain the presence of a single IR stretch for $C\equiv N$, and a single AB quartet observed in the ^{31}P NMR spectra of the [RuCl$_2$(PPh$_3$)$_2$(RCN)]$_2$ analogues, where RCN = CH_3CN, PhCN.[63] Some mononuclear complexes containing nitrile and chelating phosphine ligands (e.g. RuCl$_2$(DPPE)(RCN)$_2$; R = Me, Et) are also known.[64]

3-I   L = PhCN   3-II
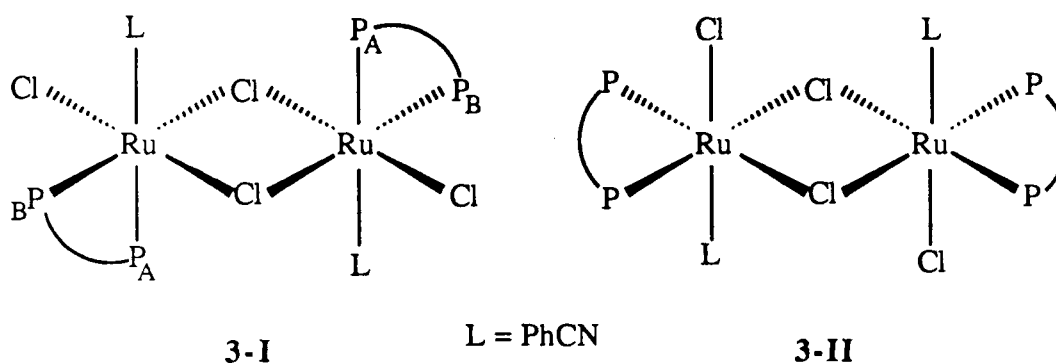
An additional pair of AB quartets of ~15% total integral intensity, seen in the phosphorus NMR spectrum of the bis(benzonitrile) complex (Figure 3.14), is assigned to the mono(benzonitrile) species [(PhCN)(DPPB)Ru(μ-Cl)$_3$RuCl(DPPB)], 14f, formed by PhCN-dissociation in solution (Equation 3.15).

$$[RuCl(DPPB)(PhCN)(\mu\text{-}Cl)]_2 \rightleftharpoons [(PhCN)(DPPB)Ru(\mu\text{-}Cl)_3RuCl(DPPB)] \quad (3.15)$$

14f
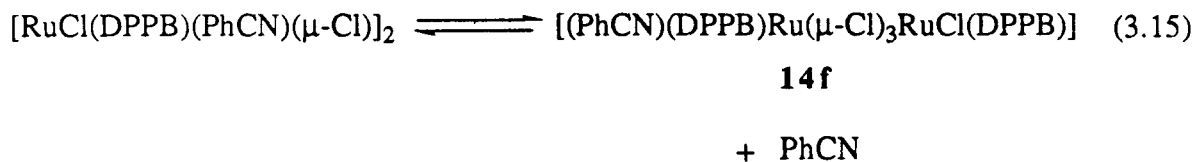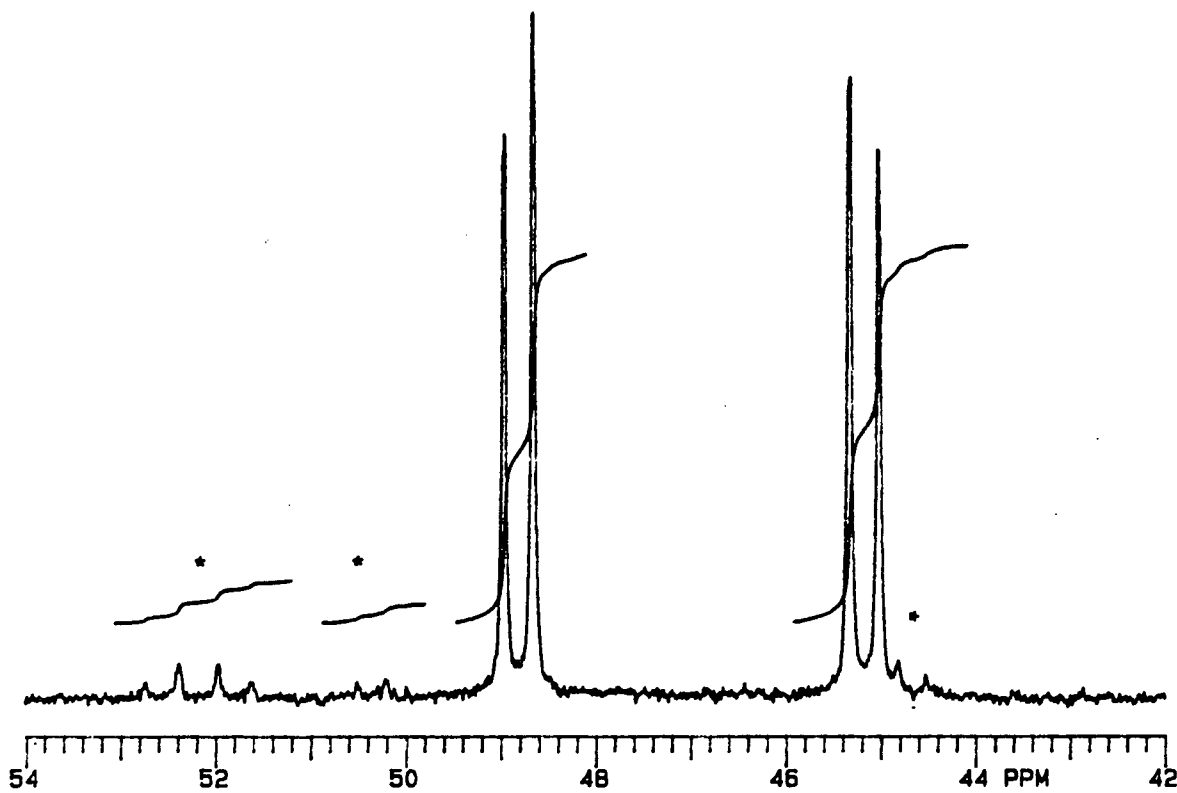
+ PhCN

Figure 3.14: $^{31}P\{^1H\}$ NMR spectrum of [RuCl$_2$(DPPB)(PhCN)]$_2$ in CDCl$_3$ (121.42 MHz).
The peaks marked with asterisks belong to Ru$_2$Cl$_4$(DPPB)$_2$(PhCN), **14f**; see text.
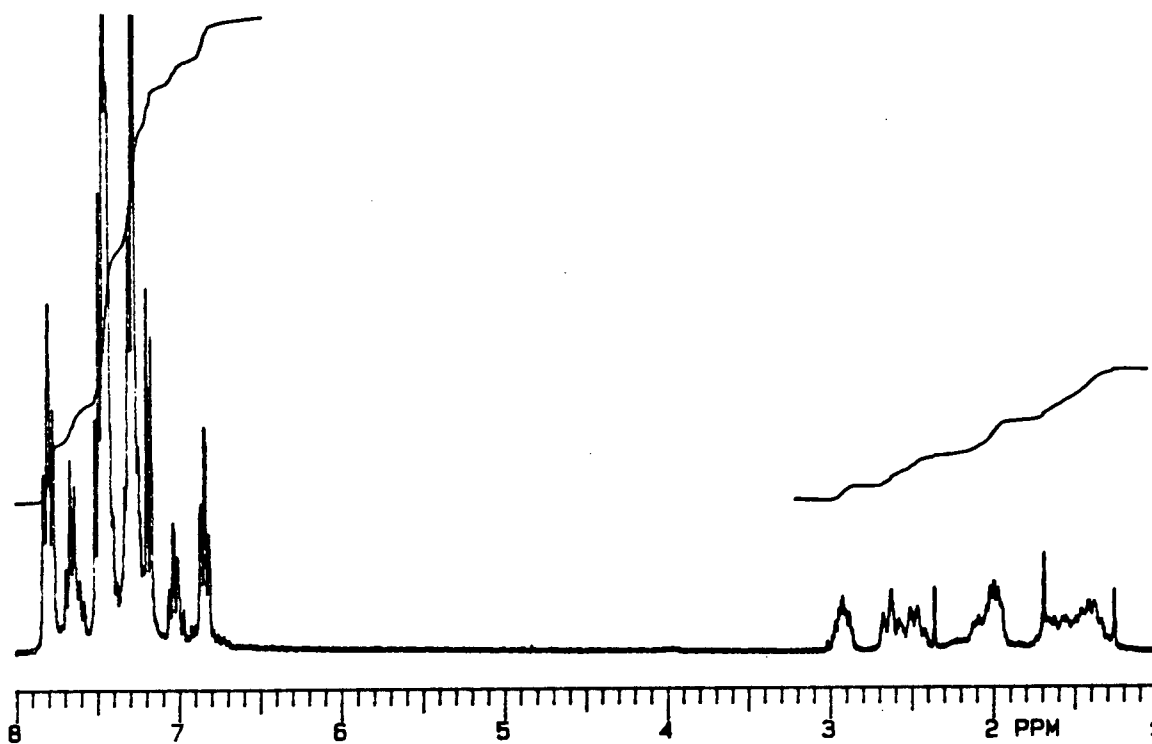
Figure 3.15: ^1H NMR spectrum of [RuCl$_2$(DPPB)(PhCN)]$_2$ in CDCl$_3$ (300 MHz, 20 °C).

3.7 NMR Studies on [(L)(DPPB)Ru(μ-Cl)₃Ru(Cl)(DPPB)] Complexes

3.7.1 ³¹P{¹H} Solution NMR Studies

The ambient temperature $^{31}P\{^{1}H\}$ NMR spectra of C_6D_6 or $CDCl_3$ solutions of the complexes $Ru_2Cl_4(DPPB)_2(L)$, where $L = Me_2CO$, CO, Me_2SO, PhCN, MeI, or DMA, all consist of two independent AB quartet patterns of equal integral intensity. The data are summarised in Table 3.6. The presence of two independent AB patterns (assigned as AB and CD) is consistent with the unsymmetric, trichloro-bridged dinuclear structure of these species in solution (Figure 3.16). In the absence of a ligand (L) dissociation/re-association process, or in a system where such a process is slow on the NMR time-scale, the two ruthenium centres are different, making all four phosphorus nuclei chemically and magnetically inequivalent; this would give rise to two ^{31}P NMR AB patterns of equal intensity. The single crystal X-ray study on the Me_2SO-adduct **14e** shows that the same unsymmetrical arrangement of the DPPB ligands relative to each other is maintained in the solid state (Section 3.6.4).
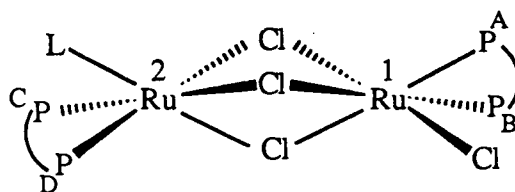
Figure 3.16: Proposed structure of $Ru_2Cl_4(DPPB)_2(L)$ complexes.

It should be noted that for a complex, containing a nonchiral diphosphine such as DPPB, a symmetric dinuclear structure possessing a plane of symmetry through the terminal and one of the bridging chlorides and the coordinated ligand L would render P_A equivalent to P_B and P_C to P_D (Figure 3.17); this would likely result in just two singlets of equal integral intensity in the ^{31}P NMR spectrum.

Table 3.6: $^{31}P\{^1H\}$ NMR Data (121.42 MHz, 20 °C) for the Trichloro-Bridged Dinuclear Complexes, $[(L)(DPPB)Ru(\mu\text{-}Cl)_3Ru(Cl)(DPPB)]$.

L (Complex)	Solvent	Chemical Shifts, δ (ppm)	$^2J_{PP}$, (Hz)
Me$_2$CO (**14a**)	C$_6$D$_6$	$\delta_A = 52.8$, $\delta_B = 51.5$	43.7
		$\delta_C = 50.1$, $\delta_D = 48.7$	38.4
CO (**14d**)	C$_6$D$_6$	$\delta_A = 53.8$, $\delta_B = 53.3$	45.2
		$\delta_C = 46.9$, $\delta_D = 33.1$	29.6
Me$_2$SO (**14e**)	C$_6$D$_6$	$\delta_A = 53.6$, $\delta_B = 50.6$	43.8
		$\delta_C = 41.6$, $\delta_D = 28.9$	32.1
	CDCl$_3$	$\delta_A = 53.5$, $\delta_B = 50.7$	42.6
		$\delta_C = 41.6$, $\delta_D = 29.3$	32.5
	DMSO-d_6	$\delta_A = 53.9$, $\delta_B = 51.6$	43.8
		$\delta_C = 42.8$, $\delta_D = 32.3$	32.0
PhCN (**14f**)	C$_6$D$_6$	$\delta_A = 52.6$, $\delta_B = 51.8$	42.1
		$\delta_C = 50.3$, $\delta_D = 44.7$	36.5
MeI (**14g**)[a]	CDCl$_3$	$\delta_A = 52.6$, $\delta_B = 51.7$	43.4
		$\delta_C = 48.6$, $\delta_D = 41.8$	36.7
DMA (**14h**)[a]	C$_6$D$_6$	$\delta_A = 53.5$, $\delta_B = 52.2$	43.6
		$\delta_C = 52.7$, $\delta_D = 50.7$	39.6
	CDCl$_3$	$\delta_A = 52.2$, $\delta_B = 50.3$	43.3
		$\delta_C = 51.4$, $\delta_D = 49.2$	39.9
NEt$_3$ (**14b**)	CDCl$_3$	48.3, s	—
NHBu$_2$ (**14c**)	CDCl$_3$	48.2, s	—
Proton Sponge[a]	CDCl$_3$	48.4, s	—
DBU[a]	CDCl$_3$	44.8, s	—

a   These complexes were prepared *in situ* by reaction of **14** with the appropriate ligand.
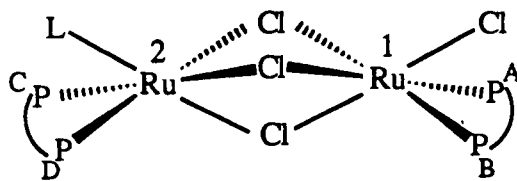
Figure 3.17: A symmetric dinuclear structure for Ru$_2$Cl$_4$(DPPB)$_2$(L) complexes.

The ^{31}P{^{1}H} spectra for some Ru$_2$Cl$_4$(DPPB)$_2$(L) complexes (L = Me$_2$CO, **14a**; CO, **14d**; Me$_2$SO, **14e**; MeI, **14g**; DMA, **14h**) are shown in Figures 3.18a through 3.18e. The relatively lower field AB pattern is quite insensitive to the nature of the coordinated ligand (L) as it remains essentially invariant in position (δ_{AB} ~52±1) as well as in the magnitude of the coupling constant ($^2J_{AB}$ ~44±1 Hz). It is therefore assigned to the resonances of the $-$Cl$_3$Ru^1(Cl)(P–P) portion of the molecule, which is in a locked conformation. The other set of signals is, however, much more sensitive to the nature of L as evidenced from the much larger spread of chemical shifts (δ_{CD} ~35–52) and coupling constants ($^2J_{CD}$ ~29–40 Hz; see Table 3.6) and is therefore attributed to the (L)(P–P)Ru^2(μ-Cl)$_3$– fragment of the molecule.

Also apparent in the spectra of the MeI, and DMA adducts (Figure 3.18d, 3.18e) are the resonances due to the dichloro-bridged complex [RuCl(DPPB)(μ-Cl)]$_2$, **14** (δ = 59.5 ppm, $^2J_{PP}$ = 47 Hz). This implies that the binding of these ligands to ruthenium is relatively weak, and only a partial equilibrium conversion to the trichloro-bridged species occurs even in the presence of *ca.* 100-fold excess of the respective ligands. Some **14** is also present in solutions of the acetone analogue **14a** (Figure 3.18a). The ligand exchange must be slow on the NMR time scale because resonances of the individual species are observed. In contrast, the Me$_2$SO and the CO complexes show no evidence of ligand dissociation to the dichloro-bridged precursor (Figure 3.18b, 3.18c), consistent with the much stronger binding of CO and Me$_2$SO to ruthenium.
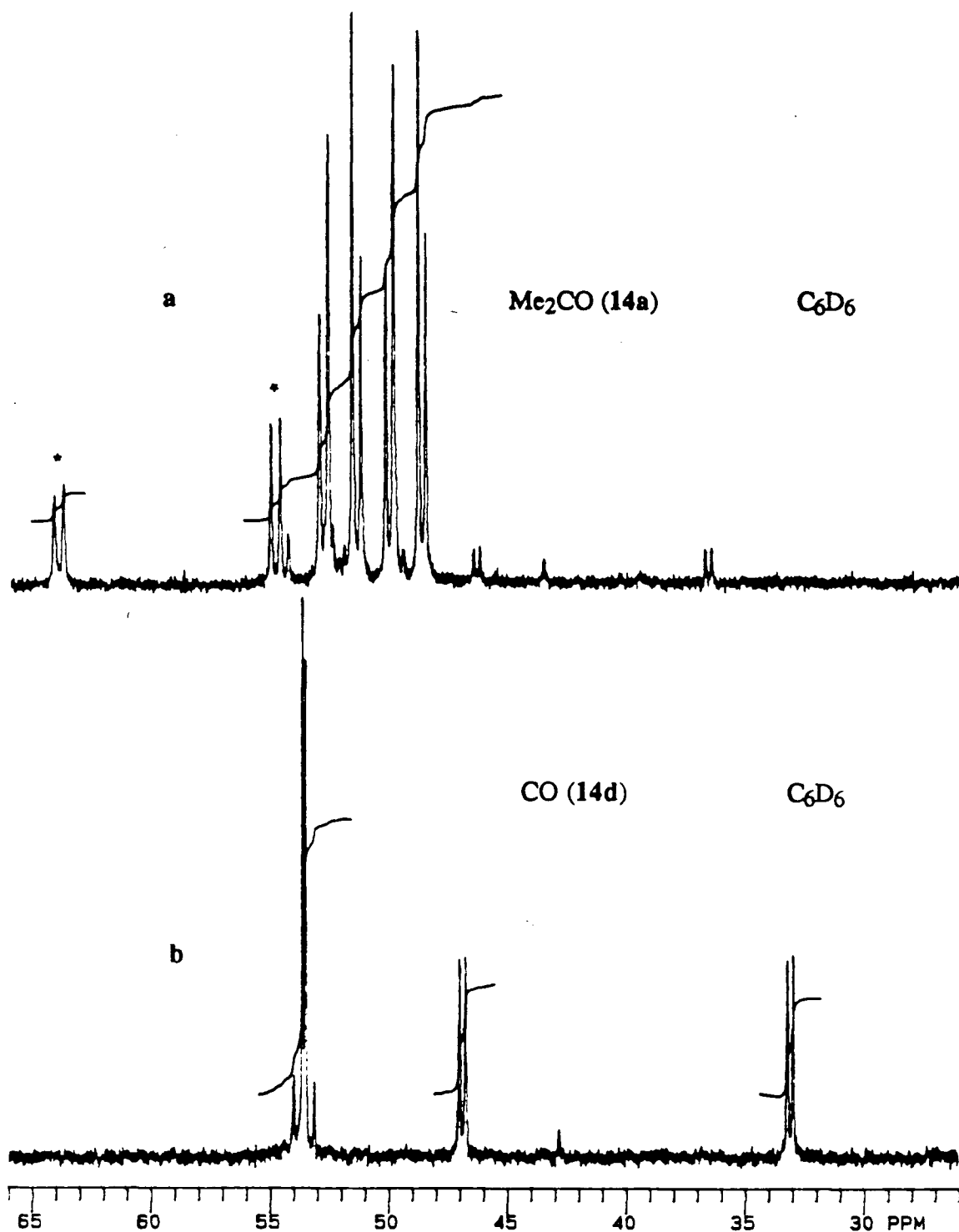
Figure 3.18a–e: $^{31}P\{^1H\}$ NMR spectra (121.42 MHz, 20 °C) of [(L)(DPPB)Ru-(μ-Cl)$_3$Ru(Cl)(DPPB)] complexes. The ligand L and the solvent are indicated with each individual spectrum. L = (a) Me$_2$CO; (b) CO; (c) Me$_2$SO; (d) MeI; and (e) DMA. The resonances due to [RuCl(DPPB)(μ-Cl)]$_2$ are marked by asterisks.

113

Figure 3.18, continued:

c

Me$_2$SO (14e)   C$_6$D$_6$

d

MeI (14g)   CDCl$_3$

65   60   55   50   45   40   35   30 PPM

114
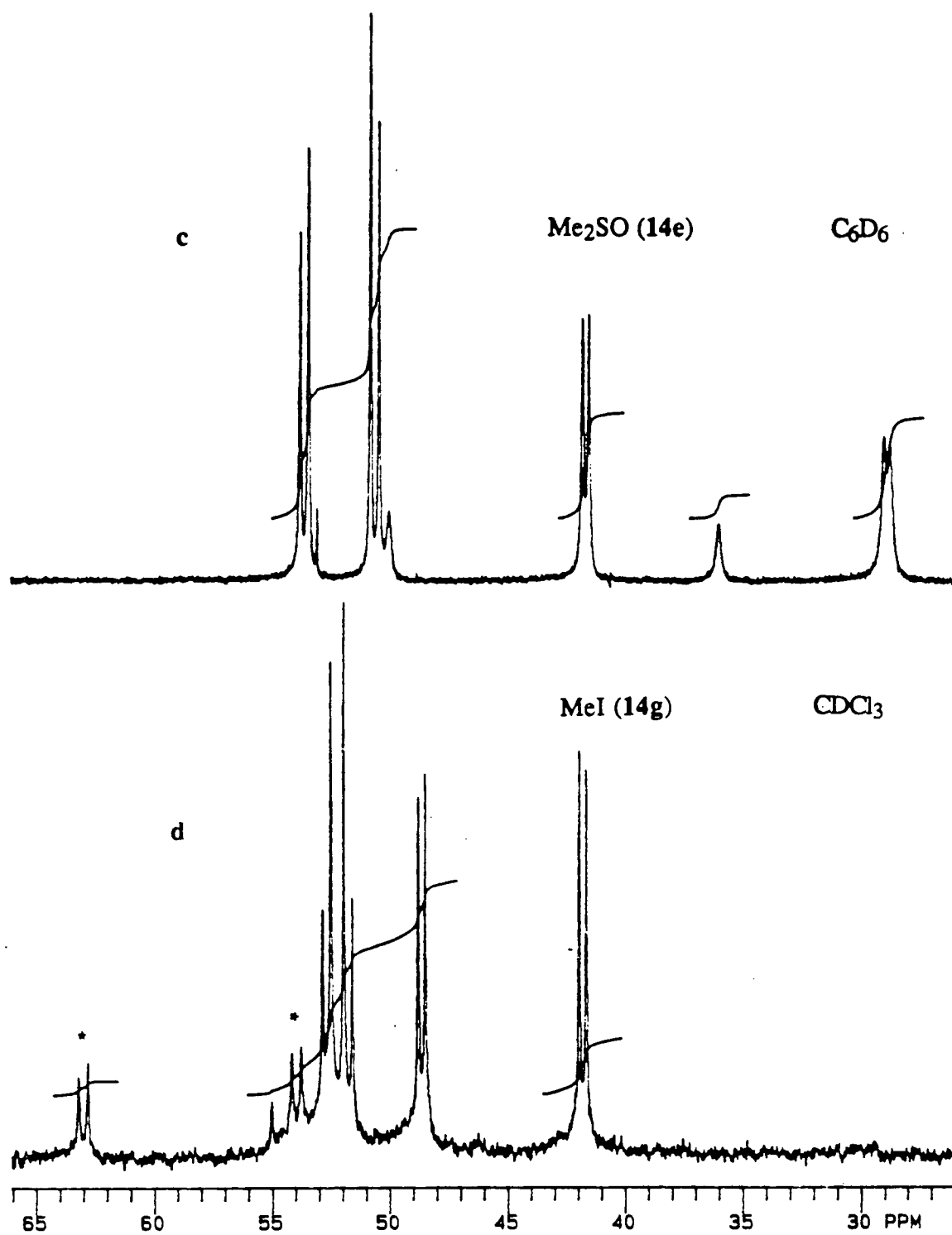
Figure 3.18, continued:
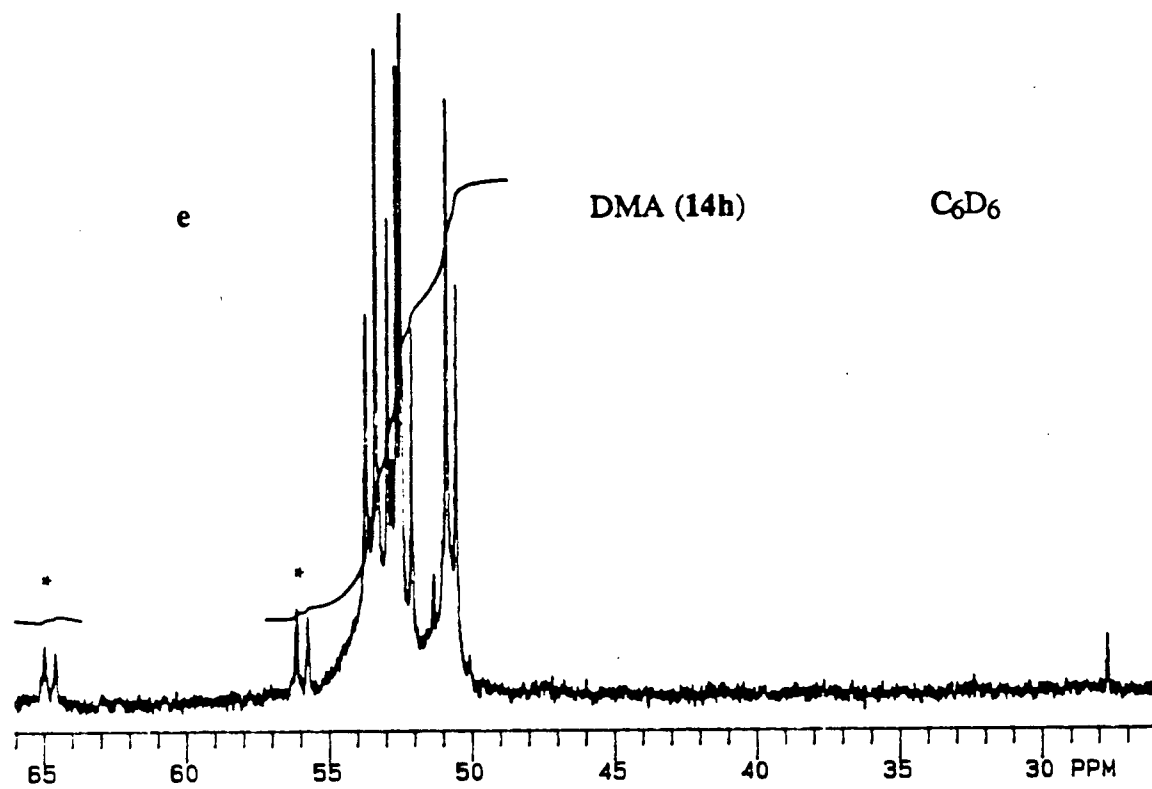
The formation of trichloro-bridged complexes of the type $(L)P_2Ru(\mu\text{-}Cl)_3RuClP_2$, where P is a monodentate phosphine (L = CO,[65] CS,[66] PF$_3$,[67] N$_2$,[68] DMA,[69] acetone[69]), has been reported previously; two sets of ^{31}P NMR AB patterns have been observed in each case, but there is no clear evidence for the existence of a dynamic equilibrium as found in the current study.

The phosphorus NMR spectra of the corresponding amine adducts (L = NEt$_3$, NHBu$_2$, PS, DBU; see Table 3.6) consist of only a sharp singlet at ~48.3 ± 0.2 ppm (at 44.8 ppm when L = DBU) even down to −60 °C. This is explained by a rapid equilibrium on the NMR time scale between the trichloro-bridged Ru$_2$Cl$_4$(DPPB)$_2$(amine) species and the dichloro-bridged complex **14** formed by dissociation of the amine ligand bound to Ru^2 in solution (*cf.* Scheme 3-II); the dissociated amine can then recoordinate to either ruthenium centre, resulting in scrambling of all four phosphorus centres. The ligand dissociation/re-association process must involve both ruthenium centres in the dinuclear complex (Ru^2 and Ru^1). The exchange at only one ruthenium centre (Ru^2) will result in scrambling of the P$_C$ and P$_D$ resonances, assuming that the amine can recoordinate at any one of the three non-bridging sites, but this will not affect the P$_A$ and P$_B$ resonances.

3.8   Reactions of *Cis*–RuCl$_2$(DMSO)$_4$ with Other Bidentate Phosphines

The successful synthesis of the dinuclear Ru(II) complex [(DMSO)(DPPB)Ru-(μ-Cl)$_3$RuCl(DPPB)], **14e**, by reaction of *cis*–RuCl$_2$(DMSO)$_4$ with one equivalent of DPPB as outlined in Sections 3.6.3 and 3.6.4, prompted further investigation into the reactivity of *cis*–RuCl$_2$(DMSO)$_4$ with other chelating phosphine ligands. The studies have been extended to include the phosphines: DPPM, DPPE, and *S,S*-BDPP.

The reactions with one equivalent of DPPM and DPPE yield bright yellow solids (Chapter 2, Section 2.5.7). The products are readily identified by NMR spectroscopy as the previously reported bis(bidentate phosphine) complexes:[9, 13, 70] RuCl$_2$(DPPM)$_2$

116

(100% *cis* isomer) and $RuCl_2(DPPE)_2$ (a 50:50 mixture of *cis* and *trans* isomers, based on NMR spectral intensities). The ^{31}P NMR data are listed in Table 3.7. In each case, resonances of the unreacted precursor complex *cis*–$RuCl_2(DMSO)_4$ (~50%) were apparent in the ^1H NMR spectrum (2–3 ppm region).[71] Addition of excess phosphine to the solution results in a complete conversion to the $RuCl_2(P-P)_2$ species as evidenced by ^1H NMR spectroscopy.

Reaction of *cis*–$RuCl_2(DMSO)_4$ with *S,S*-BDPP produced a mixture of products. The $^{31}P\{^1H\}$ NMR spectrum (Figure 3.19) of the mixture in C_6D_6 reveals two sets of AX patterns of equal intensity, centred at 59.8 and 40.3 ppm ($^2J_{PP}$ = 51.0 and 40.1 Hz, respectively), which are assigned to a trichloro-bridged DMSO adduct [(DMSO)(BDPP)Ru(μ-Cl)$_3$RuCl(BDPP)] by analogy to the corresponding DPPB complex (see Sections 3.6.3 and 3.6.4). The relatively low intensity (~6%) AX patterns centred at 61.8 and 59.6 ppm ($^2J_{PP}$ = 52.1 and 49.0 Hz, respectively) remain unassigned, but probably arise from related dinuclear species. The singlet at 9.2 ppm constituting ~40% of the total intensity is attributed to the *trans*–$RuCl_2$(*S,S*-BDPP)$_2$ complex (observed at 8.7 ppm in CDCl$_3$), which has been isolated by another route and characterised crystallographically (see Section 3.8 and Appendix A-2.3). The S=O stretch for the bound DMSO ligand of [(DMSO)(BDPP)Ru(μ-Cl)$_3$RuCl(BDPP)] is observed at 1089 cm^{-1} in the IR spectrum and is characteristic of coordination through the S atom.[50]
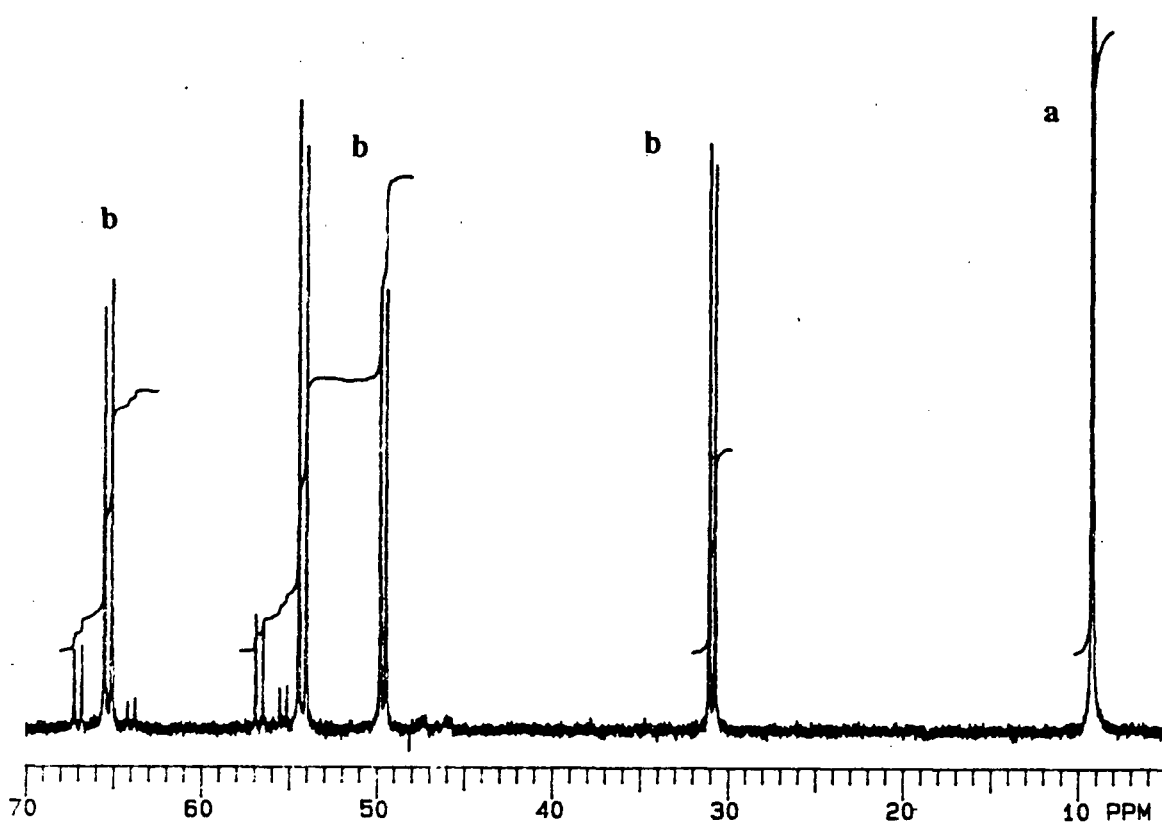
Figure 3.19: $^{31}P\{^1H\}$ NMR spectrum of the mixture of products isolated from the reaction of cis–$RuCl_2(DMSO)_4$ with one equivalent of S,S-BDPP:

(a) trans–$RuCl_2(BDPP)_2$; (b) $[(DMSO)(BDPP)Ru(\mu-Cl)_3RuCl(BDPP)]$

The comparison of reactivity of cis–$RuCl_2(DMSO)_4$ with one equivalent of various bidentate phosphines, viz. DPPM, DPPE, S,S-BDPP, and DPPB, clearly reveals the influence of relative chelate size of the respective ligands (i.e. bite angle and steric factors) on the nature and distribution of the resulting products. The diphosphines DPPM and DPPE, which form four- and five-membered rings, respectively, upon coordination to the metal, give only the bis(P–P) complexes. The use of S,S-BDPP (chelate size six) results in the formation of a mixture of dinuclear "$RuCl_2(P–P)$" species and a mononuclear $RuCl_2(P–P)_2$ complex in ca. 60:40 ratio (see above). In contrast, the reaction of DPPB with $RuCl_2(DMSO)_4$ results in the formation of the dinuclear complex $[(DMSO)(DPPB)Ru(\mu-Cl)_3RuCl(DPPB)]$, 14e, in ~80% isolated yield (see Section 2.5.6.4).

118

Table 3.7: $^{31}P\{^1H\}$ NMR Data (121.42 MHz, C_6D_6, 20 °C) for the Complexes Obtained by the Reaction of Cis–$RuCl_2(DMSO)_4$ with One Equivalent of Bidentate Phosphine.

Complex	Chemical Shifts, δ (ppm)	$^2J_{PP}$, (Hz)
cis–$RuCl_2(DPPM)_2$	$\delta_A = -1.4$, $\delta_B = -27.6$, A_2B_2 pattern	36.2
cis–$RuCl_2(DPPE)_2$	$\delta_A = 51.9$, $\delta_B = 37.2$, A_2B_2 pattern	19.7
$trans$–$RuCl_2(DPPE)_2$	44.5, s	—
$trans$–$RuCl_2(S,S$-$BDPP)_2$	9.2, s	—
[$Ru_2Cl_4(S,S$-$BDPP)_2(DMSO)$]	$\delta_A = 65.3$, $\delta_B = 54.2$, AX pattern	51.0
	$\delta_C = 49.6$, $\delta_D = 30.9$, AX pattern	40.1

3.9 Reactions of [RuCl(p-cymene)(μ-Cl)]$_2$ with Bidentate Phosphines

Previous work from this laboratory has reported on the synthesis of the mononuclear cationic Ru(II) complexes, [RuCl(MeCN)$_3$(DPPB)]$^+$PF$_6^-$ and [RuCl(η^6-$C_6H_5CH_3$)(DPPB)]$^+$PF$_6^-$ (Equation 3.16), which contain a single diphosphine per Ru.[27, 72] The acetonitrile derivative was found to be an active catalyst for the H_2-hydrogenation of imine and nitrile substrates under relatively mild conditions (50 °C, 1 atm of H_2). Reactions of Ru(arene) precursors with one equivalent of a bidentate phosphine were investigated in an attempt to find a synthetic route that would bypass the dinuclear $Ru_2^{II, II}$ complexes (cf. Equation 3.16).

$$[RuCl(DPPB)(\mu\text{-}Cl)]_2 + 2\,AgPF_6 \longrightarrow [RuCl(DPPB)(S)_3]^+PF_6^- \quad (3.16)$$

$$(S) = CH_3CN \quad \text{or} \quad (S)_3 = \eta^6\text{-toluene}$$
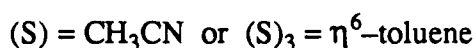
The complex $[RuCl(p\text{-cymene})(\mu\text{-}Cl)]_2$ was chosen as the precursor over other arene analogues (e.g. benzene, toluene, xylene)[73] because of its generally greater solubility in organic solvents. A recent report by Mashima *et al.* describes a series of complexes of the general formula $[RuX(\text{arene})(S\text{-BINAP})]^+X^-$ (X = Cl, Br, I; arene = benzene, toluene, or p-cymene) which have been prepared by reaction of the appropriate arene precursor with one equivalent of S--BINAP.[74]

The corresponding R-BINAP derivative, $[RuCl(p\text{-cymene})(R\text{-BINAP})]^+Cl^-$ has been prepared in high yields (90%) and characterised during the present study (see Section 2.5.8 for details). The ^{31}P NMR spectrum of this complex consists of an AX pattern (δ_A = 40.0, δ_X = 23.5 ppm, $^2J_{AX}$ = 62.5 Hz). The observed parameters are in agreement with those reported by Mashima *et al.* for the S-BINAP analogue.[74] The ^1H NMR spectrum (Figure 3.20) of the complex is consistent with the formulation suggested by Mashima *et al.* (Figure 3.21).[74] Resonances of the BINAP protons are seen spread over the 8.3–6.8 ppm region, while resonances of the aromatic protons of the η^6-bound p-cymene ligand are observed as doublets centred at 6.35, 5.95, 5.90 and 4.30 ppm, respectively (1H each). The singlet at 2.0 ppm is assigned to the lone methyl group of the p-cymene, while resonances due to the methyl of the isopropyl substituent are observed as doublets at 1.35 and 0.95 ppm, respectively. The septet pattern at 3.0 ppm is attributed to the methine proton of the isopropyl group.
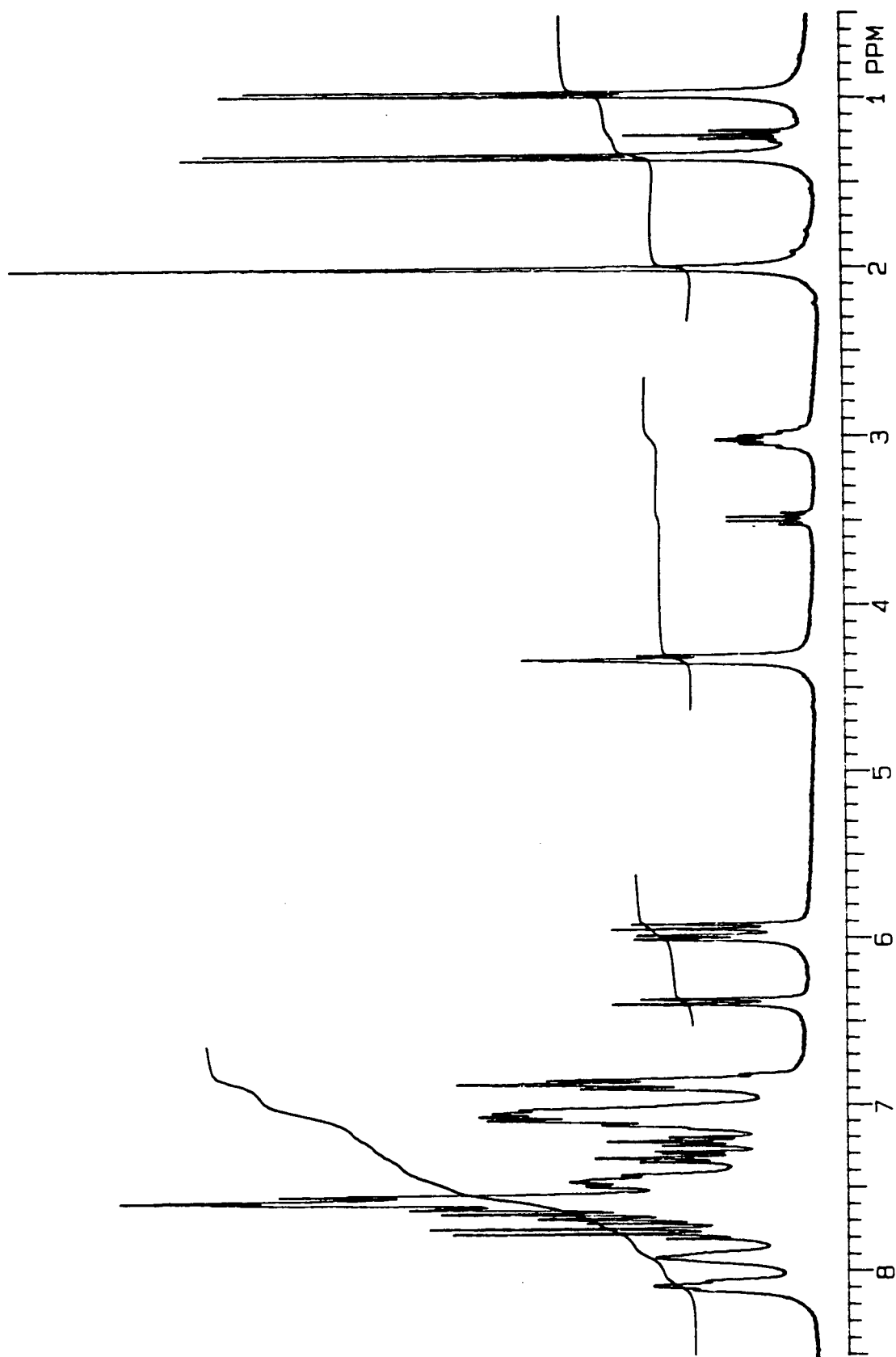
Figure 3.20: 1H NMR spectrum (300 MHz, 20 °C) of [RuCl(p-cymene)(R-BINAP)]+Cl− in CDCl3.
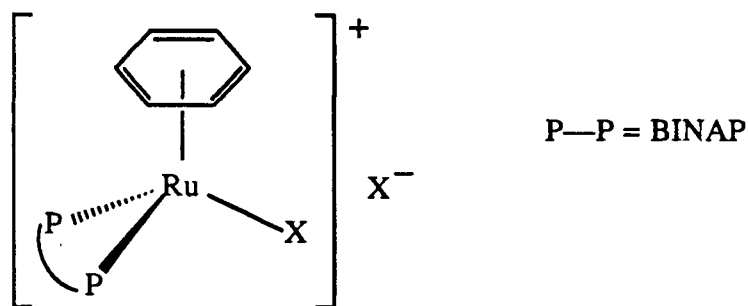
Figure 3.21: Geometry of [RuX(arene)(BINAP)]$^+$X$^-$ complexes.

The additional broad resonance observed at 4.30 ppm (~1H) in the ^{1}H NMR spectrum is tentatively assigned to a molecule of water; the chemical shift is close to that expected for hydrogen-bonded water. The presence of water in the sample is confirmed by IR spectroscopy and the elemental analysis is also consistent with the presence of 0.5 mole equivalents of water per Ru complex. One possible mode of binding is shown below:
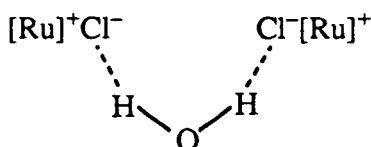
[Ru] represents [RuX(arene)(BINAP)]

Reaction of equimolar amounts of S,S-BDPP with [RuCl(p-cymene)(μ-Cl)]$_2$ under similar preparative conditions (Section 2.5.8), however, yielded a mixture of products as evidenced by the ^{31}P NMR spectroscopy. An AX pattern observed at 35.1 ppm (δ_A = 39.2, δ_B = 29.1 ppm, $^2J_{AX}$ = 60.7 Hz) and constituting $ca.$ 25% of the total integral intensity has been assigned to the desired [RuCl(p-cymene)(S,S-BDPP)]$^+$Cl$^-$ complex by comparison of the data for the BINAP analogues. One of the products was isolated and identified from its ^{31}P NMR chemical shift (8.7 ppm, s) as the bis(diphosphine) complex $trans$–RuCl$_2$(S,S-BDPP)$_2$. The $trans$ arrangement of the chloro

ligands was confirmed by a single crystal X-ray diffraction analysis (see Appendix A-2.3 for the structural details).

While the Ru-(arene)BINAP complexes could be obtained in almost quantitative yields, the corresponding BDPP derivative is formed in only about 25% yield. This observation supports the earlier suggestion (see Section 3.8) that the steric bulk and chelate size of the diphosphine ligands perhaps influence the nature of the products generated.

3.10 References – Chapter 3

1. Schroder, M.; Stephenson, T. A. in *Comprehensive Coordination Chemistry*; Wilkinson, G.; Gillard, R. D.; McCleverty, J. A., Eds.; Pergamon Press: Oxford, 1987; Vol. 4, Chapter 45.

2. Bruce, M. I. in *Comprehensive Organometallic Chemistry*; Wilkinson, G., Stone, F. G. A., Abel, E. W., Eds.; Pergamon Press: Oxford, 1982; Vol.4, p. 651.

3. Seddon, E. A.; Seddon, K. R. *The Chemistry of Ruthenium*; Elsevier: Amsterdam, 1984.

4. Jardine, F. H. *Prog. Inorg. Chem.* **1984**, *31*, 265.

5. Some journals periodically publish special reports on the chemistry of individual or a group of transition metals. See for example, Annual Survey of Ruthenium Chemistry for the Years 1983/84:
    (a) Keister, J. B. *J. Organomet. Chem.* **1987**, *318*, 297.
    (b) Shapley, P. A. *J. Organomet. Chem.* **1987**, *318*, 409.

6. James, B. R. in *Comprehensive Organometallic Chemistry*; Wilkinson, G., Stone, F. G. A., Abel, E. W., Eds.; Pergamon Press: Oxford, 1982; Vol.8, p. 285.

7. James, B. R. *Homogeneous Hydrogenation*; Wiley: New York, 1973.

8. Collman, J. P.; Hegedus, L. S.; Norton, J. R.; Finke, R. G. *Principles and Applications of Organotransition Metal Chemistry*; University Science Books: Mill Valley, CA, 1987; p. 545.

9. (a) Chatt, J.; Hayter, R. G. *J. Chem. Soc.* **1961**, 772; 896; 5507.
    (b) *ibid.*, **1963**, 6017.

10. James, B. R.; Wang, D. K. W.; Voigt, R. F. *J. Chem. Soc., Chem. Commun.* **1975**, 574.

11. Mason R.; Meek, D. W.; Scollary, G. R. *Inorg. Chim. Acta* **1976**, *16*, L11.

12. McAuliffe, C. A.; Levason, W. *Phosphine, Arsine and Stibine Complexes of the Transition Elements*; Elsevier: Amesterdam, 1979.

13. Jung, C. W.; Garrou, P. E.; Hoffman, P. R.; Caulton, K. G. *Inorg. Chem.* **1984**, *23*, 726.

14. Joshi, A. M.; Batista, A. A.; James, B. R. *unpublished results.*

15. (a) Wang, D. K. W., Ph.D. Dissertation, The University of British Columbia, Vancouver, Canada, 1978.
    (b) James, B. R.; Wang, D. K. W. *Inorg. Chim. Acta* **1976**, *19*, L17.

16. Bressan, M.; Rigo, P. *Inorg. Chem.* **1975**, *14*, 2286.

17. Henrici-Olive, G.; Olive, S. *Angew. Chem., Int. Ed. Engl.* **1971**, *10*, 105.

18. James, B. R.; McMillan, R. S.; Morris, R. H.; Wang, D. K. W. *Adv. Chem. Ser.* **1978**, *167*, 122.

19. James, B. R.; Wang, D. K. W. *Can. J. Chem.* **1980**, *58*, 245.

20. Kawano, H.; Ikariya, T.; Ishii, Y.; Saburi, M.; Yoshikawa, S.; Uchida, Y.; Kumobayashi, H. *J. Chem. Soc., Perkin Trans.* **1989**, 1571.

21. Thorburn, I. S.; James, B. R. *unpublished results.*

22. (a) Kagan, H. B. in *Asymmetric Synthesis*; Morrison, J. D., Ed.; Academic Press: New York, 1985; Vol. 5, p. 1.
    (b) Koenig, K. E., *ibid.*; p. 71.

23. Bosnich, B., Ed., *Asymmetric Catalysis*; Martinus Nijhoff: Dordrecht, 1986.

24. James, B. R.; Thompson, L. K.; Wang, D. K. W. *Inorg. Chim. Acta* **1978**, *29*, L237.

25. Dekleva, T. W.; Thorburn, I. S.; James, B. R. *Inorg. Chim. Acta* **1985**, *100*, 49.

26. Thorburn, I. S.; Rettig, S. J.; James, B. R. *Inorg. Chem.* **1986**, *25*, 234.

27. Thorburn, I. S., Ph.D. Dissertation, The University of British Columbia, Vancouver, Canada, 1985.

28. James, B. R.; Pacheco, A.; Rettig, S. J.; Thorburn, I. S.; Ball, R. G.; Ibers, J. A. *J. Mol. Catal.* **1987**, *41*, 147.

29. (a) Clark, E. P. *Indust. Eng. Chem. Anal. Ed.* **1941**, *13*, 820.
    (b) Zoellner, R. W. *J. Chem. Ed.* **1990**, *67*, 714.

30. Hoffman, P. R.; Caulton, K. G. *J. Am. Chem. Soc.* **1975**, *97*, 4221.

31. Evans, D. F. *J. Chem. Soc.* **1959**, 2003.

32. Figgis, B. N. *Introduction to Ligand Fields*; Wiley: New York, 1966; Chapter 10.

33. Day, M. C.; Selbin, J. *Theoretical Inorganic Chemistry*; Van Nostrand Reinhold: New York, 1969, 2nd Edn.; p. 483.

34. Brown, M. J.; Chaloner, P. A.; Murrer, B. A.; Parker, D. *ACS Symp. Ser.* **1980**, *119*, 170.

35. Cotton, F. A.; Wilkinson, G. *Advanced Inorganic Chemistry*; Wiley-Interscience: New York, 1980, 4th Edn.; p. 467.

36. Noyori, R.; Takaya, H. *Acc. Chem. Res.* **1990**, *23*, 345.

37.   Noyori, R. *Science* **1990**, *248*, 1194; *Chem. Soc. Rev.* **1989**, *18*, 187.

38.   Ikariya, T.; Ishii, Y.; Kawano, H.; Arai, T.; Saburi, M.; Yoshikawa, S.; Akutagawa, S. *J. Chem. Soc., Chem. Commun.* **1985**, 922.

39.   Noyori, R.; Ohkuma, T.; Kitamura, M.; Takaya, H.; Sayo, N.; Kumobayashi, H.; Akutagawa, S. *J. Am. Chem. Soc.* **1987**, *109*, 5856.

40.   Gordon, A. J.; Ford, R. A. *The Chemist's Companion, A Handbook of Practical Data, Techniques and References*; Wiley: New York, 1972; p. 186.

41.   Chaudhuri, N. K.; Servando, O.; Markus, B.; Galynker, I. *J. Indian Chem. Soc.* **1985**, *62(11)*, 899.

42.   McCrindle, R.; Ferguson, G.; Arsenault, G. J.; McAlees, A. J. *J. Chem. Soc., Chem. Commun.* **1983**, 571.

43.   Reference 8, Chapters 6, 12 and 15.

44.   Tsuji, J. in *Organic Synthesis via Metal Carbonyls*; Wender, I. and Pino, P., Eds.; Wiley-Interscience: New York, 1977; Vol. 2, p.595.

45.   Domazetis, G.; Tarpey, B.; Dolphin, D.; James, B. R. *J. Chem. Soc., Chem. Commun.* **1980**, 939.

46.   Domazetis, G.; James, B. R.; Tarpey, B.; Dolphin, D. *ACS Symp. Ser.* **1981**, *152*, 243.

47.   Varshavsky, Yu. S.; Shestakova, E. P.; Kiseleva, N. G.; Cherkasova, T. G.; Buzina, N. A.; Bresler, L. S.; Kormer, V. A. *J. Organomet. Chem.* **1979**, *170*, 81; and references therein.

48.   Kuhlman, E. J.; Alexander, J. J. *J. Organomet. Chem.* **1979**, *174*, 81; *Inorg. Chim. Acta* **1979**, *34*, 197.

49.   Albers, M. O.; Coville, N. J.; Nicolaides, C. P.; Webber, R. A.; Ashworth, T. V.; Singleton, E. *J. Organomet. Chem.* **1981**, *217*, 247.

50.   Bora, T.; Singh, M. M. *Transition Met. Chem.* **1978**, *3*, 27; and references therein.

51.   James, B. R.; Ochiai, E.; Rempel, G. I. *Inorg. Nucl. Chem. Lett.* **1971**, *7*, 781.

52.   Evans, I. P.; Spencer, A.; Wilkinson, G. *J. Chem. Soc., Dalton Trans.* **1973**, 204.

53.   Mercer, A.; Trotter, J. *J. Chem. Soc., Dalton Trans.* **1975**, 2480.

54.   McMillan, R. S.; Mercer, A.; James, B. R.; Trotter, J. *J. Chem. Soc., Dalton Trans.* **1975**, 1006.

55.   (a) LaPlaca, S. J.; Ibers, J. A. *Inorg. Chem.* **1965**, *4*, 778.
       (b) Skapski, A. C.; Troughton, P. G. H. *J. Chem. Soc., Chem. Commun.* **1968**, 1230.

56.   (a) Alcock, N. W.; Raspin, K. A. *J. Chem. Soc. (A)* **1968**, 2108.
       (b) Fraser, A. J. F.; Gould, R. O. *J. Chem. Soc., Dalton Trans.* **1974**, 1139.
       (c) Cotton, F. A.; Matusz, M.; Torralba, R. C. *Inorg. Chem.* **1989**, *28*, 1516.

57.   Chioccola, G.; Daly, J. J. *J. Chem. Soc. A* **1968**, 1981.

58.   For example: (a) Mattson, B. M.; Heiman, J. R.; Pignolet, L. H. *Inorg. Chem.* **1976**, *15*, 564; and references therein.
       (b) Schumann, H.; Opitz, J.; Pickardt, J. *J. Organomet. Chem.* **1977**, *128*, 253.
       (c) Hursthouse, M. B.; Jones, R. A.; Abdul Malik, K. M.; Wilkinson, G. *J. Am. Chem. Soc.* **1979**, *101*, 4128.
       (d) Jones, R. A.; Wilkinson, G.; Coloquohoun, I. J.; McFarlane, W.; Galas, A. M. R.; Hursthouse, M. B. *J. Chem. Soc., Dalton Trans.* **1980**, 2480.

59. Hampton, C.; Cullen, W. R.; James, B. R.; Charland, J. -P. *J. Am. Chem. Soc.* **1988**, *110*, 6918.

60. Joshi, A. M.; James, B. R. *J. Chem. Soc., Chem. Commun.* **1989**, 1785.

61. Reference 8, p. 280.

62. (a) Kulawiec, R. J.; Faller, J. W.; Crabtree, R. H. *Organometallics* **1990**, *9*, 745; and references therein.
    (b) Burk, M. J.; Segmuller, B.; Crabtree, R. H. *Organometallics* **1987**, *6*, 2241.

63. Cole-Hamilton, D. J.; Wilkinson, G. *J. Chem. Soc., Dalton Trans.* **1979**, 1283.

64. Newton, W. E.; Searles, J. E. *Inorg. Chim. Acta* **1973**, *7*, 349.

65. Armit, P. W.; Sime, W. J.; Stephenson, T. A. *J. Chem. Soc., Dalton Trans.* **1976**, 2121.

66. Stephenson, T. A.; Switkes, E. S.; Armit, P. W. *J. Chem. Soc., Dalton Trans.* **1974**, 1134.

67. Head, R. A.; Nixon, J. F. *J. Chem. Soc., Dalton Trans.* **1978**, 901.

68. Gosser, L. W.; Knoth, W. H.; Parshall, G. W. *J. Am. Chem. Soc.* **1973**, *95*, 3436.

69. Dekleva, T. W. Ph.D. Dissertation, The University of British Columbia, Vancouver, Canada, 1983.

70. Chaudret, B.; Commenges, G.; Poilblanc, R. *J. Chem. Soc., Dalton Trans.* **1984**, 1635.

71. Morris, R. H. Ph.D. Dissertation, The University of British Columbia, Vancouver, Canada, 1978.

72. Thorburn, I. S.; Rettig, S. J.; James, B. R. *J. Organomet. Chem.* **1985**, *296*, 103.

73. (a) Bennett, M. A.; Smith, A. K. *J. Chem. Soc., Dalton Trans.* **1974**, 233.
    (b) Zelonka, R. A.; Baird, M. C. *Can. J. Chem.* **1972**, *50*, 3063.

74. Mashima, K.; Kusano, K.; Ohta, T.; Noyori, R.; Takaya, H. *J. Chem. Soc., Chem. Commun.* **1989**, 1208.

CHAPTER 4

Reactions of RuCl₂(DPPB)(PPh₃) with Chelating Ligands

4.1 Introduction

The mixed-phosphine complex RuCl₂(DPPB)(PPh₃)[1] and its DIOP analogue,[2] prepared by a simple phosphine exchange reaction (Equation 4.1), have been known for several years.

$$RuCl_2(PPh_3)_3 + P–P \longrightarrow RuCl_2(P–P)(PPh_3) + 2\ PPh_3 \quad (4.1)$$

$$P–P = DPPB, DIOP$$

Caulton and coworkers re-examined the preparative chemistry of complexes of the general formula RuCl₂(P–P)(PPh₃), where P–P represents the bidentate phosphines Ph₂P(CH₂)ₙPPh₂, n = 1–4.[1] Detailed variable temperature ³¹P NMR studies of reactions of the precursor RuCl₂(PPh₃)₃ complex with one equivalent of the appropriate phosphine in CD₂Cl₂ solution showed that no mixed-phosphine complexes containing DPPM or DPPE were formed; *trans*-RuCl₂(DPPM)₂ and *trans*-RuCl₂(DPPE)₂ were the major products. A small amount of RuCl₂(DPPP)(PPh₃) was observed in solution, while only the DPPB complex RuCl₂(DPPB)(PPh₃), **23**, was isolable.[1] The authors ascribed these differences in reactivity of Ph₂P(CH₂)ₙPPh₂ ligands to the differences in chelate bite angles (∠ P–Ru–P) in the resulting RuCl₂(P–P)(PPh₃) species. They concluded that as this angle became smaller, the reduced steric crowding made the RuCl₂(P–P)(PPh₃) complex

accessible to further reaction to form a coordinatively saturated product of the type $RuCl_2(P-P)_2$.

The normal apical-to-basal angle for a square-pyramidal geometry is expected to be 104°. Crystallographic studies by Churchill and Bezman[3] on pentacoordinate iridium complexes of the general formula $Ir(COD)(CH_3)(L_2)$, where $L = PMe_2Ph$[3a] or $L_2 = DPPP$,[3b] $DPPE$,[3c] have yielded values of 101.5, 93.4 and 84.9°, respectively, for $\angle$ P–Ir–P.

As mentioned in Section 3.4.1, the mixed-phosphine complexes readily lose the triphenylphosphine ligand in solution to form the chloro-bridged dimeric complexes, $[RuCl(P-P)(\mu-Cl)]_2$, where P–P = DPPB or DIOP (Equation 4.2). Trapping such dimeric moieties, formed *in situ*, with an appropriate ligand seemed feasible. As described in Chapter 3, reactions of $RuCl_2(DPPB)(PPh_3)$, **23**, with monodentate ligands, such as NEt_3, clearly provide a synthetic route into dinuclear ruthenium complexes containing a single diphosphine (DPPB) per ruthenium (Equation 4.3).

$$RuCl_2(P-P)(PPh_3) \; \rightleftharpoons \; 1/2 \; [RuCl(P-P)(\mu-Cl)]_2 \; + \; PPh_3 \qquad (4.2)$$

$$P-P \; = \; DPPB \; or \; DIOP$$

$$RuCl_2(DPPB)(PPh_3) \; \xrightarrow[-PPh_3]{NEt_3} \; 1/2 \; [(NEt_3)(DPPB)Ru(\mu-Cl)_3RuCl(DPPB)] \qquad (4.3)$$
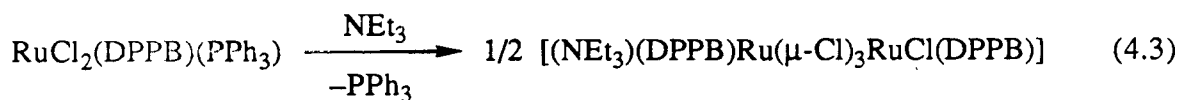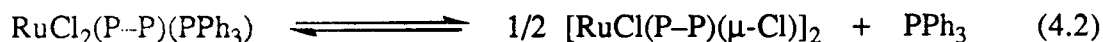
Much of the chemistry of the mixed phosphine complex $RuCl_2(DPPB)(PPh_3)$, **23**, described here has developed out of interest in the dimer chemistry. Reactions of **23** with chelating ligands produced some unusual six-coordinate compounds; their characterisation and reactivity with H_2 (including that of **23**) are described in this chapter.

The structure of $RuCl_2(DPPB)(PPh_3)$ was of particular interest. Based on a low-temperature ^{31}P NMR study of $RuCl_2(DPPB)(PPh_3)$ in CD_2Cl_2 solution, Caulton and

coworkers have proposed, for the mixed-phosphine complex **23**, a structure similar to that of the $RuCl_2(PPh_3)_3$ precursor, at least in solution. The tris(triphenylphosphine) derivative has been previously characterised crystallographically,[4] and shows a square-pyramidal arrangement of ligands about the Ru centre with *trans*-disposed chlorides and mutually *trans* PPh$_3$ ligands in the basal plane and the remaining PPh$_3$ group occupying the apical position.[4]

As attempts to grow diffraction quality crystals of **23** were unsuccessful, it was decided to conduct a comparative solid-state ^{31}P NMR study of $RuCl_2(DPPB)(PPh_3)$ and $RuCl_2(PPh_3)_3$ complexes in the hope of extracting information about the solid-state structure of the former. The results are described in the next section.

4.2   Solid-State ^{31}P NMR Studies on $RuCl_2(DPPB)(PPh_3)$ and $RuCl_2(PPh_3)_3$

The samples were packed as powders (~0.2–0.3 g) in Teflon® holders of ~8 mm ID. High-resolution, solid-state NMR spectra were obtained on a Bruker CXP200 FT-NMR machine operating at 80.99 MHz for ^{31}P, by combining high-power proton decoupling[5] with [1]H–[31]P cross polarisation (CP)[6] (5.5 µs 90°y ^{1}H pulse, 1 ms contact time, 1 s recycle time) and magic-angle spinning (MAS)[7] at ~2.5–4.0 kHz (for general reviews on CP/MAS NMR spectroscopy, see Refs. 8–10).

The CP/MAS ^{31}P NMR spectra of the complexes $RuCl_2(DPPB)(PPh_3)$ and $RuCl_2(PPh_3)_3$ are shown in Figure 4.1. The chemical shift anisotropy interaction in the solid-state results in a spectrum which consists of isotropic peaks and peaks at integral values of the spinning frequency (spinning sidebands).[8-12] The isotropic peaks were differentiated from the spinning sidebands by obtaining spectra at different rotor speeds. Positions of the spinning sidebands change with the spinning frequency of the sample
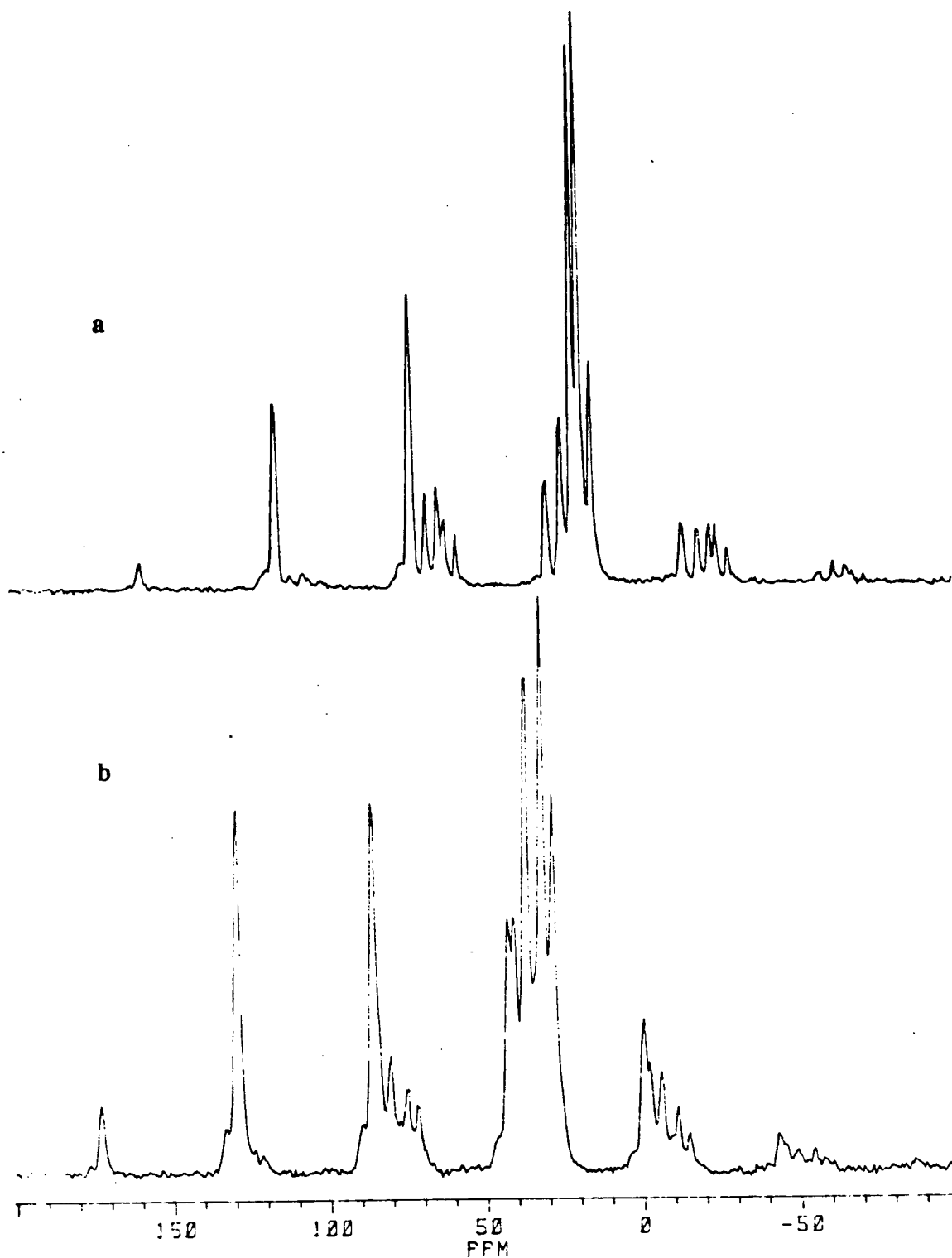
Figure 4.1: The 80.99 MHz CP/MAS ^{31}P NMR spectra of the complexes
(a) $RuCl_2(PPh_3)_3$, and (b) $RuCl_2(DPPB)(PPh_3)$, at a MA spinning frequency of 3.5 kHz.

while the isotropic peaks remain invariant in position.[8-12] Alternatively, the isotropic chemical shifts were obtained by using a routine *TOSS* (*TO*tal *S*uppression of *S*idebands) pulse sequence to suppress the sidebands.[11]

Caulton and coworkers have reported the low-temperature ^{31}P NMR data for $RuCl_2(PPh_3)_3$[13] and $RuCl_2(DPPB)(PPh_3)$[1] in dichloromethane solution (Table 4.1). The spectra of the two complexes exhibit an AX_2 and an ABX pattern, respectively. The *TOSS* spectra for the two complexes, along with the respective low-temperature solution NMR spectra which were simulated using the parameters reported in the literature,[1, 13] are shown in Figures 4.2 and 4.3. The solid-state NMR data are listed in Table 4.2.

4.2.1   Comparison of Solid-State and Solution ^{31}P NMR Data

The two mutually *trans* basal PPh$_3$ ligands of $RuCl_2(PPh_3)_3$ which are equivalent in solution become inequivalent in the solid-state, presumably because of solid-state packing effects, and give rise to the AB part of the ABX pattern (δ_{AB} ~19.9 ppm, Figure 4.2). The non-equivalence of the two basal PPh$_3$ ligands in the solid state is also evident in the molecular structure of $RuCl_2(PPh_3)_3$ in which the two basal Ru–P bond lengths differ by ~0.04 Å (2.412 and 2.374 Å).[4, 14] The coupling constant $^2J_{AB}$ of 333 Hz is within the range expected for *trans*-disposed phosphines bound to ruthenium.[15, 16] The single low-field resonance at 72.5 ppm is proposed to constitute the AX/BX part of the system, the *cis* couplings, $^2J_{AX}$ and $^2J_{BX}$, being too small (typical range –60 to +60 Hz[15, 16]) to be resolved in the relatively broad CP/MAS spectrum. The observed solid-state chemical shifts of 19.9 ppm (δ_{AB}) for the basal and of 72.5 ppm for the apical PPh$_3$ ligands are close to the corresponding solution values of 24.1 and 75.7 ppm, respectively.
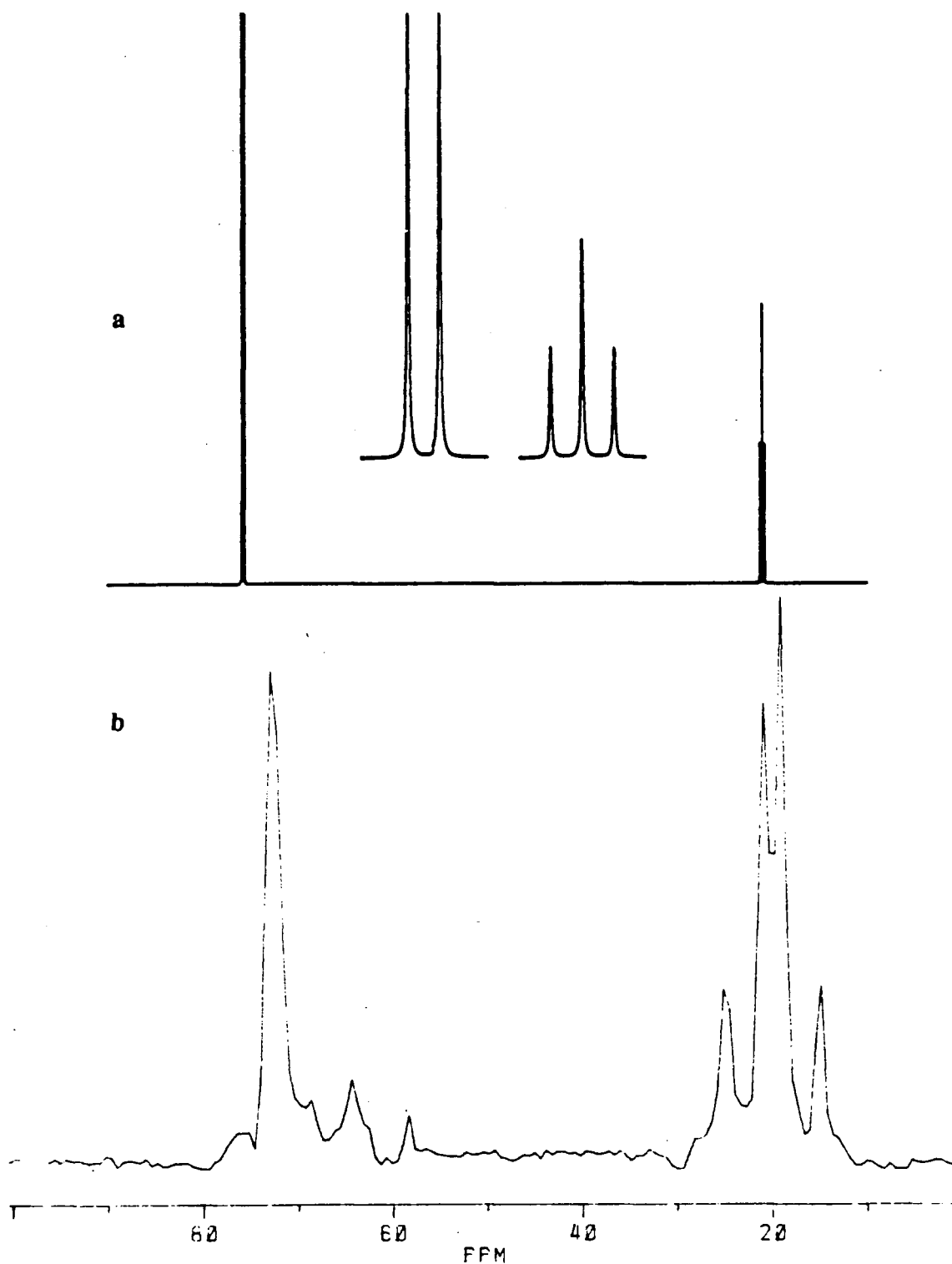
Figure 4.2: (a) A simulated solution NMR spectrum of RuCl$_2$(PPh$_3$)$_3$ obtained using the literature data[13] given in Table 4.1.

(b) A CP/MAS ^{31}P NMR (*TOSS*) spectrum of RuCl$_2$(PPh$_3$)$_3$.

136
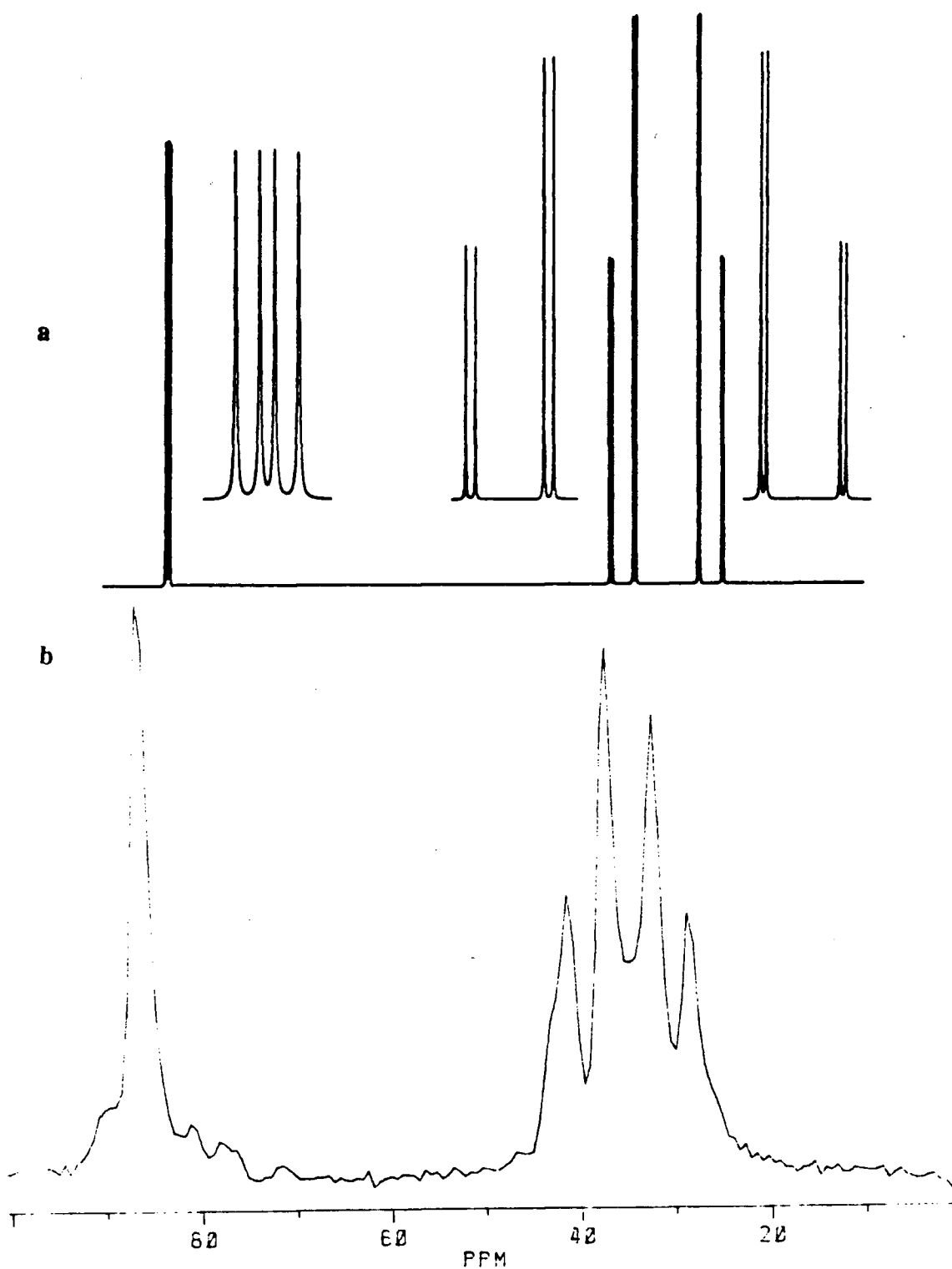
Figure 4.3: (a) A simulated solution NMR spectrum of RuCl$_2$(DPPB)(PPh$_3$) obtained using the literature data[1] given in Table 4.1.

(b) A CP/MAS ^{31}P NMR (*TOSS*) spectrum of RuCl$_2$(DPPB)(PPh$_3$).

Table 4.1: Literature $^{31}P\{^1H\}$ NMR Spectral Data for (a) $RuCl_2(PPh_3)_3$[13] at $-97\ ^\circ C$, and (b) $RuCl_2(DPPB)(PPh_3)$[1] at $-63\ ^\circ C$ in CD_2Cl_2 Solution.

Complex	Chemical Shift, δ ppm (Assignment) $(^2J_{PP},$ Hz)		
$RuCl_2(PPh_3)_3$ AX$_2$ Pattern	24.1 (P$_X$) $(^2J_{AX} = 30.5)$	75.7 (P$_A$)	
$RuCl_2(DPPB)(PPh_3)$ ABX Pattern	26.3 (P$_A$) $(^2J_{AX} = -22.6)$	35.2 (P$_B$) $(^2J_{AB} = 302.4)$	83.2 (P$_X$) $(^2J_{BX} = -37.5)$

Table 4.2: Solid-State ^{31}P CP/MAS NMR Spectral Data for (a) $RuCl_2(PPh_3)_3$, and (b) $RuCl_2(DPPB)(PPh_3)$.

Complex	Chemical Shift, δ ppm (Assignment) $(^2J_{PP},$ Hz)		
$RuCl_2(PPh_3)_3$ ABX Pattern	16.9 (P$_A$)	22.8 (P$_B$) $(^2J_{AB} = 333)$	72.5 (P$_X$)
$RuCl_2(DPPB)(PPh_3)$ ABX Pattern	30.4 (P$_A$)	39.2 (P$_B$) $(^2J_{AB} = 320)$	86.3 (P$_X$)

The move of the solid-state chemical shifts to higher field relative to the solution values implies increased shielding in the solid state, particularly for the resonance at 16.9 ppm designated as δ_A. Such chemical shift differences between the solid-state CP/MAS and solution NMR data have been observed for other compounds, including tertiary phosphines and their transition metal complexes.[17-21] Differences of a few ppm ($\leq$ 5-6 ppm) are common, and the compounds are still considered to possess similar structures in solution and in the solid state, at least qualitatively.[17-21] Larger chemical shift differences are often considered a manifestation of major structural differences.[18] The highest-field signal at 16.9 ppm may be attributed to the basal PPh_3 with a longer Ru-P bond (2.412 Å). An empirical linear correlation between the crystallographically determined Ru–P distances in a series of Ru(II)-triarylphosphine complexes and the corresponding ^{31}P-chemical shifts observed in solution has been suggested,[22] with the chemical shifts becoming more high-field with increasing Ru–P bond lengths. The difference of 52.7 ppm between the basal and the apical phosphorus chemical shifts in the CP/MAS spectrum is close to the 51.6 ppm difference observed in the solution spectrum. Overall, the ^{31}P CP/MAS NMR data for $RuCl_2(PPh_3)_3$ are consistent with the previously established solid-state geometry of the complex[4, 14] (Figure 4.4), and comparison with the solution data indicates that there are no major differences in the solid-state and the low-temperature solution structures.

Ru–P_A	2.412 Å	P_A–Ru–P_B	156.4°
Ru–P_B	2.374 Å	P_A–Ru–P_X	101.1°
Ru–P_X	2.230 Å	Cl(1)–Ru–Cl(2)	157.2°
Ru–Cl(1)	2.387 Å	P_A–Ru–Cl(1)	92.4°
Ru–Cl(2)	2.388 Å	P_A–Ru–Cl(2)	83.7°
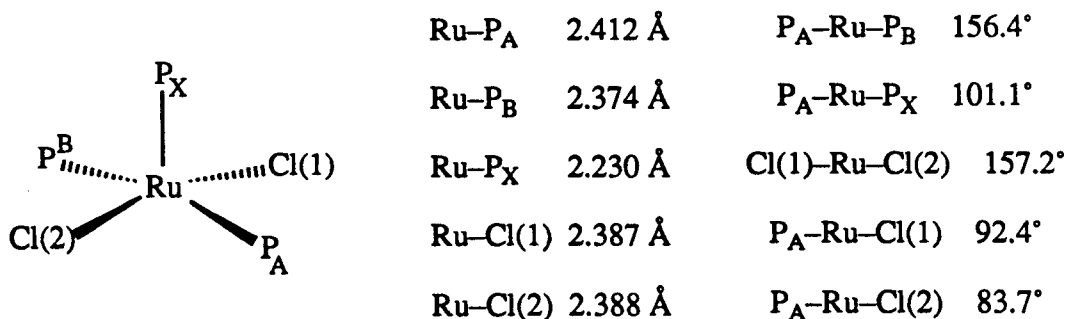
Figure 4.4: Geometry of $RuCl_2(PPh_3)_3$ as determined by an X-ray diffraction study.[4, 14] The bond length and bond angle data are taken from Reference 4.

The ambient temperature ^{31}P spectrum of **23** in $CDCl_3$ is shown in Figure 4.5. The AB quartet seen in the spectrum (δ_A = 63.1, δ_B = 53.9 ppm; $^2J_{AB}$ = 46.8 Hz) is assigned to the dichloro-bridged [RuCl(DPPB)(μ-Cl)]$_2$ species formed by dimerisation of "RuCl$_2$(DPPB)" after dissociation of PPh$_3$ from **23** (Equation 4.2). The signal due to free PPh$_3$ is evident at *ca.* –6 ppm. Caulton and coworkers have assigned the triplet-like set of resonances at ~24 ppm as a part of an AB$_2$ pattern due to **23** resulting from a fast exchange at room temperature of P$_B$ and P$_X$ belonging to the DPPB ligand (see Figure 4.7, Section 4.2.2).[1] The observed line spacing of 139.5 Hz is essentially identical to the average of the static values of $^2J_{AB}$ and $^2J_{AX}$ (302.4 and –22.6 Hz, respectively, see Table 4.1) obtained from the expected ABX pattern which is resolved at –60 °C.[1]
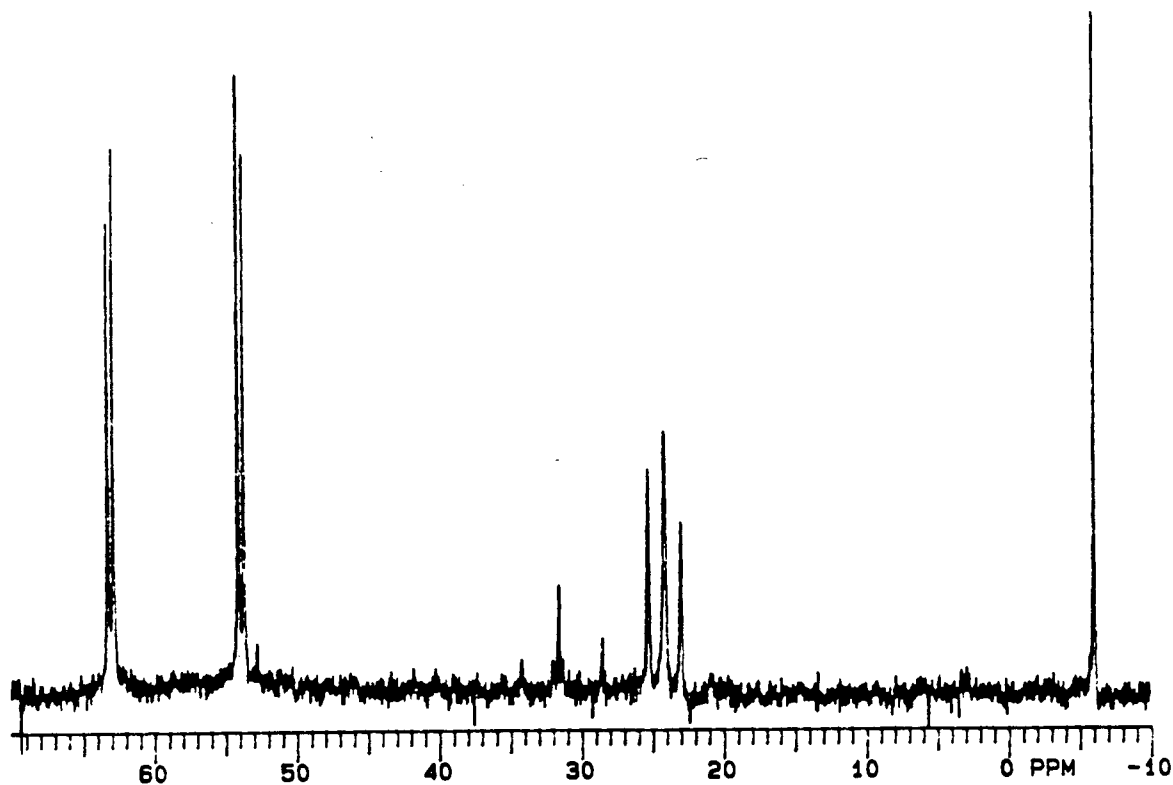
Figure 4.5: $^{31}P\{^1H\}$ NMR spectrum (121.42 MHz, 20 °C) of RuCl$_2$(DPPB)(PPh$_3$) in $CDCl_3$.

The solid-state ^{31}P CP/MAS NMR spectrum of the mixed-phosphine complex RuCl$_2$(DPPB)(PPh$_3$), **23**, exhibits an ABX pattern similar to that observed[1] in the low-temperature solution NMR spectrum (Figure 4.3). The solid-state chemical shifts of 30.4, 39.2, and 86.3 ppm correspond well with the reported solution parameters[1] of 26.3, 35.2, and 83.2 ppm, respectively. The shift of ~3–4 ppm in the CP/MAS phosphorus resonances towards low field relative to the solution values indicates reduced shielding of the phosphorus nuclei in the solid state. Interestingly, this low-field shift in going from solution to the solid state is in the direction opposite to that observed for RuCl$_2$(PPh$_3$)$_3$, which shows increased shielding in the solid state (see above). The high-field AB quartet centred at 34.8 ppm with a scalar coupling $^2J_{AB}$ of 320 Hz indicates *trans*-disposed non-equivalent phosphines. The 320 Hz value for the *trans* coupling is somewhat greater than the corresponding coupling of 302.4 Hz obtained from the solution spectrum, suggesting the presence of additional constraints and interactions in the solid-state which may not exist, or are averaged out, in solution. The low-field signal at 86.3 ppm is assigned to an apical phosphine ligand; because of the forced *cis* configuration of the chelating DPPB ligand, the apical phosphine must be a part of the diphosphine. Again, the *cis* P-Ru-P couplings, $^2J_{AX}$ and $^2J_{BX}$, cannot be seen in the CP/MAS NMR spectrum because their magnitudes are much smaller than the typical line-widths encountered in the solid-state NMR spectrum ($w_{1/2}$ ~50–100 Hz).

The resonances at 30.4 (δ_A) and 39.2 ppm (δ_B) are assigned to the PPh$_3$ ligand and the basal –PPh$_2$ part of the DPPB chelate, respectively, based on the results of a non-quaternary suppression (*NQS*) experiment,[23] in which only the peaks due to phosphorus atoms attached to a non-quaternary carbon are suppressed (presumably because of relatively fast relaxation of the phosphorus nucleus by the protons on the non-quaternary carbon). The *NQS* spectrum depicted in Figure 4.6 shows the almost complete loss of
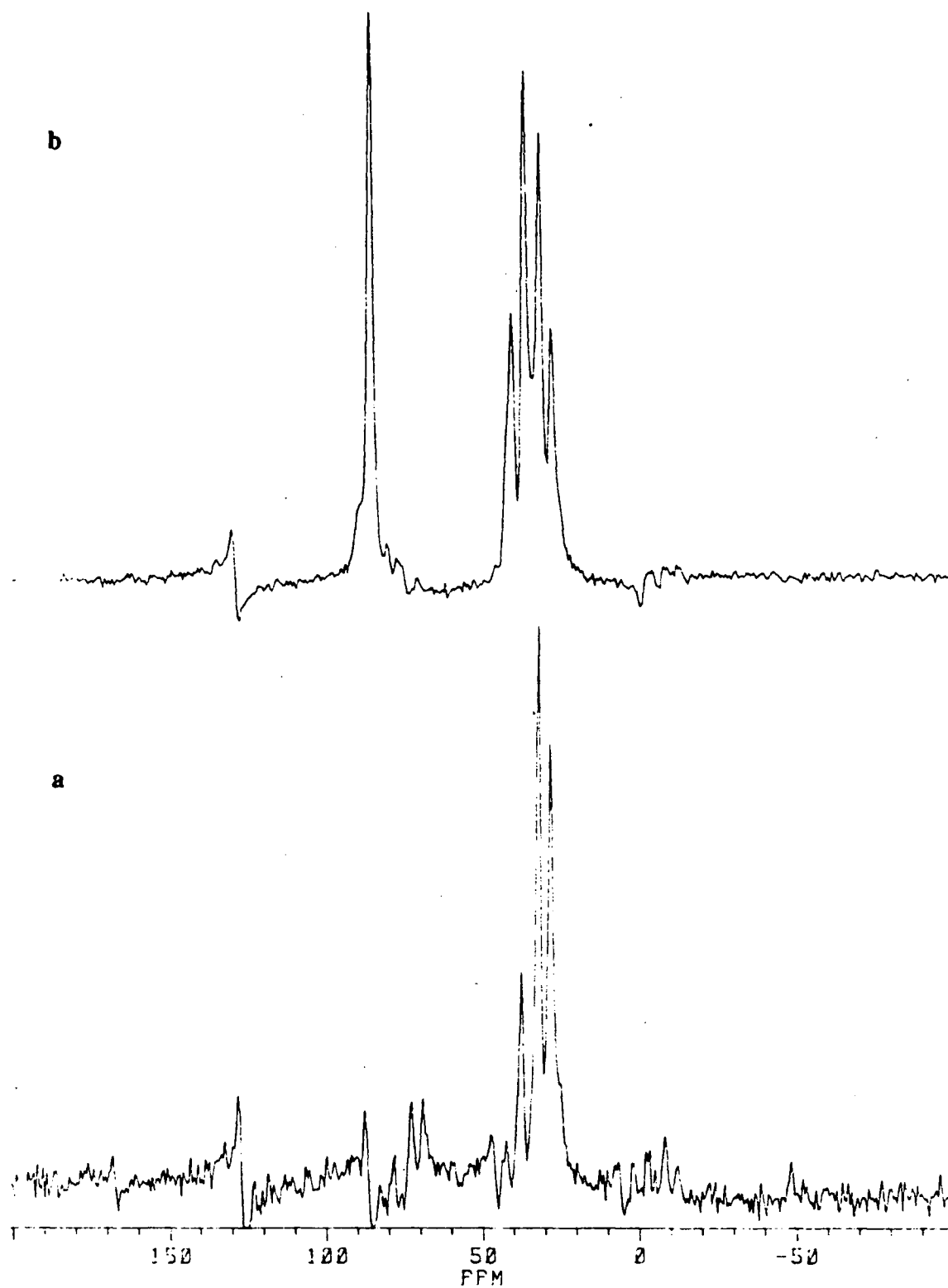
Figure 4.6: The CP/MAS ^{31}P NMR spectra of RuCl$_2$(DPPB)(PPh$_3$) showing
(a) *Non-Quaternary Suppression* (*NQS*) with a dipolar dephasing delay of 303 μs.
The corresponding *TOSS* spectrum (b) is shown for comparison.

intensity for the resonances at 86.3 and 39.2 ppm, the signals which are due to phosphorus nuclei attached to a non-quaternary carbon (*i.e.* alkyl chain of DPPB). The resonance at 30.4 ppm remains unaffected and is therefore assigned to the PPh3 ligand, in which all three P–phenyl linkages are through a quaternary carbon atom. The similarities between the solution and the solid-state NMR data for $RuCl_2(DPPB)(PPh_3)$ clearly suggest very similar solution (at least at low temperature) and solid-state structures for the mixed-phosphine complex.

4.2.2 Comparison of the ^{31}P CP/MAS NMR Data for $RuCl_2(PPh_3)_3$ and $RuCl_2(DPPB)(PPh_3)$ Complexes

Based on the comparison of the respective ^{31}P CP/MAS NMR data, the mixed-phosphine complex $RuCl_2(DPPB)(PPh_3)$ is proposed to have a solid-state geometry very similar to that of $RuCl_2(PPh_3)_3$ (Figure 4.7). The ^{31}P CP/MAS NMR spectra of $RuCl_2(PPh_3)_3$ and $RuCl_2(DPPB)(PPh_3)$, including the sideband structure, are very similar except that each of the signals (δ_A, δ_B and the δ_X) for the latter are less shielded than the corresponding signals for the tris(triphenylphosphine) complex by about 14–16 ppm (Figures 4.1–4.3, Table 4.2). The solid-state effects, structural or otherwise, which may be responsible for such a considerable and fairly uniform deshielding effect are not obvious. In any case, the deshielding (relative to $RuCl_2(PPh_3)_3$) cannot be entirely due to solid-state factors; for example, even in the solution spectra, the apical chemical shifts for $RuCl_2(PPh_3)_3$ and $RuCl_2(DPPB)(PPh_3)$ differ by 7.5 ppm. Seven-membered chelates, such as the one formed by DPPB on coordination to Ru, have been noted to exhibit considerable deshielding relative to the free ligand (coordination shift),[15] and probably also contribute to the observed relative ^{31}P-deshielding in the solid-state spectra. Assuming that the empirical correlation between the ^{31}P chemical shift and the Ru–P bond lengths observed for Ru-monophosphine complexes[22] can be extended to Ru-diphosphine

complexes, the relative ^{31}P-deshielding in **23** may reflect a shortening of Ru–P bonds. A crystal structure determination of RuCl$_2$(DPPB)(PPh$_3$), **23**, and a careful examination of solid-state ^{31}P NMR spectra for a series of analogous complexes, incorporating diphosphines of varying chelate size (e.g. 4–9, for DPPM through DPPH), may shed more light on these aspects. However, as noted earlier (Section 4.1), the mixed-phosphine complexes containing DPPM, DPPE or DPPP are not isolable.[1] Attempts during the present study to synthesise the DPPN or DPPH analogues of **23** resulted in the formation of diphosphine-bridged species of the type [RuCl$_2$(P–P)$_{1.5}$]$_2$, which have been characterised by elemental analysis and ^{31}P NMR spectroscopy (see Chapter 2, Section 2.5.11 for details).

Both RuCl$_2$(PPh$_3$)$_3$ and RuCl$_2$(DPPB)(PPh$_3$) have a *trans* arrangement of two non-equivalent phosphines in the basal plane as evidenced by the characteristic, relatively large coupling ($^2J_{AB}$) of ~325 ± 10 Hz. The chemical shift differences between the basal and the apical phosphines within the two complexes are essentially identical ($\delta_X-\delta_{AB}$ = 52 ± 1 ppm, see Table 4.2).
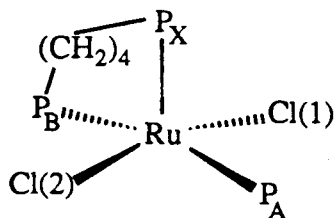
Figure 4.7: Proposed solid-state geometry of RuCl$_2$(DPPB)(PPh$_3$) based on the present ^{31}P-CP/MAS NMR studies.

In recent years, the high-resolution ^{31}P-CP/MAS NMR technique has been employed in the study of biological membranes,[24] inorganic phosphides,[25] phosphates and polyphosphates,[26] as well as phosphorus-containing polymers[27] such as poly-phosphazenes. The relatively small number of ^{31}P-CP/MAS NMR studies reported to date

on phosphines, transition metal complexes containing phosphines, and their polymer-supported analogues, has clearly established the utility of such studies in structure elucidation in the solid-state;[17–21] comparison of solid-state and solution NMR data provides a direct way of examining correlation between the solid and solution structures of such compounds.[12, 17–21] The $^2J_{PP}$ constants have been used extensively to determine the stereochemistry of metal phosphine complexes.[12, 15, 28] In solution, various fluxional processes can often result in the chemical and magnetic equivalence of two phosphine ligands with accompanying loss of such ^{31}P–^{31}P coupling information.[1, 12] However, phosphorus nuclei that may be equivalent in solution often become inequivalent in the solid state, as demonstrated for $RuCl_2(PPh_3)_3$ in the present study (see above); the $^2J_{PP}$ values, particularly for *trans*-disposed phosphorus nuclei, can be obtained by examination of CP/MAS NMR spectra of such complexes.

Despite the potential usefulness of ^{31}P-CP/MAS NMR studies of transition metal phosphine complexes, the application of this technique has remained surprisingly limited to complexes of only a few metals. Phosphine complexes of Rh,[17, 18] Pt,[19, 20] and Cu[17, 29] are perhaps the most studied, with those of Ni,[19b] Pd,[19b, 28] Au,[17] and Hg[30] completing the list. The results described above are to our knowledge the first examples of a ^{31}P-CP/MAS NMR spectroscopic investigation of ruthenium(II) monodentate and bidentate phosphine complexes. The present study clearly illustrates the potential of phosphorus solid-state NMR spectroscopy as a tool for establishing or refuting the similarity in the solid-state stereochemistry of a series of related compounds, through a simple comparative examination of their ^{31}P-CP/MAS NMR spectra, particularly when the X-ray structure of one of the compounds is known.

4.3   Reaction of RuCl$_2$(DPPB)(PPh$_3$), 23, with H$_2$

Reaction of the mixed-phosphine complex 23 with H$_2$ was investigated with the objective of synthesising a ruthenium hydride complex, RuHCl(DPPB)(PPh$_3$). Such a complex would be analogous to the triphenylphosphine complex RuHCl(PPh$_3$)$_3$,[31, 32] which is one of the most active catalysts for the hydrogenation of terminal alkenes.[32-35]

Stirring an initially brown DMA solution (5 mL) of 0.1 g of RuCl$_2$(DPPB)(PPh$_3$) under one atmosphere of H$_2$ pressure for one hour produced a dark red-brown solution. Work-up of the solution, by concentration to a viscous oil followed by addition of dry, deoxygenated methanol, yielded a green solid which was identified as the starting mixed-phosphine complex by ^{31}P NMR spectroscopy (Figure 4.5). The reaction of 23 with H$_2$ in DMA as monitored by gas-uptake studies at 50 °C, however, consistently showed ~0.20 mole equivalent H$_2$ uptake per Ru. Under the same conditions, the analogous RuCl$_2$(PPh$_3$)$_3$ takes up 1 mole equivalent of H$_2$ per Ru with the resultant formation of RuHCl(PPh$_3$)$_3$ and DMAH$^+$Cl$^-$ in accordance with Equation 4.4.[36]

$$RuCl_2(PPh_3)_3 + H_2 \xrightarrow{\text{DMA}} RuHCl(PPh_3)_3 + DMAH^+Cl^- \qquad (4.4)$$
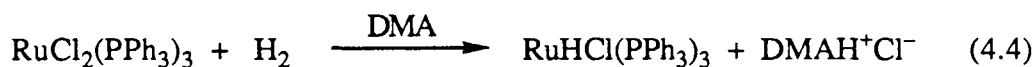
Examination of the H$_2$-uptake solution by ^{31}P NMR spectroscopy (C$_6$D$_6$ lock) clearly shows the presence of more than one species in solution (Figure 4.8); the ^{1}H NMR spectrum of the ruthenium phosphine-containing species could not be obtained because of the large amount of non-deuterated DMA solvent present. Several of the ^{31}P NMR peaks in the 45–55 ppm region could be correlated as AB quartets, simply based on the coupling constants ($^2J_{PP}$) and the observed intensities (Figure 4.8, inset). The relatively small chemical shift separations (<4 ppm) between the various related δ_A and δ_B resonances imply that the corresponding phosphorus nuclei occupy similar chemical and magnetic environments. The presence of the triplet-like resonance at ~24 ppm indicates that some 23

146
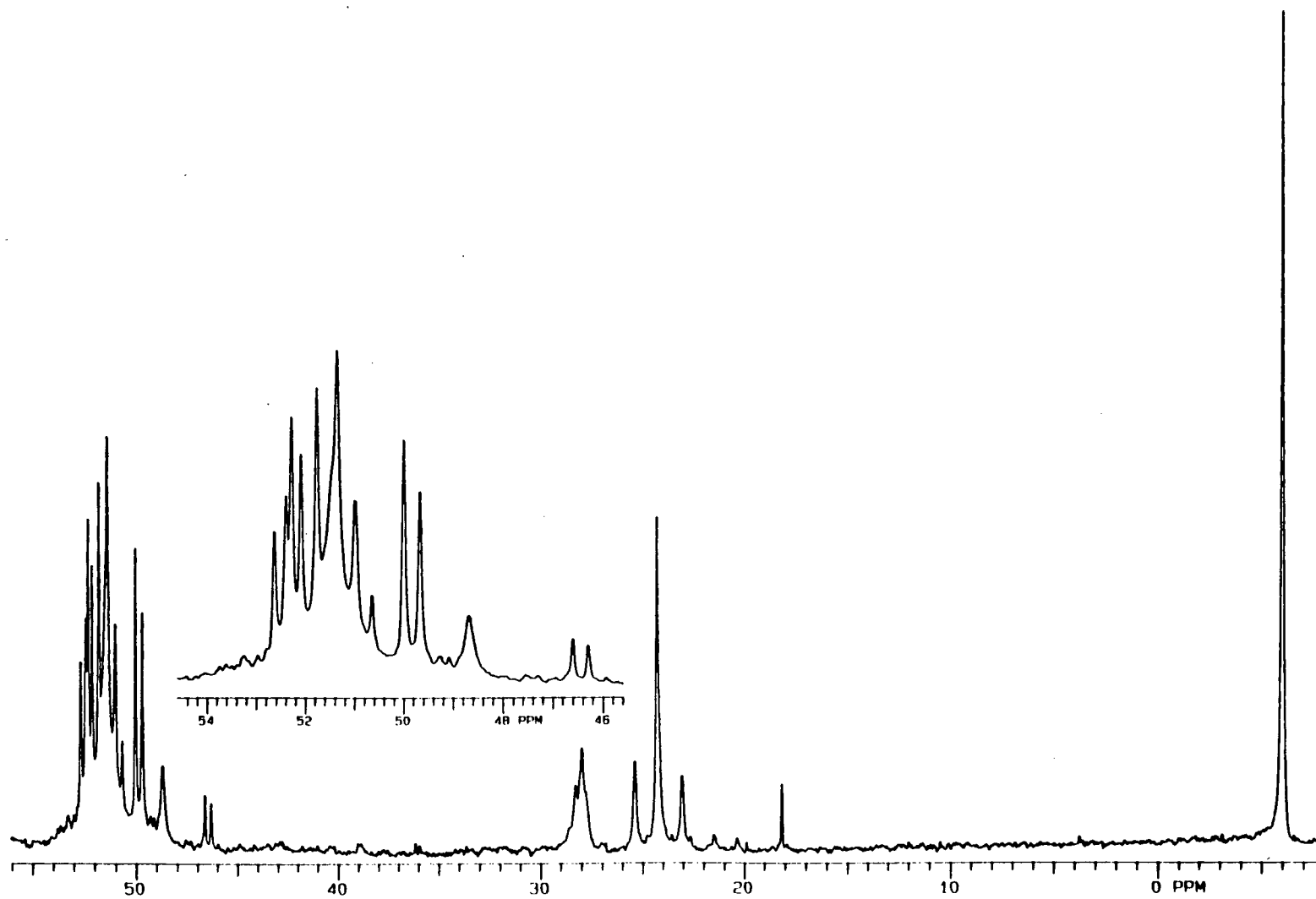
Figure 4.8: $^{31}P\{^1H\}$ NMR spectrum (121.42 MHz, C_6D_6 lock, 20 °C) of the H_2-uptake solution of $RuCl_2(DPPB)(PPh_3)$, **23**, in DMA.

is present in the solution (compare with the ambient temperature ^{31}P NMR spectrum of **23** shown in Figure 4.5). Because of the apparently reversible nature of the reaction of **23** with H_2 in DMA, and because of the large number of species produced in the reaction, further investigations into the nature of the various species in solution were not pursued.

In the presence of Proton Sponge® (PS), the mixed-phosphine complex **23** absorbed ~0.90 mole equivalent of H_2 per Ru over about 25 min (50 °C, 1 atm of H_2, DMA); the resultant solution was distinctly darker red in colour compared to the H_2-uptake solution obtained in the absence of added PS (see above). Stirring a C_6D_6 solution of $RuCl_2(DPPB)(PPh_3)$ and PS (~1.1 eq.) under 1 atm H_2-pressure, for 18 h at room temperature, also produced a dark red solution with some suspended solid (presumably PSH^+Cl^-). These red solutions generated by reaction of **23** with H_2 were extremely air-sensitive, turning green within seconds of exposure to air. The ^{31}P{^{1}H} and ^{1}H NMR spectra of the reaction mixture in C_6D_6 sealed under hydrogen atmosphere are shown in Figures 4.9 and 4.10, respectively.

The major peak in the phosphorus NMR spectrum is a singlet at 48.4 ppm which is assigned to the trichloro-bridged dinuclear complex containing coordinated PS, *viz*. $[(PS)(DPPB)Ru(\mu-Cl)_3RuCl(DPPB)]$ mentioned in Chapter 3 (Section 3.6.5); addition of PS to a solution of **23** *in the absence of hydrogen* does indeed result in the appearance of the 48.4 ppm resonance. The triplet-like resonance at *ca.* 39.5 ppm with a line spacing of 129 Hz is assigned, by analogy to the phosphorus spectrum of the starting dichloro complex **23** (Figure 4.5),[1] as part of an AB_2 pattern due to the desired $RuHCl(DPPB)(PPh_3)$ species.
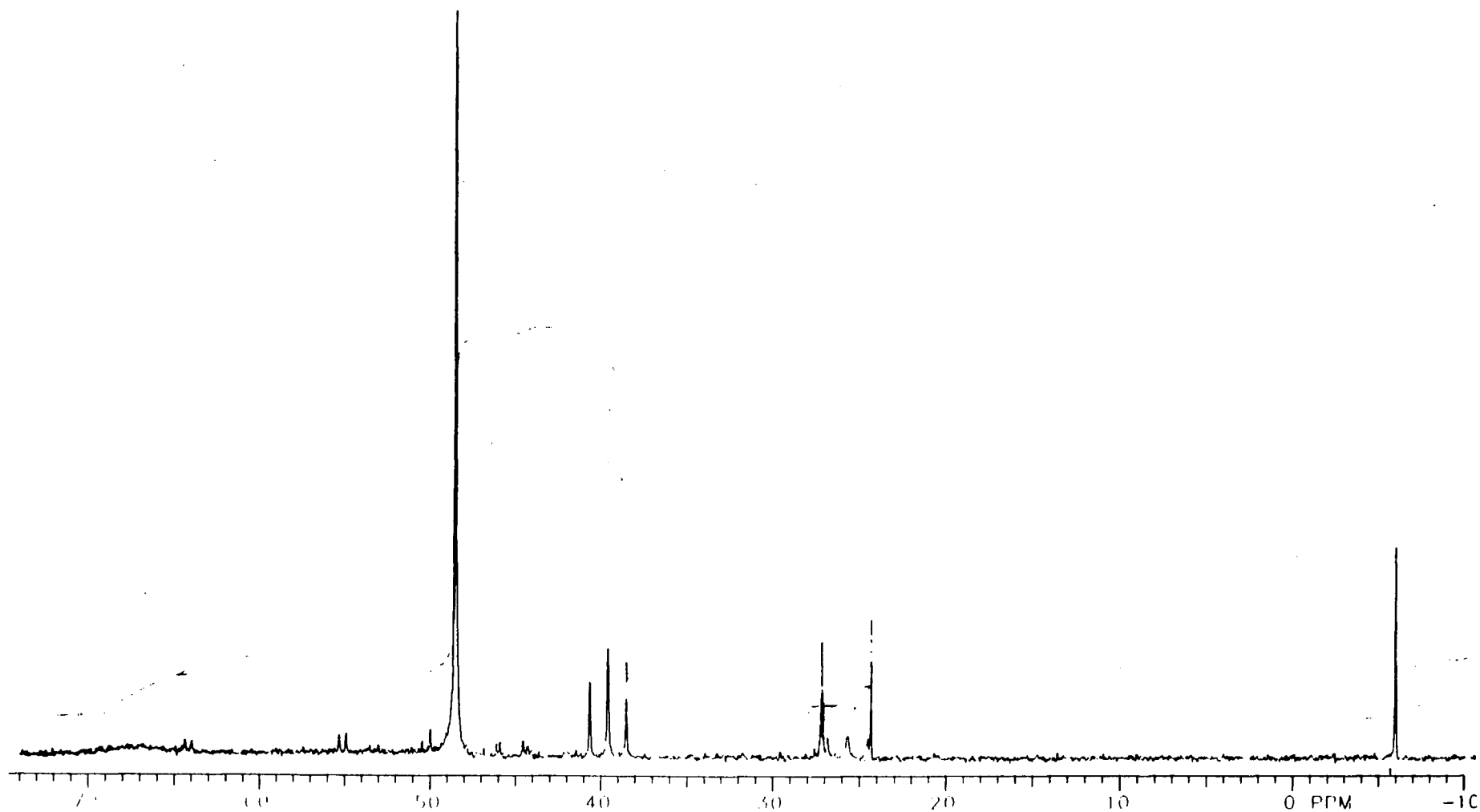
Figure 4.9: $^{31}P\{^1H\}$ NMR spectrum (121.42 MHz, 20 °C) of the reaction mixture obtained after stirring **23** in C_6D_6 solution under 1 atm H_2 for 18 h in the presence of Proton Sponge® (~1 equiv./Ru).
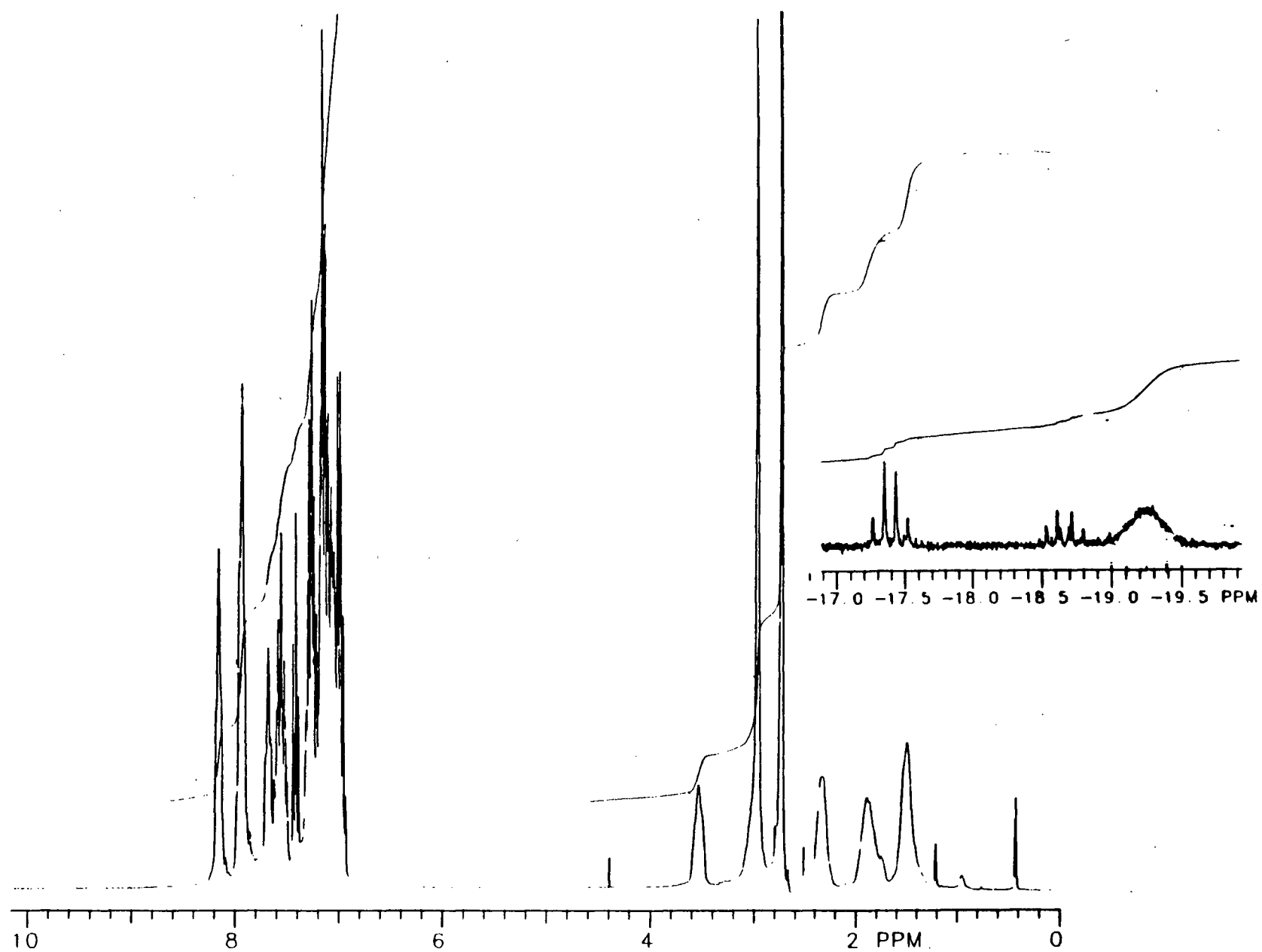
Figure 4.10: ^1H NMR spectrum (300 MHz, 20 °C) of the reaction mixture obtained after stirring **23** in C_6D_6 solution under 1 atm H_2 for 18 h in the presence of Proton Sponge® (~1 equiv./Ru).

The dark red colour of the reaction mixtures obtained after reaction with H_2 in the presence of DMA or PS is consistent with the formation of five-coordinate hydride(s); six-coordinate Ru-hydride complexes are typically pale yellow in colour whereas the five-coordinate complexes are generally intensely coloured.[37] The extremely air-sensitive nature of the red solutions also supports the presence of pentacoordinate Ru(II) species.

The proton NMR spectrum (Figure 4.10) principally consists of resonances due to [(PS)(DPPB)Ru(μ-Cl)$_3$RuCl(DPPB)]. The phenyl and naphthyl proton resonances span the δ 8.3–6.8 ppm region and the methylene protons of DPPB appear as broad multiplets at δ 3.5, 2.3, 1.9 and 1.5 ppm (4H each). The singlets at 2.85 and 2.6 ppm are assigned to the N-methyl protons of the bound and the free PS, respectively. Support for the presence of small amounts of Ru-hydride moieties in the solution comes from the signals in high-field region of the proton NMR spectrum, which consists of a pseudo-quartet (an overlapping doublet of triplet, dt, pattern) at δ –17.4 ppm, a doublet of triplets centred at –18.65, and a very broad peak at –19.25 ppm ($w_{1/2}$ ~90 Hz). The peaks at –17.4 and –18.65 ppm are tentatively assigned to two different species of the composition 'RuHCl(DPPB)(PPh$_3$)' (Figure 4.11); of note, the hydride resonance of the analogous RuHCl(PPh$_3$)$_3$ is observed at –17.75 ppm (q, $^2J_{PH}$ = 26.0 Hz, CDCl$_3$).[31] The observed $^2J_{PH}$ of ~25–30 Hz for the pseudo-quartet and the doublet of triplets indicate that the hydride is *cis* to the three phosphine ligands in both the 'RuHCl(DPPB)(PPh$_3$)' species (Figure 4.11). The broad resonance at –19.25 ppm, which is of approximately double the integral intensity of the pseudo-quartet at –17.4, may be due to a coordinated dihydrogen ligand (η^2-H$_2$)[38–40] likely *trans* to the Ru-hydride (Structure 4-IV in Figure 4.11). Reliable spin-lattice relaxation time (T_1) measurements on this signal could not be obtained because of the very low intensity of the hydride peaks. Alternatively, the 2:1 integral intensity ratio for the broad resonance at –19.25 and the dt pattern at –17.4 ppm may be purely coincidental, then the –19.25 ppm resonance could belong to a different species such as 4-II, with all three hydrogens (a hydride and a molecular H$_2$ moiety) in mutually

cis positions. Fast exchange among the three hydrogens at ambient temperature would give a broad proton NMR signal. Such fast exchange, at least on the NMR time-scale, and the consequent broadening of hydride signals in proton NMR spectra, have been observed for other polyhydride complexes containing three mutually *cis* hydrogens. The complexes $Co(H)(\eta^2-H_2)(Pr^i_2P(CH_2)_3PPr^i_2)$,[41] $[(\eta^5-C_5H_5)Ir(L)H_3]^+$ (L = PCy_3, PMe_2Ph, PPr^i_3, $AsPh_3$),[42] and $[\{\eta^5-(1,3-SiMe_3)_2-C_5H_3\}NbH_3]$[43] are some examples of complexes which exhibit exchanging hydride ligands. The resonance at -18.65 ppm (dt, $^2J_{PH} = 29$ and 25 Hz) could result from either of the two species, 4-I or 4-III, depicted in Figure 4.11.
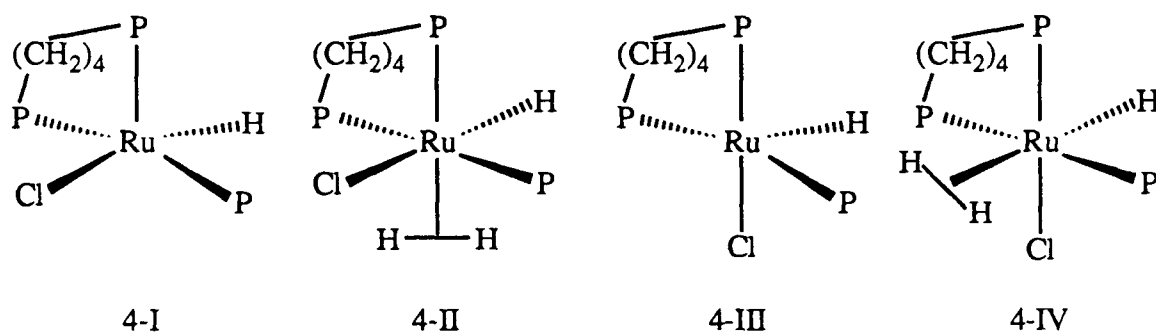
Figure 4.11: Possible structures for Ru-hydrides formed from $RuCl_2(DPPB)(PPh_3)$.

On the whole, H_2-reactivity of $RuCl_2(DPPB)(PPh_3)$ in the presence of either DMA or PS as an external base parallels that noted by C. Hampton of this department for some related mixed-phosphine complexes of general formula $RuCl_2(P-N)(PPh_3)$,[44] where P–N represents a ferrocenylaminophosphine ligand such as PPFA or isoPFA,[45] which is similar to the BPPFA ligand shown in Chapter 1, Figure 1.1. Hampton's studies showed that the PPFA and isoPFA derivatives reacted with 1 atm H_2 in the presence of DMA or PS in an apparently reversible fashion; the H_2-uptake in DMA for these complexes corresponded to ~0.39 and 0.19 mole/Ru at 30 and 50 °C, respectively. An H_2-uptake of ~0.57 mole/Ru was observed in the presence of Proton Sponge® at 30 °C.[44] The ^{31}P NMR spectra of solutions of $RuCl_2(P-N)(PPh_3)$ complexes sealed under hydrogen consisted of a large

number of peaks suggesting the presence of several species in the reaction mixture, most of which could not be isolated and identified with certainty. The presence of some Ru-hydride species was evident from signals in the high-field region of the proton NMR spectra. The hydrides RuHCl(isoPFA)(PPh$_3$) and RuHCl(PPh$_3$)$_3$, and a dinuclear dihydrogen complex, [(η^2-H$_2$)(isoPFA)Ru(μ-Cl)$_2$(μ-H)RuH(PPh$_3$)$_2$],[46] were the only products that could be isolated and characterised from the reaction of RuCl$_2$(isoPFA)(PPh$_3$) with H$_2$ in benzene/methanol solutions.[44]

During the present study, attempts to isolate 'RuHCl(DPPB)(PPh$_3$)' and related hydrides formed in the reaction of 23 with H$_2$ were not successful; however, as described in the following sections, reactions with chelating reagents L–L (see Sections 4.4, 4.5 and 6.2) of these hydrides prepared *in situ* generally resulted in the displacement of the triphenylphosphine ligand to afford six-coordinate RuHCl(DPPB)(L–L) complexes.

4.4 Synthesis of RuCl$_2$(DPPB)(PPh$_2$Py)

Reaction of RuCl$_2$(DPPB)(PPh$_3$) with one equivalent of diphenyl(2-pyridyl)-phosphine, PPh$_2$Py, in dichloromethane gave an orange-yellow product which was identified as *trans*–RuCl$_2$(DPPB)(PPh$_2$Py), 24, as shown in Figure 4.12. The complex was characterised by NMR spectroscopy and elemental analysis.
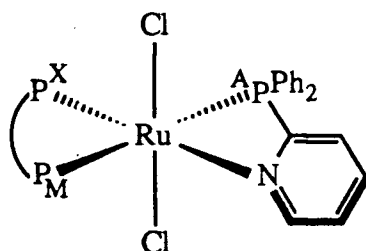
Figure 4.12: *Trans*–RuCl$_2$(DPPB)(PPh$_2$Py), 24.

The ^{31}P NMR spectrum of this compound in C_6D_6 solution displayed an AMX pattern which consisted of three doublet of doublets of equal integral intensity (Figure 4.13). The doublet of doublets centred at –21.0 ppm is assigned to the PPh$_2$Py ligand (P_A) and the remaining two sets at 24.9 (P_M) and 45.0 (P_X) ppm, respectively, are attributed to the DPPB ligand. The $^2J_{AM}$ of 328.5 Hz is indicative of two mutually *trans* phosphines, each of which shows a further coupling of 28.1 and 36.9 Hz, respectively, due to the third phosphine (P_X) in the *cis* position. The coordination shift of –16 ppm for the Ru(II)-bound PPh$_2$Py, relative to the free ligand singlet at –5.0 ppm, is in the same direction and range as that observed for an *ortho*-metallated PPh$_3$ ligand bound to a Ru(II) centre.[47] A ring contribution[15] (Δ_R) can be calculated for the chelating PPh$_2$Py by subtracting from its chemical shift that for the non-chelating PPh$_3$ ligand in the formally analogous RuCl$_2$(DPPB)(PPh$_3$) complex, **23**; the Δ_R value of –47.3 ppm (Δ_R = –21.0 – 26.3 = –47.3 ppm) is characteristic of formation of a four-membered ring.[15] The 45.0 ppm resonance for **24** is ~38 ppm high-field of the resonance due to the apical phosphorus of **23**, strongly suggesting that the *trans* site in the PPh$_2$Py derivative is occupied by the pyridyl group giving a six-coordinate complex. The additional sets of resonances in the ^{31}P NMR spectrum of *trans*–RuCl$_2$(DPPB)(PPh$_2$Py) at 47.2, 35.9 and –21.4 ppm are attributed to the *cis*–RuCl$_2$(DPPB)(PPh$_2$Py) complex (see below). The ^{1}H NMR spectrum of **24** (Figure 4.14) shows the pyridyl proton resonances shifted upfield of the corresponding free ligand proton values of ~7.2–7.1 ppm (m, 4H) to ~6.6 (m, 3H) and 6.2 (m, 1H) ppm.

The reaction of **23** with PPh$_2$Py was carried out with a view of incorporating a nitrogenous base, in this case the pyridyl group, in a ruthenium-bound ligand. Because of what appeared to be a reversible reaction of **23** with H$_2$ in the presence of an external base such as DMA (Section 4.3), it seemed appropriate to introduce a basic site in a coordinated
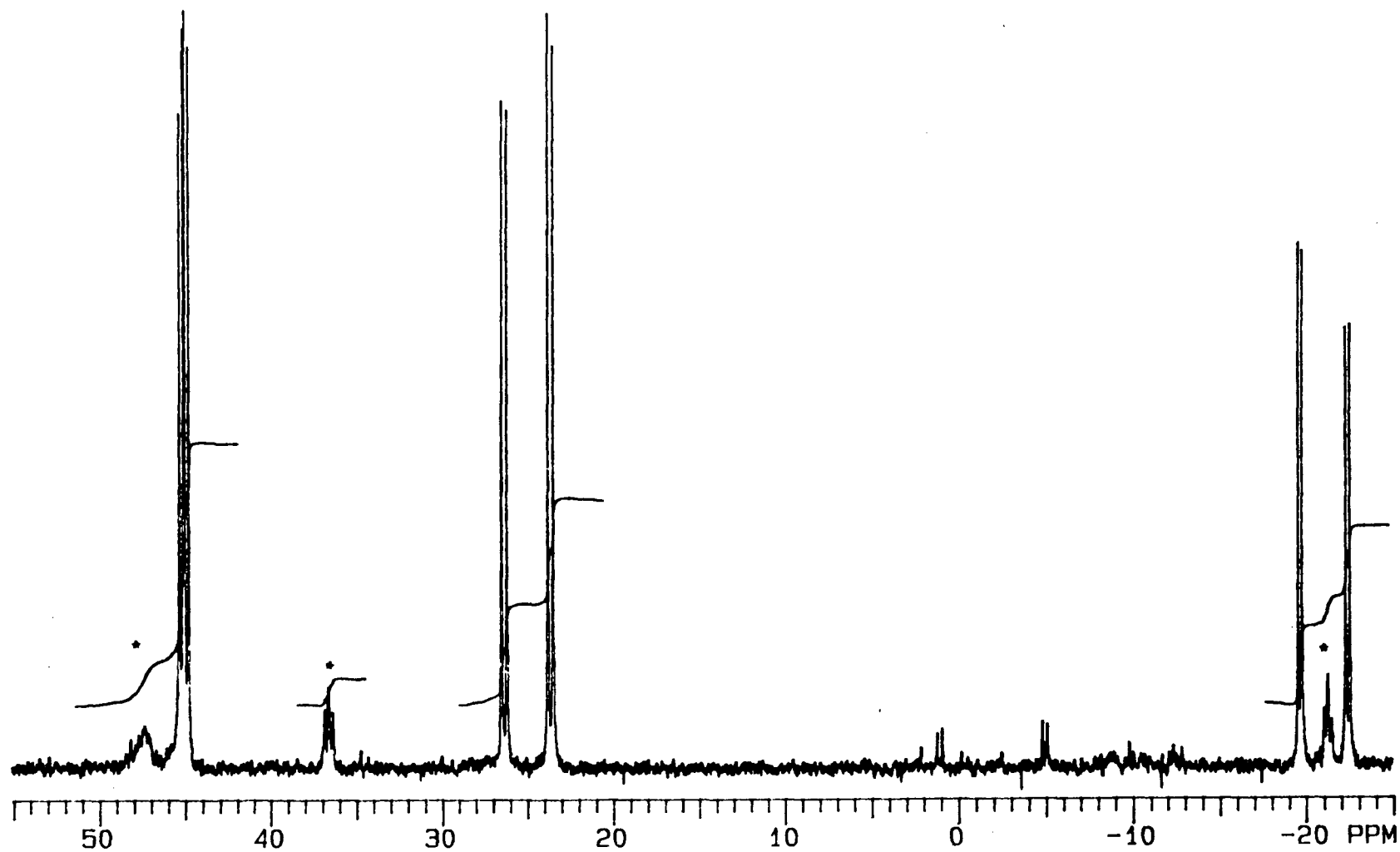
Figure 4.13: The $^{31}P\{^{1}H\}$ NMR spectrum (121.42 MHz, C_6D_6, 20 °C) of *trans*-$RuCl_2(DPPB)(PPh_2Py)$. The peaks marked with asterisks are due to the *cis* isomer (~12% of total integral intensity).
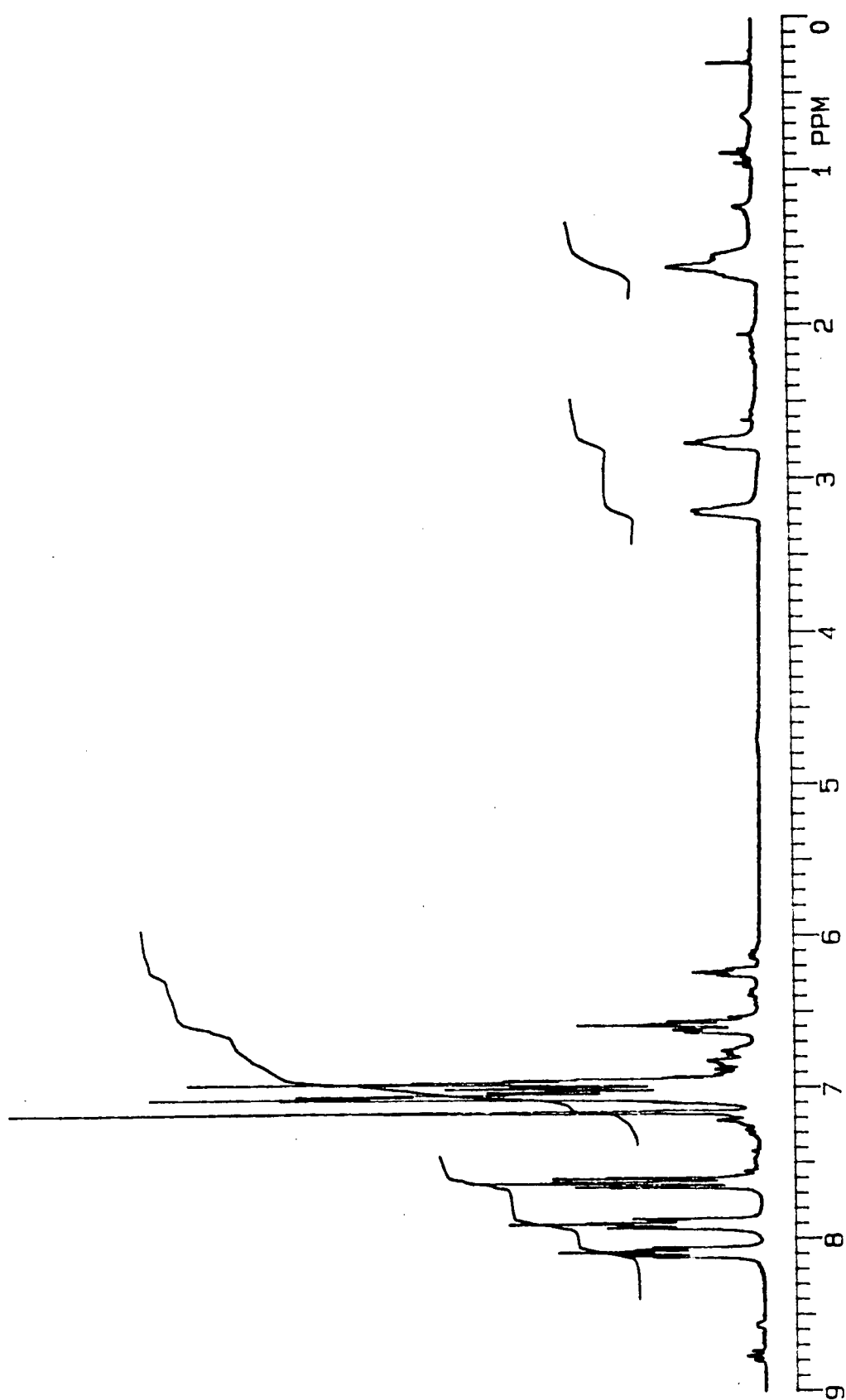
Figure 4.14: The ^{1}H NMR spectrum (300 MHz, C$_6$D$_6$, 20 °C) of *trans*–RuCl$_2$(DPPB)(PPh$_2$Py).

ligand which could, under hydrogenation conditions, perhaps promote hydride formation by "picking up" the HCl (heterolytic cleavage of H_2;[33, 34] *cf.* Chapter 1, Section 1.3), and simultaneously providing a coordination site for subsequent substrate binding (Equation 4.5).

(4.5)
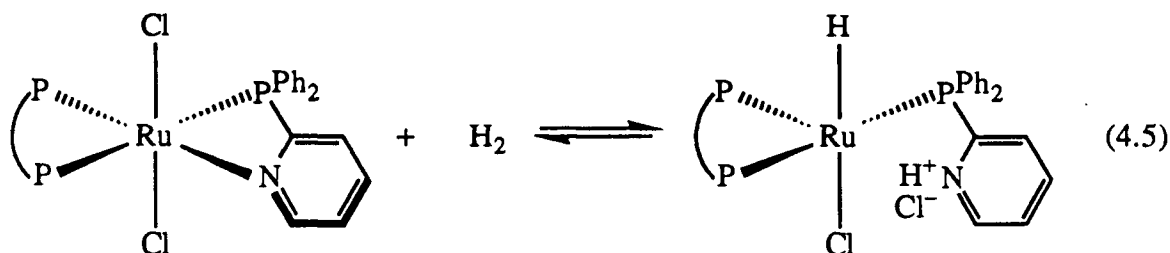
As mentioned at the end of the previous section, ongoing H_2-activation work from this department has involved Ru(II) complexes of ferrocenylaminophosphine ligands, such as PPFA and isoPFA, which contain both phosphorus and nitrogen centres (*cf.* Chapter 1, Figure 1.1).[44–46, 48] The amino group of the PPFA ligand in $RuCl_2(PPFA)(PPh_3)$ has been shown to participate in dihydrogen activation.[44]

Heating a toluene solution of *trans*–$RuCl_2(DPPB)(PPh_2Py)$ at 80 °C under 1 atm of H_2 for 8 h resulted in the precipitation of a yellow-orange solid, **25**. The $^{31}P\{^1H\}$ and the ^1H NMR spectra of the product in $CDCl_3$ solution at 20 °C are shown in Figures 4.15 and 4.16, respectively. The absence of proton resonances in the high-field region (0 to –30 ppm) means no hydride(s) were formed during the reaction. The ^{31}P NMR spectrum shows overlapping doublet of doublet patterns centred at –21.4, 35.9 and 47.2 ppm with $^2J_{PP}$ of 23–35 Hz, which are characteristic of a mutually *cis* arrangement of the three phosphine groups. The same resonances are also present in the ^{31}P spectrum of the *trans* isomer in about 12% of the integral intensity (see Figure 4.13). Furthermore, heating a solution of the *trans* isomer in the absence of H_2 leads to the formation of the same product(s) as evidenced by ^1H and the ^{31}P NMR spectroscopy. All of these observations are consistent with the *cis* formulation for **25** as illustrated in Figure 4.17.
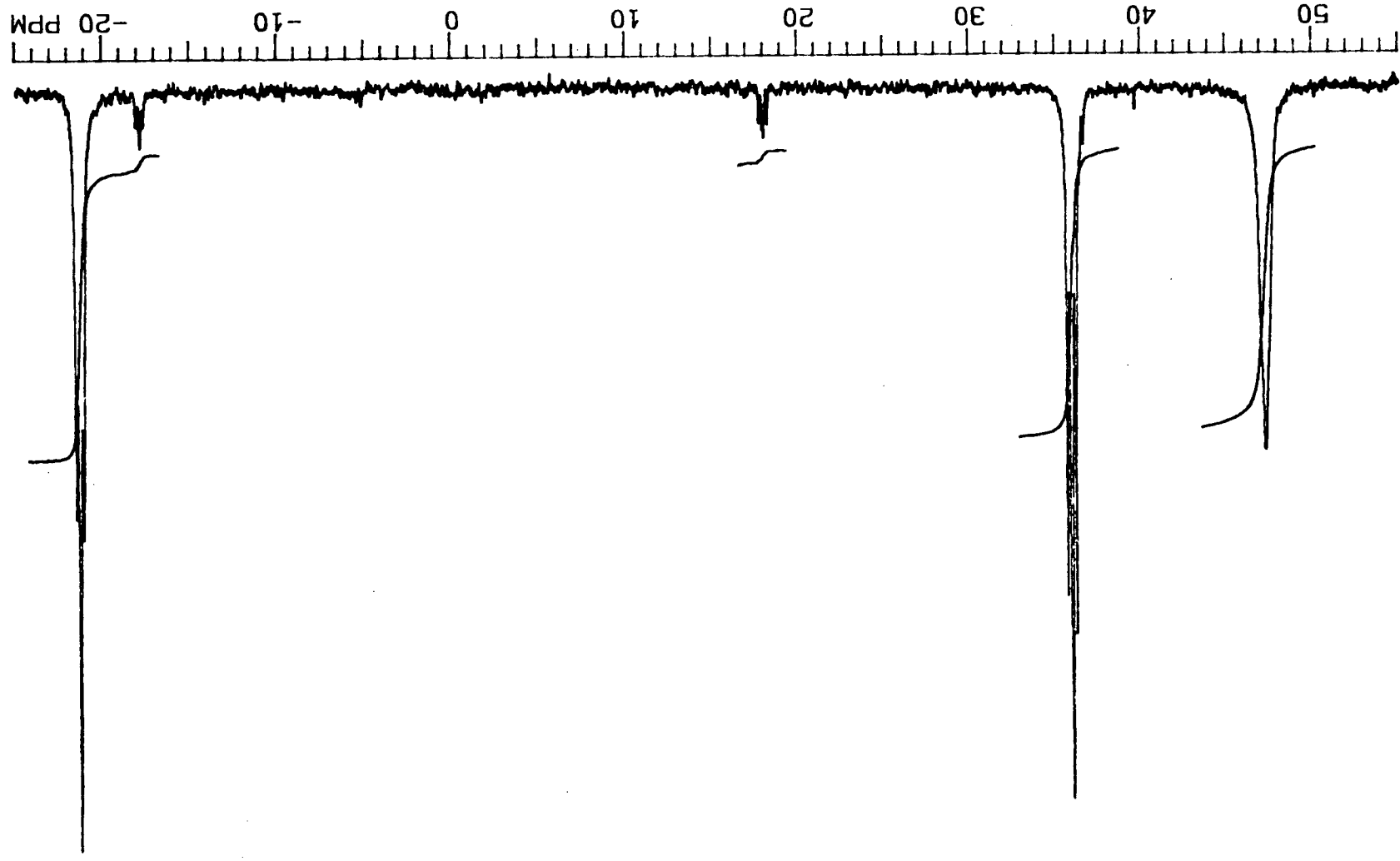
Figure 4.15: The 31P{1H} NMR spectrum (121.42 MHz, CDCl$_3$, 20 °C) of *cis*-RuCl$_2$(DPPB)(PPh$_2$Py)
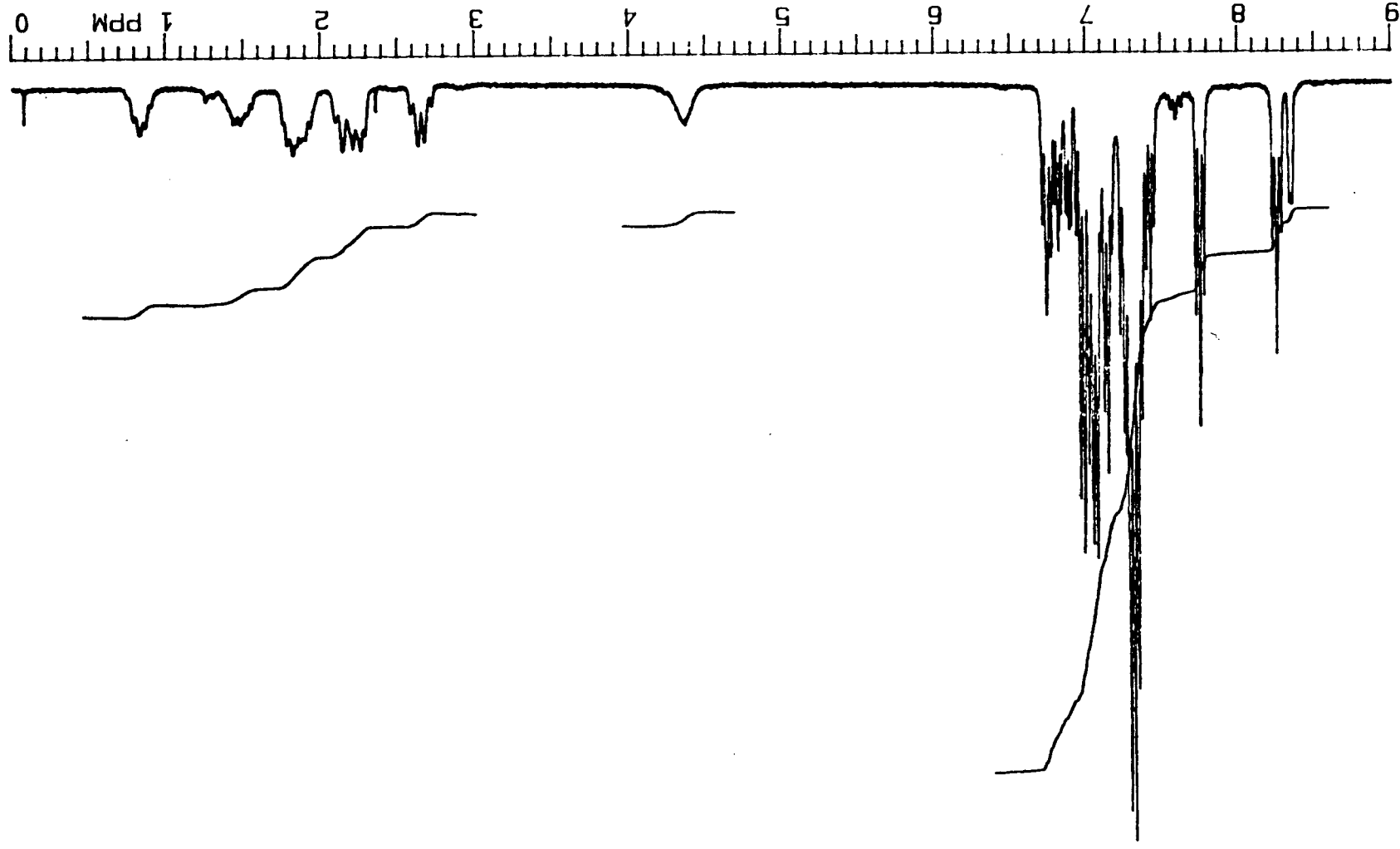
Figure 4.16: The 1H NMR spectrum (300 MHz, CDCl₃, 20 °C) of *cis*-RuCl₂(DPPB)(PPh₂Py).

159
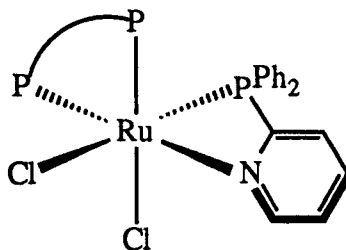
Figure 4.17: *Cis*—RuCl$_2$(DPPB)(PPh$_2$Py), **25**.

The additional set of three 1:1:1 doublet of doublet ^{31}P NMR patterns of *ca.* 4% integral intensity, and centred at −18.0, 17.8 and 36.0 ppm in the spectrum of **25** (Figure 4.15), remains unassigned. The observed P-Ru-P coupling constants ($^2J_{PP}$ ~25–30 Hz) for this as yet unidentified product are characteristic of a mutually *cis* arrangement of the three phosphine groups.

The relative insolubility of the *cis* isomer **25** (*vs. trans*) in nonpolar solvents such as benzene or toluene is consistent with a higher dipole moment, and therefore an increased polarity, expected for the *cis* complex. Such differences in solubility in polar and nonpolar solvents have been noted for other *cis/trans* six-coordinate Ru(II) complexes (e.g. *cis,cis,trans*– and all *trans*–RuHCl(CO)$_2$(PPh$_3$)$_2$[49]), the *cis* isomers generally being relatively less soluble in nonpolar solvents and the *trans* complexes in polar solvents.

The observed isomerisation of the *trans* derivative, **24**, to the corresponding *cis* complex, **25**, under hydrogenation conditions specified earlier was unexpected, but in retrospect not surprising. Complex **24** obtained by reaction of **23** with PPh$_2$Py must be the kinetic product, which on heating isomerises to the thermodynamically more stable *cis* species **25**. The relative insolubility of **25** in aromatic solvents likely aids the isomerisation process by continually driving the equilibrium toward the formation of more *cis* isomer which continues to precipitate from the benzene or toluene solutions. For Ru(II) complexes such as RuCl$_2$(Ph$_2$P(CH$_2$)$_{1-3}$PPh$_2$)$_2$, which contain two chelating phosphine ligands, the *cis*-dichloro arrangement is often thermodynamically favoured over the *trans*

configuration.[50]   Interestingly however, the kinetically favoured *trans–*RuCl$_2$(diphosphine)$_2$ complexes are almost always more prevalent.[51] Presumably, the diphosphines bind to Ru too strongly to permit dissociation of one end of the chelate to produce a five-coordinate fluxional intermediate that could undergo rearrangement to give the *cis* isomer.

A possible mechanism for the formation of **24** from **23** and the subsequent isomerisation of **24** to **25** is outlined in Scheme 4-I. The incoming pyridylphosphine ligand occupies the vacant coordination site *trans* to the apical phosphine end of the DPPB ligand of **23** to give a six-coordinate intermediate (**A**);   dissociation of PPh$_3$ and coordination of the pyridyl nitrogen would give the observed *trans-* kinetic product (**24**).

In view of the relative inertness of the *trans–*RuCl$_2$(diphosphine)$_2$ complexes to isomerisation to the respective *cis* analogues, it is reasonable to assume that the pyridyl group, rather than a phosphine, undergoes dissociation to give a five-coordinate intermediate (**B**). The coordinated DPPB ligand, however, is known to dissociate at one end and become "dangling" in some Ru(II) systems.[52] To test for possible involvement of DPPB, the new complex *trans–*RuCl$_2$(DPPB)(DPPM), **27**, analogous to **24** in geometry and also in that it contains a four-membered chelate similar to PPh$_2$Py, but without a nitrogen centre, was synthesised. No isomerisation to the *cis* isomer was detected for **27**, even after heating in toluene solution at 80 °C for 48 h (see Section 4.5 for details). This observation provides some indirect support for the non-involvement of the DPPB ligand in the isomerisation of **24**, and by the same token suggests that the presence of the pyridyl group in **24** plays a key role in the isomerisation of **24** to the *cis* derivative **25**. Related isomerisation reactions in some pyridylphosphine Pt and Pd complexes also occur *via* dissociation of the pyridyl functionality.[53] Five-coordinate Ru(II) complexes are known to be stereochemically non-rigid,[1, 3, 13, 54] and can readily rearrange via a Berry pseudo-
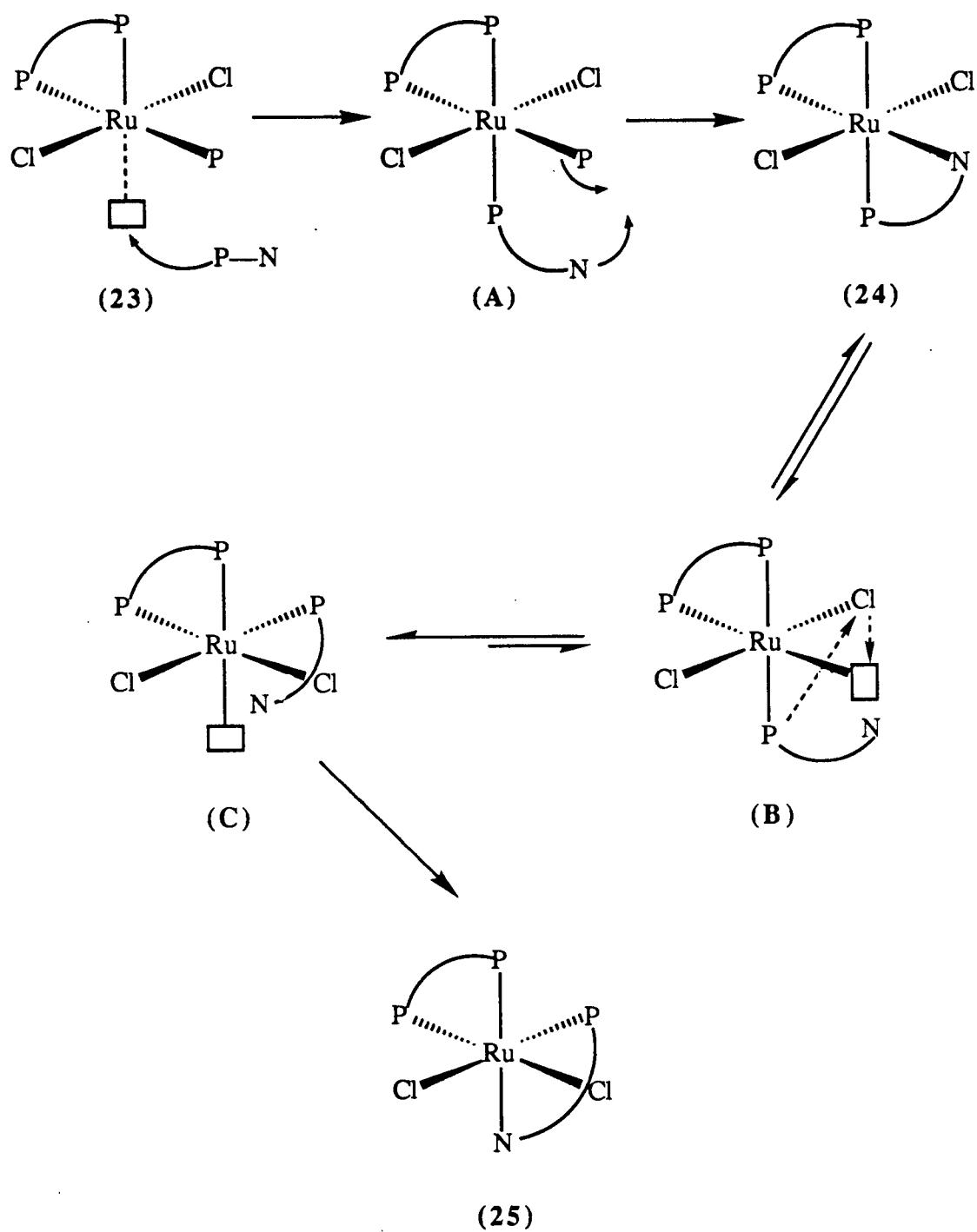
Scheme 4-I: A possible mechanism for the formation of **24** and **25** from **23**; DPPB and PPh$_2$Py are denoted by P—P and P—N, respectively.

rotation mechanism.[55] Recoordination of the pyridyl group to the ruthenium centre in the rearranged five-coordinate intermediate C then produces the *cis* isomer 25.

The *cis* complex 25 can exist in two enantiomeric forms designated Δ and Λ[54b, 56] as illustrated in Figure 4.18; however, the two isomers cannot be differentiated from each other by NMR spectroscopy. However, substitution of the nonchiral DPPB ligand by a chiral DIOP or BINAP ligand would result in the formation of diastereomers, and would be of interest.

Δ Λ
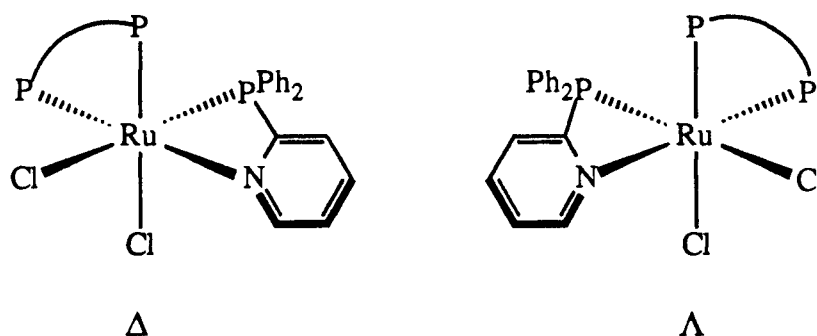
Figure 4.18: Enantiomeric forms of *cis-(fac)*–$RuCl_2$(DPPB)(PPh_2Py), 25.

Although the attempts to make the hydride complex RuHCl(DPPB)(PPh_2Py) or RuHCl(DPPB)($PPh_2PyH^+Cl^-$) by reaction of *trans*–$RuCl_2$(DPPB)(PPh_2Py) with H_2 were unsuccessful, and instead resulted in the isomerisation of the starting complex to the corresponding *cis* isomer, 25, the former hydride complex was eventually synthesised using a different approach.

As described earlier (Section 4.3), the reaction of $RuCl_2$(DPPB)(PPh_3) with H_2 in the presence of Proton Sponge® produces hydride species such as RuHCl(DPPB)(PPh_3) in solution. Addition of PPh_2Py (1 equiv./Ru) to a dark red solution of ruthenium hydrides, generated *in situ* by treating 23 (0.2 g, 0.23 mmol) in ~20 mL toluene with 1 atm H_2 in the presence of PS at 65 °C, resulted in a rapid colour-change to orange. The yellow-orange solid that precipitated over two hours of stirring the reaction mixture under

H_2 was separated by filtration, washed with ethanol to remove any PSH^+Cl^-, and vacuum-dried (yield: 0.08 g). The ^{31}P and ^{1}H NMR spectra of the yellow-orange solid were identical to those observed for the cis–$RuCl_2$(DPPB)(PPh_2Py) complex (see Figures 4.15–4.17). An orange-brown solid was then isolated from the toluene filtrate by concentration to ~5 mL followed by addition of hexanes (yield: 0.08 g).

The ^{31}P and ^{1}H NMR spectra of the orange-brown product in C_6D_6 solution are shown in Figures 4.19 and 4.20, respectively. The high-field overlapping doublet of triplet pattern at −13.7 ppm in the proton NMR spectrum is indicative of a hydride species, **26** (see Figure 4.21). The magnitude of the H-Ru-P coupling constants suggests that the hydride is cis to the three phosphine groups ($^2J_{PH}$ = 23.1 Hz, d; 21.6 Hz, t). Proton NMR signals due to Ru-H moieties trans to a chloride ligand of trans–$RuHCl(Ph_2P(CH_2)_nPPh_2)_2$ species for n = 1–4 have been reported, and are observed in the range δ −13 to −20 ppm (q, $^2J_{PH}$ ~19–22 Hz).[2]

Examination of the phosphorus NMR spectrum points to the presence of at least three species. One of the products is readily identified as the trans–$RuCl_2$(DPPB)(PPh_2Py) complex, **24** (~43% based on integral intensity), by comparison of the phosphorus NMR data (Figure 4.13); a small amount of the cis isomer **25** is also evident (~7% based on integral intensity). The new sets of resonances centred at −12.9, 40.9 and 59.9 ppm (AMX pattern), amounting to ~50% of the total integral intensity, are assigned to the hydride species; one trans and two cis P-Ru-P couplings ($^2J_{P-P}$) are evident. The resonances centred at −12.9 ppm (δ_A) are attributed to the bound PPh_2Py and the remaining two sets of signals centred at 40.9 (δ_M), 59.9 (δ_X) ppm to the DPPB ligand for reasons elucidated earlier. All phosphorus resonances of **26** show a small residual coupling of ~8–11 Hz because of inadequate broadband proton decoupling, particularly of the high-field ruthenium hydride; the extra splittings disappeared when the broadband decoupler power was increased to the maximum available.
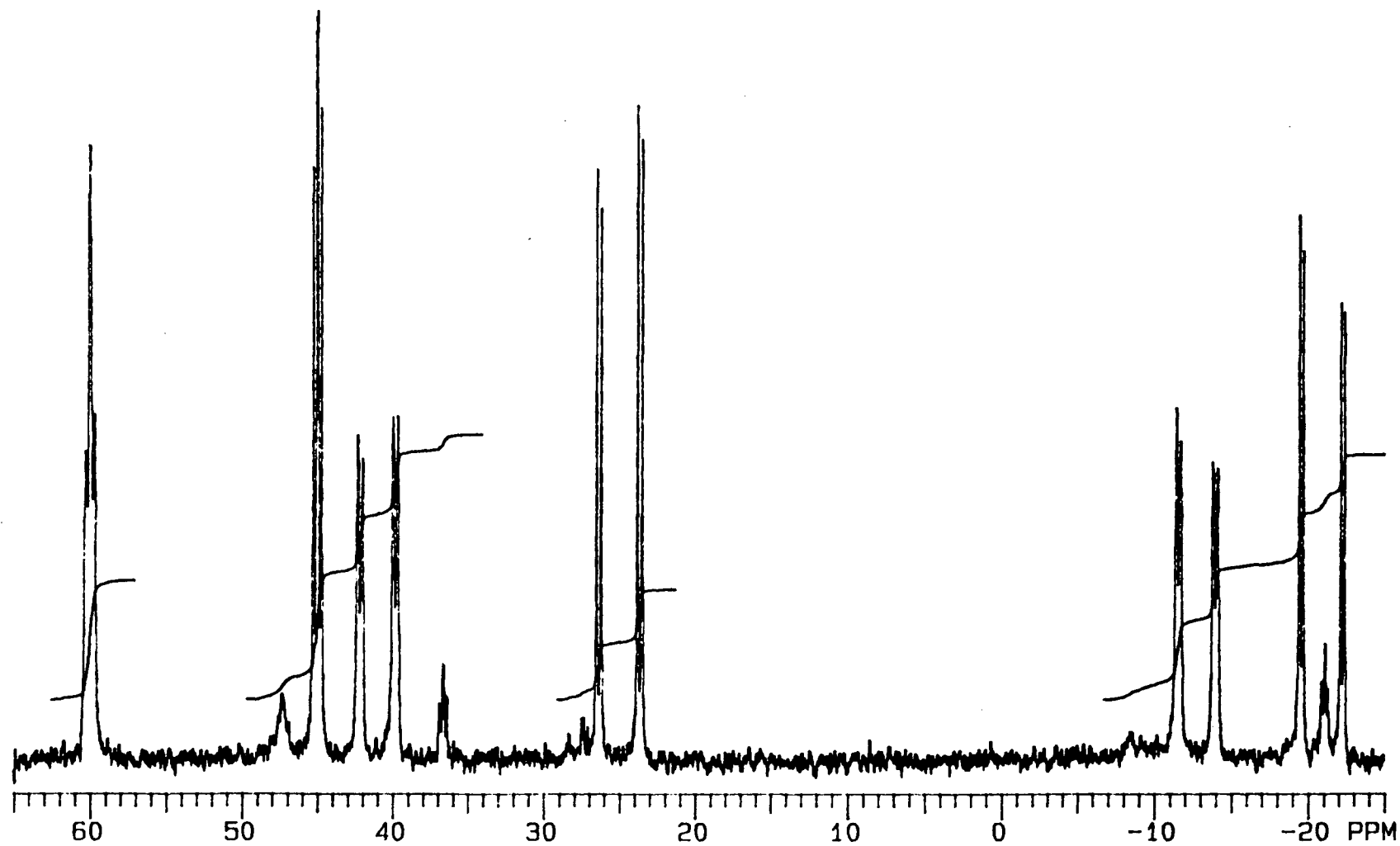
Figure 4.19: The ^{31}P NMR spectrum (121.42 MHz, C_6D_6, 20 °C) of the orange-brown solid obtained from the reaction of PPh_2Py with hydrides formed *in situ* from the reaction of **23** with H_2 in the presence of Proton Sponge®.
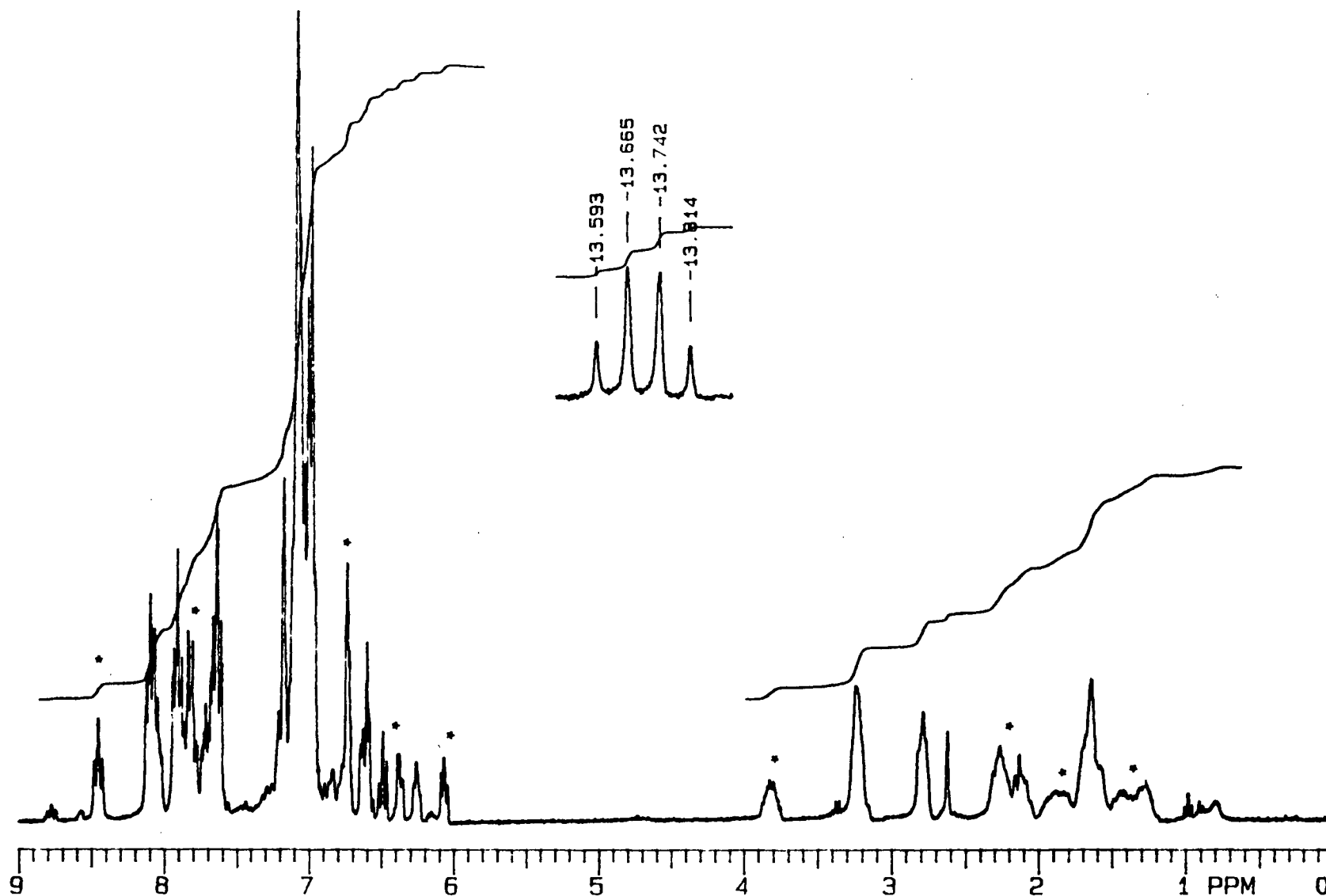
Figure 4.20: The ^{1}H NMR spectrum (300 MHz, C_6D_6, 20 °C) of the orange-brown solid obtained from the reaction of PPh$_2$Py with hydrides formed *in situ* from the reaction of **23** with H$_2$ in the presence of Proton Sponge®. The peaks assigned to the hydride complex **26** (see text) are marked by asterisks. The hydride resonance is also shown (INSET).

Overall, the dichloro- complexes (24 and 25 together) and the hydridochloro-derivative (26) were produced in *ca.* 2:1 ratio based on relative NMR integral intensities; further purification and isolation of the hydride derivative were not attempted. Consistent with the available NMR spectral data, the hydride complex, 26, is assigned the *trans* geometry shown in Figure 4.21. The ^{31}P NMR spectral data for the Ru(II)-pyridylphosphine complexes 24–26 are listed in Table 4.3.
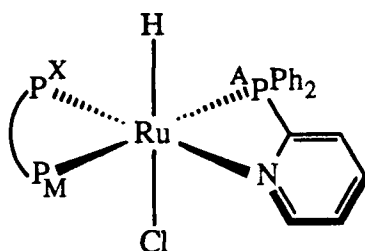
Figure 4.21: *Trans*–RuHCl(DPPB)(PPh₂Py), 26.

The phosphorus chemical shifts of the hydridochloro complex 26 are observed to low field of the corresponding resonances of the dichloro analogue 24. A similar relative low-field shift in ^{31}P chemical shifts on replacing a chloride by a hydride ligand is observed for other Ru(II)-phosphine complexes; for example, the ^{31}P chemical shifts for *trans*–RuHCl(P–P)₂ complexes[2] are: P–P, δ ppm (s) = DPPM, –3.8; DPPE, 60.8; DPPP, 15.6, as compared to the chemical shifts for the corresponding *trans*–RuCl₂(P–P)₂ complexes:[1] P–P, δ ppm = DPPM, –7.7; DPPE, 44.3; DPPP, –5.0.

Table 4.3: $^{31}P\{^1H\}$ NMR Spectral Data[a] for RuXCl(DPPB)(PPh$_2$Py) Complexes **24–26** (X = Cl, H).

Complex	Chemical Shift, δ ppm (Assignment) ($^2J_{PP}$, Hz)		
Trans-(mer)–RuCl$_2$(DPPB)(PPh$_2$Py)	–21.0 (P$_A$)	24.9 (P$_M$)	45.0 (P$_X$)
(24) AMX Pattern	($^2J_{AX}$ = 28.1)	($^2J_{AM}$ = 328.5)	($^2J_{MX}$ = 36.9)
Cis-(fac)–RuCl$_2$(DPPB)(PPh$_2$Py)	–21.4 (P$_A$)	35.9 (P$_M$)	47.2 (P$_X$)
(25) AMX Pattern	($^2J_{AX}$ = 23.7)	($^2J_{AM}$ = 27.3)	($^2J_{MX}$ = 34.7)
Trans-(mer)–RuHCl(DPPB)(PPh$_2$Py)[b]	–12.9 (P$_A$)	40.9 (P$_M$)	59.9 (P$_X$)
(26) AMX Pattern	($^2J_{AX}$ = 31.2)	($^2J_{AM}$ = 288.3)	($^2J_{MX}$ = 36.7)

[a] 121.42 MHz, at 20 °C; in C$_6$D$_6$ for complexes **24** and **26**, in CDCl$_3$ for **25**. PPh$_2$Py is designated as P$_A$ while P$_M$ and P$_X$ refer to the phosphorus nuclei of the DPPB ligand.

[b] ^{1}H NMR (300 MHz, C$_6$D$_6$, 20 °C) signal for Ru–H is observed at –13.7 ppm (dt; $^2J_{PH}$ = 23.1 Hz, d; 21.6 Hz, t).

4.5 Synthesis of *Trans*–RuCl$_2$(DPPB)(DPPM)

Addition of one equivalent of the diphosphine DPPM to a dichloromethane or benzene solution of RuCl$_2$(DPPB)(PPh$_3$) resulted in a rapid colour change from the initial green to yellow. A pale brownish-yellow solid that was isolated from the yellow solution is identified as *trans*–RuCl$_2$(DPPB)(DPPM), **27** (Figure 4.22), by ^{1}H and ^{31}P NMR spectroscopy and elemental analysis; full preparative details are given in Section 2.5.9.2.

168
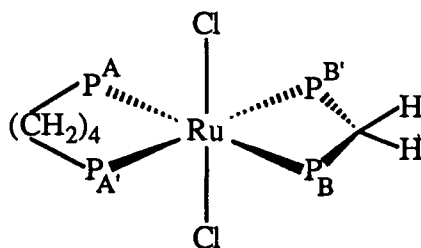
Figure 4.22: *Trans*-RuCl₂(DPPB)(DPPM), **27**.

The ^{1}H NMR spectrum of **27** in C_6D_6 (Figure 4.23) shows a triplet at δ 4.65 (2H) for the methylene protons of DPPM, and broad multiplets at δ 2.95 (4H) and 2.60 (4H) for the methylene protons of DPPB. The resonances for the *ortho*-phenyl protons are observed at δ 7.65 (8H, DPPB) and 7.45 (8H, DPPM) while those for the *meta*- and *para*-phenyl protons of DPPB and DPPM are observed as overlapping multiplets in the 7.0–6.8 ppm region (total 24H).

The ^{31}P NMR spectrum of **27** is second order in nature ($\Delta\delta/J < 6$;[9] Figure 4.24). That the complex patterns seen in the spectrum of **27** arise from a single compound was confirmed by a ^{31}P–^{31}P homonuclear correlation (*COSY*) experiment. It is evident from the contour plot shown in Figure 4.25 that all the resonances are connected with each other *via* off-diagonal peaks, thus indicating that all four phosphorus nuclei within **27** are coupled with each other.

Complexes of the type *trans*-RuCl₂(P–P)₂ generally exhibit just a singlet in the ^{31}P NMR spectrum, all four phosphorus nuclei being chemically and magnetically equivalent. For example, the chiral Ru(II) analogues containing the diphosphines *S,S*-CHIRAPHOS[56] or *S,S*-BDPP (present work, see Chapter 2, Section 2.5.8.4), for which the two ends of the chiral diphosphine are magnetically equivalent, show just a singlet in the ^{31}P spectra (*cf.* Chapter 3, Section 3.4). A combination of relative flexibility of diphosphine backbone and molecular motion in solution can sometimes result in the apparent equivalence of the phosphorus nuclei as seen for RuHCl(CHIRAPHOS)₂.[12, 56] The relatively large scalar
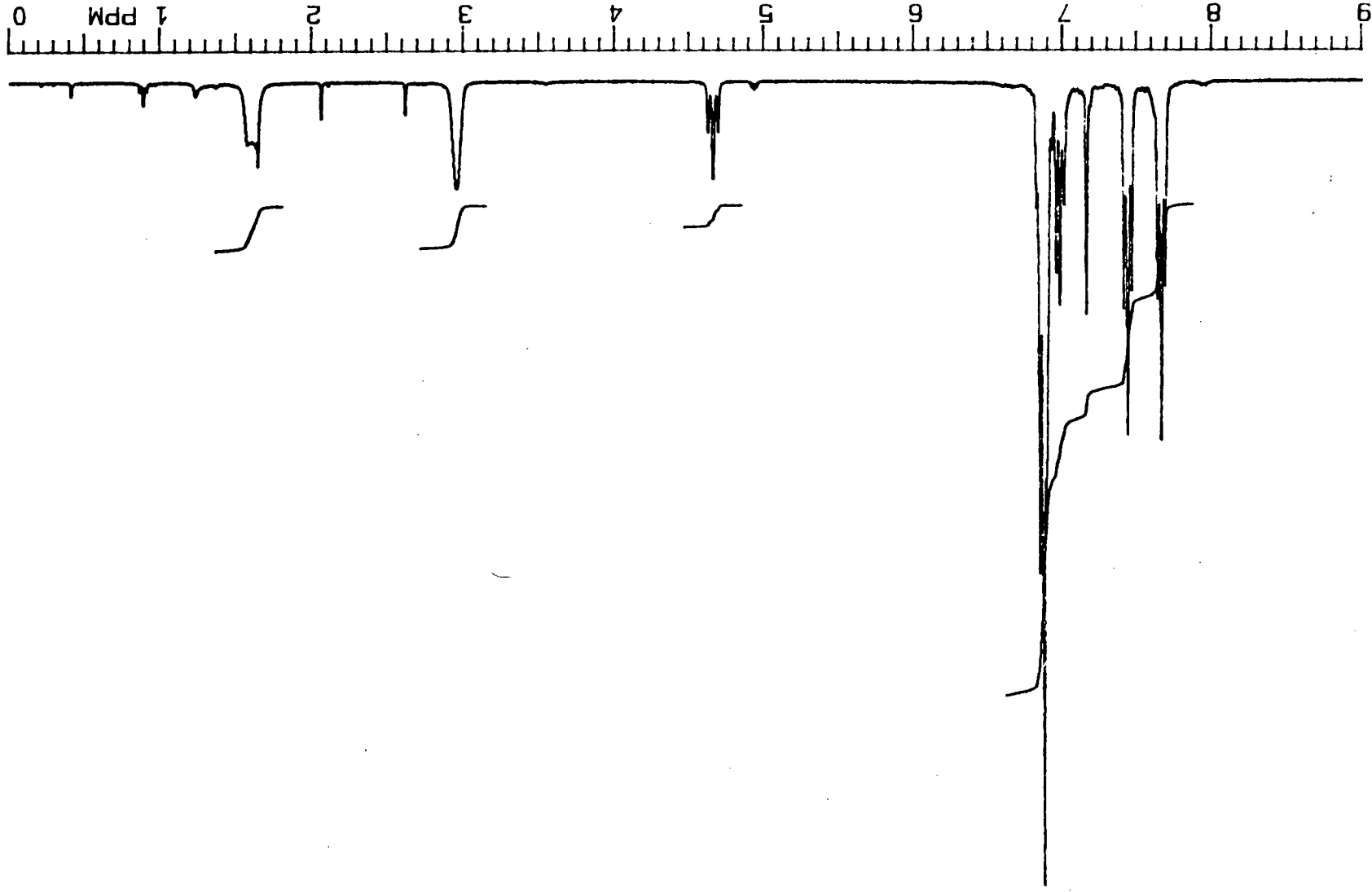
Figure 4.23: Proton NMR spectrum (300 MHz, C_6D_6, 20 °C) of *trans*-RuCl$_2$(DPPB)(DPPM), 27.

170

Figure 4.24: ³¹P{¹H} NMR spectrum (121.42 MHz, C₆D₆, 20 °C) of *trans*-RuCl₂(DPPB)(DPPM), **27**.
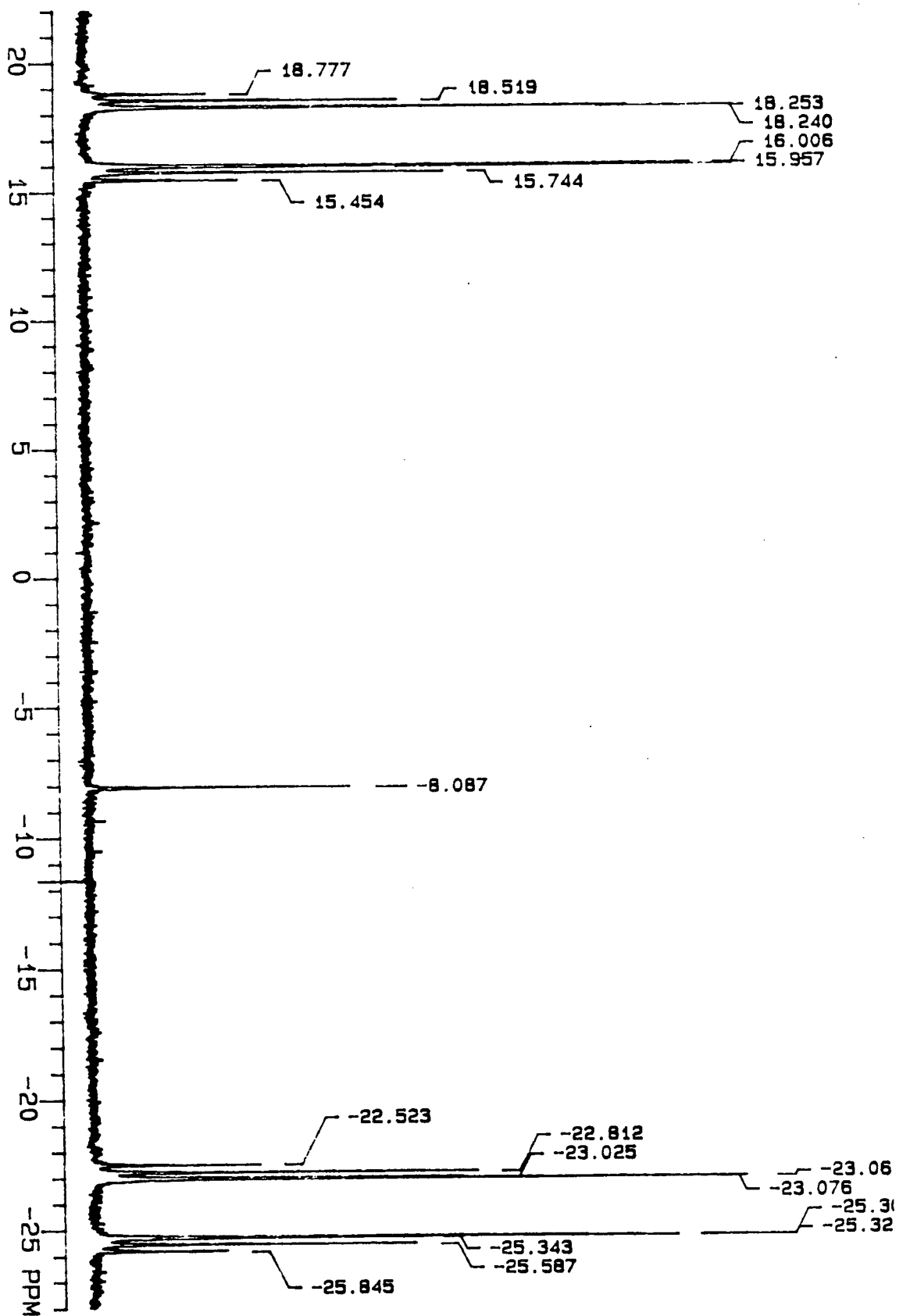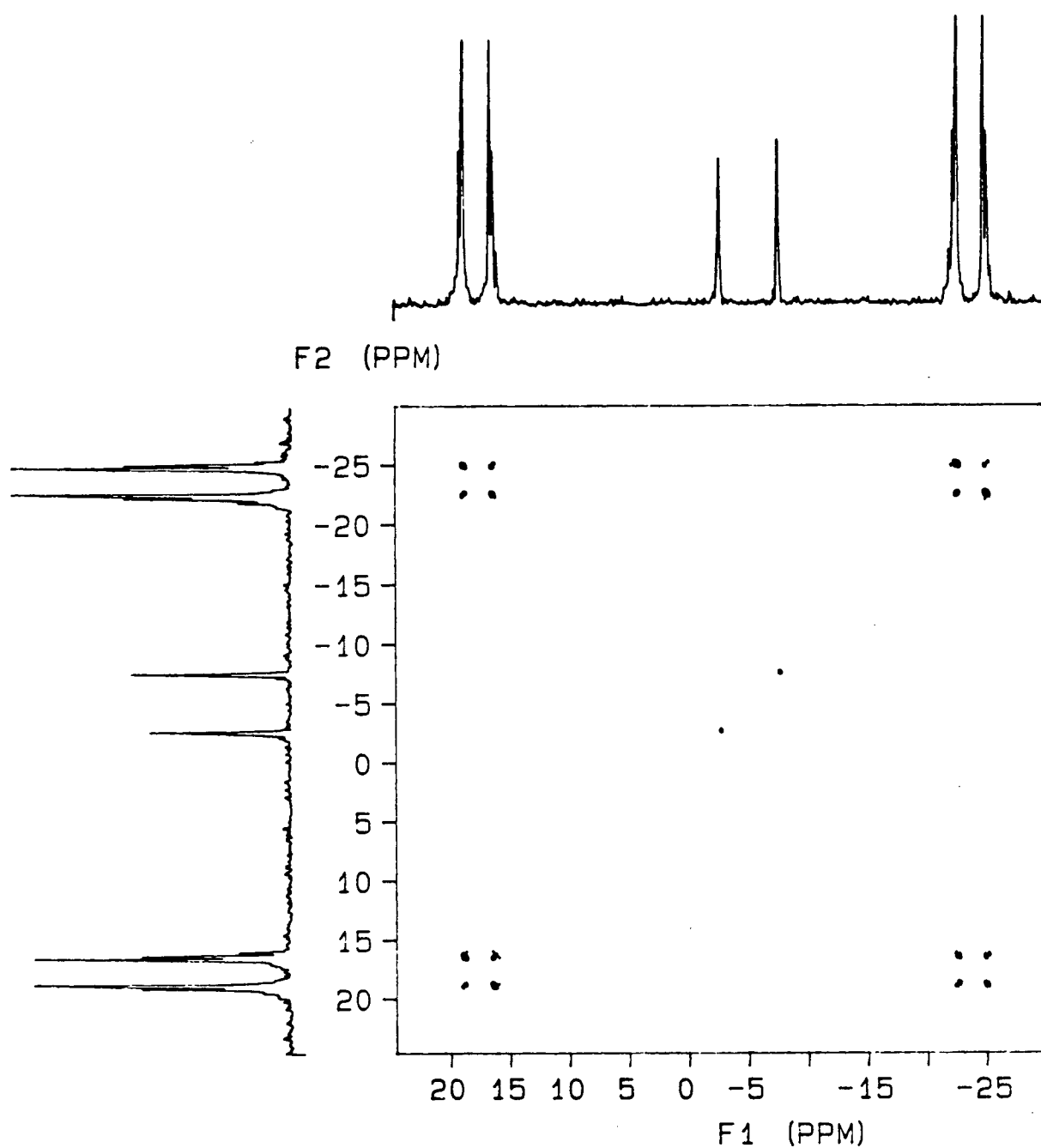
Figure 4.25: $^{31}P-^{31}P$ homonuclear *COSY* contour plot (121.42 MHz, 20 °C) of
trans-RuCl$_2$(DPPB)(DPPM), **27**, in C$_6$D$_6$ solution.

172

due to *trans*-disposed phosphines, $^2J_{PP}$ (~200–350 Hz[15]), is in fact seldom seen in solution spectra of *trans*–RuCl$_2$(P–P)$_2$ complexes. In complex **27**, however, the two diphosphine ligands, *viz*. DPPB and DPPM, are sufficiently different from each other that separate resonances are observed, giving rise to the second order AA'BB' ^{31}P NMR pattern in solution (Figures 4.24, 4.26). The high-field pattern centred at –24.2 ppm is assigned to DPPM, and the pattern at 17.1 ppm to the DPPB ligand, in keeping with the reported shielding of phosphorus nuclei in four-membered rings and the observed deshielding of phosphorus nuclei in seven-membered chelates.[1, 15, 57]

Figure 4.26 shows a simulated ^{31}P NMR spectrum for an AA'BB' spin-system which corresponds well with that observed for **27** (Figure 4.24). The P-P coupling constants obtained from the simulated spectrum are listed in Table 4.4.

Table 4.4: ^{31}P NMR Spectral Parameters[a] (121.42 MHz) Used to Obtain the Simulated Spectrum for *Trans*–RuCl$_2$(DPPB)(DPPM), **27**, Shown in Figure 4.26.

Spectral Parameter[b]	Value	Spectral Parameter[b]	Value
δ_A, $\delta_{A'}$ (DPPB)	6854.0 (17.1 ppm)	δ_B, $\delta_{B'}$ (DPPM)	1847.0 (–24.2 ppm)
$^2J_{AB}$	303.0	$^2J_{A'B'}$	303.0
$^2J_{AA'}$	29.6	$^2J_{BB'}$	31.3
$^2J_{AB'}$ (or $^2J_{A'B}$)	–30.6	$^2J_{A'B}$ (or $^2J_{AB'}$)	–34.3

a Obtained using a Varian spectral simulation package, assuming an AA'BB' spin-system. All values are in Hz, unless indicated otherwise, with a reference frequency of 4779.9 Hz for 85% H$_3$PO$_4$ at 0.0 ppm.

b The coupling constants $^2J_{AB}$ and $^2J_{A'B'}$ are due to *trans*-disposed phosphines ($^2J_{trans}$); the rest arise from mutually *cis* phosphines ($^2J_{cis}$). Signs of $^2J_{cis}$ are reported relative to one another while the $^2J_{trans}$ is positive.
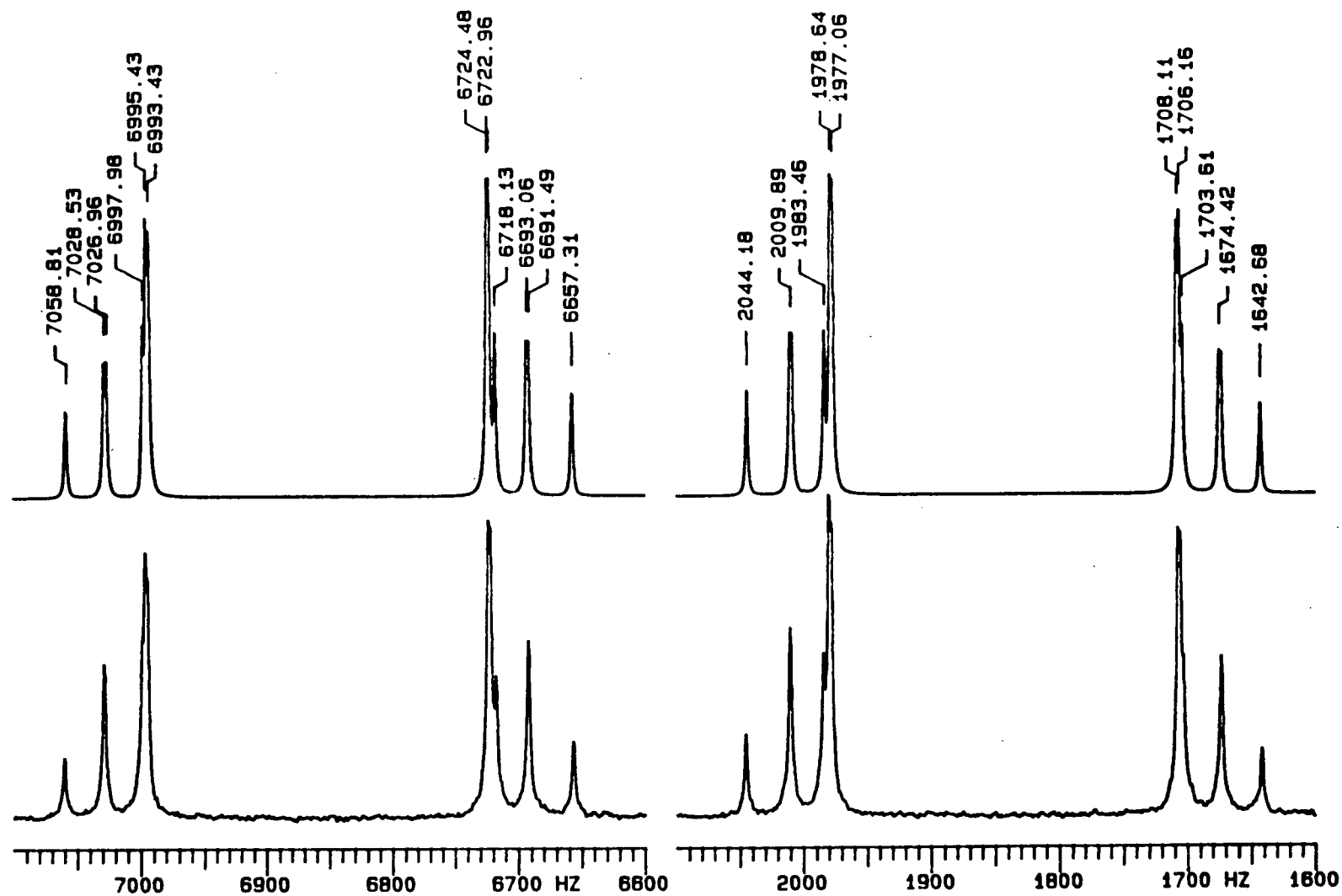
Figure 4.26: A simulated ^{31}P NMR spectrum (121.42 MHz, AA'BB' spin-system) for *trans*–RuCl$_2$(DPPB)(DPPM), **27**, obtained using the parameters listed in Table 4.4.

As mentioned in the previous section, synthesis of **27** was undertaken in order to check, albeit indirectly, if DPPB dissociation was involved in the isomerisation of *trans*-RuCl$_2$(DPPB)(PPh$_2$Py), **24**, to the corresponding *cis* derivative, **25**. The phosphine DPPM was chosen to replace the chelating PPh$_2$Py ligand of **24** because it forms a similar four-membered ring upon coordination to a metal centre. Moreover, it was thought that a study of the isomerisation behaviour of *trans*-RuCl$_2$(DPPB)(DPPM) might indicate whether the presence of pyridyl moiety in **24** was important for the isomerisation of **24** to **25**.

The ^{31}P NMR spectrum of a toluene solution of **27** remained unchanged even after heating the solution at 80 °C for 48 h under argon, showing that no isomerisation of the *trans* derivative to the corresponding *cis* species occurred under these conditions. The stability of **27** to isomerisation must result from its inability to dissociate a phosphine-end, of either DPPB or DPPM, to give a fluxional five-coordinate intermediate that is likely essential for the isomerisation to proceed. As mentioned in the previous section, this result provides some indirect evidence of the coordinative stability of DPPB, and support for the involvement (dissociation) of the pyridyl group of the PPh$_2$Py ligand in the *trans* to *cis* isomerisation of RuCl$_2$(DPPB)(PPh$_2$Py).

Reaction of 'RuHCl(DPPB)(PPh$_3$)' (prepared *in situ* from **23** and H$_2$/PS in 10 mL benzene as described in Section 4.3) with one mole equivalent DPPM ligand produced a yellow solution. Addition of hexanes (20 mL) to the reaction mixture after concentration of the benzene solution to ~5 mL resulted in precipitation of a yellow solid which was isolated by filtration, washed with diethyl ether (5 mL) and vacuum-dried (yield: 0.075 g). The ^{1}H NMR high-field quintet at –15.55 ppm ($^2J_{PH}$ = 18.9 Hz) observed for the yellow solid in C$_6$D$_6$ solution is indicative of the Ru-hydride complex, *trans*-RuHCl(DPPB)(DPPM), **28**, with the hydride being *cis* to all four phosphorus nuclei. The proton NMR spectrum also shows that RuCl$_2$(DPPB)(DPPM), **27**, is present in substantial amounts – in *ca.* 2:1 ratio relative to the hydride as calculated from the integral intensities (Figure 4.27).
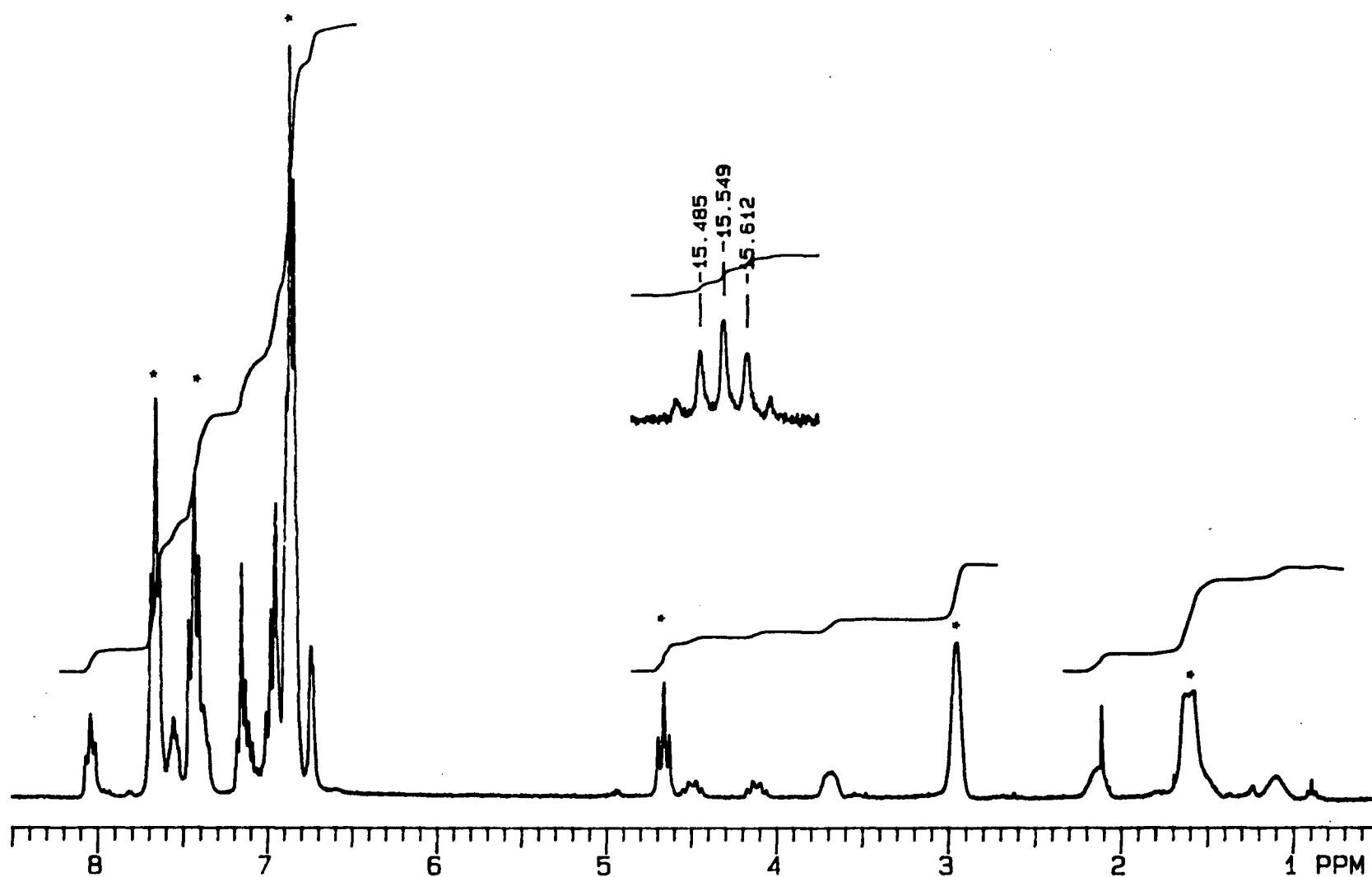
Figure 4.27: The ^{1}H NMR spectrum (300 MHz, C_6D_6, 20 °C) of the yellow solid obtained from the reaction of DPPM (1 eq./Ru) with hydrides formed *in situ* from the reaction of **23** with H_2 in the presence of Proton Sponge®. The peaks due to the dichloro complex **27** (see text) and impurities are marked while the rest are assigned to *trans*-RuHCl(DPPB)(DPPM).
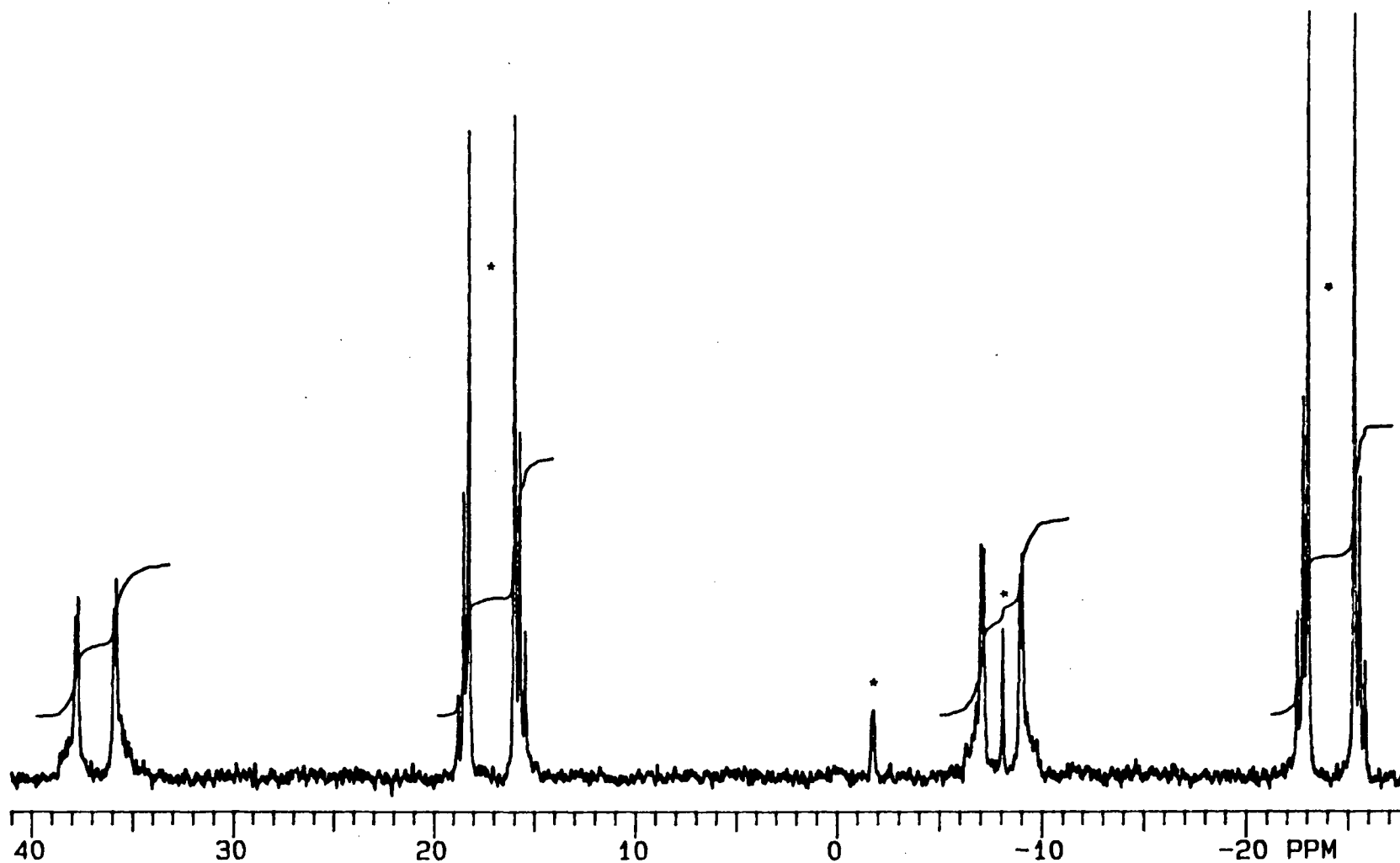
Figure 4.28: The $^{31}P\{^1H\}$ NMR spectrum (121.42 MHz, C_6D_6, 20 °C) of the yellow solid obtained from the reaction of DPPM with hydrides formed *in situ* from the reaction of 23 with H_2 in the presence of Proton Sponge®. The peaks due to the dichloro complex 27 (see text) and impurities are marked while the rest are assigned to *trans*-RuHCl(DPPB)(DPPM).

The ^{31}P NMR spectrum of the yellow solid confirms the presence of **27** in the product mixture (Figure 4.28, see above). Resonances centred at 37.8 and –8.0 ppm are attributed to the DPPB and DPPM ligands, respectively, of *trans*–RuHCl(DPPB)(DPPM), **28**. These NMR patterns are similar in appearance to those observed for **27**, but are shifted to high field of the corresponding signals due to **27**, as expected for a hydridochloro complex (see the previous section).

Spectral simulation to obtain various ^{31}P-^{31}P coupling constants by comparison with the observed spectrum was not carried out for the hydridochloro complex **28**. Of note, attempts to synthesise **28** by reaction of **27** with NaBH$_4$ in refluxing ethanol were unsuccessful, the starting complex **27** being recovered unchanged after 24 h (^{31}P NMR evidence).

Significantly, comparison of reactions of 'RuHCl(DPPB)(PPh$_3$)' with the phosphines PPh$_2$Py and DPPM shows that the corresponding hydridochloro complexes **26** and **28** are formed in approximately the same ratio (*ca.* 1:2, i.e. ~34% formation of the hydridochloro products) relative to the respective dichloro derivatives (**24+25** and **27**, ~66% formation), which are the other products in these reactions. It should be noted that in each case 'RuHCl(DPPB)(PPh$_3$)' was prepared *in situ* from RuCl$_2$(DPPB)(PPh$_3$). Provided that the PPh$_2$Py and DPPM ligands react with the 'RuHCl(DPPB)(PPh$_3$)'/ RuCl$_2$(DPPB)(PPh$_3$) equilibrium mixture irreversibly and much more rapidly than the equilibrium could be re-established to form 'RuHCl(DPPB)(PPh$_3$)' from **23** and H$_2$/PS, the observed distribution of the hydridochloro (34±3%) and the dichloro products (~66%) may be a reflection of the initial proportions of 'RuHCl(DPPB)(PPh$_3$)' and RuCl$_2$(DPPB)(PPh$_3$) in solution at the time of phosphine addition (Scheme 4-II).

$$\text{RuCl}_2(\text{DPPB})(\text{PPh}_3) \underset{\text{C}_6\text{H}_6}{\overset{\text{H}_2/\text{Proton Sponge}\circledR}{\rightleftharpoons}} \text{'RuHCl(DPPB)(PPh}_3\text{)'} + \text{HCl}$$

66%   34%

fast | $\begin{array}{c} -\text{PPh}_3 \\ +\text{L--L} \end{array}$ L–L = PPh$_2$Py or DPPM   *fast* | $\begin{array}{c} -\text{PPh}_3 \\ +\text{L--L} \end{array}$

RuCl$_2$(DPPB)(L–L)   RuHCl(DPPB)(L–L)

66%   34%
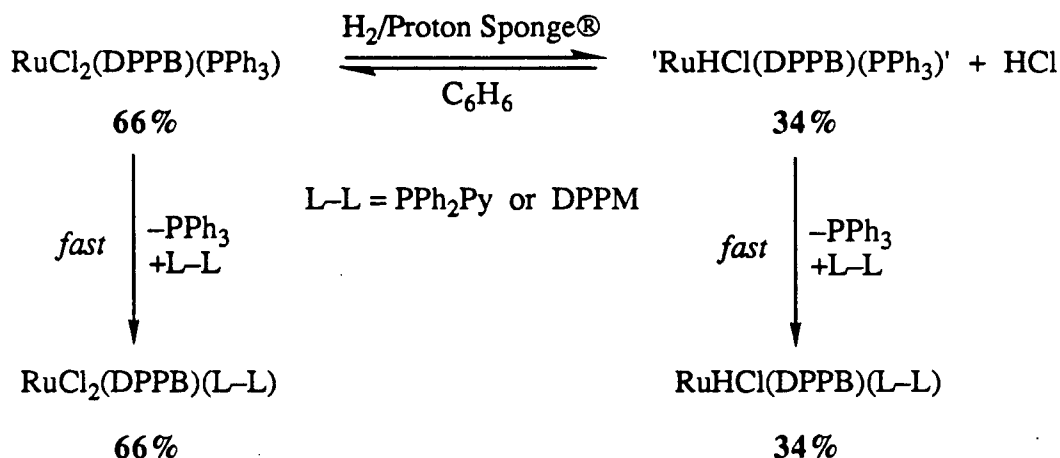
Scheme 4-II

4.6 Characterisation of RuCl$_2$(R-BINAP)(PPh$_3$), 21

The reaction of RuCl$_2$(PPh$_3$)$_3$ with one equivalent of BINAP affords the BINAP

analogue of the mixed-phosphine complex in high yield; the preparative details are given in

Section 2.5.2.2. The ^{31}P NMR spectrum of RuCl$_2$(R-BINAP)(PPh$_3$), 21 (Figure 4.29) is

similar to that observed for the DPPB derivative (Figure 4.5), and consists of resonances

due to the dimeric [RuCl$_2$(R-BINAP)]$_2$ species (δ_A = 75.8, δ_B = 5.8 ppm, $^2J_{AB}$ = 40.6

Hz; δ_C = 58.6, δ_D = 58.2 ppm, $^2J_{AB}$ = 43.2 Hz), which is formed by partial dissociation

of the PPh$_3$ ligand in solution (δ –6.0 ppm. s). The additional reasonances at 65.8 and

56.1 ppm and the triplet-like pattern centred at 21.0 ppm are assigned to the mixed-

phosphine species RuCl$_2$(R-BINAP)(PPh$_3$), 21, by comparison with the corresponding

spectrum of RuCl$_2$(DPPB)(PPh$_3$), 23. Based on the similarity of the ^{31}P NMR spectra of

21 and 23, the BINAP complex is assigned a structure similar to that of the DPPB

complex (*cf.* Figure 4.7).

Figure 4.29: 31p{1H} NMR spectrum (121.42 MHz, 20 °C) of RuCl$_2$(R-BINAP)(PPh$_3$), 21, in C$_6$D$_6$.

180
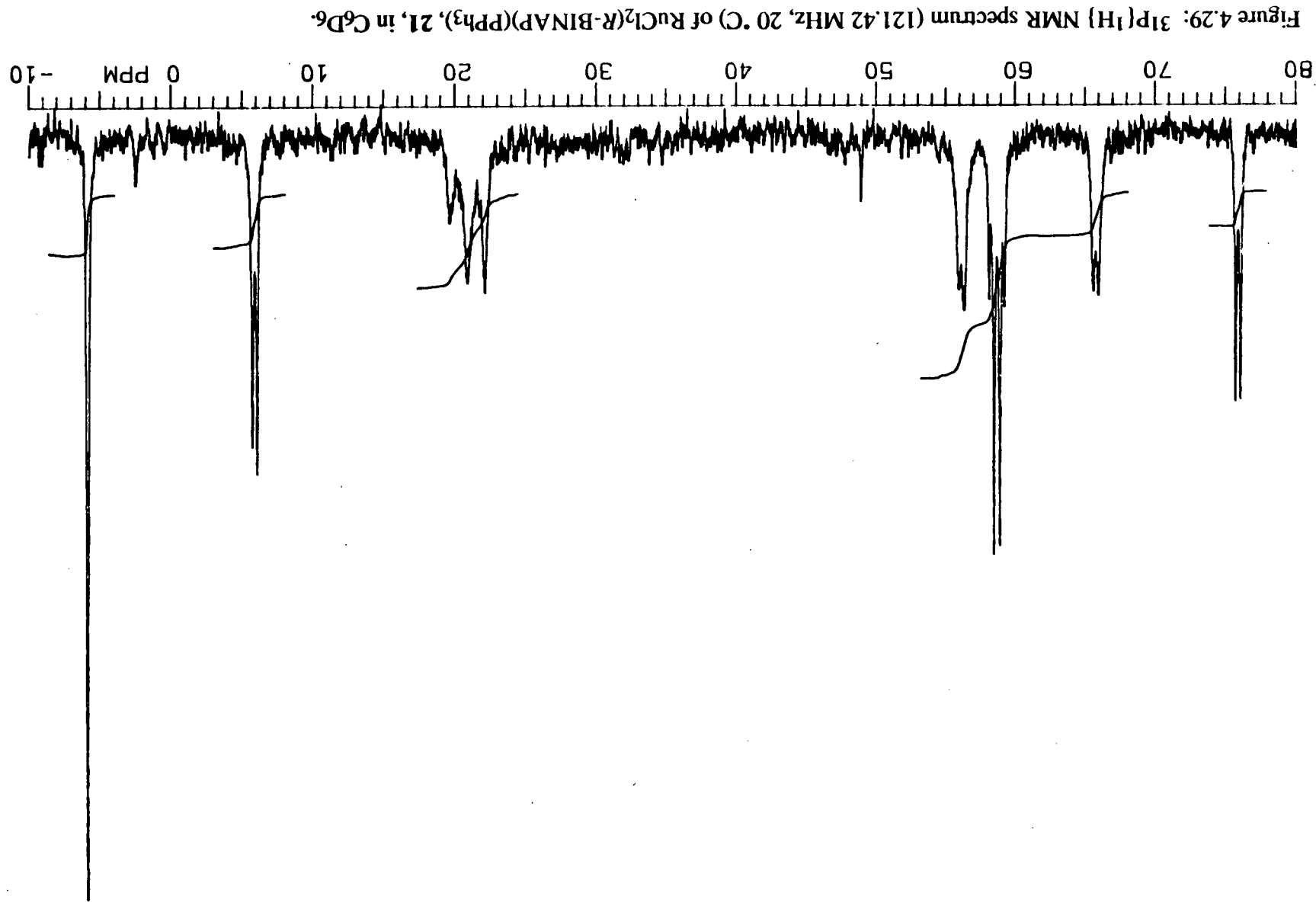
4.7 References – Chapter 4

1. Jung, C. W.; Garrou, P. E.; Hoffman, P. R.; Caulton, K. G. *Inorg. Chem.* **1984**, *23*, 726.

2. (a) Wang, D. K. W., Ph.D. Dissertation, The University of British Columbia, Vancouver, Canada, 1978.
   (b) James, B. R.; Wang, D. K. W. *Inorg. Chim. Acta* **1976**, *19*, L17.

3. (a) Churchill, M. R.; Bezman, S. A. *Inorg. Chem.* **1972**, *11*, 2243.
   (b) *Ibid.* **1973**, *12*, 531.
   (c) *Ibid.* **1973**, *12*, 260.

4. LaPlaca, S. J.; Ibers, J. A. *Inorg. Chem.* **1965**, *4*, 778.

5. Schaefer, J.; Stejskal, E. O. *J. Am. Chem. Soc.* **1976**, *98*, 1031.

6. Pines, A.; Gibby, M. G.; Waugh, J. S. *J. Chem. Phys.* **1972**, *56*, 1776; **1973**, *59*, 569.

7. Andrew, E. R. *Prog. Nucl. Magn. Reson. Spectrosc.* **1971**, *8*, 1.

8. (a) Fyfe, C. A. *Solid State NMR for Chemists*; C.F.C. Press: Guelph, Ont, Canada, 1983; and references therein.
   (b) Wasylishen, R. E.; Fyfe, C. A. *Ann. Rep. NMR Spectrosc.* **1982**, *12*, 1; and references therein.

9. Sanders, J. K. M.; Hunter, B. K. *Modern NMR Spectroscopy: A Guide for Chemists*; Oxford Press: Oxford, U.K., 1987; Chapter 9.

10. (a) Mehring, M. in *NMR Basic Principles and Progress*; Diehl, P., Fluck, E. and Kosfeld, R., Eds.; Springer Verlag: New York, 1976; Vol. 11.
    (b) Fukushima, E.; Roeder, S. B. W. *Experimental Pulse NMR*; Addison-Wesley: Reading, MA, USA, 1981; Chapter 4.

11. Dixon, W. T.; Schaefer, J.; Sefcik, M. D.; Stejskal, E. O.; McKay, R. A. *J. Magn. Reson.* **1982**, *49*, 341.

12. Mann, B. E. *Adv. Organomet. Chem.* **1988**, *28*, 397.

13. Hoffman, P. R.; Caulton, K. G. *J. Am. Chem. Soc.* **1975**, *97*, 4221.

14. For a review of chemistry and properties of $RuCl_2(PPh_3)_3$, see: Jardine, F. H. *Prog. Inorg. Chem.* **1984**, *31*, 265.

15. Garrou, P. E. *Chem. Rev.* **1981**, *81*, 229.

16. (a) Pregosin, P. S.; Kunz, R. W. in *NMR Basic Principles and Progress*; Springer-Verlag: Heidelberg, 1979; Vol. 16, p. 55.
    (b) Collman, J. P.; Hegedus, L. S.; Norton, J. R.; Finke, R. G. *Principles and Applications of Organotransition Metal Chemistery*; University Science Books: Mill Valley, CA, 1987; p. 72.

17. Diesveld, J. W.; Menger, E. M.; Edzes, H. T.; Veeman, W. S. *J. Am. Chem. Soc.* **1980**, *102*, 7935.

18. Maciel, G. E.; O'Donnel, D. J.; Greaves, R. *Adv. Chem. Ser.* **1982**, *196*, 389.

19. a) Bemi, L.; Clark, H. C.; Davies, J. A.; Drexler, D.; Fyfe, C. A.; Wasylishen, R. E. *J. Organomet. Chem.* **1982**, *224*, C5.
    b) Bemi, L.; Clark, H. C.; Davies, J. A.; Fyfe, C. A.; Wasylishen, R. E. *J. Am. Chem. Soc.* **1982**, *104*, 438.
    c) Clark, H. C.; Davies, J. A.; Fyfe, C. A.; Hayes, P. J.; Wasylishen, R. E. *Organometallics* **1983**, *2*, 177.
    d) Fyfe, C. A.; Clark, H. C.; Davies, J. A.; Hayes, P. J.; Wasylishen, R. E. *J. Am. Chem. Soc.* **1983**, *105*, 6577.

20. Kroto, H. W.; Klein, S. I.; Meidine, M. F.; Nixon, J. F.; Harris, R. K.; Packer, K. J.; Reams, P. *J. Organomet. Chem.* **1985**, *280*, 281.

21. Komoroski, R. A.; Magistro, A. J.; Nicholas, P. P. *Inorg. Chem.* **1986**, *25*, 3917.

22. Dekleva, T. W., Ph.D. Dissertation, The University of British Columbia, Vancouver, Canada, 1983; Chapter 2.

23. Opella, S. J.; Frey, D. M. H. *J. Am. Chem. Soc.* **1979**, *101*, 5855.

24. a) Haberkorn, R. A.; Herzfeld, J.; Griffin, R. G. *J. Am. Chem. Soc.* **1978**, *100*, 1296.
    b) Waltham, M. C.; Cornell, B. A.; Smith, R. *Biochim. Biophys. Acta* **1986**, *862*, 451.

25. Nissan, R. A.; Vanderah, T. A. *J. Phys. Chem. Solids* **1989**, *50*, 347.

26. a) Rothwell, W. R.; Waugh, J. S.; Yesinowski, J. P. *J. Am. Chem. Soc.* **1980**, *102*, 2637.
    b) Rao, K. M.; Gobetto, R.; Iannibello, A.; Zecchina, A. *J. Catal.* **1989**, *119*, 512.

27. a) Haw, J. E.; Crosby, R. C.; Maynard, S. J.; Reese, R. L. *Polym. Prepr.* **1988**, *29*, 78.
    b) Pratt, R. G.; Ackerman, J. L. *Polym. Mater. Sci. Eng.* **1983**, *49*, 293.

28. Nixon, J. F. and Pidcock, A. in *Ann. Rev. NMR Spectrosc.*; Mooney, E. F., Ed.; Academic Press: New York, 1969; Vol. 2, p. 345.

29. Bowmaker, G. A.; Cotton, J. D.; Healy, P. C.; Kildea, J. D.; Silong, S. B.; Skelton, B. W.; White, A. H. *Inorg. Chem.* **1989**, *28*, 1462; and references therein.

30. Allman, T. *J. Magn. Reson.* **1989**, *83*, 637.

31. Schunn, R. A.; Wonchoba, E. R.; Wilkinson, G. *Inorg. Syntheses* **1972**, *13*, 131.

32.   Hallman, P. S.; McGarvey, B. R.; Wilkinson, G. *J. Chem. Soc., A* **1968**, 3143.

33.   James, B. R. in *Comprehensive Organometallic Chemistry*; Wilkinson, G., Stone, F. G. A., Abel, E. W., Eds.; Pergamon Press: Oxford, 1982; Vol.8, p. 285.

34.   James, B. R. *Homogeneous Hydrogenation*; Wiley: New York, 1973.

35.   Reference 16b; p. 545.

36.   Markham, L. D., Ph.D. Dissertation, The University of British Columbia, Vancouver, Canada, 1973.

37.   Chaudret, B. N.; Cole-Hamilton, D. J.; Nohr, R. S.; Wilkinson, G. *J. Chem. Soc., Dalton Trans.* **1977**, 1546.

38.   (a) Kubas, G. J.; Ryan, R. R.; Swanson, B. I.; Vergamini, P. J.; Wasserman, H. J. *J. Am. Chem. Soc.* **1984**, *106*, 451.
       (b) Crabtree, R. H.; Lavin, M. *J. Chem. Soc., Chem. Commun.* **1985**, 794; *ibid.*, 1661.
       (c) Morris, R. H.; Sawyer, J. F.; Shiralian, M.; Zubkowski, J. D. *J. Am. Chem. Soc.* **1985**, *107*, 5581.

39.   Kubas, G. J. *Acc. Chem. Res.* **1988**, *21*, 120; and references therein.

40.   (a) Crabtree, R. H.; Hamilton, D. F. *Adv. Oraganomet. Chem.* **1988**, *28*, 299; and references therein.
       (b) Crabtree, R. H. *Acc. Chem. Res.* **1990**, *23*, 95; and references therein.

41.   Ng, J. B., Ph.D. Dissertation, The University of British Columbia, Vancouver, Canada, 1990; Chapter 5.

42.   Heinekey, D. M.; Millar, J. M.; Koetzle, T. F.; Payne, N. G.; Zilm, K. W. *J. Am. Chem. Soc.* **1990**, *112*, 909.

43. Antinolo, A.; Chaudret, B.; Commenges, G.; Fajardo, M.; Jalon, F.; Morris, R. H.; Otero, A.; Schweitzer, C. T. *J. Chem. Soc., Chem. Commun.* **1988**, 1210.

44. Hampton, C., Ph.D. Dissertation, The University of British Columbia, Vancouver, Canada, 1989; Chapter 4.

45. (a) Cullen, W. R.; Einstein, F. W. B.; Huang, C.-H.; Willis, A. C.; Yeh, E.-S. *J. Am. Chem. Soc.* **1980**, *102*, 988.
    (b) Butler, I. R.; Cullen, W. R.; Kim, T.-J. *Synth. React. Inorg. Met.-Org. Chem.* **1985**, *15*, 109.

46. Hampton, C.; Cullen, W. R.; James, B. R.; Charland, J.-P. *J. Am. Chem. Soc.* **1988**, *110*, 6918.

47. (a) Cole-Hamilton, D. J.; Wilkinson, G. *J. Chem. Soc., Dalton Trans.* **1977**, 797.
    (b) Pez, G. P.; Grey, R. A.; Corsi, J. *J. Am. Chem. Soc.* **1981**, *103*, 7528.

48. Rodgers, G. E.; Cullen, W. R.; James, B. R. *Can. J. Chem.* **1985**, *61*, 1314.

49. Markham, L. D.; James, B. R. *unpublished results.*

50. Schroder, M.; Stephenson, T. A. in *Comprehensive Coordination Chemistry*; Wilkinson, G.; Gillard, R. D.; McCleverty, J. A., Eds.; Pergamon Press: Oxford, 1987; Vol. 4, Chapter 45, pp. 379–390.

51. (a) Chatt, J; Hayter, R. G. *J. Chem. Soc.* **1961**, 772; 896; 5507; *ibid.* **1963**, 6017.
    (b) James, B. R.; Wang, D. K. W.; Voigt, R. F. *J. Chem. Soc., Chem. Commun.*, **1975**, 574.
    (c) Mason, R.; Meek, D. W.; Scollary, G. R. *Inorg. Chim. Acta* **1976**, *16*, L11.

52.   (a) James, B. R.; Mahajan, D. *J. Orgamomet. Chem.* **1985,** *279,* 31.; *Can. J. Chem.* **1980,** *58,* 996.
(b) James, B. R.; McMillan, R. S.; Morris, R. H.; Wang, D. K. W. *Adv. Chem. Ser.* **1978,** *167,* 122.

53.   Xie, Y., Ph.D. Dissertation, The University of British Columbia, Vancouver, Canada, 1990.

54.   (a) Cotton, F. A. and Wilkinson, G. *Advanced Inorganic Chemistry*; Wiley-Interscience: New York, 1980, 4th Edn.; Chapter 28, pp. 1217–1233.
(b) Douglas, B. E.; McDaniel, D. H.; Alexander, J. J. *Concepts and Models of Inorganic Chemistry*; Wiley: New York, 1983, 2nd Edn.; Chapter 8.

55.   Berry, R. S. *J. Chem. Phys.* **1960,** *32,* 933.

56.   "IUPAC Proposals for Nomenclature of Absolute Configurations Concerned with Six-Coordinated Complexes Based on the Octahedron" *Inorg. Chem.* **1970,** *9,* 1.

57.   (a) Thorburn, I. S., Ph.D. Dissertation, The University of British Columbia, Vancouver, Canada, 1985; Chapters 3 and 4.

CHAPTER 5

Activation of Dihydrogen by Chloro-Bridged Diruthenium(II,II) Complexes Containing Chelating Ditertiary Phosphines

5.1 Introduction

Although direct addition of dihydrogen to an unsaturated substrate is thermodynamically favourable in the ground state, the process is symmetry forbidden and mediation by a catalyst is generally essential in order to overcome the net symmetry restrictions.[1] Transition metal complex-catalysed H_2-hydrogenation of unsaturated substrates proceeds presumably through a series of symmetry allowed reaction steps involving metal hydride intermediate(s), wherein in general activation of both dihydrogen and substrate at the metal centre must be followed by a successful stepwise hydrogen transfer to the substrate and release of the reduced product.[2-4] Recently, however, Eisenberg and coworkers have demonstrated evidence for a "pairwise" hydride transfer to alkene substrates, with the transfers occurring faster than relaxation of the hydrogen nuclear spins in *para* hydrogen.[5]

Transition metal hydride complexes have been synthesised by a number of routes.[2-4] These include, for example, the use of molecular hydrogen, oxidative addition of HX, protonation, reactions with hydride reagents such as $NaBH_4$ and $LiAlH_4$, and hydrogen transfer from organic donors (e.g. alcohols). The choice of a synthetic route obviously depends on the nature of the starting material and the desired hydride product.

Reaction of ruthenium halide precursors with H_2 provides a convenient route to ruthenium hydride complexes; a base is usually necessary to remove the HX formed in such a reaction . Thus ruthenium hydrido(phosphine) complexes of the type $RuHClP_3$, where P represents a monodentate phosphine, are prepared by reaction of $RuCl_2P_3$ precursors with H_2 in the presence of an appropriate base (Equation 5.1).[6] The choice of base is also important as exemplified by reactions 5.2 and 5.3, in which the nature of the product is clearly influenced by the choice of the base employed (DMA[7] *vs.* Proton Sponge[8, 9]). The highly nucleophilic character of the strongly basic trialkylamines, such as NEt_3, can sometimes lead to complications through coordination and/or dehydrogenation and dealkylation of the amines.[10]

$$RuCl_2(PR_3)_3 + H_2 \xrightarrow{\quad NEt_3 \quad} RuHCl(PR_3)_3 + Et_3NH^+Cl^- \qquad (5.1)$$

$$2\,RuCl_3(PR_3)_2 + H_2 \xrightarrow{\quad DMA \quad} [RuCl_2(PR_3)_2]_2 + 2\,DMAH^+Cl^- \qquad (5.2)$$

$$\Big\downarrow H_2/PS$$

$$2\,RuCl_3(PR_3)_2 + 4\,H_2 \xrightarrow{\quad PS \quad} [RuH_2Cl(PR_3)_2]_2 + 4\,PSH^+Cl^- \qquad (5.3)$$
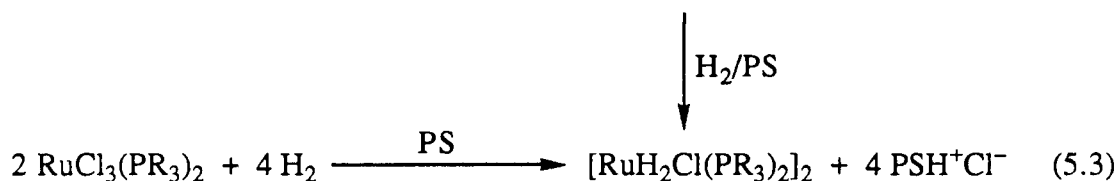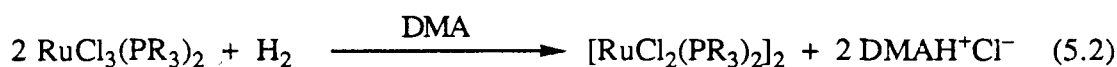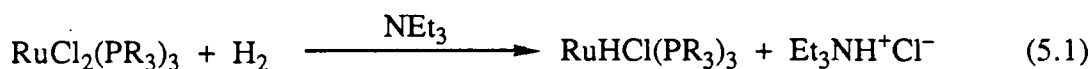
The reasons for interest in the synthesis and catalytic applications of Ru(II) complexes containing a single chelating phosphine per ruthenium have been elucidated in an earlier chapter (Chapter 3, Sections 3.1, 3.2), and some synthetic routes to dichloro complexes of the stoichiometry "$RuCl_2(P–P)$" have been described. Generation of the corresponding hydride species is the next logical step.

Thorburn's attempts to synthesise a hydride complex from chloro-bridged dinuclear $Ru_2Cl_5(DPPB)_2$ or $Ru_2Cl_4(DPPB)_2$ precursors by reaction in benzene solution with H_2 in the presence of added Proton Sponge® yielded trichloro-bridged dinuclear anionic species $[Ru_2Cl_5(DPPB)_2]^-PSH^+$ as the major isolable product (~60–65% yield; $^{31}P\{^1H\}$ NMR,

CD$_2$Cl$_2$, 20 °C: 54.6 ppm, s).[11, 12] Examination of the minor component (5–10%) by ^{1}H NMR spectroscopy in CD$_2$Cl$_2$ solution did indicate the presence of a small amount of hydride species, which was evident from broad triplet resonances at δ –17.65 and –21.90 ppm in *ca.* 1:1 ratio ($^2J_{PH}$ ~32 Hz).[11] The rather high solubility of [Ru$_2$Cl$_5$(DPPB)$_2$]$^-$-PSH$^+$, even in the relatively nonpolar solvent benzene, complicated the separation of products, and attempts to isolate the hydride derivative(s) in a pure form were unsuccessful. The high 'chloride-affinity' of Ru$_2$Cl$_4$(P–P)$_2$ complexes is thought to be responsible for formation of the anionic complexes through reaction with the initially formed PSH$^+$Cl$^-$ (Equation 5.4).[11, 12]

$$\text{Ru}_2\text{Cl}_5(\text{P–P})_2 + \text{H}_2 \xrightarrow{\text{PS}} \text{Ru}_2\text{Cl}_4(\text{P–P})_2 + \text{PSH}^+\text{Cl}^- \qquad (5.4)$$

$$\Big\downarrow \text{PSH}^+\text{Cl}^-$$

$$[\text{Ru}_2\text{Cl}_5(\text{P–P})_2]^-\text{PSH}^+$$
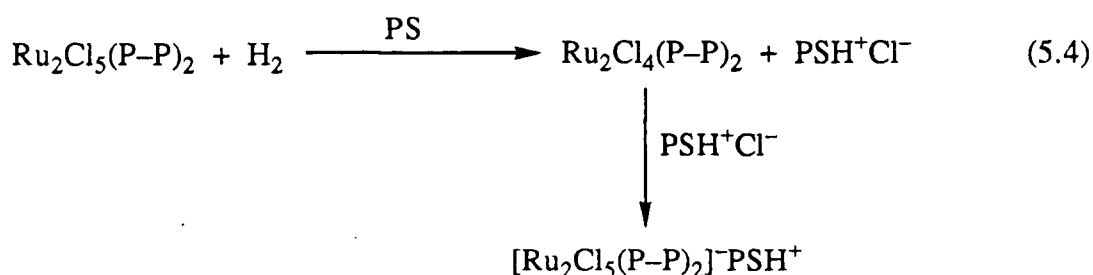
The choice of base proved to be an important factor in the reaction of [RuCl(P–P)(μ-Cl)]$_2$ with H$_2$, where P–P = DPPB (**14**) or *S,S*-CHIRAPHOS (**16**). In preliminary studies carried out by Thorburn, the use of NEt$_3$ (1 equiv./Ru or 2 equiv./Ru$_2$) in place of Proton Sponge® in reaction 5.4 resulted in the formation and subsequent isolation, albeit in very low yields (5–10%), of novel hydridochloro derivatives of the stoichiometry 'RuHCl(P–P)' (see below). The triethylamine adducts [(Et$_3$N)(P–P)Ru-(μ-Cl)$_3$RuCl(P–P)] (**14b** and **16b**), presumably formed by coordination of the added amine to the corresponding Ru$_2^{II,II}$ precursors (see Chapter 3, Section 3.6.1), were the major products of the respective reactions (~70% yield). The hydride complexes were characterised by proton NMR spectroscopy, and identified as the trinuclear Ru(II)-hydride species [RuHCl(P–P)]$_3$ (P–P = DPPB, **29**; CHIRAPHOS, **30**), on the basis of a single

crystal X-ray diffraction study on the CHIRAPHOS complex **30**. These preliminary results have been published as part of a review.[12]

More recently, dimeric Ru-BINAP analogues of **14** and **16**, including the corresponding triethylamine derivative, $[Ru_2Cl_4(BINAP)_2](NEt_3)$, have proved to be highly effective as catalyst precursors for asymmetric H_2-hydrogenation of a wide range of substrates, with enantiomeric excesses close to 100% being achieved in a number of cases.[13-16] As outlined in the introduction to Chapter 3, the possible involvement of 'RuHCl(DIOP)' species in RuHCl(DIOP)$_2$-catalysed H_2-hydrogenation of alkene substrates, as indicated by a detailed kinetic study,[17, 18] provided the impetus for devising ways of accessing such 1:1 'Ru(P–P)' complexes in pure form. Involvement of 'RuHCl(BINAP)' as the catalytically active species in related systems, including those incorporating dimeric Ru-BINAP analogues of the complexes **14** and **16**, has also been suggested.[12, 19, 20]

Described in this chapter are the results of a detailed investigation into the H_2-reactivity of dichloro-bridged dimeric $[RuCl(P–P)(\mu-Cl)]_2$ complexes leading to the corresponding trinuclear $[RuHCl(P–P)]_3$ derivatives. The original synthetic procedure has been optimised during the course of this work to obtain the hydridochloro trimers **29** and **30** in >50% isolated yield. A detailed spectroscopic characterisation of complexes **29** and **30** is presented. A mechanism for their formation is proposed; much of the work was done on complexes **14** and **29** containing the nonchiral DPPB ligand.

The present study reveals the intermediacy of molecular hydrogen $(\eta^2\text{-}H_2)$[21] species in the synthesis of the hydridochloro trimers and, therefore, a brief look at the general properties of transition metal molecular hydrogen complexes, including the various criteria used for their characterisation, seems appropriate.

5.2 Molecular Hydrogen Complexes: A Brief Review

The initial interaction of molecular hydrogen with a transition metal during H_2-activation processes has been considered for many years, but remained a topic of speculation until recently.[21] In 1976, Ashworth and Singleton, based on their observations that all the reactions of the complexes $RuH_4(PPh_3)_3$ and $RuH_3(DPPE)_2^+$ occurred by initial loss of H_2 and by analogy with the similar behaviour found for complexes containing reversibly bonded dioxygen ligand, proposed the possibility of stable H_2 binding at the Ru centre whereby these complexes could be considered as H_2 adducts of Ru(II).[22]

Further, Kubas in a 1980 report inferred, from an IR spectroscopic study and the observed lability of hydrogen, that the bonding of H_2 in $MH_2(CO)_3(PR_3)_2$ (M = Mo, W; R = Pr^i, Cy) complexes "may be novel".[23] The first direct evidence for the unusual H_2 binding in these and other reported systems came with the discovery in 1983, also by Kubas et al.,[24] of the first molecular hydrogen complex, viz. $W(CO)_3(PPr^i_3)_2(\eta^2\text{-}H_2)$ (cf. Chapter 1, Figure 1.13), which was shown to contain a side-on (η^2-) bonded H_2 ligand by X-ray (H—H = 0.75 (16) Å) and neutron diffraction (H—H = 0.84 Å) analysis.[25] The ^1H NMR spectrum of the HD isotopomer showed a 1:1:1 triplet with a $^1J_{HD}$ of 33.5 Hz;[21, 25] the coupling in hydride-deuteride complexes is typically <2 Hz.[21] The large HD coupling value, which is close to that found for free gaseous HD ($^1J_{HD}$ = 43.2 Hz[26]), clearly indicated a somewhat reduced H–D bond order and provided conclusive evidence for the presence of a 'nonclassical' dihydrogen ($\eta^2\text{-}H_2$) ligand.[21]

The report by Kubas et al. was followed by the reported synthesis of $[IrH(\eta^2\text{-}H_2)(bq)(PPh_3)_2]^+$ (Figure 5.1; bq = 7,8-benzoquinolinate) by Crabtree and Lavin.[27] The report by Morris et al., that the complexes $[MH(H_2)(DPPE)_2]^+$ (M = Fe, Ru; Figure 5.1) formed by protonation of $MH_2(DPPE)_2$ contained bound dihydrogen,[28] followed in quick succession. The X-ray crystal structure of the Fe complex showed a short H–H bond length (Å) for the $\eta^2\text{-}H_2$ moiety, and the observation of large ^1H NMR HD coupling

191

constants for the respective HD isotopomers confirmed the 'nonclassical' nature of H_2 ligand,[28] consistent with Ashworth and Singleton's original speculation about the Ru complex.[22]

M = Mo, W

R = Pr^i, Cy   N—C = 7,8-benzoquinolinate   P—P = DPPE

M = Fe, Ru
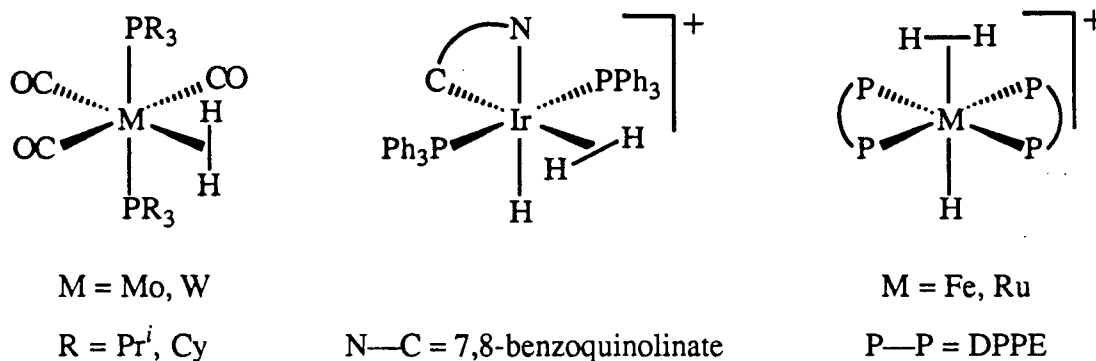
Figure 5.1: Some early examples of molecular hydrogen complexes.

Since their initial discovery,[24, 25] molecular hydrogen complexes of transition metals have continued to be of great interest as evidenced by the large number of literature reports in recent years,[27-34] including review articles[21, 35-37] and studies on theoretical aspects of metal-dihydrogen bonding.[38] A number of previously known polyhydrides are now reformulated as containing an η^2-H_2 ligand. For example, the complex $RuH_4(PPh_3)_3$ has been reformulated as $RuH_2(\eta^2$-$H_2)(PPh_3)_3$,[39] while a dinuclear complex of the empirical formula $[RuH_2Cl(PPh_3)_2]_2$ is now recognized as being $[(\eta^2$-$H_2)(PPh_3)_2Ru(\mu$-H)(μ-Cl)$_2$RuH(PPh$_3$)$_2$].[40, 41] Transition metals for which molecular hydrogen complexes have been reported to date are shown in Table 5.1. While the known dihydrogen complexes span a range of formal d-electron configurations (d^0–d^{10}), coordination numbers (4–9) and formal oxidation states (0–VI), all are either neutral or cationic, formally 18 electron species, with a large majority being of octahedral geometry.[21, 36, 41] Interestingly, more than half the known dihydrogen complexes contain ruthenium;[21] almost all contain one or more π-acceptor ligands, the "ligand-free" cluster complexes $Cu_2H_2(H_2)_x$ and $Cu_3(H_2)$,[42] and the matrix-isolated $Pd(H_2)$[43] being the only exceptions.

Some interesting examples, such as an η^2-H_2 ligand bound to a lanthanide metal (Eu)[44] and in an osmium-porphyrin system,[45] have also appeared in the literature.

Table 5.1: Transition Elements Found in Molecular Hydrogen (η^2-H_2) Complexes.

V	Cr	Mn	Fe	Co	Ni	Cu
Nb	Mo		Ru	Rh	Pd	
	W	Re	Os	Ir	Pt	

The existence of a dihydrogen–dihydride tautomerism in solution has been demonstrated for some complexes (Equation 5.5), which lends credence to the notion that dihydride formation *via* oxidative addition of H_2 may be preceded by the formation of an η^2-H_2 complex.[21, 36, 37]

$$(5.5)$$
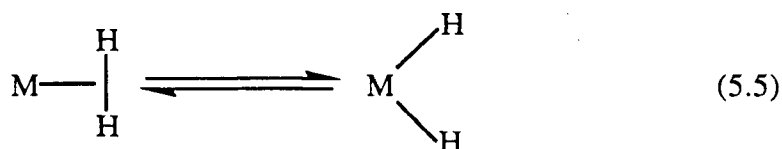
The η^2-H_2 ligand can be considered as a neutral, σ-bonded two-electron donor. The bonding scheme can be represented by a Dewar-Chatt-Duncanson type model[21, 36, 37] (Figure 5.2) commonly used to elucidate metal-alkene bonding.
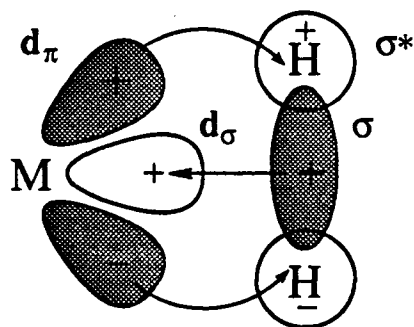
Figure 5.2: A bonding scheme for M–(η^2-H$_2$) moiety; the shaded areas represent occupied orbitals (based on Ref. 37).

According to this model, the occupied $\sigma(H_2)$ to empty $d_\sigma(M)$ electron donation constitutes the principal component of the M–(η^2-H$_2$) bonding, with a small back-bonding contribution from the filled metal d_π to the empty $\sigma^*(H_2)$ orbitals. A complete back-transfer of electrons from the metal to the σ^* orbitals of the dihydrogen ligand, however, would result in a H–H bond scisson (oxidative addition) to give a dihydride species (cf. Equation 5.5).[21, 36, 37] Thus weakly π-basic metals, high oxidation states (e.g. +II vs. 0), and the presence of π-acidic ligands are expected to stabilise the dihydrogen form over the dihydride. More detailed discussions on the various factors affecting the stability of η^2-H$_2$ complexes are available in the literature.[21, 35–37, 40]

Several criteria have been suggested for the recognition of a *nonclassical* dihydrogen ligand. Detection by X-ray crystal structure determination and neutron diffraction analysis provide the most direct proof in the solid state. Unfortunately, crystals suitable for such studies can be obtained in very few cases, and even then, locating the η^2-H$_2$ moiety may be extremely difficult because of problems of chemical instability and/or physical disorder.[21, 35–37] Vibrational spectroscopy (IR, Raman) is of limited use, particularly for noncarbonyl complexes.[21, 35–37]

Proton NMR spectroscopy has emerged as by far the most useful method for characterisation of dihydrogen complexes. A relatively large H–D coupling ($^1J_{HD}$), similar to that observed for free HD (43.2 Hz,[26] see above), is a particularly useful diagnostic tool

for complexes that contain a relatively nonfluxional dihydrogen ligand (η^2-HD); H–D coupling values in the range 18–33 Hz have been reported.[21, 36] However, the H–D coupling is often unresolved for many polyhydride complexes, e.g. [IrH$_2$(η^2-H$_2$)$_2$(PCy$_3$)$_2$]$^+$,[46] wherein fast scrambling of protons results in the loss of coupling information.

The ^{1}H NMR short T_1-relaxation time criterion (or more accurately, a short $T_1(min)$, of <100 ms[37]), introduced by Crabtree et al.[46, 47] and refined by Morris and coworkers,[32a] for identifying a dihapto bonded dihydrogen species in solution is now well-established,[21, 35–37] although some reports have advised caution.[37, 48] This method relies on the fact that for protons less than ~2 Å apart, dipole-dipole or spin-lattice relaxation constitutes the principal mode of NMR relaxation in solution. The rate of spin-lattice relaxation, R(DD), is related to the internuclear distance by the equation shown below:

$$R(DD) = \{T_1(DD)\}^{-1} = 0.3\gamma_H^4(h/2\pi)^2(r_{HH})^{-6}\left\{\frac{\tau_c}{1 + \omega^2\tau_c^2} + \frac{4\tau_c}{1 + 4\omega^2\tau_c^2}\right\} \qquad (5.6)$$

where,

τ_c	rotational correlation time (s rad^{-1})	= 0.62/ω at $\theta_{(min)}$; θ = temperature (K)
γ	gyromagnetic ratio	
ω	Larmor frequency (rad s^{-1})	
h	Planck's constant (6.626 x 10^{-34} J s)	
r_{HH}	H–H internuclear distance (cm).	

Binding of H$_2$ in a dihapto fashion to a metal causes some lengthening of the H–H bond (from 0.74 Å in free H$_2$[21] to an estimated range of ~0.8–1.2 Å); H–H(η^2-H$_2$) distances of 0.75–1.0 Å have been determined by X-ray or neutron diffraction techniques in a few cases.[21, 36, 40] On the other hand, the H–H distance in a dihydride complex is typically of the order of 1.5 Å or more. Because of the high order of spin-lattice relaxation

time dependence on the internuclear distance $(T_1(DD) \propto r^6$, see Equation 5.6), the $T_1(\eta^2\text{-}H_2)$ is expected to be an order of magnitude shorter (r = 0.8–1.2 Å, T_1 ~4–100 ms) than the T_1 observed for a *classical* dihydride moiety (r = 1.5 Å, T_1 ~1 s).[36, 37] Further, Equation 5.6 predicts that the T_1 value should pass through a minimum, $T_1(min)$ at $\theta_{(min)}$, when the correlation time $\tau_c = 0.62/\omega$, from which the internuclear distance r_{HH} can be estimated.[36, 37]

In the absence of structural characterisation, spectroscopic evidence by more than one techniques is desirable for a definite, positive identification of a *nonclassical* dihydrogen ligand.

5.3 Interaction of [RuCl(DPPB)(μ-Cl)]₂, <u>14</u>, with H₂ and N₂ in the Absence of an Added Base

5.3.1 Interaction with H₂: Formation of a Molecular Hydrogen Complex

In the absence of an added base, interaction of [RuCl(DPPB)(μ-Cl)]₂, **14**, with H₂ (1 atm) in benzene or toluene solution leads to the rapid, reversible *in situ* formation of the molecular hydrogen complex **31a** (Equation 5.7), as identified by ^{1}H and ^{31}P NMR spectroscopy (Figures 5.3 and 5.4).[49]

$$[RuCl(DPPB)(\mu\text{-}Cl)]_2 + H_2 \rightleftharpoons [(\eta^2\text{-}H_2)(DPPB)Ru(\mu\text{-}Cl)_3RuCl(DPPB)]$$

<p align="center">14   31a</p>

$$(5.7)$$

<p align="center">P—P = DPPB</p>
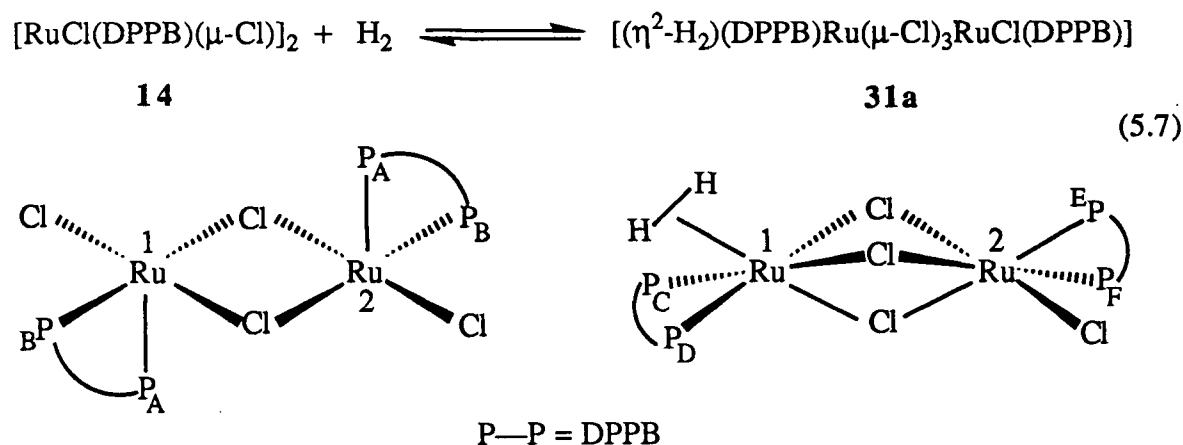
The ^{1}H NMR spectrum of a C_7D_8 solution of **14** under H_2 atmosphere shows a new broad resonance at δ −11.02 ppm, with a typically short T_1 relaxation time of 14 ms (300 MHz, 292 K, $w_{1/2}$ = 30 Hz, see Table 5.2), which is assigned to the η^2-H_2 moiety of **31a** (*cf.* Equation 5.7); the resonance disappears if the H_2 atmosphere is removed under vacuum, or replaced by argon. Species **31a** is akin to other dinuclear Ru-(η^2-H_2) complexes that contain monodentate PR_3 ligands, and terminal and bridging H^- ligands in place of some or all of the chlorides of **31a**.[40, 41]

Temperature dependence of the T_1 relaxation times was studied in the temperature range 235–324 K. The ^{1}H NMR η^2-H_2 resonance of **31a** broadens with decrease in temperature (Table 5.2). The plot of ln T_1 against $1/\theta$ is sharp V-shaped (Figure 5.5) as predicted by Equation 5.6. Only four dinuclear η^2-H_2 complexes, all containing ruthenium, have been reported so far.[40, 41, 50, 51] In case of the other dinuclear Ru(II)-(η^2-H_2) complexes,[40, 41, 50, 51] rapid exchange among the η^2-H_2 and the terminal or bridging hydride hydrogens results in averaging of the T_1 times of the respective ligands, and consequently, such V-shaped ln T_1 *vs.* $1/\theta$ plots with a clearcut minimum are not obtained.

The ^{31}P{^{1}H} NMR spectrum (Figure 5.4) of the same solution of **14** under H_2 shows, in addition to the single AB pattern of **14**, two other independent AB patterns of equal integrated intensity which are assigned to the dihydrogen complex **31a**; the data are summarised in Table 5.3. The existence of two sets of ^{31}P{^{1}H} NMR AB patterns is consistent with the suggested geometry of **31a** (*cf.* Equation 5.7). Also, the chemical shifts and $^2J_{PP}$ coupling constants are very similar to those observed for other related triply chloro-bridged complexes [(L)(DPPB)Ru(μ-Cl)$_3$Ru(Cl)(DPPB)], also prepared from **14** (L = Me_2CO, **14a**; CO, **14d**; Me_2SO, **14e**; PhCN, **14f**; MeI, **14g**; see Chapter 3: Sections 3.6, 3.7, and Table 3.6). The ^{1}H and ^{31}P NMR spectra indicate *ca.* 60%
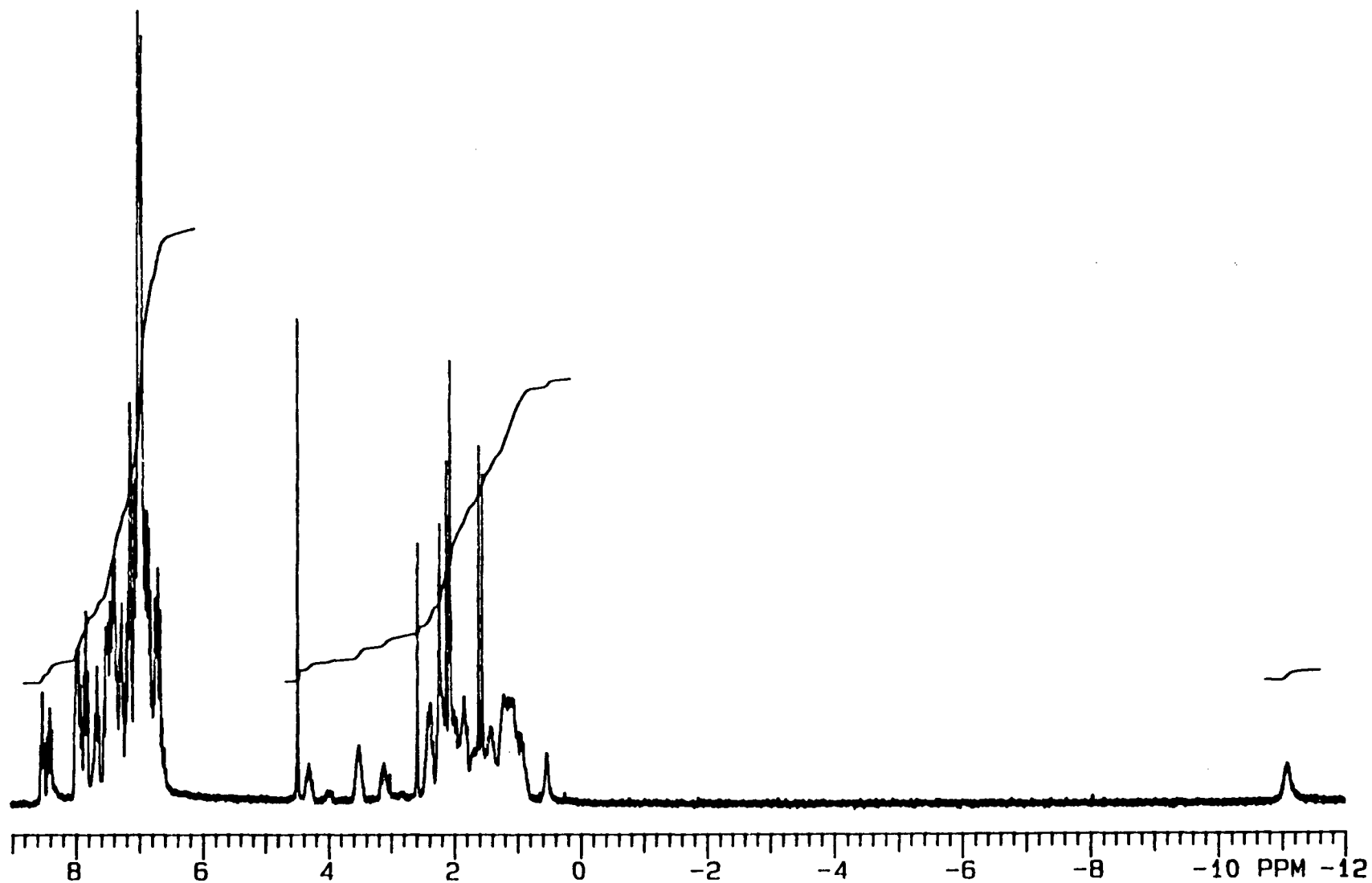
Figure 5.3: ^1H NMR spectrum (300 MHz, toluene-d_8, 292 K) of the complex [RuCl(DPPB)(μ-Cl)]$_2$, **14**, sealed under ~1 atm H_2 pressure. The resonance due to the η^2-H_2 moiety is observed at δ –11.02 ppm ·
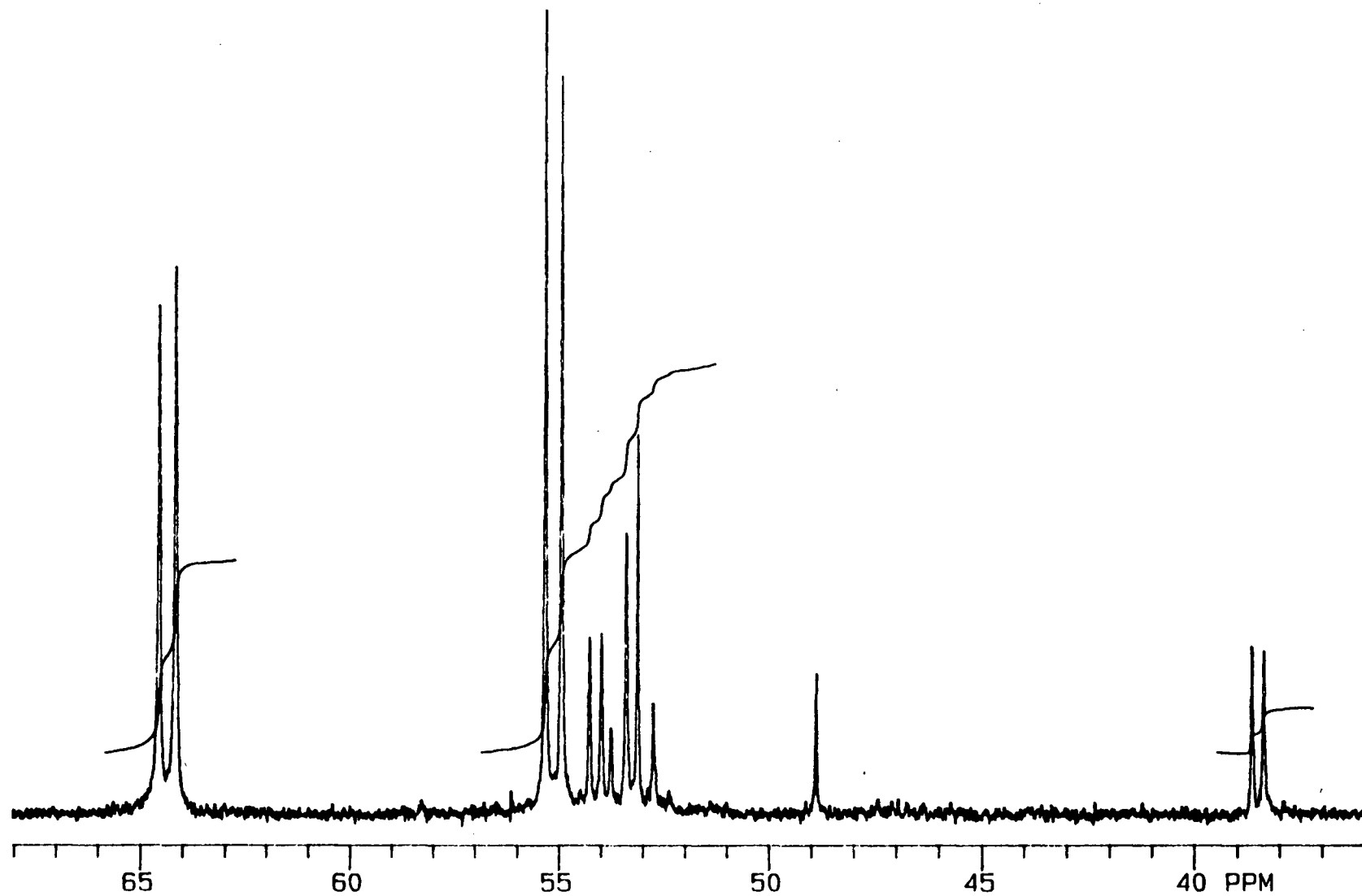
Figure 5.4: $^{31}P\{^1H\}$ NMR spectrum (121.42 MHz, toluene-d_8, 292 K) of a sample of [RuCl(DPPB)(μ-Cl)]$_2$, **14**, sealed under ~1 atm H$_2$ pressure.

Table 5.2: Temperature Dependence of the ^{1}H NMR T_1 Relaxation Time Data[a] (300 MHz, toluene-d_8) for the (η^2-H_2) resonance of **31a** at δ −11.0 ppm.

Temperature, θ, K	T_1, ms	Linewidth, $w_{1/2}$, Hz	T_2^*, ms[b]
324	19 ± 2	19	16.8
313	17 ± 1	24	13.5
292	14 ± 1	30	10.6
276	12 ± 1	36	8.9
255	15 ± 2	61	5.2
235	19 ± 2	68	4.7

[a] T_1 data were obtained by the inversion-recovery method[52] using the conventional 180°−t−90° pulse sequence.

[b] T_2^* values were calculated from the observed linewidths, according to the relation:

$$\text{linewidth} = 1/\pi T_2^*$$
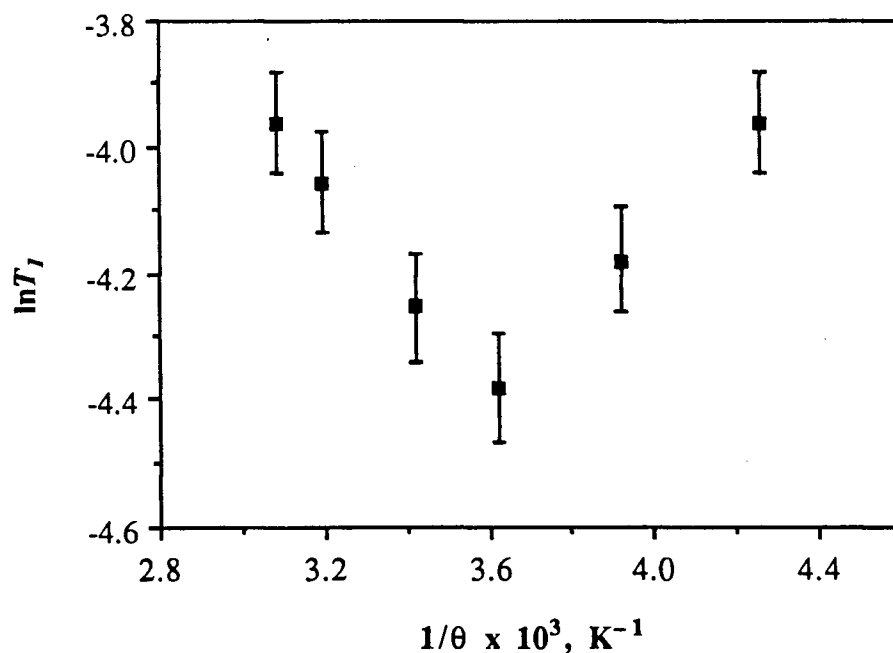
Figure 5.5: Temperature dependence of T_1 for the molecular hydrogen (η^2-H_2) moiety in [(η^2-H_2)(DPPB)Ru(μ-Cl)$_3$RuCl(DPPB)], **31a**.

equilibrium conversion of **14** to **31a** (see Figures 5.3 and 5.4) at 1 atm of H_2 and 20 °C; removal of H_2 atmosphere results in a complete disappearance of the two AB patterns due to **31a**.

<u>Table 5.3</u>: $^{31}P\{^1H\}$ NMR Data (121.42 MHz, C_6D_6 or toluene-d_8, 20 °C) for the Complexes [(L)(DPPB)Ru(μ-Cl)$_3$RuCl(DPPB)] (L = η^2-H_2, **31a**; σ-N_2, **31b**).[a]

Complex: L =	δ_A, ppm	δ_B, ppm	$^2J_{AB}$, Hz
14	64.0	54.9	47.3
η^2-H_2, **31a**	53.7	53.2	44.4
	53.8	38.3	33.8
σ-N_2, **31b**	54.4	53.5	45.1
	46.6	36.8	32.1

[a] The complexes were prepared *in situ* by sealing solutions of **14** under 1 atm of the respective gas. Further characterisation of the dinitrogen complex **31b** is described in Section 5.3.3.

The presence of two relatively sharp, independent sets of ^{31}P NMR AB patterns for **31a** suggests that exchange between bound and free H_2 is slow on the NMR time scale and thus, in the absence of inter- or intra-molecular hydrogen exchange, the broadness of the η^2-H_2 resonance of **31a** may be due to rapid internal rotation of the η^2-H_2 ligand as suggested by some workers.[21, 30a, 32a, 36] Further broadening of the η^2-H_2 signal on cooling (*cf.* Table 5.2) implies slowing of the internal motion, consistent with the behaviour of many other dihydrogen complexes.[21, 30a, 32a, 33a, 36]

From the $T_1(min)$ value of 12 ms at 277 K ($\theta_{(min)}$) obtained from the plot of ln T_1 vs. $1/\theta$ (Figure 5.5), an internuclear H–H distance of 1.08C Å, where C is a correction factor, is calculated for the η^2-H_2 moiety of **31a** following the method described by Crabtree and Hamilton.[36, 37, 47] Using a value of C = 0.794 suggested by Morris and coworkers,[32a] when the η^2-H_2 rotation is relatively rapid, and assuming a ±20% error in the $T_1(min)$ value, an H–H distance of 0.86 ± 0.02 Å is obtained. The estimated bond distance is comparable with that determined by X-ray crystallography, 0.80(6) Å, within one of the related dinuclear Ru species,[40, 51] as well as with distances reported for other mononuclear transition metal-dihydrogen complexes.[21, 32a, 36, 37]

Of particular interest, the complex **14** catalyses, presumably via **31a**, isotope exchange between H_2 and D_2 to give HD and the η^2-HD isotopomer of **31a**. A C_6D_6 solution (2 mL) of **14** (0.020 g) was stirred under 1.2 atm of H_2 and 1.8 atm of D_2 for 24 h at 20 °C; a portion of the solution was carefully transferred under hydrogen atmosphere to an NMR tube for examination by proton NMR spectroscopy.

The ^1H NMR signal of the η^2-HD ligand (C_6D_6, 292 K) is a relatively narrow 1:1:1 triplet ($w_{1/2}$ = 4.5 Hz, $^1J_{HD}$ = 29.4 Hz) of 1:2:1 triplets (cis, $^2J_{HP}$ = 7.5 Hz) centred at δ –11.07 ppm (Figure 5.6). The resonance due to free HD dissolved in C_6D_6 is seen as a 1:1:1 triplet ($^1J_{HD}$ = 42.7 Hz; cf. reported value of 43.2 Hz[26]) at 4.43 ppm. While the $^1J_{HD}$ for the η^2-HD isotopomer is within the range 18–34 Hz reported for other η^2-HD complexes,[21, 36] resolution of further coupling to phosphorus ($^2J_{HP}$) or other nuclei is unusual.[21, 36] Resolved $^2J_{HP}$ coupling with values of 2.0–3.6 Hz has been observed previously in some η^2-HD complexes.[30d, 31c, 53] Morris and coworkers have calculated using NMR simulations $^2J_{HP}$ values of 5.0 and 5.8 Hz for [M(η^2-H_2)(H)(DEPE)$_2$]$^+$ where M = Fe and Os, respectively, and DEPE = 1,2-bis(diethylphosphino)ethane.[54] The value of 7.5 Hz observed for the η^2-HD isotopomer of **31a** is the second largest seen so
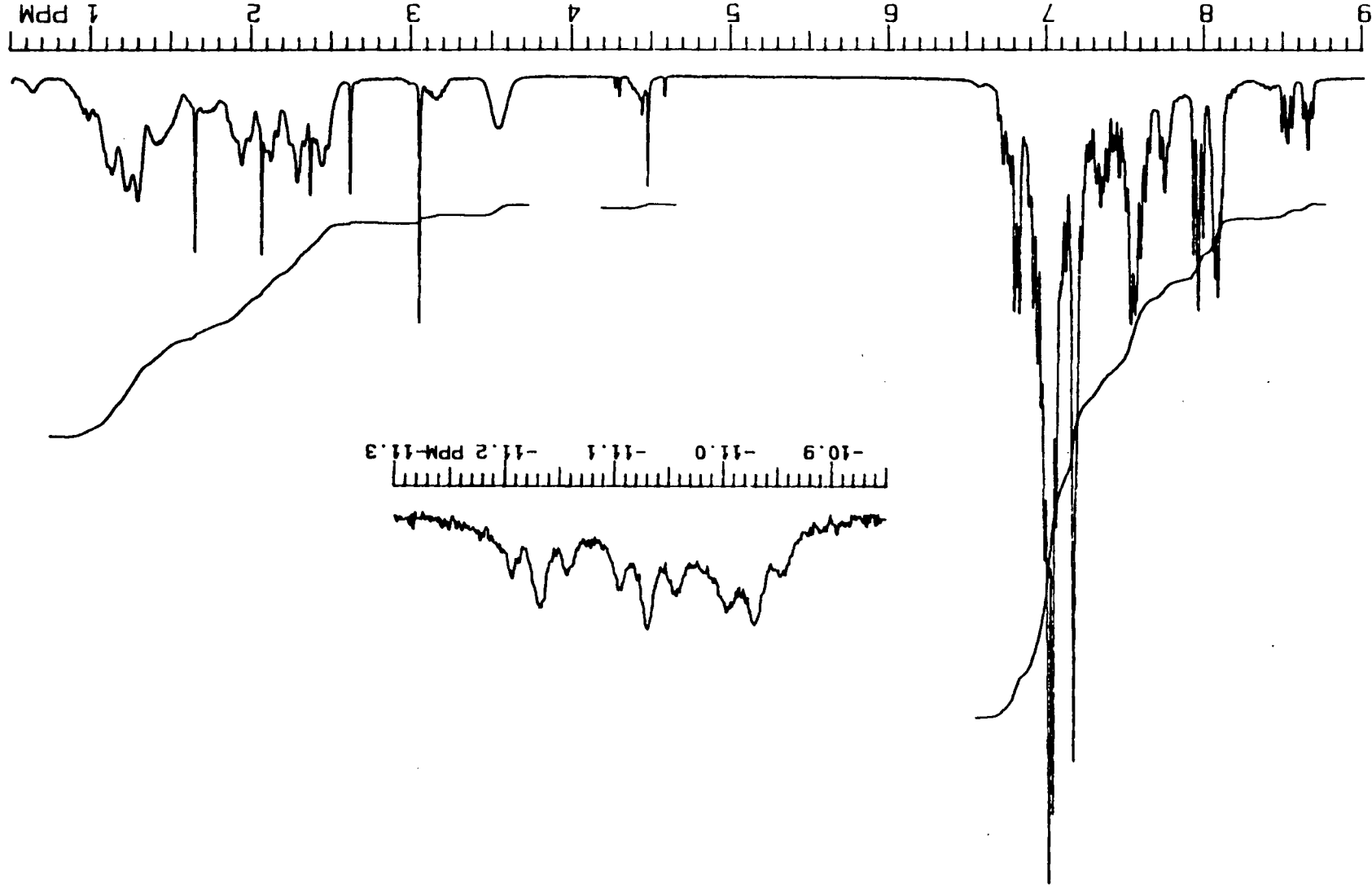
Figure 5.6: 1H NMR spectrum (300 MHz, C_6D_6, 20 °C) of [(η^2-HD)(DPPB)Ru(μ-Cl)$_3$RuCl(DPPB)], formed *in situ* by leaving [RuCl(DPPB)(μ-Cl)]$_2$, 14, under 1.2 atm of H_2 and 1.8 atm of D_2. The high-field region is expanded (INSET).

far for such complexes; Cotton and Luck have reported a $^2J_{HP}$ of 19 Hz for $ReCl(\eta^2\text{-}H_2)(PMePh_2)_4$.[55] The observation of $^2J_{HP}$ in the ^1H NMR spectrum of the η^2-HD isotopomer of **31a** is further evidence that the on/off exchange between the bound and free dihydrogen must be slow on the NMR time scale.

Facile $H_2/D_2 \rightleftharpoons$ HD exchange in the presence of other $\eta^2\text{-}H_2$ complexes has been noted previously.[30a] For example, the complexes $RuCp(PPh_3)(Bu^tNC)(H_2)^+$,[30d] and $W(CO)_3(PPr^i_3)_2(\eta^2\text{-}H_2)$[30a] are known to catalyse the isotope exchange reaction; interestingly, the latter species catalyses the exchange even in the solid state by an as yet unexplained mechanism.[30a] A similar gas-solid reaction using H_2/D_2 and **31a** (i.e. **14**) was not attempted during the current work. In another interesting case, Upmacis *et al.* observed that while $H_2/D_2 \rightleftharpoons$ HD exchange ocurred in the presence of $Cr(CO)_4(H_2)_2$ in liquid xenon at −70 °C, the analogous $Cr(CO)_5(H_2)$ complex was completely inactive,[56] implying that simultaneous coordination of two H_2 ligands at the same metal centre may be important in the formation of HD from H_2/D_2 mixtures. Based on molecular orbital calculations, Pacchioni has suggested the formation of a polyhydrogen chain at the Cr centre in $Cr(H_2)(D_2)$ leading to a seven-coordinate dihydrogen-dihydride intermediate on the way to $Cr(HD)_2$ species (Scheme 5-I):[38a]
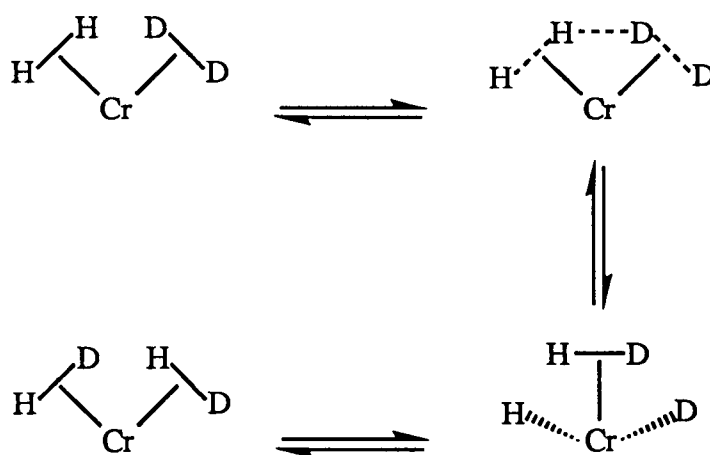
Scheme 5-I

Formation of HD from H_2/D_2 mixtures in the presence of **14** may be proceeding by a similar mechanism, possibly through a bis(dihydrogen) intermediate formed from **31a**, in which the dinuclearity of the complex is maintained (Figure 5.7a). Involvement of a mononuclear species of the type $RuCl_2(DPPB)(H_2)_2$ (Figure 5.7b), which would be analogous to the known $RuH_2(PR_3)_2(H_2)_2$ complexes,[50] cannot be ruled out completely. However, it is considered less likely because the dinuclear structure of the precursor seems to be maintained even in the presence of large excess (~50 eq.) of ligands such as amines and nitriles (see Chapter 3, Sections 3.6 and 3.7), which are known to coordinate much more strongly compared to H_2. Indeed, the addition of PhCN to **14**, for example, yields a bis(PhCN) derivative, [RuCl(DPPB)(PhCN)(μ-Cl)]$_2$, with the dinuclear structure still intact (Chapter 3, Section 3.6.5).
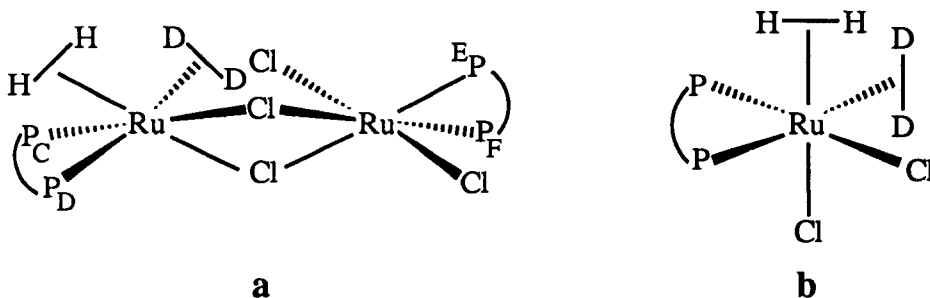
Figure 5.7: Possible intermediates in **14**-catalysed $H_2/D_2 \rightleftharpoons$ HD isotope exchange.

5.3.2 Gas-Uptake Studies

Rapid H_2 uptakes of ~0.4 equiv. per dimer are observed for DMA solutions of **14** at 1 atm of H_2 pressure and 30 °C; these fractional uptakes can be attributed to the partial formation of the dihydrogen complex **31a**. Interestingly, **14** itself is prepared by reduction of the mixed valence precursor $Ru_2Cl_5(DPPB)_2$, **2**, also in DMA solution under identical hydrogenation conditions (see Sections 2.5.5 and 3.3.1). However, it should be pointed

out that $[Ru_2Cl_5(DPPB)_2]^-DMAH^+$ is the initial product in the reduction of **2**, and the neutral dimeric product $[RuCl(DPPB)(\mu\text{-}Cl)]_2$, **14**, is obtained only after the addition of methanol which breaks up the ionic species into $DMAH^+Cl^-$ and **14**.[11, 12]

5.3.3   Interaction of Other $[RuCl(P\text{-}P)(\mu\text{-}Cl)]_2$ Complexes with H_2

DMA solutions of $[RuCl(S,S\text{-}CHIRAPHOS)(\mu\text{-}Cl)]_2$, **16**, were found to absorb *ca.* 0.40 mole equivalents of H_2 per dimer at 1 atm of H_2 and 30 °C. However, the proton NMR spectrum of a solution of **16** in C_6D_6 sealed under 1 atm of H_2 failed to reveal a broad high-field signal (down to −30 ppm) assignable to a bound dihydrogen ligand. Although the CHIRAPHOS complex **16** could be considered to form a dihydrogen complex, simply by analogy to the H_2-uptake behaviour of its DPPB counterpart, further work, including low temperature NMR studies possibly on samples sealed under relatively high H_2 pressures (1–10 atm) will be necessary in order to substantiate the presence or absence of the corresponding dihydrogen complex.

5.3.4   Interaction of <u>14</u> with N_2:   Formation of a Dinitrogen Complex

Complex **14** also reacts reversibly with 1 atm of N_2 to give a dinitrogen complex, **31b**, with an equilibrium conversion of *ca.* 70% at 20 °C. The spectroscopic data are consistent with a structure akin to **31a** with the $\eta^2\text{-}H_2$ replaced by $\sigma\text{-}N_2$ (see below).
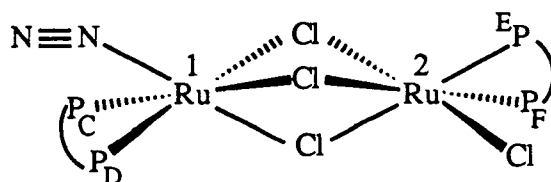
Figure 5.8: Suggested geometry for the dinitrogen complex, **31b**.

The ^{1}H and the ^{31}P{^{1}H} NMR spectra of the dinitrogen complex **31b** (i.e. of **14** under a N$_2$ atmosphere; C$_6$D$_6$, 20 °C) shown in Figures 5.9 and 5.10, respectively, closely resemble those of other trichloro-bridged dinuclear species (*cf.* corresponding spectra of compounds **14a, 14d–14g** and **31a**; also see Tables 5.3 and 3.6). The phosphorus NMR signals for **31b** are relatively sharp, again implying that the inter- and intra- molecular N$_2$ exchange is likely slow on the NMR time-scale.

The presence of σ-N$_2$ ligand in **31b** is confirmed by the $v_{N\equiv N}$ IR stretch at 2175 cm^{-1} (m, CH$_2$Cl$_2$ solution in 0.1 mm anaerobic NaCl cell, Figure 5.11), which is absent in the IR spectrum of **14** under argon atmosphere. The 2175 cm^{-1} value compares well with those found for the related ruthenium dinuclear complexes (complex, $v_{N\equiv N}$ cm^{-1}): Ru$_2$H$_4$(PCy$_3$)$_4$(N$_2$), 2145;[50] Ru$_2$H$_4$(PPh$_3$)$_4$(N$_2$), 2140;[57] and Ru$_2$Cl$_4$(PPh$_3$)$_4$(N$_2$), 2165.[58] It also lends further support to Morris' suggestion that "when the dinitrogen stretching frequency in ML$_n$(N$_2$) is >2060 cm^{-1}, then the corresponding η^2-H$_2$ adduct will be stable near room temperature" (and *vice versa*);[50] indeed, stable dihydrogen adducts have been characterised for all the dinuclear ruthenium complexes mentioned above.[40, 50]
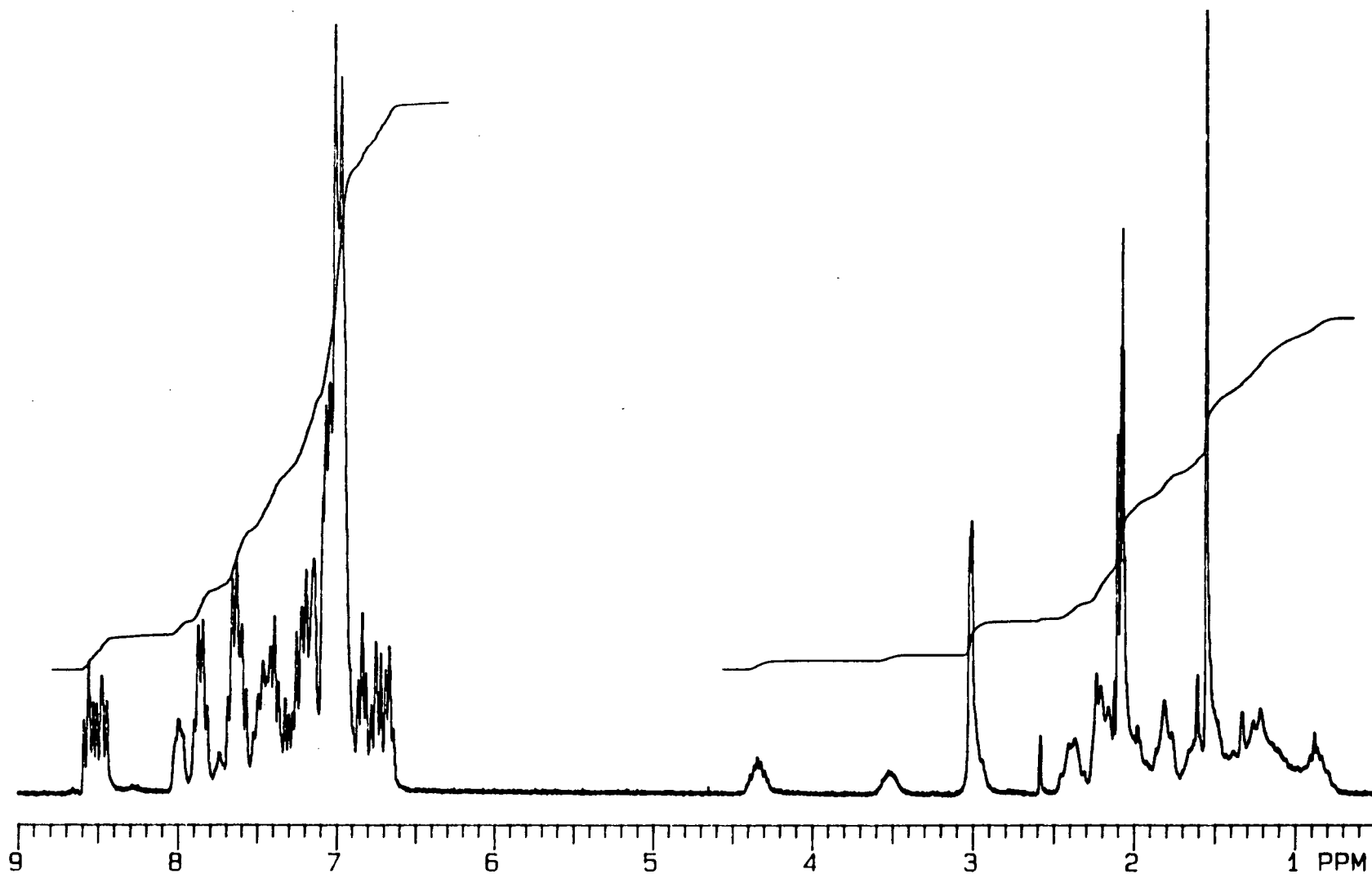
Figure 5.9: ^{1}H NMR spectrum (300 MHz, C$_6$D$_6$, 20 °C) of the dinitrogen complex **31b** formed *in situ* from [RuCl(DPPB)(μ-Cl)]$_2$, **14**, under ~1 atm N$_2$ pressure.
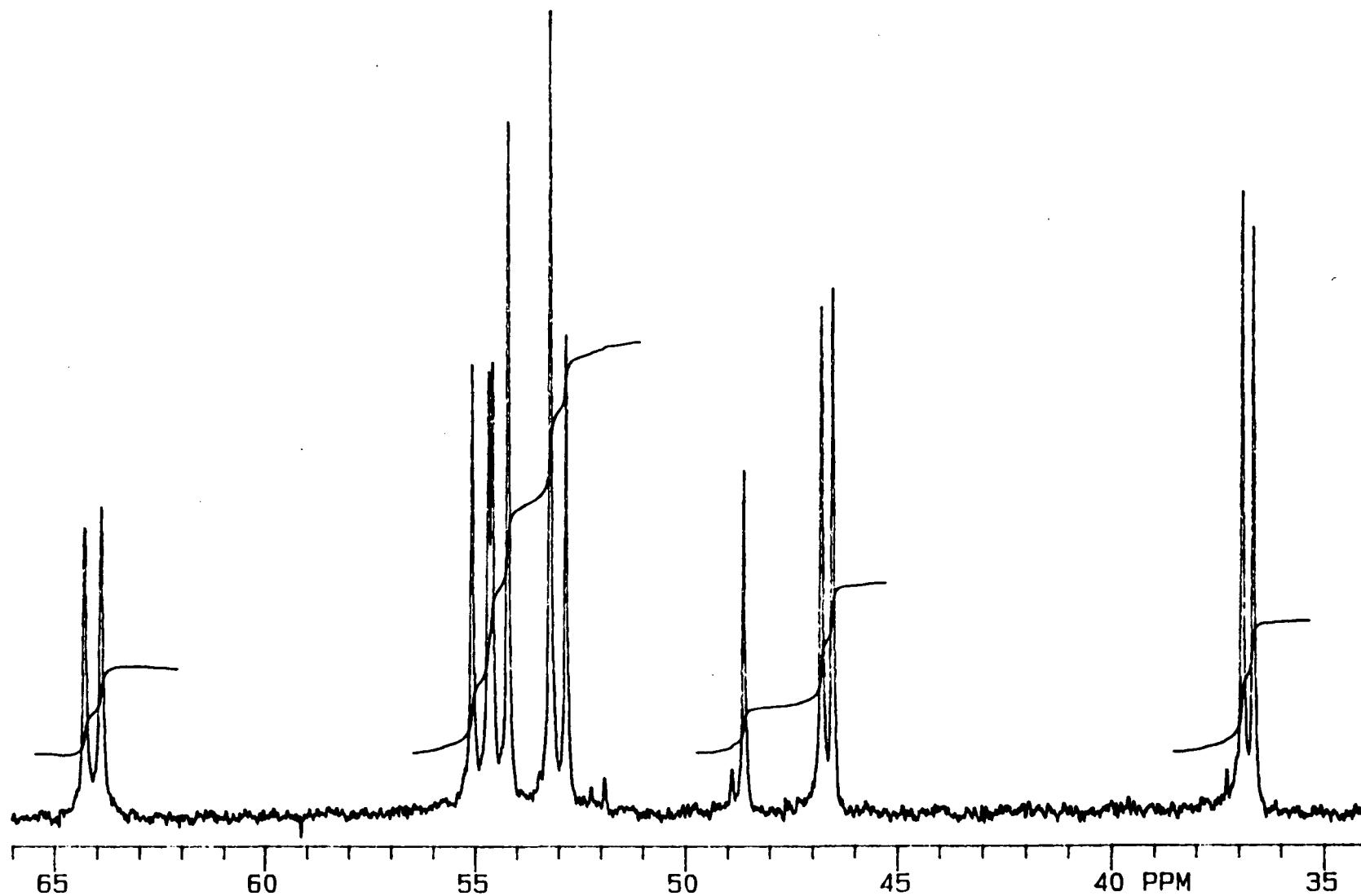
Figure 5.10: $^{31}P\{^{1}H\}$ NMR spectrum (121.42 MHz, C_6D_6, 20 °C) of the dinitrogen complex **31b** formed *in situ* from [RuCl(DPPB)(μ-Cl)]$_2$, **14**, under ~1 atm N_2 pressure.
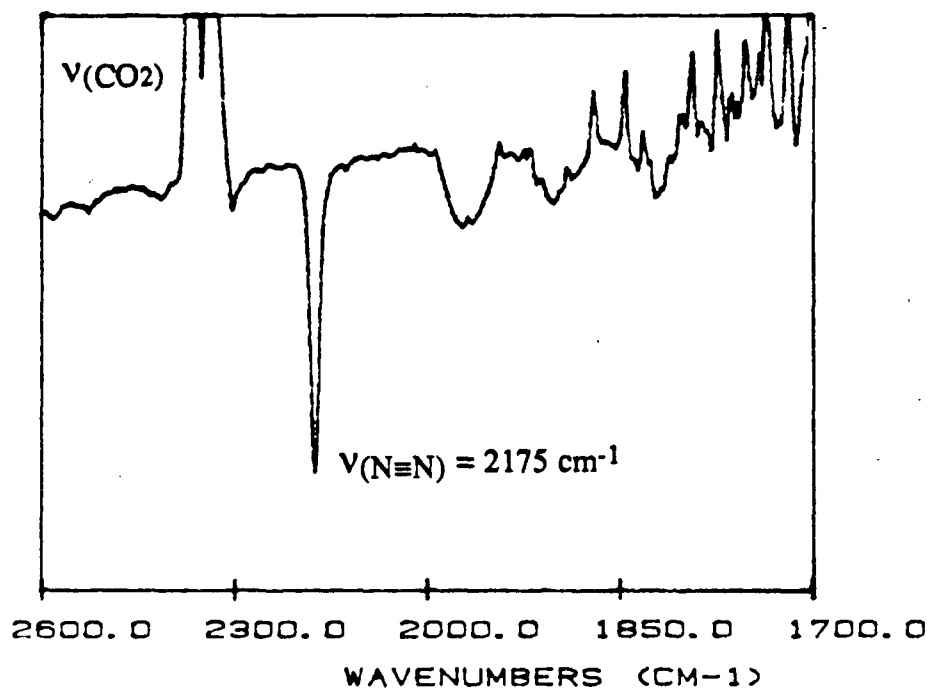
Figure 5.11: Infra-red spectrum of a CH_2Cl_2 solution of **14** sealed under N_2 atmosphere. The solvent spectrum has been subtracted.

5.4 Reaction of [RuCl(P–P)(µ-Cl)]$_2$ Dimers with H$_2$ in the Presence of Triethylamine: Synthesis of [RuHCl(P–P)]$_3$ Complexes

As described in the introduction (Section 5.1), reaction of [RuCl(P–P)(µ-Cl)]$_2$ dimers with H$_2$ in the presence of two mole equivalents of NEt$_3$ led to the formation and subsequent isolation of Ru$_2$Cl$_4$(P–P)$_2$(NEt$_3$) (*ca.* 70%) and small amounts of trimeric hydride complexes of formula [RuHCl(P–P)]$_3$ (*ca.* 5–10%).[12] The essential chemistry leading to the formation of the trinuclear hydrides and the NEt$_3$ adducts is summarised in Scheme 5-II.

$$\text{a) argon, } C_6H_6 \longrightarrow [(\text{Et}_3N)(P-P)Ru(\mu\text{-Cl})_3RuCl(P-P)]$$

a) 90%   b) 70%

$$\boxed{\begin{array}{c}[\text{RuCl}(P-P)(\mu\text{-Cl})]_2 \\ + \\ 2 \text{ equiv. NEt}_3\end{array}}$$

$$\text{b) 1 atm } H_2 \over C_6H_6, \text{ 24 h, 25 °C}$$

+

$$[\text{RuHCl}(P-P)]_3 \quad + \quad \text{Et}_3N^+Cl^-$$

5–10%   10–20%

P–P = DPPB or S,S-CHIRAPHOS
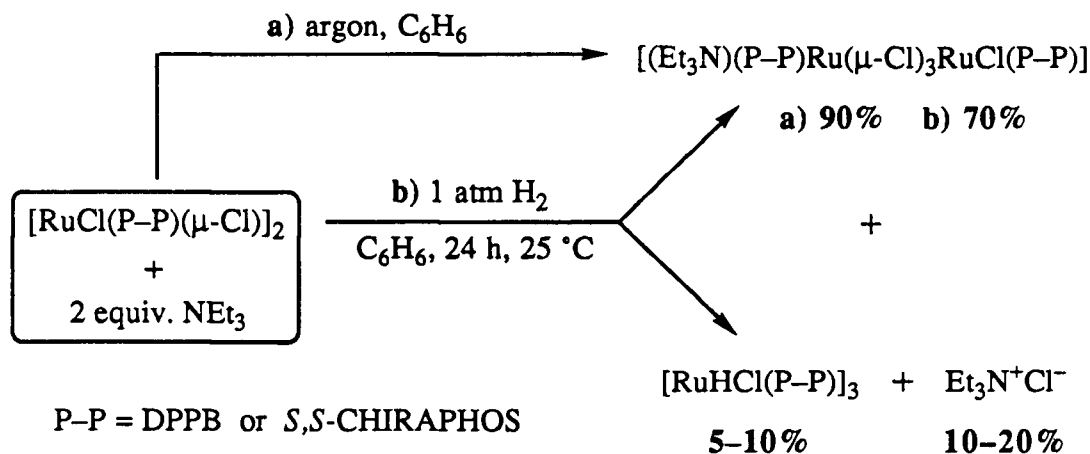
Scheme 5-II

5.4.1 Improved Synthesis of [RuHCl(P–P)]₃

The original procedure for the synthesis of the novel trimeric hydridochloro complexes, [RuHCl(P–P)]₃, involved addition of two equivalents of triethylamine to a benzene suspension/solution of the appropriate dimer precursor [RuCl(P–P)(μ-Cl)]₂ (P–P = DPPB, **14**; S,S-CHIRAPHOS, **16**); the mixture was then stirred under an atmosphere of H_2 for 24 h at room temperature. Formation of large amounts (>70%) of the triethylamine adducts (**14b** or **16b**; Scheme 5-II), which are essentially unreactive toward H_2, appears to be the principal reason for poor yields of the hydridochloro trimers. Reaction of the dimer precursors with NEt₃ in the absence of H_2 does result in quantitative formation of the corresponding amine adducts, which have been characterised by elemental analysis and NMR spectroscopy (see Section 2.5.6.1 for **14b**, and Section 2.5.9.2 for **16b**).

The procedure for the synthesis of the hydridochloro trimers has been revised during the course of this work, particularly in view of the finding that the DPPB dimer **14** formed a molecular hydrogen complex under H_2 atmosphere (Section 5.3.1).[49] In the modified synthesis, a benzene solution of the appropriate dimeric [RuCl(P–P)(μ-Cl)]₂ precursor was stirred under H_2 atmosphere for about one hour, prior to the addition of two

equivalents of NEt$_3$ base, which was then added under a blancket of hydrogen. This simple change in the order of addition of the two reagents (i.e. from NEt$_3$ + H$_2$ to H$_2$ + NEt$_3$) resulted in a dramatic increase in the yields of the hydridochloro trimers (**29, 30**), from the <10% obtained in the original synthesis to >50%, with concomittant decrease in the yields of the NEt$_3$-adducts (**14b, 16b**). Indeed, the *in situ* yield of the hydride trimers is at least as high as 65–70%, based on the isolated yield of NEt$_3$H$^+$Cl$^-$.

5.5 Characterisation of [RuHCl(P–P)]$_3$ Complexes

5.5.1 Molecular Structure of [RuHCl(*S,S*-CHIRAPHOS)]$_3$, <u>30</u>

A single crystal X-ray diffraction study of the CHIRAPHOS complex, **30**, carrried out by Thorburn and Ball, reveals a highly unsymmetrical trinuclear structure for **30** as shown in Figure 5.12.[12] The structural parameters are listed in the Appendix (A-2), and some selected bond distances and bond angles are given in Tables 5.4 and 5.5, respectively. The three hydride ligands could not be detected in the X-ray structure, but NMR spectral studies (next section) suggest the presence of two terminal and one bridging hydride in **30** and its DPPB analogue **29**.

The highly unsymmetrical structure shows just one metal–metal bond (Ru1–Ru2 = 2.8079(6) Å), with three bridging chlorides between Ru1 and Ru3, while Ru2 is bonded to a single chloride Cl1 that bridges all three Ru atoms. The chloride bridges are unsymmetric with the Ru–Cl distances ranging from 2.452 Å for Ru1–Cl2 to 2.569 Å for Ru3–Cl2. Interestingly, the observation of the shortest and the longest Ru–Cl distances for Ru–Cl bonds which are very likely *trans* to a bridging and a terminal hydride ligand, respectively (see the following section), is consistent with the lower *trans* influence of a bridging vs. a terminal hydride ligand. The Ru–P distances are within the normal range expected for Ru(II)-phosphine complexes.

Figure 5.12: Molecular structure of [RuHCl(*S,S*-CHIRAPHOS)]$_3$, **30**, showing the atom numbering scheme used. For the sake of clarity, the hydrogen atoms and all atoms of the phenyl rings except the α-carbon have been omitted.

another view:
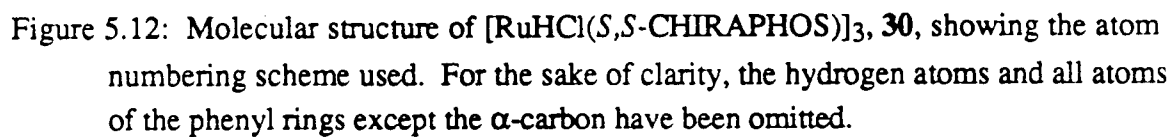
Table 5.4: Selected Bond Lengths (Å) for [RuHCl(*S,S*-CHIRAPHOS)]₃, **30**, with Estimated Standard Deviations in Parentheses.

Bond	Length (Å)	Bond	Length (Å)
Ru(1)—Cl(1)	2.519()	Ru(1)—Ru(2)	2.808()
Ru(1)—Cl(2)	2.452()	Ru(1)—Ru(3)	3.357()
Ru(1)—Cl(3)	2.521()	Ru(1)—P(1)	()
Ru(2)—Cl(1)	2.488()	Ru(1)—P(2)	()
Ru(2)—Cl(3)	2.827()	Ru(2)—P(3)	()
Ru(3)—Cl(1)	2.539()	Ru(2)—P(4)	()
Ru(3)—Cl(3)	2.551()	Ru(3)—P(5)	()
Ru(3)—Cl(2)	2.569()	Ru(3)—P(6)	()

Table 5.5: Selected Bond Angles (deg) for [RuHCl(*S,S*-CHIRAPHOS)]₃, **30**, with Estimated Standard Deviations in Parentheses.

Bonds	Angle (deg)	Bonds	Angle (deg)
Ru(2)—Ru(1)—Cl(1)	55.38()	Ru(1)—Cl(1)—Ru(3)	
Ru(2)—Ru(1)—Cl(2)	130.82()	Ru(1)—Cl(2)—Ru(3)	
Ru(2)—Ru(1)—Cl(3)	63.81()	Ru(1)—Cl(3)—Ru(3)	
Ru(2)—Ru(1)—P(1)	102.74()		
Ru(2)—Ru(1)—P(2)	123.79()		

5.5.2 ^{1}H and ^{31}P NMR Studies

The trimeric [RuHCl(P–P)]$_3$ complexes **29** and **30** in C$_6$D$_6$ solution at ambient temperature exhibit three 1:1:1 high-field resonances, one each for the three hydride ligands, in the respective ^{1}H NMR spectra. The observed $^2J_{PH}$ coupling constants, which range from 13 to 33 Hz, are indicative of a *cis* arrangement of hydride and phosphine ligands. The ^{31}P{^{1}H} NMR spectra of both complexes consist of six discrete resonances. The similarity of the respective ^{1}H (hydride region) and ^{31}P NMR spectra for the DPPB- and the CHIRAPHOS-derivatives suggests similar structure for the two complexes (see below).

The proton NMR spectrum (300 MHz, C$_6$D$_6$, 20 °C) of the DPPB trimer is shown in Figure 5.13. The hydride resonances for [RuHCl(DPPB)]$_3$, **29**, are observed as a triplet at –17.65 ($^2J_{PH}$ = 31.7 Hz), a complex multiplet at –21.1 ($^2J_{PH}$ ~13–18 Hz), and another triplet centred at –21.9 ppm ($^2J_{PH}$ = 33.2 Hz), the triplets being assigned to two terminal hydrides and the complex multiplet to a bridging hydride ligand of **29**. The ratio of combined integration of the hydride resonances to that for the DPPB ligand resonances is close to the expected value of 1:28.

The ^{31}P{^{1}H} NMR spectrum of **29** (121.42 MHz, C$_6$D$_6$, 20 °C; Figure 5.15) consists of six discrete resonances of equal intensity ratio centred at 71.8, 69.5, 61.9, 59.7, 57.6 and 48.9 ppm, each being part of an AB quartet pattern. The P–P couplings are unresolved as they are comparable to the unusually large line-widths ($w_{1/2}$ ~40 Hz) of the resonances. The spectrum remained essentially unchanged over +40 to –80 °C temperature range, except for even more broadening at lower temperatures.

In the absence of well-resolved P–P couplings, the phosphorus chemical shifts could not be assigned with certainty; attempts to obtain ^{31}P–^{31}P *2D-COSY* maps were unsuccessful because of high level of spectral noise and limited instrument time. However, the apparent line-shapes of the phosphorus resonances (Figure 5.14) do give some hint of

215
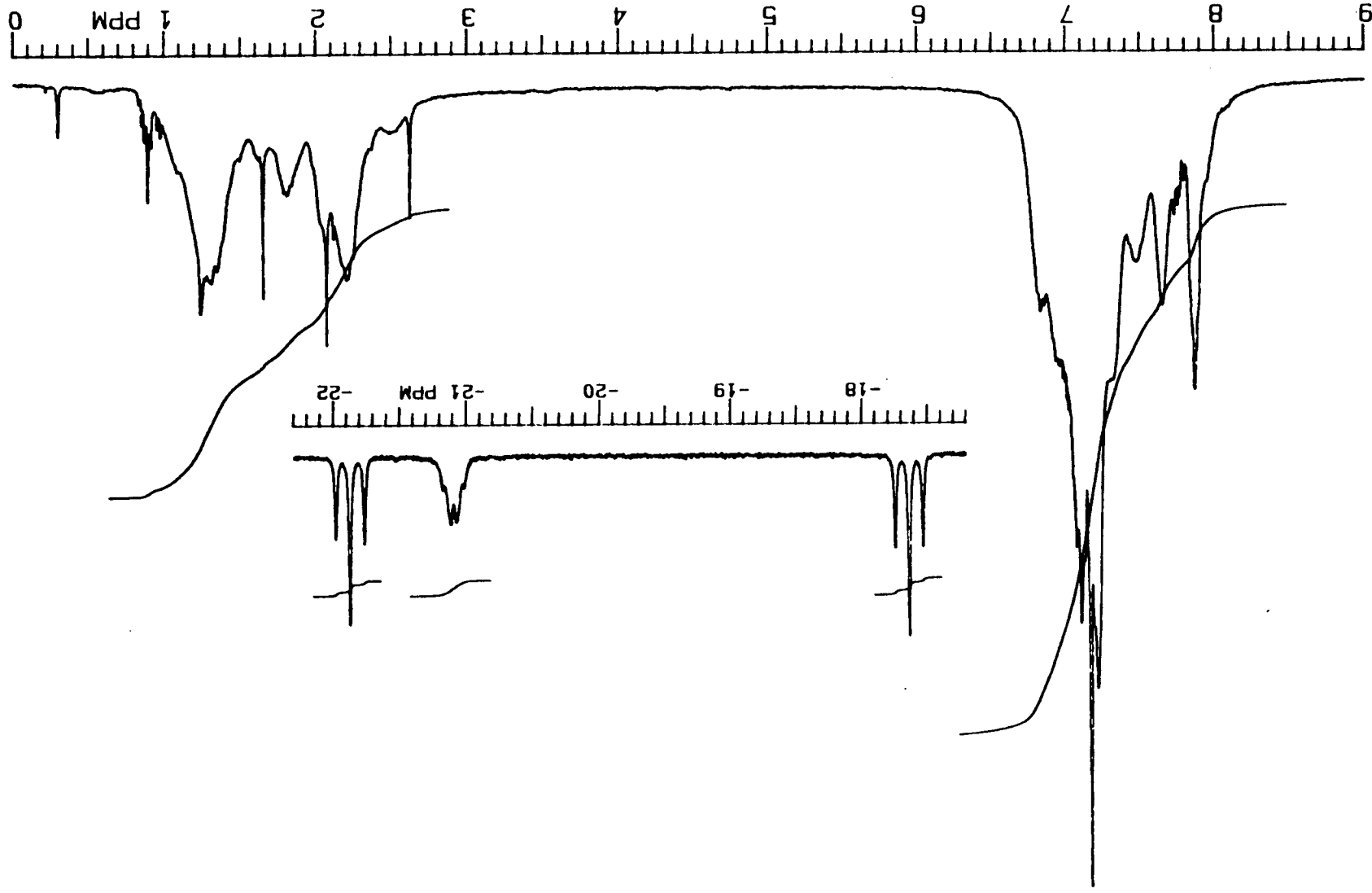
Figure 5.13: 1H NMR spectrum of [RuHCl(DPPB)]₃, 29, in C₆D₆ solution (300 MHz, 20 °C) showing the hydride region in the inset.

216
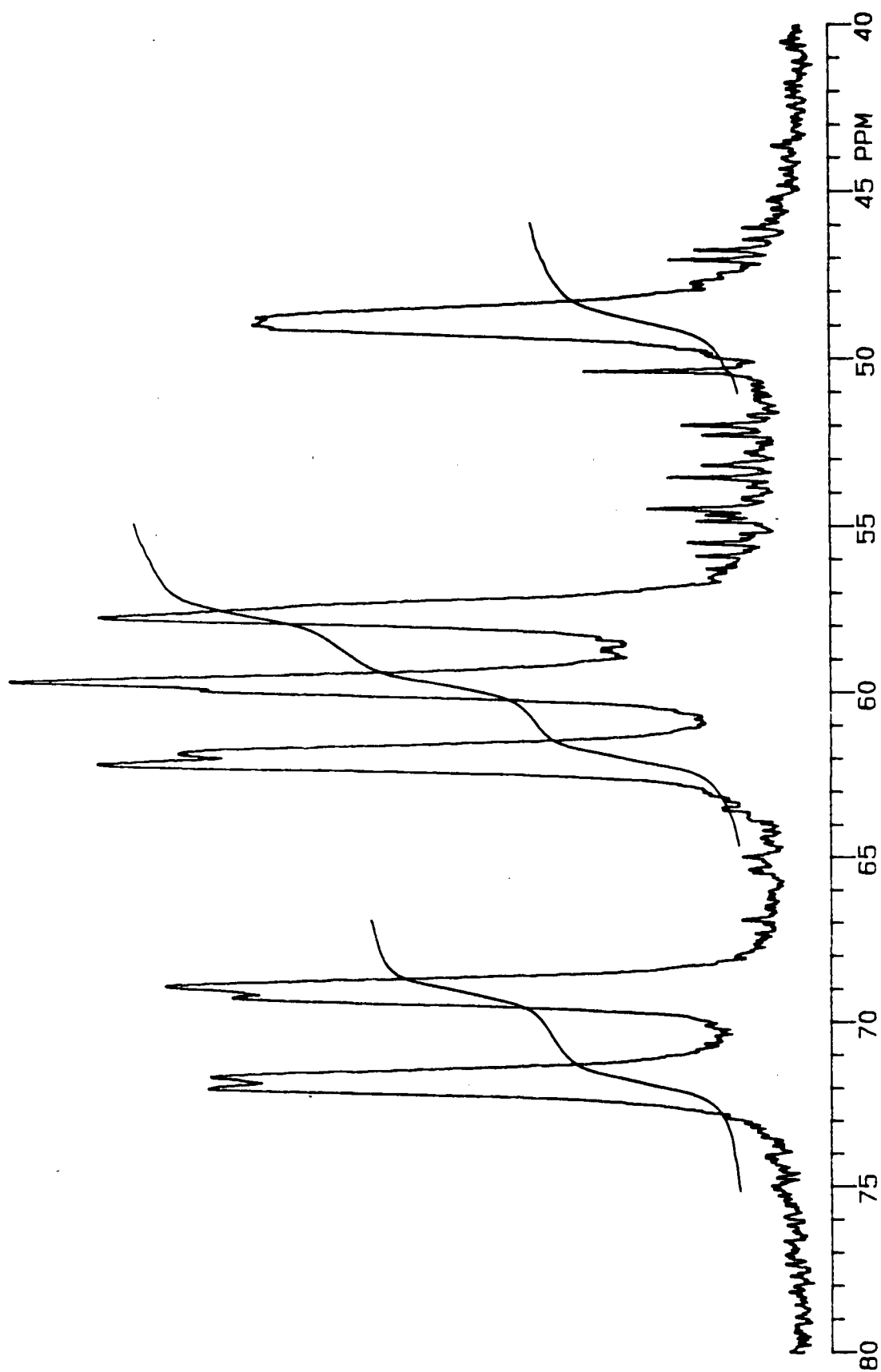
Figure 5.14: $^{31}P\{^1H\}$ NMR spectrum (121.42 MHz, 20 °C) of [RuHCl(DPPB)]$_3$, **29**, in C$_6$D$_6$ solution.

217

possible correlations. Thus the resonances at 71.8, 69.5 and 59.7 ppm can be tentatively correlated to the ones at 48.9, 61.9 and 57.6 ppm, respectively. This assignment was confirmed by selective phosphorus decoupled-proton ($^1H\{^{31}P\}$) NMR studies, which proved to be a powerful tool in assigning not only the mutually coupled phosphorus resonances, but also in establishing correlations between hydride and phosphorus NMR signals.

The $^1H\{^{31}P\}$ NMR spectra for [RuHCl(DPPB)]₃, **29**, are shown in Figure 5.15. The ^1H NMR triplet at −17.65 ppm due to a terminal hydride shows loss of coupling when the phosphorus resonances at 69.5 and 61.9 ppm are decoupled selectively (Figure 5.15b and 5.15c), confirming mutual coupling between the two phosphorus resonances and their correlation to the hydride ligand that resonates at −17.65 ppm. Irradiation of δ 71.8 and 48.9 ppm ^{31}P signals causes loss of coupling for the signals at −21.1 and −21.9 ppm in the proton NMR spectrum (Figure 5.15a and 5.15f), while selective ^{31}P-decoupling at 59.7 and 57.6 ppm affects only the −21.1 ppm proton NMR multiplet assigned to the bridging hydride (Figure 5.15d and 5.15e). Finally, broad-band phosphorus decoupling results in collapse of the hydride signals to three singlets (Figure 5.15g). These results along with the assignments of the phosphorus and the hydride signals are summarised in Table 5.6.
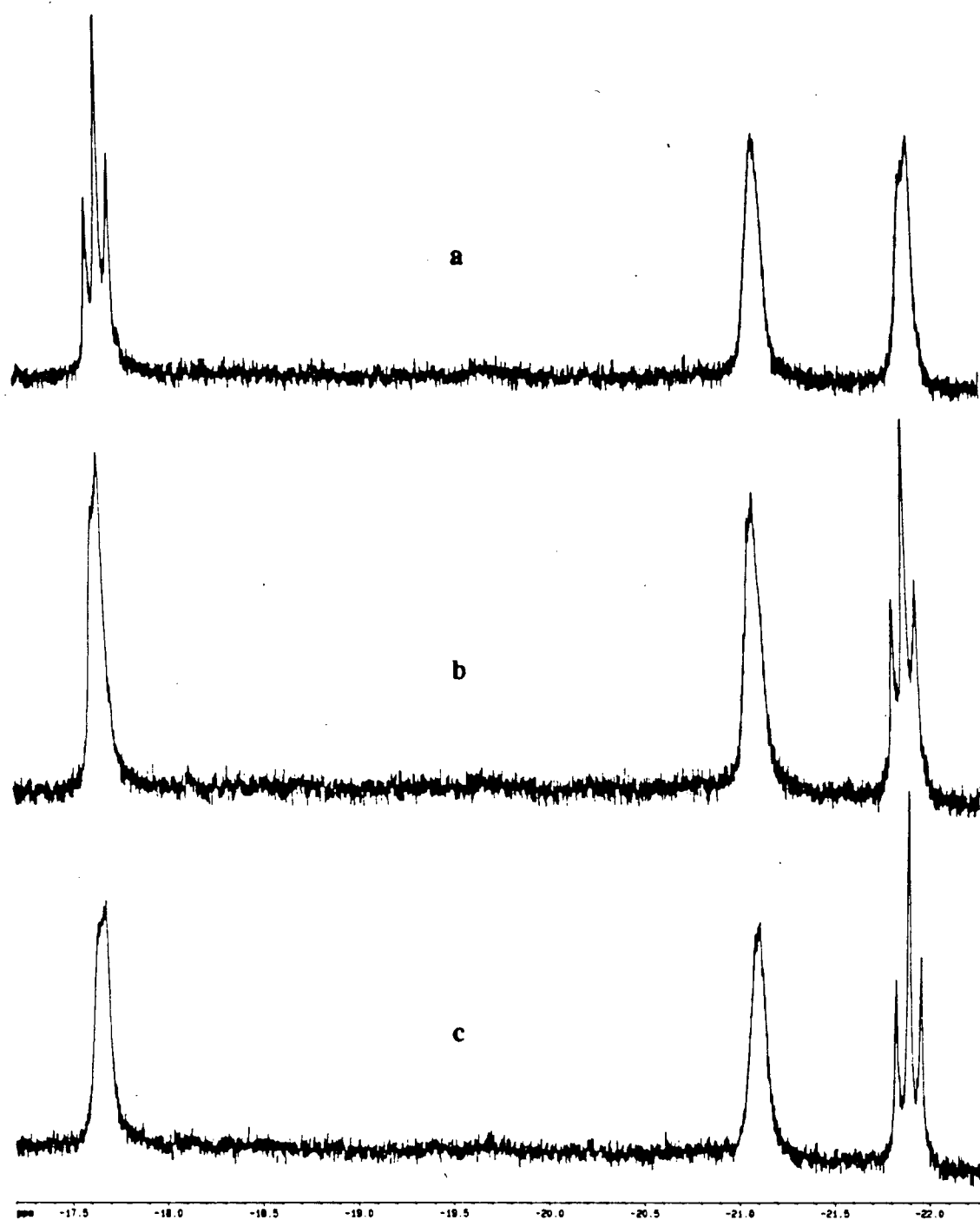
Figure 5.15: ^{1}H{^{31}P} high-field NMR spectra of [RuHCl(DPPB)]$_3$, **29**, in C_6D_6 solution (500.13 MHz for ^{1}H, 202.46 MHz for ^{31}P, 23 °C) with selective phosphorus decoupling at: (a) 71.8; (b) 69.5; (c) 61.9; (d) 59.7; (e) 57.6; (f) 48.9 ppm; and (g) with broad-band decoupling.

Figure 5.15, continued.
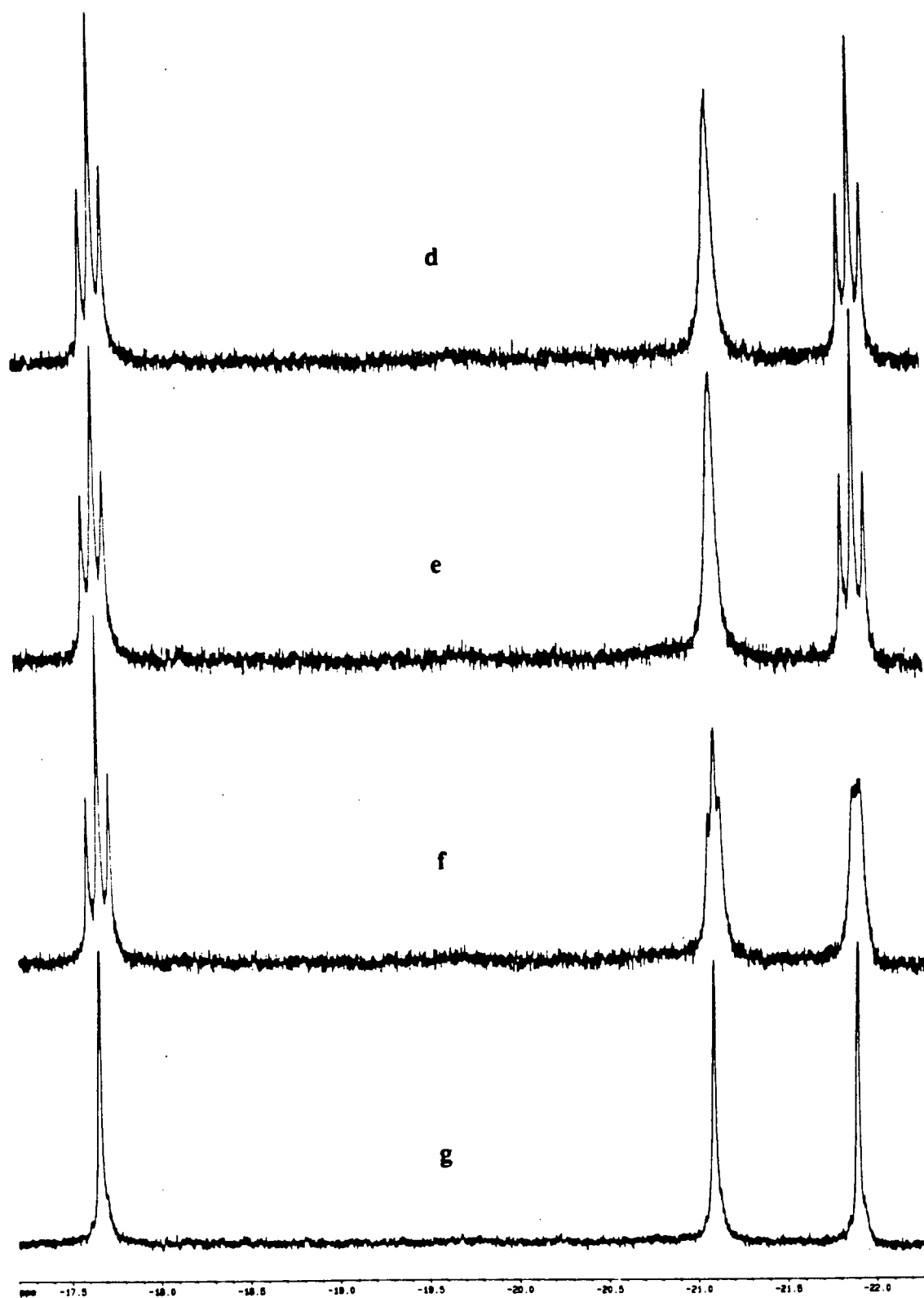
Table 5.6: Results of a Selective {³¹P}-Decoupled ¹H NMR Spectral Study of [RuHCl(DPPB)]₃, **29**, in C₆D₆ Solution.[a]

δ(Ru-H) ppm	Coupled to δ(Ru-P) ppm	Placement of Ru-H Ru Atom[b]	Placement of Ru-P Ru Atom[b]
–17.65 (t)	69.5, 61.9	Terminal, at Ru(3)	Ru(3)
–21.1 (m)	71.8, 48.9	Bridging between	Ru(2)
	59.7, 57.6	Ru(1) and Ru(2)	Ru(1)
–21.9 (t)	71.8, 48.9	Terminal, at Ru(2)	

[a] C₆D₆ solvent, 23 °C; 500.13 MHz for ¹H, 202.46 MHz for ³¹P.

[b] Atom numbering based on the molecular structure of the CHIRAPHOS trimer **30**; also see Figure 5.16 below
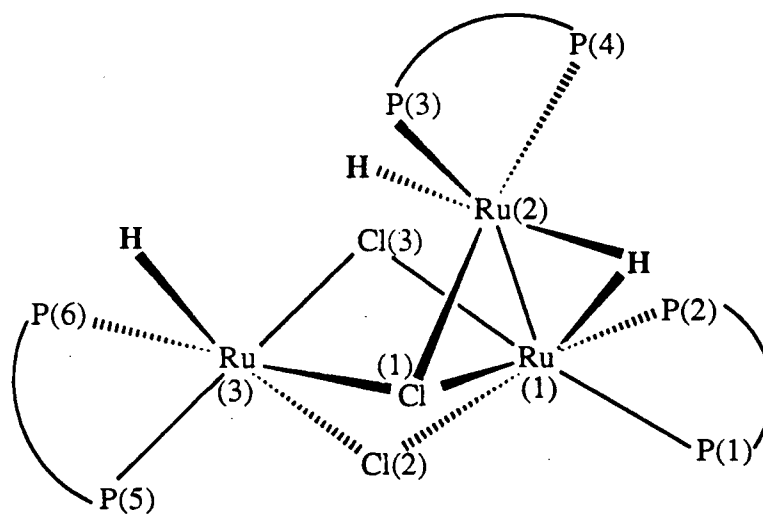
P—P = chelating phosphine

Figure 5.16: Schematic structural representation of [RuHCl(P–P)]₃ complexes (based on the X-ray structure of the CHIRAPHOS derivative; Figure 5.12).

The three hydride ligand resonances for [RuHCl(CHIRAPHOS)]$_3$, **30**, in the proton NMR spectrum (C$_6$D$_6$, 20 °C; Figure 5.18) are observed as doublet of doublet (dd) patterns centred at –17.0 ($^2J_{PH}$ = 36.6, 26.4 Hz) and –24.8 ppm ($^2J_{PH}$ = 36.3, 31.8 Hz) and a complex multiplet centred at –19.4 ppm with $^2J_{PH}$ in the 8–21 Hz range. Again, by analogy to the ^{1}H NMR spectrum for the DPPB analogue (see above), the two dd patterns are respectively assigned to two terminal hydride ligands – one each on Ru(3) and Ru(2), while the complex multiplet is assigned to the bridging hydride between Ru(1) and Ru(2) (see Figures 5.12 and 5.16).
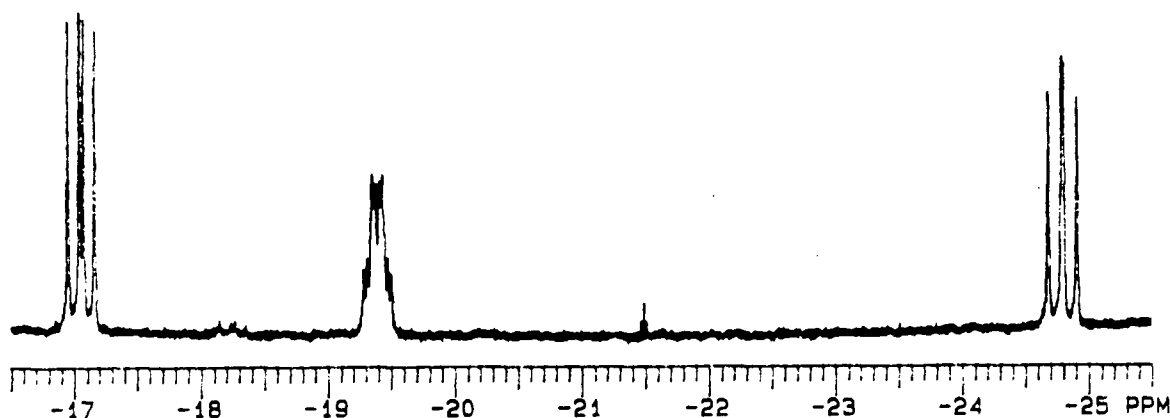
Figure 5.17: ^{1}H NMR spectrum (hydride region, 300 MHz, C$_6$D$_6$, 20 °C) of [RuHCl(*S,S*-CHIRAPHOS)]$_3$, **30**.

The ^{31}P{^{1}H} NMR spectrum of a crude reaction mixture containing **30** and the NEt$_3$ adduct **16b**, recorded at ambient temperature in C$_6$D$_6$ solution, is shown in Figure 5.18. The spectrum consists of six doublet resonances centred at δ 102.7, 100.5, 97.0, 94.0, and 86.5 ppm in a 1:1:1:1:2 integral ratio, the two highest-field signals (86.5 ppm)
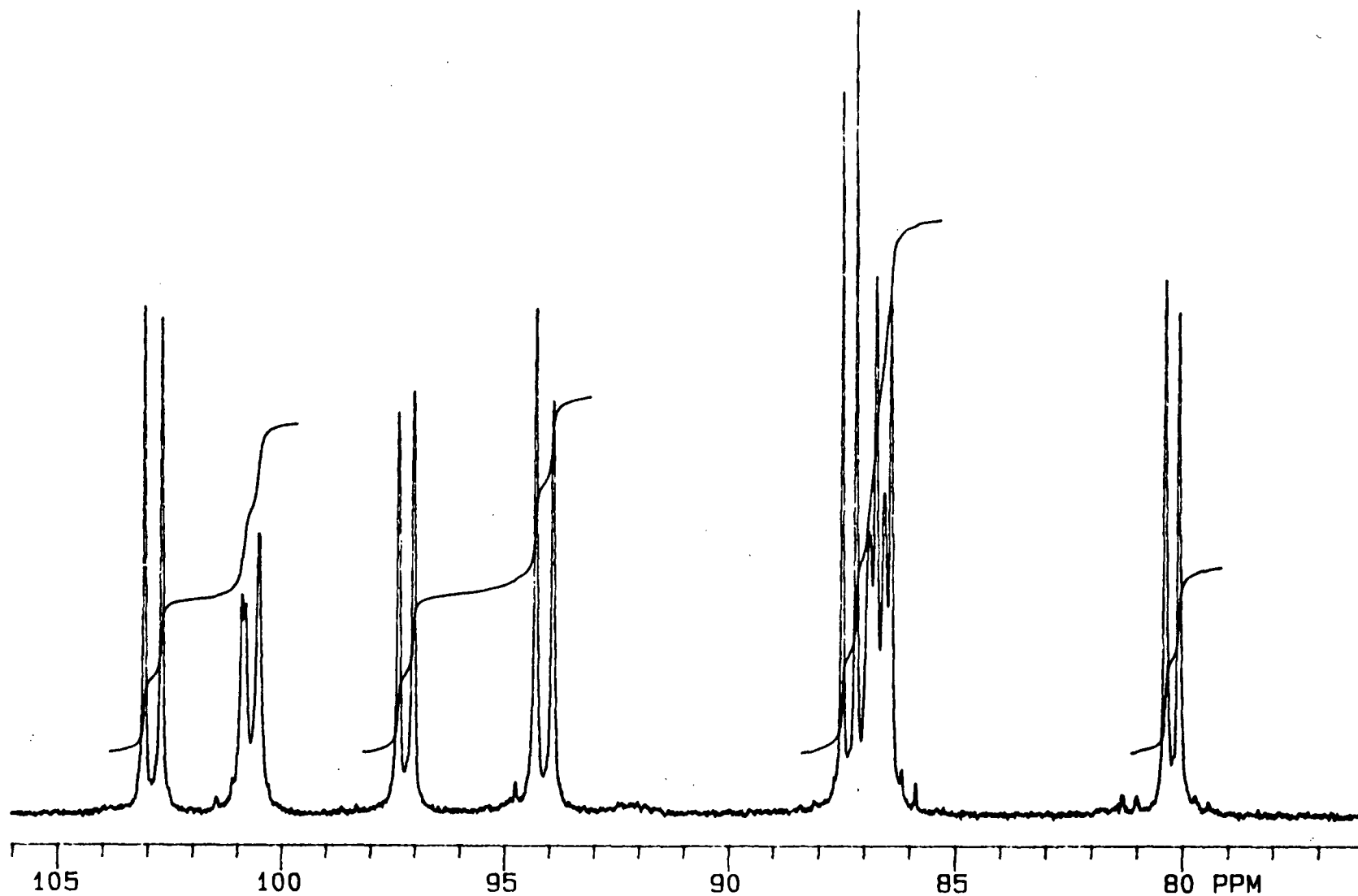
Figure 5.18: $^{31}P\{^1H\}$ NMR spectrum (121.42 MHz, C_6D_6, 20 °C) of a crude reaction mixture showing resonances of the hydridochloro trimer [RuHCl(CHIRAPHOS)]$_3$, **30**, and the dinuclear coproduct [(Et$_3$N)(CHIRAPHOS)Ru-(μ-Cl)$_3$RuCl(CHIRAPHOS)], **16b**.

being coincidentally degenerate. Unlike the $^{31}P\{^1H\}$ NMR spectrum for the DPPB analogue (see above), the spectrum for the CHIRAPHOS complex exhibits relatively sharp peaks with well-resolved $^{31}P-^{31}P$ couplings. The six resonances constitute three AX patterns, as expected for a trinuclear complex containing only one chelating phosphine per Ru centre, and are readily assigned based on the observed coupling constants; δ_A, δ_X ppm ($^2J_{AX}$ Hz): 102.7, 94.0 (46.6); 100.5, 86.5 (40.6); and 97.0, 86.5 (41.4). The additional AB quartet (δ_A = 87.3, δ_B = 80.2 ppm, $^2J_{AB}$ = 37.3 Hz) is assigned to the triethylamine adduct **16b**, which has been isolated and characterised (see Section 2.5.10.2). The BINAP analogue [RuCl$_2$(BINAP)]$_2$(NEt$_3$) reported by Ikariya *et al.* also exhibits an AB quartet pattern (62 and 57 ppm, $^2J_{PP}$ = 35 Hz).[15b]

The ^{31}P NMR spectrum is solvent dependent, with slight variation in the chemical shifts being observed with a change in the solvent; for example, the two overlapping resonances of **30** (85.5 ppm, C$_6$D$_6$) are sufficiently resolved to permit measurement of the respective coupling constants when toluene-d_8 is used as the solvent. Also, extra splittings are sometimes apparent because of insufficient/incomplete ^1H decoupling of the hydride region.

5.6. Interaction of [RuHCl(DPPB)]₃ with H₂ and Nitriles

Interaction of the hydridochloro trimers [RuHCl(P–P)]$_3$ with hydrogen was of interest because these complexes are effective catalysts for hydrogenation of a variety of substrates (Chapter 7). Also, the corresponding Ru(II) tertiary phosphine analogues, previously characterised in our laboratory,[8] were later shown to be the dinuclear hydridochloro species containing a molecular hydrogen ligand: (η^2-H$_2$)[RuHCl(PR$_3$)$_2$]$_2$, R = phenyl or *p*-tolyl.[9]

Addition of 1 atm of H$_2$ to a solution of [RuHCl(DPPB)]$_3$, **29**, in toluene-d_8 did not produce any visible colour change, but the ^1H NMR spectrum of the solution showed a

broad resonance ($w_{1/2}$ = 50 Hz at 20 °C) at –13.05 ppm with a short T_1 relaxation time of 24 ms. The three original hydride resonances of **29** (see Table 5.6) could be discerned only at the noise level. The ^{31}P NMR spectrum showed two new broad resonances of equal intensity at 63.5 and 40.2 ppm ($w_{1/2}$ ~60 Hz); the resonances of **29** (Table 5.6) had disappeared. Removal of H_2 under vacuum resulted in the reappearance of the NMR signals due to [RuHCl(DPPB)]$_3$, **29**, indicating a reversible binding of H_2. The limited data are consistent with the formation of a dinuclear hydridochloro derivative, **32**, containing a molecular hydrogen ligand (η^2-H_2), which is assigned a geometry similar to that found for the corresponding tertiary phosphine analogues (Figure 5.19).[8, 9]

P—P = DPPB
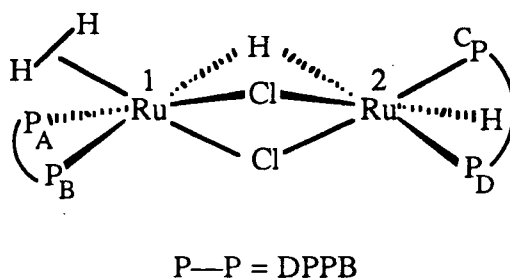
Figure 5.19: Suggested geometry for [RuHCl(DPPB)]$_2$(η^2-H_2) complex, **32**.

The variable temperature ^1H NMR spectra (hydride region, toluene-d_8) of **32** are shown in Figure 5.20. The signal at –13 ppm broadens with decrease in temperature and decoalesces ~224 K. Below 220 K, three broad signals centred at *ca.* –7, –13 and –18 ppm become apparent, with the two outer signals sharpening on further cooling. By analogy to the corresponding spectra reported for (η^2-H_2)[RuHCl(PR$_3$)$_2$]$_2$,[9, 40] the resonances at –7 and –18 ppm are respectively assigned to the bridging and the terminal hydride ligands of **32**, while the relatively broad signal at –13 ppm (estimated $w_{1/2}$ ~500 Hz at 199K) is attributed to the bound dihydrogen moiety.

Both intramolecular and intermolecular H-exchange processes are evident from the NMR spectra of **32**. The –13 ppm resonance in the ^1H NMR spectrum obtained at ambient

temperature is an average signal due to the exchanging η^2-H_2 ligand and the bridging and the terminal hydrides of **32**, and the corresponding T_1 relaxation time of 24 ms is also an averaged value. The T_1 relaxation time for the η^2-H_2 moiety (as opposed to an averaged value) could not be measured accurately because of the very large linewidth of the signal at low temperature (Figure 5.20). The signal for dissolved H_2 (4.46 ppm) was also relatively broad ($w_{1/2}$ ~10 Hz), implying exchange between the bound and the free dihydrogen.

Further evidence of intra- and intermolecular exchange processes comes from the ^{31}P NMR spectrum. For a species of the geometry suggested in Figure 5.19, two sets of AB patterns will be expected if the exchange is too slow (or non-existent) on the NMR time-scale. A fast intermolecular on/off equilibrium between the bound and the free H_2 at the Ru^1 centre will result in scrambling of the P_A and P_B signals provided that the H_2 can bind any of the three non-bridging sites on Ru^1, but will not affect P_C and P_D pair on Ru^2 if the $-(\mu\text{-H})(\mu\text{-Cl})_2Ru^2H(DPPB)$ fragment remains in a locked conformation. The observed scrambling of the P_C and P_D resonances, at ambient temperature, indicates that the intramolecular exchange between the bridging and the terminal hydride on Ru^2 must also be fast on the NMR time-scale. Exchange between η^2-H_2 and the bridging hydride constitutes the third mode of exchange. It has been observed previously for the dinuclear hydridochloro Ru(II) tertiary phosphine analogoues of **32**.[9, 40] Interestingly, the resonances of $(P_A, P_B)Ru^1$ and $(P_C, P_D)Ru^2$ remained distinct, at least at 20 °C, implying $(\eta^2\text{-}H_2)Ru^1 \leftrightarrow Ru^2(\eta^2\text{-}H_2)$ process (if occuring) is slow on the NMR time-scale. The lower field ^{31}P resonance at 63.5 ppm is tentatively assigned to the $(P_C, P_D)Ru^2$ pair consistent with the general trend observed for Ru-phosphine complexes containing a terminal hydride ligand (see Section 4.4, p.167), while the 40.3 ppm signal is attributed to the $(P_A, P_B)Ru^1$ pair.
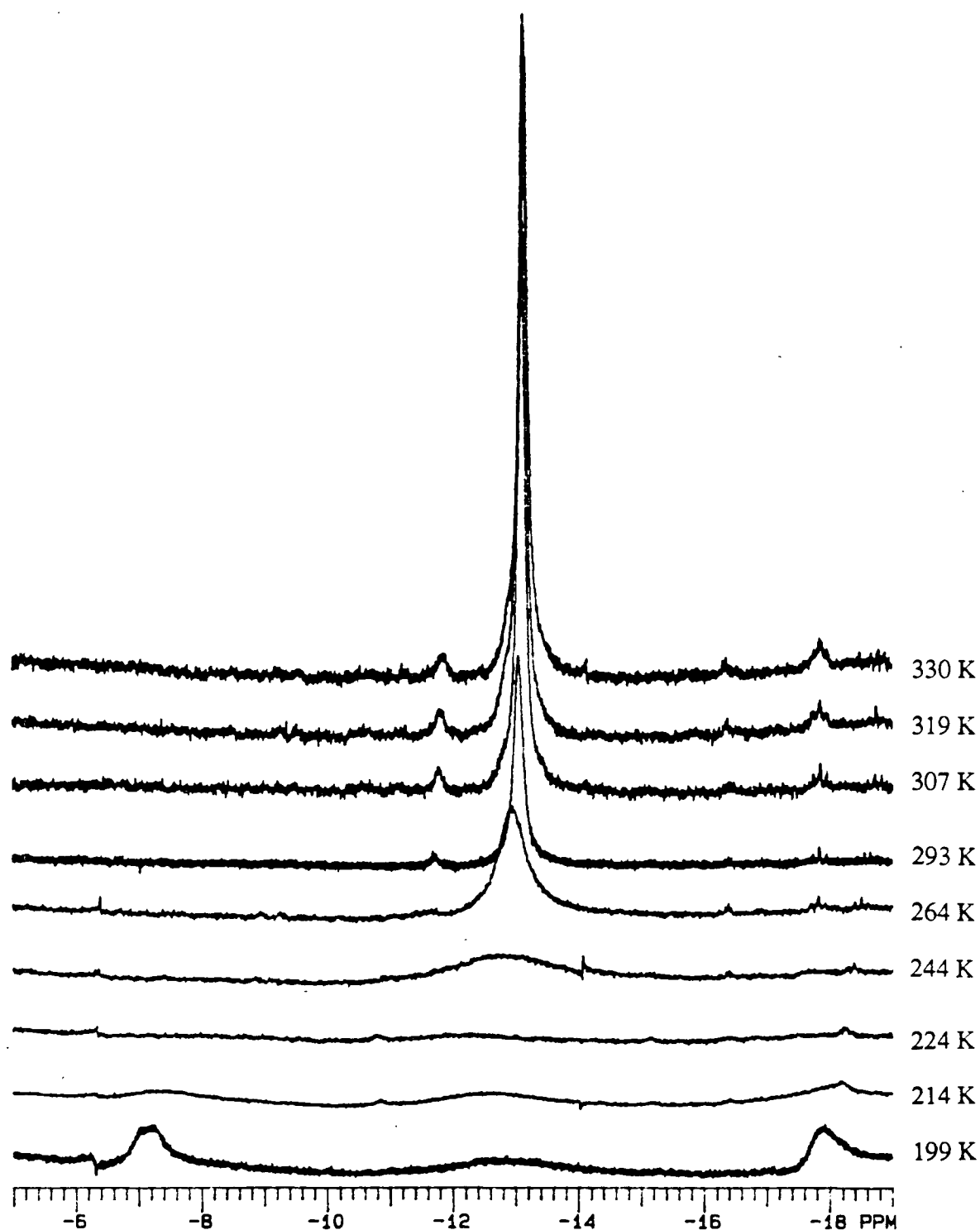
Figure 5.20: Variable temperature ^1H NMR spectra of the dinuclear η^2-H_2 complex [(η^2-H_2)(DPPB)Ru(μ-H)(μ-Cl)$_2$RuH(DPPB)], **32**, generated *in situ* from the reaction of [RuHCl(DPPB)]$_3$ with H_2.

Addition of one equivalent of MeCN or PhCN per Ru to a solution of **29** also resulted in complete *in situ* conversion of the trimeric hydride to give dinuclear complexes similar to the η^2-H_2 complex **32** described above; the products have been characterised *in situ* by NMR spectroscopy. The ^1H and ^{31}P NMR data are listed in Table 5.7.

The ^{31}P NMR spectra of the nitrile derivatives (MeCN, **33a**; PhCN, **33b**) consisted of two AB quartet patterns of equal intensity, indicating that unlike the η^2-H_2 complex **32**, the ligand exchange was slow on the NMR time-scale. The ^1H NMR spectra (hydride region) consisted of a complex multiplet assigned to the bridging hydride ligand, and a triplet resonance attributed to the terminal hydride.

The breakdown of the hydridochloro trimer [RuHCl(DPPB)]$_3$, **29**, under an atmosphere of H_2 to give the dinuclear (η^2-H_2) derivative, **32**, is a significant finding. The complex **29** and its CHIRAPHOS analogue **30** are catalyst precursors for hydrogenation of a variety of substrates (see Chapter 7); the dinuclear dihydrogen complex **32** must be the species present under hydrogenation conditions. The studies should be extended to the CHIRAPHOS system. Generation of nitrile derivatives **33a** and **33b** (which appear to be analogous to **32**), in the presence of equimolar quantities of the nitriles MeCN or PhCN, also suggests that dinuclear species are likely to be present during hydrogenation of nitrile substrates for which **29** is an effective catalyst.

5.7   Suggested Mechanism for Formation of [RuHCl(P–P)]$_3$ Complexes

Based on the results described in the previous sections, the following mechanism (Scheme 5-III) is proposed for the formation of the trimeric hydride derivatives [RuHCl(P–P)]$_3$, **29** and **30**, from the corresponding dimeric [RuCl(P–P)(μ-Cl)]$_2$ complexes (**14** and **16**). The mechanism involves formation of a molecular hydrogen complex followed by deprotonation of the bound H_2 by triethylamine to give the

RCN =	Chemical Shift δ ppm	Coupling Constant Hz	Assignment[b]
^1H NMR data, Hydride Region			
MeCN, **33a**	−17.5 (br, complex m)	$^2J_{PH} \sim 16-20$	Bridging Hydride
	−17.7 (br, t)	$^2J_{PH} = 30$	Terminal Hydride
PhCN, **33b**	−16.65 (br, pseudo q)	$^2J_{PH} \sim 16-25$	Bridging Hydride
	−17.55 (br, t)	$^2J_{PH} = 35$	Terminal Hydride
$^{31}P\{^1H\}$ NMR data			
MeCN, **33a**	$\delta_A = 60.0, \delta_B = 57.6$	$^2J_{AB} = 35$	
	$\delta_C = 71.7, \delta_D = 58.8$	$^2J_{CD} = 52$	
PhCN, **33b**	$\delta_A = 59.6, \delta_B = 56.8$	$^2J_{AB} = 37.7$	
	$\delta_C = 71.7, \delta_D = 58.8$	$^2J_{CD} = 41.3$	

[a] C_6D_6 solvent, 20 °C; 300 MHz for ^1H, 121.42 MHz for ^{31}P.

[b] *Cf.* Figure 5.19 for assignments

intermediate **I**. A repeat of this sequence via the intermediate **II** would yield the dinuclear $[RuCl(P-P)]_2$ species (intermediate **III**) which, under H_2 atmosphere, could generate the dinuclear hydridochloro species containing an η^2-H_2 moiety, **32**. During work-up of the reaction mixture, when the H_2 atmosphere is removed under vacuum, the complex **32** converts to the trimeric hydride species **29** which is the isolated product. The reaction of **29** with H_2 is reversible, and affords the molecular hydrogen complex **32**. Similarly, reactions of **29** with nitriles generate the dimeric species with a coordinated nitrile (**33a**, **33b**), as evidenced by NMR spectroscopy.

L = MeCN, **33a**; PhCN, **33b**
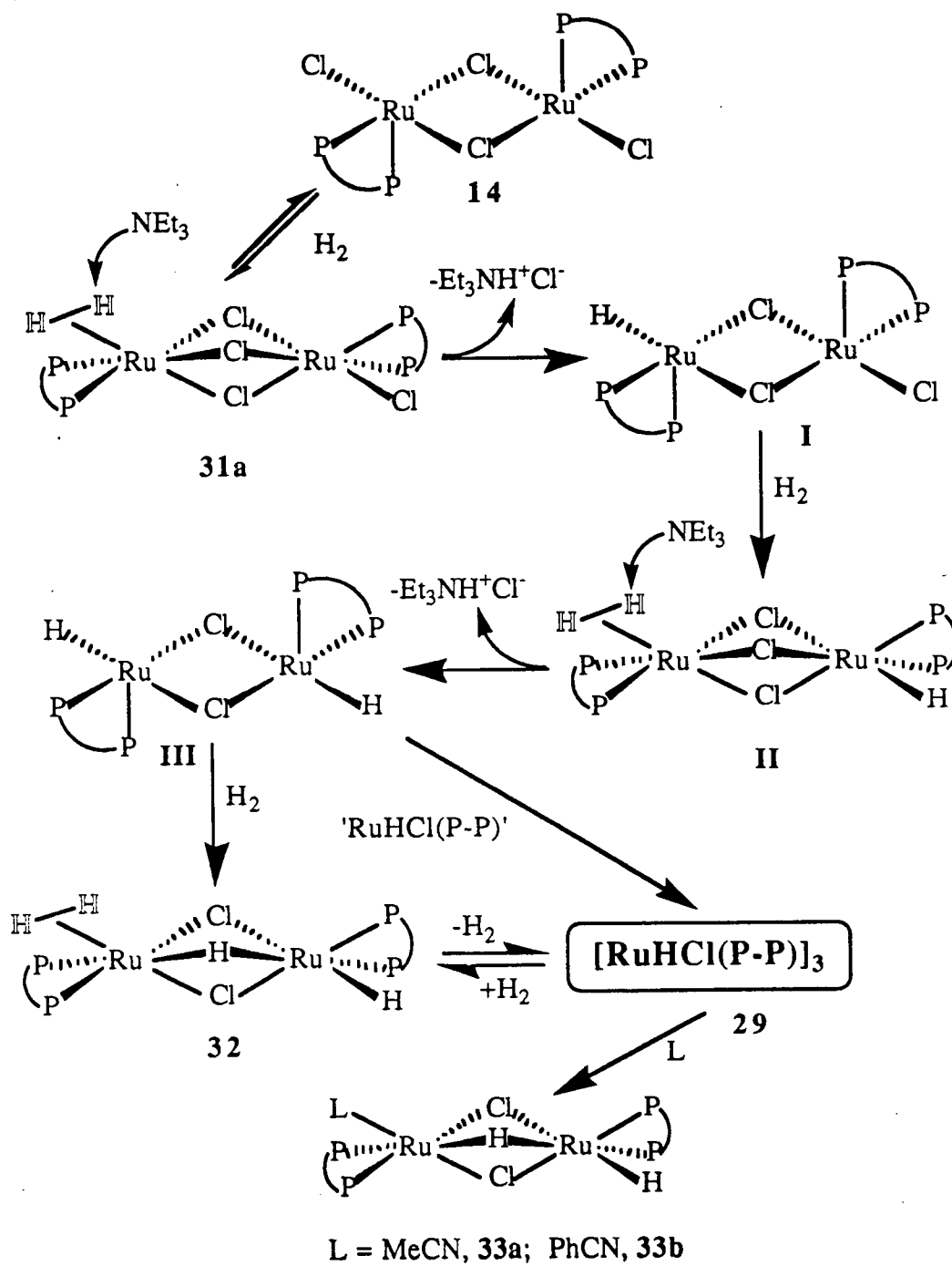
Scheme 5-III

5.8 References – Chapter 5

1. Pearson, R. G. *Acc. Chem. Res.* **1971**, *4*, 152.

2. James, B. R. in *Comprehensive Organometallic Chemistry*; Wilkinson, G., Stone, F. G. A., Abel, E. W., Eds.; Pergamon Press: Oxford, 1982; Vol. 8, Chapter 51.

3. James B. R. *Adv. Organomet. Chem.* **1979**, *17*, 319.

4. James, B. R. *Homogeneous Hydrogenation*; Wiley: New York, 1973.

5. (a) Eisenschmid, T. C.; Kirss, R. U.; Deutsch, P. P.; Hommeltoft, S. I.; Eisenberg, R.; Bargon, J.; Lawler, R. G.; Balch, A. L. *J. Am. Chem. Soc.* **1987**, *109*, 8089.
   (b) Kirss, R. U.; Eisenschmid, T. C.; Eisenberg, R. *J. Am. Chem. Soc.* **1988**, *110*, 8564.
   (c) Kirss, R. U.; Eisenberg, R. *J. Organomet. Chem.* **1989**, *359*, C22.
   (d) Eisenschmid, T. C.; McDonald, J.; Eisenberg, R.; Lawler, R. G. *J. Am. Chem. Soc.* **1989**, *111*, 7267.

6. Hallman, P. S.; McGarvey, B. R.; Wilkinson, G. *J. Chem. Soc., A* **1968**, 3143.

7. James, B. R.; Wang, D. K. W. *Inorg. Chim. Acta* **1978**, *29*, L237.

8. Dekleva, T. W.; Thorburn, I. S.; James, B. R. *Inorg. Chim. Acta* **1985**, *100*, 49.

9. Hampton, C.; Dekleva, T. W.; James, B. R.; Cullen, W. R. *Inorg. Chim. Acta* **1988**, *145*, 165.

10. McCrindle, R.; Fergusson, G.; Arsenalut, J.; McAlees, A. J. *J. Chem. Soc., Chem. Commun.* **1983**, 571.

11. Thorburn, I. S., Ph.D. Dissertation, The University of British Columbia, Vancouver, Canada, 1985.

12. James, B. R.; Pacheco, A.; Rettig, S. J.; Thorburn, I. S.; Ball, R. C.; Ibers, J. A. *J. Mol. Catal.* **1987,** *41,* 147.

13. Noyori, R. *Science* **1990,** *248,* 1194; *Chem. Soc. Rev.* **1989,** *18,* 187.

14. (a) Miyashita, A.; Yasuda, A.; Takaya, H.; Toriumi, K.; Ito, T.; Souchi, T.; Noyori, R. *J. Am. Chem. Soc.* **1980,** *102,* 7932.
    (b) Miyashita, A.; Takaya, H.; Souchi, T.; Noyori, R. *Tetrahedron* **1984,** *40,* 1245.
    (c) Takaya, H.; Mashima, K.; Koyano, K.; Yagi, M.; Kumobayashi, H.; Taketomi, T.; Akutagawa, S.; Noyori, R. *J. Org. Chem.* **1986,** *51,* 629.

15. (a) Kawano, H.; Ishii, Y.; Ikariya, T.; Saburi, M.; Yoshikawa, S.; Uchida, Y.; Kumobayashi, H. *Tetrahedron Lett.* **1987,** *28,* 1905.
    (b) Ikariya, T.; Ishii, Y.; Kawano, H.; Arai, T.; Saburi, M.; Yoshikawa, S.; Akutagawa, S. *J. Chem. Soc., Chem. Commun.* **1985,** 922.

16. (a) Mashima, K.; Kusano, K.; Ohta, T.; Noyori, R.; Takaya, H. *J. Chem. Soc., Chem. Commun.* **1989,** 1208.
    (b) Kitamura, M.; Ohkuma, T.; Inoue, S.; Sayo, N.; Kumobayashi, H.; Akutagawa, S.; Ohta, T.; Takaya, H.; Noyori, R. *J. Am. Chem. Soc.* **1988,** *110,* 629.
    (c) Noyori, R.; Ohkuma, T.; Kitamura, M.; Takaya, H.; Sayo, N.; Kumobayashi, H.; Akutagawa, S. *J. Am. Chem. Soc.* **1988,** *109,* 5856.

17. James, B. R.; McMillan, R. S.; Morris, R. H.; Wang, D. K. W. *Adv. Chem. Ser.* **1978,** *167,* 122.

18. James, B. R.; Wang, D. K. W. *Can. J. Chem.* **1980,** *58,* 245.

19. Kawano, H.; Ikariya, T.; Ishii, Y.; Saburi, M.; Yoshikawa, S.; Uchida, Y.; Kumobayashi, H. *J. Chem. Soc., Perkin Trans.* **1989,** 1571.

20. James, B. R.; Joshi, A. M.; Kvintovics, P.; Morris, R. H.; Thorburn, I. S. in *Catalysis of Organic Reactions*; Blackburn, D. W., Ed.; Marcel Dekker: New York, 1990; Chapter 2.

21. (a) Kubas, G. J. *Acc. Chem. Res.* **1988**, *21*, 120; and references therein.
    (b) Kubas, G. J. *Comments Inorg. Chem.* **1988**, *7*, 17; and references therein.

22. Ashworth, T. V.; Singleton, E. *J. Chem. Soc., Chem. Commun.* **1976**, 705.

23. Kubas, G. J. *J. Chem. Soc., Chem. Commun.* **1980**, 61.

24. (a) Kubas, G. J.; Ryan, R. R.; Vergamini, P. J.; Wasserman, H. J. 185th Am. Chem. Soc. National Meeting, Seattle, WA, 1983; Abstr. # INOR 229.
    (b) *C&EN* **1983**, *61(13)*, 4.

25. Kubas, G. J.; Ryan, R. R.; Swanson, B. I.; Vergamini, P. J.; Wasserman, H. J. *J. Am. Chem. Soc.* **1984**, *106*, 451.

26. Nageswara Rao, B. D.; Anders, L. R. *Phys. Rev.* **1965**, *140*, A112.

27. Crabtree, R. H.; Lavin, M. *J. Chem. Soc., Chem. Commun.* **1985**, 794; 1661.

28. Morris, R. H.; Sawyer, J. F.; Shiralian, M.; Zubkowski, J. D. *J. Am. Chem. Soc.* **1985**, *107*, 5581.

29. A recent Chemical Abstracts computer search (July 1990) on molecular hydrogen complexes yielded a listing consisting of about seventy references. Some representative examples are cited in references 30 through 34.

30. (a) Kubas, G. J.; Unkefer, C. J.; Swanson, B. I.; Fukushima, E. *J. Am. Chem. Soc.* **1986**, *108*, 7000.
    (b) Wasserman, H. J.; Kubas, G. J.; Ryan, R. R. *J. Am. Chem. Soc.* **1986**, *108*, 2294.
    (c) Kubas, G. J.; Ryan, R. R.; Wrobleski, D. A. *J. Am. Chem. Soc.* **1986**, *108*, 1339.

(d) Conroy-Lewis, F. M.; Simpson, S. J. *J. Chem. Soc., Chem. Commun.* **1986**, 506.

31. (a) Morris, R. H.; Earl, K. A.; Luck, R. L.; Lazarowych, N. J.; Sella, A. *Inorg. Chem.* **1987**, *26*, 2674.
(b) Kubas, G. J.; Ryan, R. R.; Unkefer, C. J. *J. Am. Chem. Soc.* **1987**, *109*, 8113.
(c) Chinn, M. S.; Heinekey, D. M. *J. Am. Chem. Soc.* **1987**, *109*, 5865.
(d) Bianchini, C.; Mealli, C.; Peruzzini, M.; Zanobini, F. *J. Am. Chem. Soc.* **1987**, *109*, 5548.

32. (a) Bautista, M. T.; Earl, K. A.; Maltby, P. A.; Morris, R. H.; Schweitzer, C. T.; Sella, A. *J. Am. Chem. Soc.* **1988**, *110*, 7031.
(b) Bautista, M. T.; Earl, K. A.; Maltby, P. A.; Morris, R. H. *J. Am. Chem. Soc.* **1988**, *110*, 4056.
(c) Bianchini, C.; Peruzzini, M.; Zanobini, F. *J. Organomet. Chem.* **1988**, *354*, C19.
(d) Fontaine, X. L. R.; Fowles, E. H.; Shaw, B. L. *J. Chem. Soc., Chem. Commun.* **1988**, 482.

33. (a) Jia, G.; Meek, D. W. *J. Am. Chem. Soc.* **1989**, *111*, 757.
(b) Arliguie, T.; Chaudret, B. *J. Chem. Soc., Chem. Commun.* **1989**, 155.
(c) Chinn, M. S.; Heinekey, D. M.; Payne, N. G.; Sofield, C. D. *Organometallics* **1989**, *8*, 1824.
(d) Cappellani, E. P.; Maltby, P. A.; Morris, R. H.; Schweitzer, C. T.; Steele, M. R. *Inorg. Chem.* **1989**, *28*, 4437.
(e) Howdle, S. M.; Poliakoff, M. *J. Chem. Soc., Chem. Commun.* **1989**, 1099.

34. (a) Chinn, M. S.; Heinekey, D. M. *J. Am. Chem. Soc.* **1990**, *112*, 5166.
(b) Van der Sluys, L. S.; Eckert, J.; Eisenstein, O.; Hall, J. H.; Huffman, J. C.; Jackson, S. A.; Koetzle, T. F.; Kubas, G. J.; Vergamini, P. J.; Caulton, K. G. *J. Am. Chem. Soc.* **1990**, *112*, 4831.
(c) Howdle, S. M.; Healy, M. A.; Poliakoff, M. *J. Am. Chem. Soc.* **1990**, *112*, 4804.
(d) Harman, W. D.; Taube, H. *J. Am. Chem. Soc.* **1990**, *112*, 2261.

(e) Jia, G.; Morris, R. H. *Inorg. Chem.* **1990,** *29,* 581.

(f) Amendola, P.; Antoniutti, S.; Albertin, G.; Bordignon, E. *Inorg. Chem.* **1990,** *29,* 318.

(g) Mediati, M.; Tachibana, G. N.; Jensen, C. M. *Inorg. Chem.* **1990,** *29,* 3.

35. Henderson, R. A. *Transition Met. Chem.* **1988,** *13(6),* 474.

36. Crabtree, R. H.; Hamilton, D. G. *Adv. Organomet. Chem.* **1988,** *28,* 299; and references therein.

37. Crabtree, R. H. *Acc. Chem. Res.* **1990,** *23,* 95.

38. (a) Pacchioni, G. *J. Am. Chem. Soc.* **1990,** *112,* 80; *J. Organomet. Chem.* **1989,** *377,* C13.

(b) Burdett, J. K.; Pourian, M. R. *Inorg. Chem.* **1988,** *27,* 4445.

(c) Burdett, J. K.; Phillips, J. R.; Pourian, M.; Turner, J. J.; Upmacis, R. *Inorg. Chem.* **1987,** *26,* 3054.

(d) Hay, P. J. *J. Am. Chem. Soc.* **1987,** *109,* 705.

(e) Jean, Y.; Einstein, O.; Volatron, F.; Mouche, B.; Sefta, F. *J. Am. Chem. Soc.* **1986,** *108,* 6587.

39. Crabtree, R. H.; Hamilton, D. G. *J. Am. Chem. Soc.* **1986,** *108,* 3124.

40. Hampton, C., Ph.D. Dissertation, The University of British Columbia, Vancouver, Canada, 1989; Chapter 3.

41. (a) Hampton, C.; Dekleva, T. W.; James, B. R.; Cullen, W. R. *Inorg. Chim. Acta* **1988,** *145,* 165.

(b) Dekleva, T. W.; Thorburn, I. S.; James, B. R. *Inorg. Chim. Acta* **1985,** *100,* 49.

42. Hauge, R. H.; Kafafi, Z. H.; Margrave, J. L. *Proceedings, The Physics and Chemistry of Small Clusters,* Richmond, VA, Oct. 1986; through Reference 21.

43. Ozin, G. A.; Garcia-Prieto, J. *J. Am. Chem. Soc.* **1986,** *108,* 3099.

44.   Nolan, S. P.; Marks, T. J. *J. Am. Chem. Soc.* **1989**, *111*, 8538.

45.   Collman J. P.; Wagenknecht, P. S.; Hembre, R. T.; Lewis, N. S. *J. Am. Chem. Soc.* **1990**, *112*, 1294.

46.   Crabtree, R. H.; Lavin, M.; Bonneviot, L. *J. Am. Chem. Soc.* **1986**, *108*, 4032.

47.   Hamilton, D. G.; Crabtree, R. H. *J. Am. Chem. Soc.* **1988**, *110*, 4126.

48.   (a) Antoniutti, S.; Albertin, G.; Amendola, P.; Bordignon, E. *J. Chem. Soc., Chem. Commun.* **1989**, 229.
       (b) Cotton, F. A.; Luck, R. L. *Inorg. Chem.* **1989**, *28*, 6.

49.   Joshi, A. M.; James, B. R. *J. Chem. Soc., Chem. Commun.* **1989**, 1785.

50.   Arliguie, T.; Chaudret, B.; Morris, R. H.; Sella, A. *Inorg. Chem.* **1988**, *27*, 598.

51.   Hampton, C.; Cullen, W. R.; James, B. R.; Charland, J. -P. *J. Am. Chem. Soc.* **1988**, *110*, 6918.

52.   Sanders, J. K. M.; Hunter, B. K. *Modern NMR Spectroscopy: A Guide for Chemists*; Oxford University Press: Oxford, 1987; pp. 61–65.

53.   Conroy-Lewis, F. M.; Simpson, S. J. *J. Chem. Soc., Chem. Commun.* **1987**, 1675.

54.   Bautista, M.; Earl, K. A.; Morris, R. H.; Sella, A. *J. Am. Chem. Soc.* **1987**, *109*, 3780.

55.   Cotton, F. A.; Luck, R. L. *J. Chem. Soc., Chem. Commun.* **1988**, 1277.

56.   Upmacis, R. K.; Poliakoff, M.; Turner, J. J. *J. Am. Chem. Soc.* **1986**, *108*, 3645.

57.   (a) Chaudret, B.; Devillers, J.; Poilblanc, R. *Organometallics* **1985**, *4*, 1727; *J. Chem. Soc., Chem. Commun.* **1983**, 641.

58.   Gosser, L. W.; Knoth, W. H.; Parshall, G. W. *J. Am. Chem. Soc.* **1973**, *95*, 3436.

CHAPTER 6

Ruthenium(II) Hydrido-Diene Complexes Containing Bidentate Phosphines

6.1 Introduction

The ruthenium(II) hydrido(diene) complex $RuHCl(nbd)(PPh_3)_2$, first reported by Wilkinson *et al.* in 1968,[1] exists in solution as a single (*trans*) isomer in which the metal, the hydride, and the alkene π-bond form a coplanar *cis* arrangement[2, 3] which is favourable for olefin insertion into the Ru–H bond. Earlier work from this laboratory[2, 3] has reported formation of the stable six-coordinate norbornenoyl complex $RuCl(COC_7H_9)(CO)_2(PPh_3)_2$ *via* an irreversible reaction of CO with *trans*–$RuHCl(nbd)(PPh_3)_2$, **34** (Equation 6.1). Coordination of CO, presumably to a five-coordinate intermediate, promotes the hydride migratory-insertion to give a carbonyl(alkenyl) species which subsequently undergoes CO migratory-insertion to give the acyl; coordinative saturation is attained via further coordination of CO. Detailed NMR studies, including selective homonuclear decoupling experiments by Dekleva from this laboratory, established the geometry for the norbornenoyl complex, as depicted in Equation 6.1.[2, 3]

$$2 RuHCl(nbd)(PPh_3)_2 \quad \xrightarrow{\text{5 H}_2} \quad (\eta^2\text{-H}_2)(PPh_3)_2Ru(\mu\text{-Cl})_2(\mu\text{-H})Ru(H)(PPh_3)_2 \quad (6.2)$$

(6.1)

34
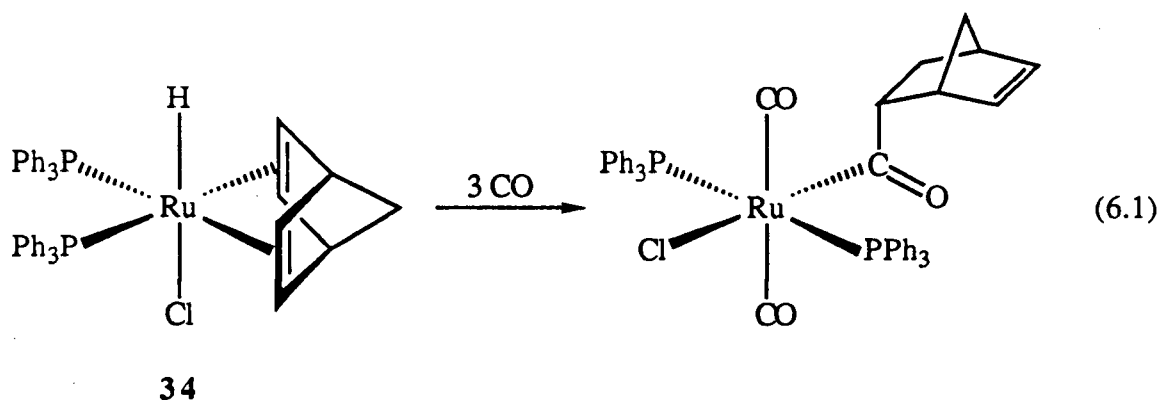
The unusual stability of this acyl species (acyls are typically kinetically unstable with respect to carbonyl-deinsertion[4] or reductive elimination[5, 6]) permitted further investigation into its reactivity with H_2.[7] The H_2-hydrogenolysis of a transition metal-acyl complex to afford the product aldehyde and the metal hydride –often the catalyst precursor– is commonly the final step in both stoichiometric and catalytic hydroformylation of alkenes, but has been little studied.[7–9] Hydrogenolysis of $RuCl(COC_7H_9)(CO)_2(PPh_3)_2$ in DMA or toluene solutions (1 atm H_2, 40–70 °C) results in the formation of 2-norbornene-5-carboxaldehyde and *cis,cis,trans*–$RuHCl(CO)_2(PPh_3)_2$ (Scheme 6-I). A detailed kinetic study of this reaction was undertaken and a mechanism, involving PPh_3 dissociation as the rate-determining first step followed by hydrogenolysis of the resulting intermediate, was proposed to account for the observed kinetic data (Scheme 6-I).[7, 8]

Further, the hydrido(diene) complex, **34**, reacts with H_2 with loss of norbornane to yield a dinuclear η^2-H_2 complex,[10] (Equation 6.2):

+ Norbornane
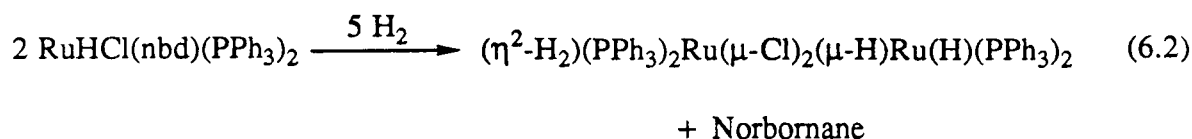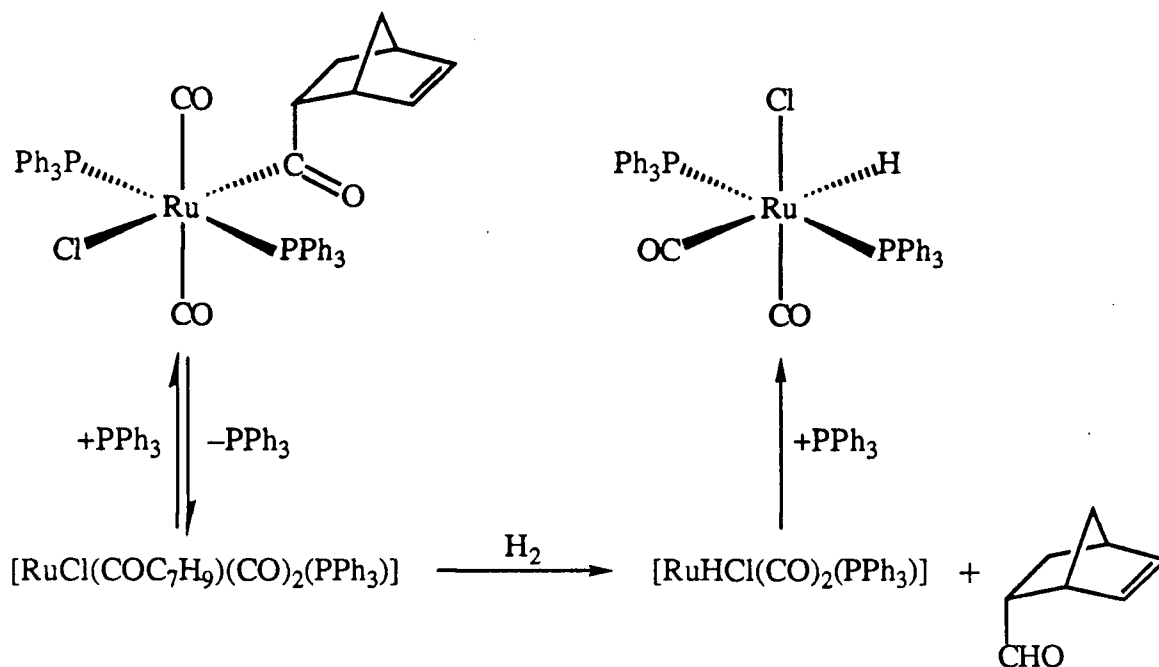
Scheme 6-I: Proposed mechanism for the H_2-hydrogenolysis of the Ru(II) acyl complex $RuCl(COC_7H_9)(CO)_2(PPh_3)_2$.

The work described in this chapter was undertaken to explore further reactions as outlined in Equations 6.1 and 6.2 by using a chelating ditertiary phosphine (P–P) in place of two PPh_3 ligands in the 'precursor' complex 34. The phosphine $Ph_2P(CH_2)_nPPh_2$ (n = 4, DPPB) was chosen as the chelating phosphine particularly because of: (a) the known tendency of DPPB (compared to the n = 1–3 analogues) to become monodentate at a metal centre, i.e. to become dangling,[11] (b) its formation of seven-membered chelate rings, similar to the well-known, chiral DIOP[11, 12] and BINAP ligands,[13, 14] (c) isolation of the dinuclear molecular hydrogen complexes containing DPPB, $(\eta^2-H_2)(DPPB)Ru(\mu-Cl)_2$-$(\mu-X)Ru(X)(DPPB)$ (X = Cl,[15] H; cf. Equation 6.2; also see Chapter 5), and finally, because of (d) the related dichloro(norbornadiene)Ru(II) complex[16] was previously synthesised in this laboratory (see below).

Thorburn[16] investigated the reaction of the dichloro-bridged dinuclear complex $[RuCl(DPPB)(\mu-Cl)]_2$, 14, with excess norbornadiene in benzene. The orange product,

characterised by elemental analysis and ^{1}H and ^{31}P{^{1}H} NMR spectroscopy,[§] was identified as *trans*–RuCl$_2$(nbd)(DPPB)·0.5 C$_6$H$_6$ solvate, **35** (64% yield). An X-ray crystal structure determination confirmed the mutually *trans* chloride ligands.[16, 17] Thorburn also noted that the norbornadiene ligand of **35** slowly dissociated in solution to give the dinuclear precursor **14** (Equation 6.3), which was evident from the gradual disappearance of the 17.0 ppm singlet due to **35** and the concomitant appearance of the AB quartet pattern due to **14** (δ_A = 62.8, δ_B = 53.5 ppm, $^2J_{AB}$ = 46.8 Hz) in the ^{31}P NMR spectrum of an aged solution of **35**.[16, 17] In the corresponding ^{1}H NMR spectrum, free nbd (δ 6.8 ppm, t, olefinic protons) soon became detectable, and after 24 h peaks due to **35** constituted only ~40% of the total integral intensity.

$$RuCl_2(nbd)(DPPB) \rightleftharpoons 1/2\ [RuCl(DPPB)(\mu\text{-}Cl)]_2 + nbd \qquad (6.3)$$

$$\mathbf{35} \qquad\qquad\qquad\qquad\qquad \mathbf{14}$$
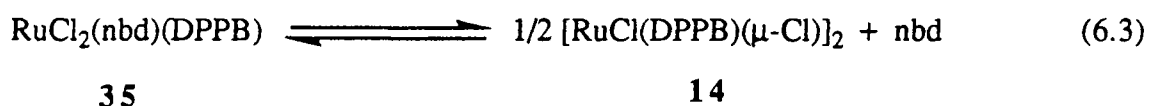
Interestingly, a preparative scale reaction of the dichlorodiene complex **35** with H$_2$ in the presence of Proton Sponge® led to the isolation of the previously known [Ru$_2$Cl$_5$(DPPB)$_2$]$^-$PSH$^+$ complex[16–19] as the major product (~63% yield, ^{31}P{^{1}H} NMR, CD$_2$Cl$_2$, 20 °C: 53.6 ppm, s) instead of a hydridochloro species such as "RuHCl(DPPB)" or an η^2-H$_2$ analogue containing DPPB (*cf.* Equation 6.2). A small amount of brown solid (~5% yield) subsequently isolated from the reaction mixture (filtrate), though analytically impure, showed evidence of hydride formation. The proton NMR spectrum of the brown solid principally consisted of a high-field resonance at –9.69 ppm (t, $^2J_{PH}$ = 21 Hz; C$_6$D$_6$,

20 °C) characteristic of a Ru-hydride species, along with resonances in the 4.0–0.8 ppm region characteristic of bound norbornadiene protons; the resonances were tentatively assigned to *trans*-RuHCl(nbd)(DPPB), **36**.[16, 17]

6.2   Synthesis and Characterisation of *Trans*-RuHCl(nbd)(DPPB), **36**

The minor, impure product obtained by Thorburn from the reaction of **35** with H_2 (see above), and tentatively identified as *trans*-RuHCl(nbd)(DPPB), was synthesised in pure form by two routes (Section 2.5.3).

One, giving a 40% yield, involves the simple displacement of the PPh₃ ligands of *trans*-RuHCl(nbd)(PPh₃)₂, **34**, by DPPB in benzene solution (Equation 6.4).

$$RuHCl(nbd)(PPh_3)_2 + DPPB \xrightarrow{C_6H_6} RuHCl(nbd)(DPPB) + 2\,PPh_3 \qquad (6.4)$$

34   **36**
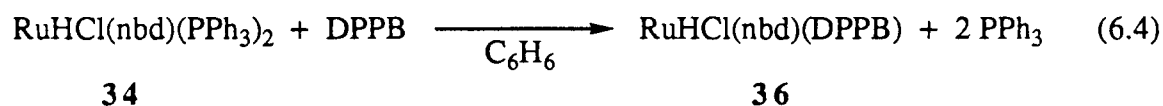
The second method for the preparation of **36** also involves PPh₃ displacement, this time by nobornadiene, from the mixed phosphine Ru(II) precursor RuCl₂(dppb)(PPh₃), **23**, under hydrogenation conditions (1 atm H_2, Proton Sponge, 60 °C) in benzene (Equation 6.5). The off-white **36** is isolated in 62% yield, although the accompanying PSH⁺Cl⁻ salt, which was identified by ¹H NMR spectroscopy, is formed in quantitative yield.

$$RuCl_2(DPPB)(PPh_3) + nbd \xrightarrow[C_6H_6]{H_2/PS} RuHCl(nbd)(DPPB) + PPh_3 \qquad (6.5)$$

23   **36**   + PSH⁺Cl⁻
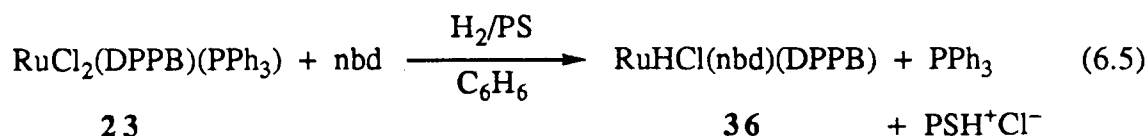
The ³¹P{¹H} NMR spectrum of **36** in C₆D₆ solution consists of a singlet at 43.2 ppm, while the ¹H NMR Ru-hydride resonance is observed as a triplet at δ –9.69 ppm,

with $^2J_{PH}$ = 20.7 Hz (Figure 6.1). This means the two phosphorus atoms of the DPPB ligand are chemically and magnetically equivalent, and are *cis* to the hydride.
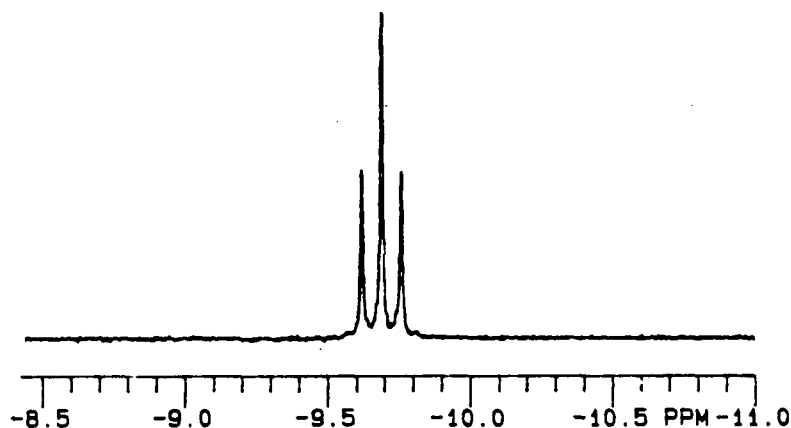
Figure 6.1: The ^1H NMR (300 MHz, C_6D_6, 20 °C) hydride region for *trans*–RuHCl(nbd)(DPPB), **36**.

The ^1H NMR spectrum of **36** was fully assigned using a combination of *2D-COSY* and *NOEDIFF* experiments (Figures 6.2 and 6.3, respectively). The replacement of an 'axial' chloride of RuCl$_2$(nbd)(DPPB), **35**, by a hydride ligand to give **36** leads to the expected doubling in number of peaks for the olefinic protons (δ 3.89, 2.84 ppm, 2H each, br m) and methine protons (δ 3.67, 3.36 ppm, 1H each, br m) of nbd, and the methylene backbone protons (δ 3.75, 2.07, 1.22, 0.98 ppm, 2H each, br m) of the DPPB ligand (compare with the proton NMR data for **35** given in the previous section). This doubling of the number of proton NMR peaks is due to the presence in **36** of two different ligands (H$^-$, Cl$^-$) above and below the Ru-DPPB plane. The two multiplets for the *ortho*-phenyl protons of the DPPB ligand are separated by over 0.9 ppm (δ 8.25, 7.33), again reflecting the axial asymmetry across the Ru-DPPB plane. Irradiation of the δ 8.25 resonance induces a large positive *NOE* enhancement of the Ru–H resonance at –9.69 ppm and *vice versa* (Figure 6.3); thus the 8.25 ppm resonance is assigned to the four *ortho*-phenyl protons (one from each of the phenyl groups on the two P atoms) closest to the hydride,

243

while the higher field 7.33 ppm signal is attributed to the remaining four *ortho*-phenyl protons.

Figure 6.2: The ¹H NMR *2D-COSY* spectrum (300 MHz, C₆D₆, 20 °C, aliphatic proton region) of *trans*–RuHCl(nbd)(DPPB), **36**.
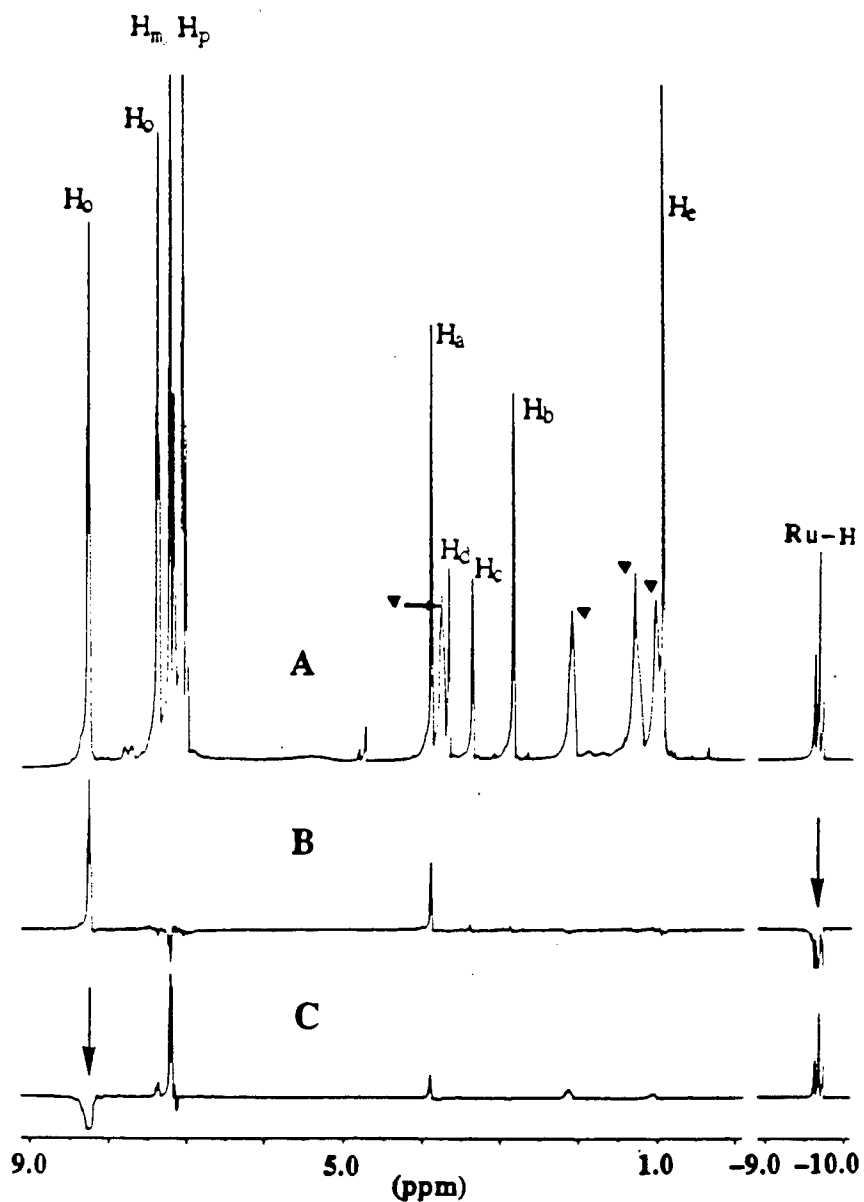
Figure 6.3: The ^{1}H NMR *NOEDIFF* spectra (400 MHz, C$_6$D$_6$, 20 °C) of *trans*-RuHCl(nbd)(DPPB), **36**.

(A) ^{1}H NMR spectrum of **36**; see Figure 6.4 for assignments.

(B) Spectrum with irradiation of the Ru–H resonance (δ –9.69 ppm).

(C) Spectrum with irradiation of the δ 8.25 ppm resonance (see text).

Irradiation of the hydride signal also results in a large positive enhancement of the δ 3.89 ppm resonance, which is therefore assigned to the pair of olefinic protons (H_a) closest to the hydride; H_c and H_d are then assigned because of their observed coupling to H_a and H_b, respectively. The $\nu_{(Ru-H)}$ IR absorption band for **36** is observed at 2045 cm^{-1} (w). The spectroscopic data of **36** resemble closely those for the corresponding RuHCl(nbd)(PPh$_3$)$_2$ complex, **34**, and are consistent with the *trans*-RuHCl(nbd)(DPPB) formulation shown in Figure 6.4.
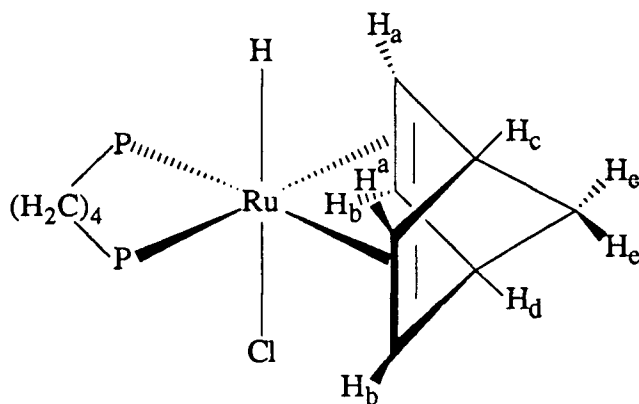
Figure 6.4: Proposed geometry for RuHCl(nbd)(DPPB), **36**, including the proton assignment, based on analysis of the solution NMR spectral data.

Reactions of the mixed-phosphine complex RuCl$_2$(DPPB)(PPh$_3$), **23**, with nbd in the absence of H$_2$ and PS were also investigated. The complex **23** reacts with excess norbornadiene in benzene at 60 °C to produce a greenish yellow suspension. Complete removal of the solvent from the reaction mixture at this stage yields mostly the green starting complex **23**, while addition of hexanes precipitates a mixture of green and yellow solids. Examination by ^{31}P NMR spectroscopy of a reaction mixture in C$_6$D$_6$ indicates equilibrium formation of the dichloronorbornadiene derivative RuCl$_2$(nbd)(DPPB), **35** (Equation 6.6), as evidenced by the resonance at 17.0 ppm (s); additional signals assignable to **23** and free PPh$_3$ are also apparent (for a ^{31}P{^{1}H} NMR spectrum of **23**, see Chapter 4, Figure 4.5).

$$\text{RuCl}_2(\text{DPPB})(\text{PPh}_3) + \text{nbd} \underset{C_6H_6}{\rightleftharpoons} \text{RuCl}_2(\text{nbd})(\text{DPPB}) + \text{PPh}_3 \qquad (6.6)$$

$$\mathbf{23} \qquad\qquad\qquad\qquad\qquad\qquad \mathbf{35}$$
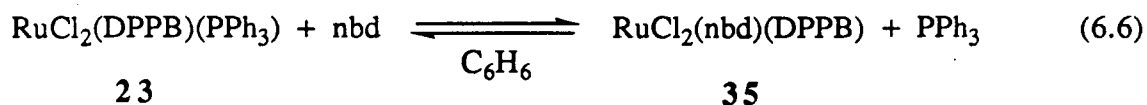
6.3 Discussion

The overall chemistry of formation of **35** and **36** from various starting materials, coupled with the solution behaviour (PPh$_3$ disociation) and H$_2$-reactivity of **23** (to give 'RuHCl(DPPB)(PPh$_3$)' species; see Chapter 4, Section 4.3), are summarised in Scheme 6-II.
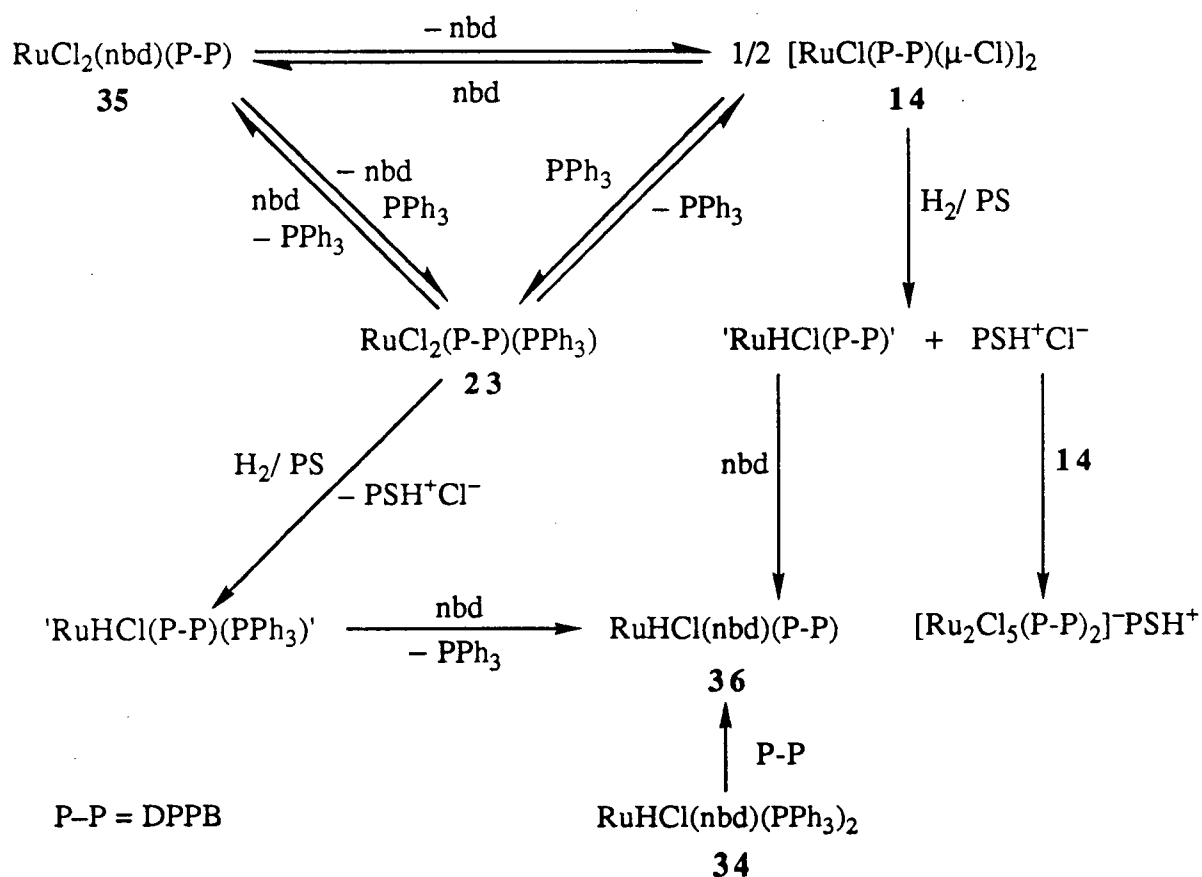
Scheme 6-II

Thorburn has noted the dissociation of coordinated nbd from $RuCl_2(nbd)(DPPB)$, **35**, in solution (see above).[16] Interestingly, the corresponding $RuCl_2(nbd)(PR_3)_2$ complexes (where R = Ph,[20] *p*-tolyl[3]) or $RuHCl(nbd)(PPh_3)_2$, **34**, do not undergo dissociation of the diene,[2, 3] and indeed solution reactivity of **34** probably stems from the loss of PPh_3 (see Section 6.1, and see below). Structural data are not available for the monodentate phosphine systems, but steric factors (e.g. two *cis*–PPh_3 ligands *vs*. DPPB) probably promote PPh_3 dissociation.

Complex **35** had seemed initially to be an appropriate precursor either to (a) the target hydrido(diene) complex $RuHCl(nbd)(DPPB)$, **36**, by treatment with H_2, if necessary by addition of a base to consume liberated HCl,[21] or (b) coordinatively unsaturated hydrides, following hydrogenation of and displacement of the diene as norbornene and/or norbornane. In retrospect , however, the chemistry becomes more complicated because of the loss of diene from **35**. Treatment with H_2 in the presence of Proton Sponge® (PS), in fact, yields mainly the trichloro-bridged species $[Ru_2Cl_5(DPPB)_2]^-PSH^+$ (**A**) and only small amounts of impure **36**. Complex **A** was synthesised previously by reaction of **14** with H_2 in the presence of PS,[16, 18, 19] and this likely provides the pathway for synthesis of **A** from **35** (Scheme 6-II). Some **36** could presumably be formed by direct reaction of H_2 with **35**, or *via* **14** and the intermediate 'RuHCl(DPPB)' shown in Scheme 6-II; the non-reactivity of monodentate phosphine analogues of **35**, $RuCl_2(nbd)(PR_3)_2$, toward H_2 tends to favour the latter suggestion. Indeed, addition of norbornadiene (~1 equiv./Ru) to a C_6D_6 solution of $[RuHCl(DPPB)]_3$ (*cf*. Chapter 5, Section 5.4) resulted in the formation of **36**, as confirmed by NMR spectroscopy.

The reaction of **35** with H_2 (1 atm H_2, 50 °C, DMA solvent) in the presence of PS was monitored using a conventional gas uptake apparatus; the final uptake corresponded to 1.7 mole equivalents H_2 per mole of the complex in about 1.5 h.[16] Formation of **36** by hydrogenation of **35** would require 0.5 H_2/Ru, whereas complete hydrogenation of

coordinated nbd on **35** would utilise 2.0 H_2/Ru. The less than 2.0 (or 2.5) equivalent H_2-uptake probably corresponds to partial formation of **36** and partial hydrogenation of the diene, the ratio being governed by loss of nbd from **35**. The low yield of **36** *via* this '**35** + H_2 route' must result in part from loss of available diene as hydrogenated product. Support for this comes from the attempted catalytic hydrogenation of norbornadiene, using as catalyst **14** (1.0 mM), which readily hydrogenates 1-hexene, styrene and acrylamide (max. rate = 4.9, 3.0 and 1.3 x 10^{-4} M s^{-1}, respectively; [alkene] = 0.40 M, 1 atm H_2, 50 °C, DMA).[16] Under identical conditions, hydrogenation of norbornadiene is much slower (max. rate = 1.4 x 10^{-5} M s^{-1}) and stops after *ca.* 3 h with an uptake corresponding to the reduction of only 2.5% of the available substrate (total turnovers, norbornane/Ru, ~10).[16] The inability to effectively reduce norbornadiene suggests that a catalytically inactive complex is being formed during the reaction with H_2.

The simple displacement of PPh3 from RuHCl(nbd)(PPh3)2, **34**, by the chelating DPPB ligand to yield **36** (Equation 6.4) appears to be general; under similar reaction conditions (see Section 2.5.3), use of Ph2P(CH2)6PPh2 (DPPH) yields the corresponding *trans*–RuHCl(nbd)(DPPH) complex.§ The norbornadiene ligand in **34** must be bound to ruthenium more strongly than PPh3. Alkenes are generally considered to have both a higher *trans* influence (thermodynamic), and *trans* effect (kinetic), compared to PR3 ligands.[22] Displacement by DPPB of the monodentate PPh3 of **34**, rather than the dialkene, is therefore not surprising. In addition, the chelate effects of the bidentate nbd and the incoming DPPB ligands presumably play an important role in the phosphine exchange reaction.

---

§ Spectroscopic data for *trans*-RuHCl(nbd)(DPPH): IR (cm^{-1}), v_{Ru-H} 2016(w); ^1H NMR (CDCl3, 20 °C), δ –10.56 (1H, t, Ru-H, $^2J_{PH}$ = 23 Hz); $^{31}P\{^1H\}$ NMR (CDCl3, 20 °C), 35.7 ppm (s).

Formation of **36** under hydrogenation conditions from RuCl$_2$(DPPB)(PPh$_3$), **23**, and excess nbd (Equation 6.5) almost certainly occurs *via* the intermediate RuHCl(DPPB)(PPh$_3$) as shown in Scheme 6-II. In solution, the bright green species **23** exists in rapid equilibrium with the orange-brown **14** and free phosphine (see Chapters 3 and 4); addition of nbd to **23** in solution leads to formation of **35** in a reversible equilibrium. However, as described in Section 4.3, DMA solutions of **23** in the presence of added PS take up ~0.9 equivalents of H$_2$ per Ru to generate *in situ* a hydride species which is considered to be 'RuHCl(DPPB)(PPh$_3$)'. This is then trapped by nbd by displacement of PPh$_3$ to give **36**. Conversion of **23** to **36** cannot proceed *via* **14** because A is not formed as a co-product (Scheme 6-II). It should be noted also that RuHCl(nbd)(PPh$_3$)$_2$, **34**, is formed similarly from RuHCl(PPh$_3$)$_3$ by displacement of PPh$_3$.[1]

Of note is the relatively high isolated yield (62%), and perhaps close to quantitative conversion (based on yield of PSH$^+$Cl$^-$, see above), of the hydridochloro(diene)-complex, **36**, obtained by the '**23** + H$_2$/PS + nbd' route (Equation 6.5). Although the dichloro analogue **35** is also formed during the course of the reaction (Equation 6.6), only trace amounts (< 5%) of **35** could be sometimes detected at the end of the reaction. Under similar conditions, however, reactions involving PPh$_2$Py or DPPM in place of nbd produced mixtures of the corresponding hydridochloro and dichloro products in *ca.* 1:2 ratio (complexes **26**:**24**+**25** for PPh$_2$Py and **28**:**27** for DPPM, respectively; see Chapter 4, Scheme 4-II); the observed distribution of hydridochloro *vs.* dichloro products was suggested to reflect initial (or more likely, equilibrium) ratios of 'RuHCl(DPPB)(PPh$_3$)' and RuCl$_2$(DPPB)(PPh$_3$) species, reactions of the phosphines with *both* species being rapid and irreversible (see Chapter 4, Section 4.5). As noted earlier, reaction of nbd with RuCl$_2$(DPPB)(PPh$_3$) to produce **35** and free PPh$_3$, however, *is* reversible (^{31}P NMR evidence, see above; Equation 6.6) while that with 'RuHCl(DPPB)(PPh$_3$)' to give **36** is

not. A possible explanation for the almost exclusive formation of **36**, in accordance with Equation 6.5, is presented in Scheme 6-III.

$$RuCl_2(DPPB)(PPh_3) \quad \underset{C_6H_6}{\overset{H_2/\text{Proton Sponge}®}{\rightleftharpoons}} \quad 'RuHCl(DPPB)(PPh_3)' \; + \; HCl$$

23   **B**

+PPh₃ / −nbd   −PPh₃ / +nbd **A**   **C**   −PPh₃ / +nbd

RuCl₂(nbd)(DPPB)   RuHCl(nbd)(DPPB)

35   **36**
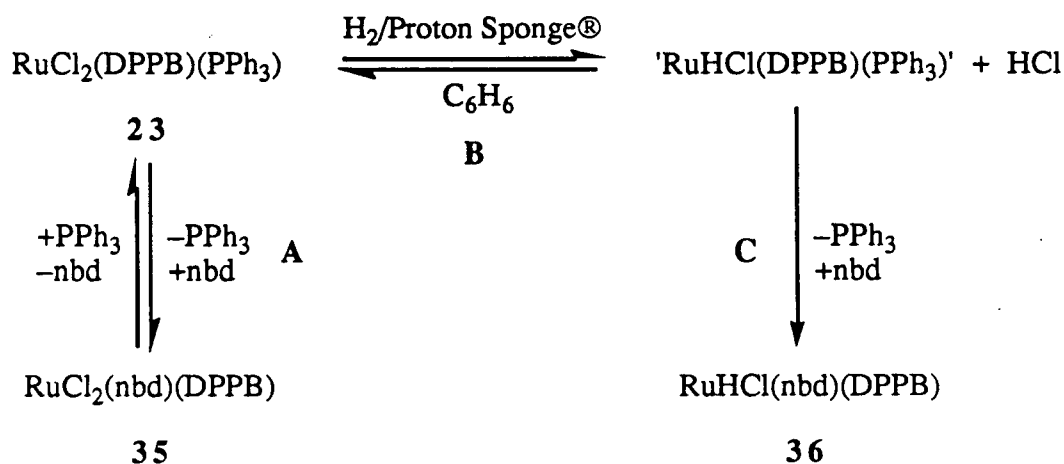
Scheme 6-III

Reaction of nbd with an equilibrium mixture of $RuCl_2(DPPB)(PPh_3)$ and 'RuHCl(DPPB)(PPh_3)' may lead initially to formation of **35** and **36** in the expected proportion (steps A and C, respectively, in Scheme 6-III). However, the reversibility of step A and the irreversible nature of step C together ensure further formation of 'RuHCl(DPPB)(PPh₃)' through a continual shift in equilibrium steps A and B in favour of the five-coordinate hydridochloro complex, which is then trapped irreversibly by the dialkene to give more of the hydrido(diene) complex **36**.

6.4 Reactivity of *Trans*-RuHCl(nbd)(DPPB), **36**, toward H₂ and CO

Benzene or DMA solutions of **36**, in the absence or presence of added PS (or DBU, 1,8-diazabicyclo-[5.4.0]-undec-7-ene), do not react with 1 atm H₂ at 30–50 °C. This is consistent with the formation of **36** as the catalytically inactive species during the ineffective hydrogenation of nbd catalysed by **14** (see above). Although **36** is best synthesised by a procedure carried out under H₂, the failure of **36** to react with H₂ was

251

somewhat surprising in view of the known behaviour of the PPh$_3$ analogue, **34**, which gives cleanly a binuclear η^2-H$_2$ complex[10] and reduction of the bound diene to norbornane (Equation 6.2). Mechanistic details of reaction 6.2 are not known, but ^{1}H and ^{31}P NMR studies carried out by Dekleva[3] showed initial formation of some RuHCl(PPh$_3$)$_3$ (C$_6$D$_6$, δ_{Ru-H} −17.5 ppm, q, $^2J_{PH}$ = 26 Hz)[23] and slower subsequent generation of the η^2-H$_2$ complex and norbornane. Which of **34**, the trisphosphine species, or a necessarily present phosphine-deficient species, effects hydrogenation of the diene is unclear. Perhaps phosphine dissociation is a critical step for reactivity toward H$_2$, and this is not realized with the bidentate DPPB ligand, although (as noted in the Introduction) dissociation to monodentate DPPB[11] is well substantiated.

The hydrido(diene) complex **36** also shows no reaction with 1 atm CO in refluxing benzene or in DMA at 70 °C. Although **36** has the coplanar arrangement of metal, hydride and alkene π-bond required for stereospecific migratory-insertion of the dialkene to form an alkenyl species,[24, 25] the insertion is not promoted by coordination of CO. Such an insertion was however found earlier for the bis(PPh$_3$) analogue **34** under 1 atm CO at 20 °C (Equation 6.1).[2, 3] Again, the inability of DPPB to dissociate in order to provide the required site for CO-binding perhaps leads to the observed unreactivity of this complex; also important, however, will be the enforced *cis* disposition of the two P donors of DPPB in any resulting product. Of note, the PPh$_3$ ligands in the acyl product of Equation 6.1 are mutually *trans*; the disposition of the phosphines in the alkenyl intermediate(s), prior to CO insertion, is not known, but any step requiring the initially dissociated PPh$_3$ to re-associate *trans* to the remaining PPh$_3$ (for steric or electronic reasons) cannot be accommodated with the DPPB ligand.

Of interest, the nature of the diene can also determine whether migratory-insertion occurs. The bis(PPh$_3$) complex *trans*–RuHCl(1,3-cyclohexadiene)(PPh$_3$)$_2$,[7] in contrast to the nbd analogue **34**, reacts with two equivalents of CO to yield, with displacement of the diene, the well-known *cis,cis,trans*–RuHCl(CO)$_2$(PPh$_3$)$_2$ species.[7, 8] The factors

affecting the choice between coordination of CO to (a) promote olefin insertion or (b) replace coordinated diene are probably balanced quite closely. This conclusion is supported by other findings where 'subtle' changes in the incoming nucleophile also determine the reaction pathway. Thus the hydrido(ethylene) complex $[CpRhH(C_2H_4)PMe_3]^+$ gives on reaction with CO the hydrido(carbonyl) species $[CpRhH(CO)PMe_3]^+$ *via* displacement of ethylene, while the insertion reaction to give an ethyl product, $[Rh(C_2H_5)Cp(C_2H_4)PMe_3]^+$, is promoted by addition of C_2H_4 itself.[26] Similarly, within a related hydrido(ethylene) complex of Mo, again CO gives a hydrido(carbonyl) complex while PPh_3 promotes the insertion reaction.[27]

Thus the 'minor' change of replacing two *cis*–PPh_3 ligands by a flexible chelating diphosphine ligand (DPPB) within a precursor complex (*trans*–$RuHCl(nbd)(PPh_3)_2$, **34**) induces for the DPPB-derivative relative non-reactivity toward H_2 and CO.

6.5   References – Chapter 6

1.   Hallman, P. S.; McGarvey, B. R.; Wilkinson, G. *J. Chem. Soc. A*, **1968**, 3143.

2.   Dekleva, T. W.; James, B. R. *J. Chem. Soc., Chem. Commun.* **1983**, 1350.

3.   Dekleva, T. W., Ph.D. Dissertation, The University of British Columbia, Vancouver, Canada, 1983; Chapters 2 and 7.

4.   Tsuji, J. in *Organic Synthesis via Metal Carbonyls*; Wender, I. and Pino, P., Eds.; Wiley-Interscience: New York, 1977; p. 595.

5.   Collman, J. P.; Hegedus, L. S.; Norton, J. R.; Finke, R. G. *Principles and Applications of Organotransition Metal Chemistry*; University Science Books: Mill Valley, CA, 1987; Chapter 5.

6.   (a) Cardaci, G.; Reichenbach, G.; Bellachioma, G.; Wassink, B.; Baird, M. C. *Organometallics*, **1988**, *7*, 2475.
     (b) Webb, S. L.; Giandomenico, C. M.; Halpern, J. *J. Am. Chem. Soc.* **1986**, *108*, 345.
     (c) Nappa, M. J.; Santi, R.; Halpern, J. *Organometallics*, **1985**, *4*, 34.
     (d) Nappa, M. J.; Santi, R.; Diefennbach, S. P.; Halpern, J. *J. Am. Chem. Soc.* **1982**, *104*, 619.

7.   Joshi, A. M., M.Sc. Dissertation, The University of British Columbia, Vancouver, Canada, 1986; Chapters 2 and 3.

8.   Joshi, A. M.; James, B. R. *Organometallics* **1990**, *9*, 199.

9.   Hoff, C. D.; Ungvary, F.; King, R. B.; Marko, L. *J. Am. Chem. Soc.* **1985**, *107*, 666.

10. (a) Dekleva, T. W.; Thorburn, I. S.; James, B. R. *Inorg. Chim. Acta* **1985**, *100*, 49.

    (b) Hampton, C.; Dekleva, T. W.; James, B. R.; Cullen, W. R. *Inorg. Chim. Acta* **1988**, *145*, 165.

11. (a) James, B. R.; Mahajan, D. *J. Organomet. Chem.* **1985**, *279*, 31; *Can. J. Chem.* **1980**, *58*, 996.

    (b) James, B. R.; McMillan, R. S.; Morris, R. H.; Wang, D. K. W. *Adv. Chem. Ser.* **1978**, *167*, 122.

12. Dumont, W.; Poulin, J.-C.; Dang, T.-P.; Kagan, H. B. *J. Am. Chem. Soc.* **1973**, *95*, 8295.

13. Noyori, R. *Science* **1990**, *248*, 1194; *Chem. Soc. Rev.* **1989**, *18*, 187.

14. Mashima, K.; Kusano, K.; Ohta, T.; Noyori, R.; Takaya, H. *J. Chem. Soc., Chem. Commun.* **1989**, 1208.

15. Joshi, A. M.; James, B. R. *J. Chem. Soc., Chem. Commun.* **1989**, 1785.

16. Thorburn, I. S. Ph.D. Dissertation, The University of British Columbia, Vancouver, Canada, 1985; Chapter 5.

17. Dekleva, T. W.; Joshi, A. M.; Thorburn, I. S.; James, B. R.; Evans, S. V.; Trotter, J. *Isr. J. Chem.* **1990**; in press.

18. James, B. R.; Pacheco, A.; Rettig, S. J.; Thorburn, I. S.; Ball, R. C.; Ibers, J. A. *J. Mol. Catal.* **1987**, *41*, 147.

19. Gamage, S. N.; Morris, R. H.; Rettig, S. J.; Thackray, D. C.; Thorburn, I. S.; James, B. R. *J. Chem. Soc., Chem. Commun.* **1987**, 894.

20. Robinson, S. D.; Wilkinson, G. *J. Chem. Soc. A* **1966**, 300.

21. James, B. R. in *Comprehensive Organometallic Chemistry*; Wilkinson, G., Stone, F. G. A. and Abel, E. W., Eds.; Pergamon Press: Oxford, 1982; Vol. 8, p. 295.

22. Appleton, T. G.; Clark, H. C.; Manzer, L. E. *Coord. Chem. Rev.* **1973**, *10*, 335.

23. Hoffman, P. R.; Caulton, K. G. *J. Am. Chem. Soc.* **1975**, *97*, 4221.

24. Crabtree, R. H. *Acc. Chem. Res.* **1979**, *12*, 331.

25. Reference 5, p. 383.

26. Werner, H.; Feser, R. *Angew. Chem. Int. Ed. Engl.* **1979**, *18*, 157.

27. Benfield, F. W. S.; Green, M. L. H. *J. Chem. Soc., Dalton Trans.* **1974**, 1324.

CHAPTER 7

Catalytic Hydrogenation Studies

7.1 Introduction

The di- and trinuclear ruthenium complexes containing a single bidentate phosphine per Ru ([RuCl(P–P)(μ-Cl)]₂ and [RuHCl(P–P)]₃, respectively), described in the previous chapters, were found to catalyse hydrogenation of a range of unsaturated organic substrates, including alkenes, ketones, imines, and nitriles under relatively mild conditions (1–12 atm H₂, 30–100 °C). The hydrogenation reactions proceeded at measurable rates under ~1 atm of H₂ pressure, thus making the kinetics and mechanisms of these hydrogenation systems amenable to detailed studies. Such studies were undertaken toward the end of this work, and some results are presented in this chapter.

7.2 Hydrogenation of Styrene Catalysed by [RuCl(DPPB)(μ-Cl)]₂, 14

The kinetics of H₂-hydrogenation reactions catalysed by [RuCl(DPPB)(μ-Cl)]₂, 14, and its analogues containing other diphosphine ligands (e.g. CHIRAPHOS, 16) are of interest because of the dimeric nature of the catalyst precursor and the possible involvement of the η²-H₂ species, 31a (see Chapter 5, Section 5.3), in the catalytic cycle. The results of a kinetic investigation into the hydrogenation of styrene to ethylbenzene catalysed by 14 are presented here.

DMA solutions of styrene rapidly absorbed hydrogen (30 °C, 1 atm of H₂) in the presence of catalytic amounts of [RuCl(DPPB)(μ-Cl)]₂, 14. The presence of ethylbenzene as the hydrogenation product was confirmed by examination of the final H₂-uptake solution

by ^{1}H NMR spectroscopy (δ 1.03, t, PhCH$_2$CH_3; 2.04, q, PhCH_2CH$_3$). Resonances due to styrene protons (7.3–5.0 ppm region) had disappeared indicating that the reduction was essentially complete. The catalyst precursor **14**, which remains dimeric in DMA solution (see Chapter 3, Section 3.7.1), was recovered intact at the end of the catalytic run as evidenced by the ^{31}P{^{1}H} NMR spectrum of the red-brown residue (obtained by pumping off the DMA and ethylbenzene under vacuum at 50 °C) in C$_6$D$_6$ (AB q: δ_A = 64, δ_B = 54.9 ppm ,$^2J_{AB}$ = 47 Hz; see Chapter 3, Table 3.3). The ^{31}P NMR spectrum of **14** in C$_6$D$_6$ in the presence of ~50-fold excess of styrene was essentially unchanged, except for a slight broadening of the resonances from initial linewidths of ~7 Hz observed in the absence of styrene to ~11 Hz.

7.2.1 Solubility of Hydrogen in DMA

The solubility of hydrogen in DMA has been determined previously in our laboratory, at a range of temperatures (15–80 °C) and at various H$_2$-pressures (100–800 Torr),[1-6] employing a constant pressure gas-uptake apparatus and by a procedure described elsewhere.[6] The H$_2$-solubility in DMA obeys Henry's law at least up to one atmosphere pressure of hydrogen over the temperature range studied, the plots of molar solubility against partial pressure of H$_2$ being linear. The solubility data at various temperatures, expressed as Henry's law constants K$_H$ derived from the slope of such straight-line plots (K$_H$ = [H$_2$]/P(H$_2$) M Torr^{-1}), are listed in Table 7.1.

The constant K$_H$ essentially represents an equilibrium constant for the dissolution of H$_2$: H$_2$(gas) $\rightleftharpoons$ H$_2$(solution). The van't Hoff plot for the temperature dependence of H$_2$-solubility in DMA is linear (Figure 7.1). The values of –655 K and –10.8 for the slope and the Y-intercept, respectively, obtained from this ln K$_H$ vs. 1/temperature plot, can be used to calculate the H$_2$-solubility in DMA at any temperature at least within the 15–80 °C range.

Table 7.1: Solubility[a] of H_2 in N,N-Dimethylacetamide.

Temperature, K (°C)	$K_H \times 10^6$, M Torr^{-1}	Reference
288.2 (15.0)	2.11 (±0.02)	1
298.2 (25.0)	2.24	2
303.2 (30.0)	2.32	3
308.2 (35.0)	2.37	1
308.2 (35.0)	2.38	4
323.2 (50.0)	2.70	5
333.2 (60.0)	2.82	5
333.2 (60.0)	2.83	1
338.2 (65.0)	2.86	6
353.2 (80.0)	3.20	4

[a] Expressed as Henry's law constant K_H, where $K_H = [H_2]/P(H_2)$.

$$y = -10.81 - 655.1x \quad R^2 = 0.992$$
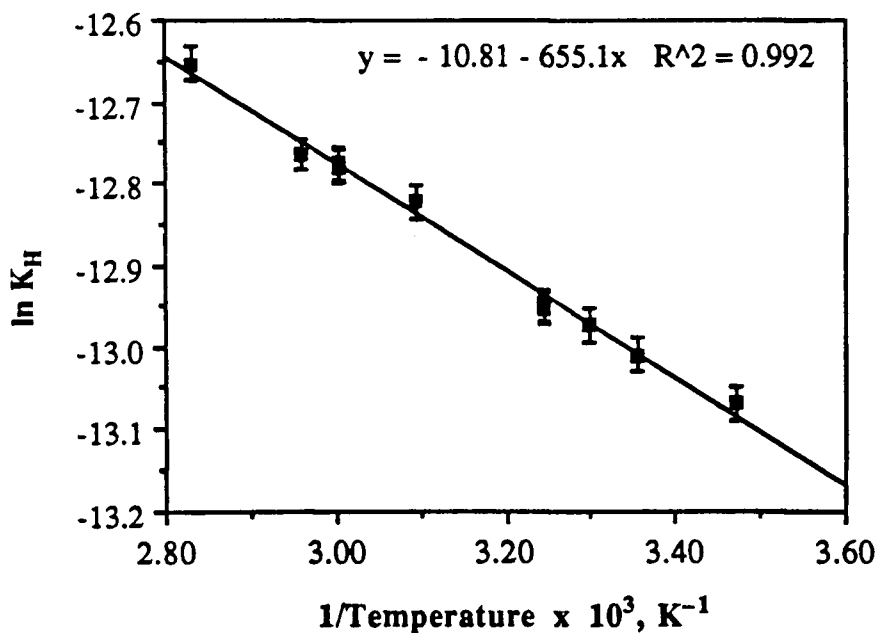
Figure 7.1: The van't Hoff plot for the temperature dependence of H_2-solubility in DMA.

7.2.2 Rate Measurements

The hydrogenation of styrene was monitored using a constant pressure gas-uptake apparatus.[6] A typical plot of H_2-uptake against time in DMA for the hydrogenation of styrene is shown in Figure 7.2. The uptake-plots were *S*-shaped, and showed an induction period of ~100–200 s. Maximum linear rates were attained in the initial 10–20% H_2-uptake region.

The H_2-uptakes were measured at total ruthenium (monomer) concentrations, $[Ru]_T$, ranging from 1.0×10^{-3} to 3.1×10^{-3} M, at different H_2-pressures (410–785 Torr), and at various substrate concentrations ($[styrene] = 0.010$–42 M), changing only one parameter at a time. *N,N*-Dimethylacetamide (DMA) was chosen as the solvent because of its convenient low vapour pressure (<5 Torr at 30 °C).[7]
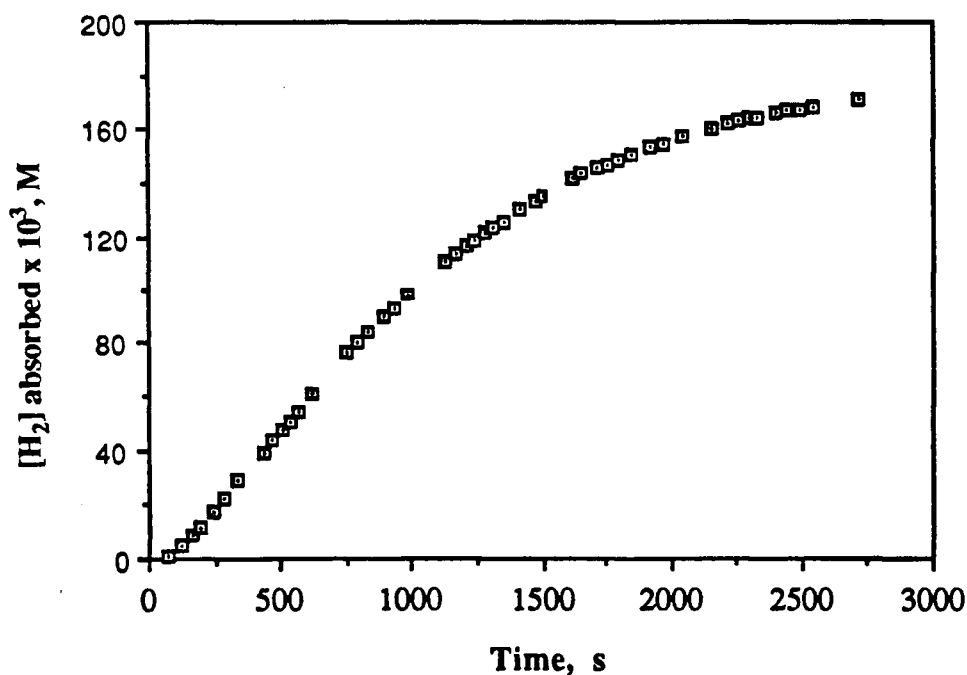
Figure 7.2: A typical H_2-uptake plot for the hydrogenation of styrene catalysed by $[RuCl(DPPB)(\mu\text{-}Cl)]_2$, **14**, in DMA at 30 °C and 785 Torr pressure of H_2. [Styrene] = 0.18 M, $[Ru]_T = 1.58 \times 10^{-3}$ M, $[H_2] = 1.82 \times 10^{-3}$ M.

The dependence of the maximum rates on the total ruthenium monomer concentration $[Ru]_T$, initial substrate concentration [styrene], and hydrogen concentration $[H_2]$ were investigated at 30 °C. The rate data for hydrogenation of styrene in DMA at 30 °C are summarised in Table 7.2.

The ruthenium dependence of hydrogenation rates was studied at the initial substrate concentration [styrene] = 0.415 M, under 785 Torr of H_2 pressure ($[H_2]$ = 1.82 $\times 10^{-3}$ M), for total ruthenium monomer concentrations $[Ru]_T$ ranging between 1.0–3.1 $\times 10^{-3}$ M. The individual rate plots are shown in Figure 7.3. The plot of the maximum rate against $[Ru]_T$ is shown in Figure 7.4 and is linear, implying a first-order dependence on $[Ru]_T$ for the hydrogenation rate.

The dependence of the maximum hydrogenation rate on the initial substrate concentration was studied at 30 °C, for [styrene] = 0.009–0.415 M, at $[Ru]_T$ = 1.58 $\times 10^{-3}$ M, under 785 Torr of H_2 pressure. The plot of maximum rate vs. [styrene] is shown in Figure 7.5. The rate of hydrogenation was found to increase on increasing the substrate concentration, but levelled off at higher substrate concentrations (≥ 0.2 M). The increase in rates was close to linear at lower styrene concentrations (< 0.05 M), indicating a first-order dependence, while a transition from first- to zero-order dependence was apparent at the higher styrene concentrations.

The effect of varying the H_2 pressure was studied at $[Ru]_T$ = 1.58 $\times 10^{-3}$ M and at [styrene] = 0.043 M (Figure 7.6). A less than first-order dependence on H_2 pressure (i.e. $[H_2]$ concentration) was observed from 785 to 410 Torr ($[H_2]$ = 1.82–0.95 $\times 10^{-3}$ M).

Table 7.2: Kinetic Data for Hydrogenation of Styrene Catalysed by [RuCl(DPPB)(μ-Cl)]$_2$ in DMA at 30 °C.

[Ru]$_T$ x 10^3 M	[styrene] x 10^2 M	P(H$_2$) Torr	[H$_2$] x 10^3 M	Max. Rate[a] x 10^5 M s^{-1}
3.04	41.5	785	1.82	20.5
2.05	41.5	785	1.82	12.7
1.58	41.5	785	1.82	11.1
1.01	41.5	785	1.82	6.57
1.58	18.0	785	1.82	10.6
1.58	4.30	785	1.82	4.84
1.58	3.70	785	1.82	4.00
1.58	2.40	785	1.82	3.10
1.58	1.80	785	1.82	2.53
1.58	1.80	785	1.82	2.49
1.58	0.90	785	1.82	1.39
1.58	4.30	685	1.59	4.11
1.58	4.30	590	1.37	3.93
1.58	4.30	500	1.16	3.57
1.58	4.30	410	0.95	3.13

[a] Error in rate values is estimated at *ca.* ±5%.
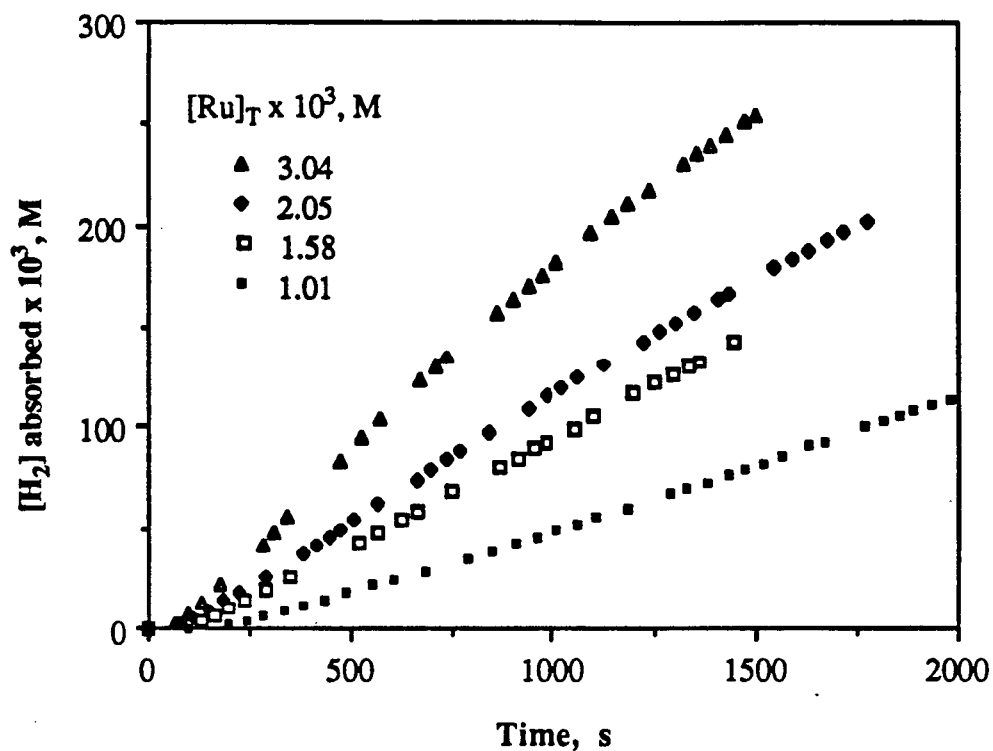
Figure 7.3: Rate plots for styrene hydrogenation catalysed by **14** in DMA, at 30 °C, at various $[Ru]_T$. [styrene] = 0.415 M, $[H_2]$ = 1.82 x 10^{-3} M.
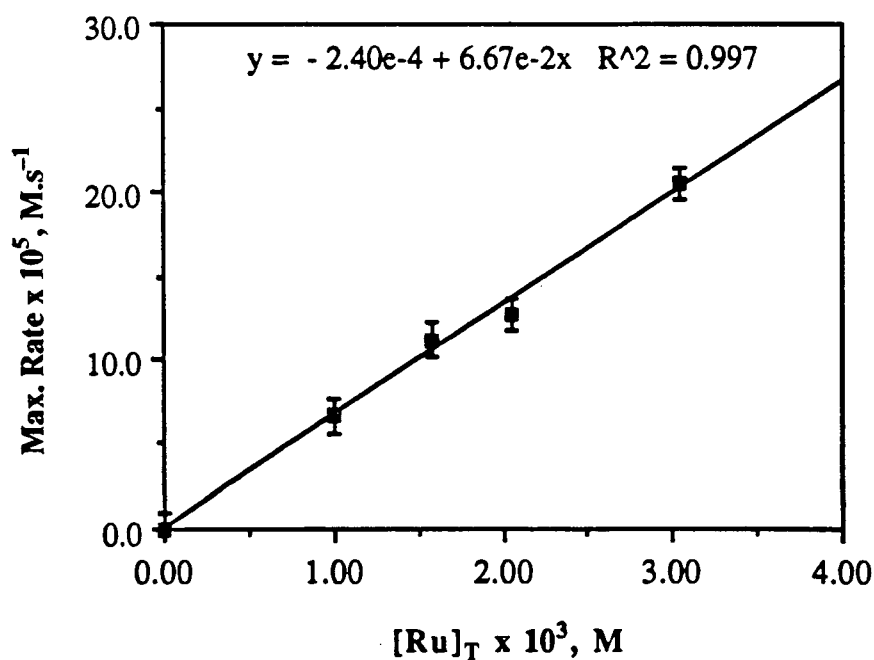
Figure 7.4: Dependence of the maximum hydrogenation rate on $[Ru]_T$ at 30 °C.
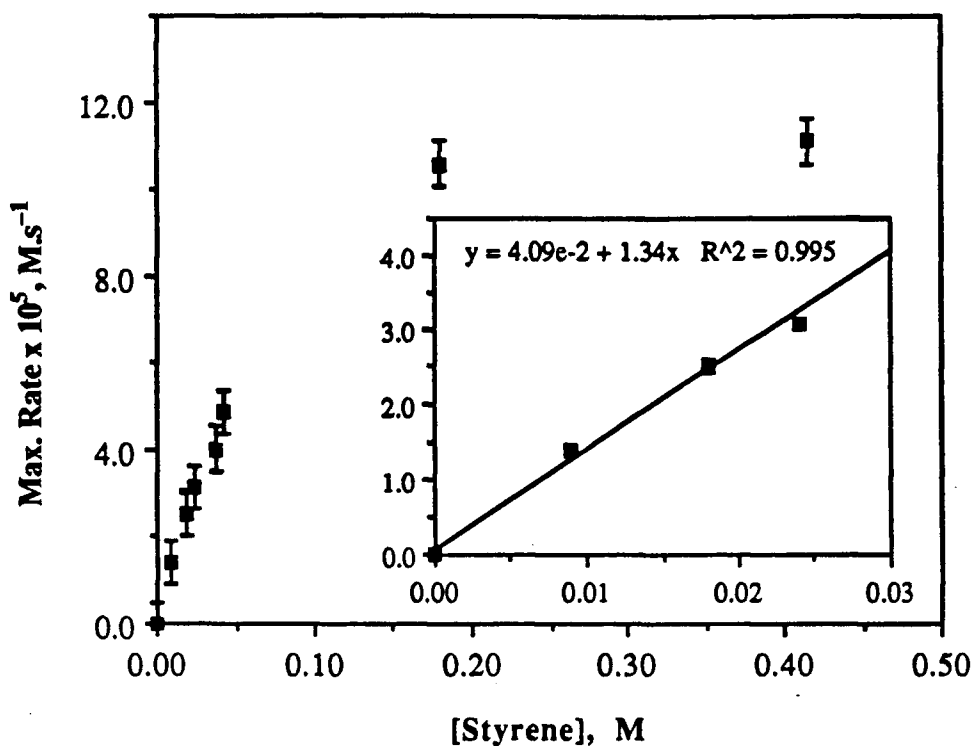
Figure 7.5: Dependence of the maximum hydrogenation rate on [styrene] at 30 °C.
$[Ru]_T = 1.58 \times 10^{-3}$ M, $P(H_2) = 785$ Torr ($[H_2] = 1.82 \times 10^{-3}$ M). The INSET
shows the initial portion of the rate plot expanded.
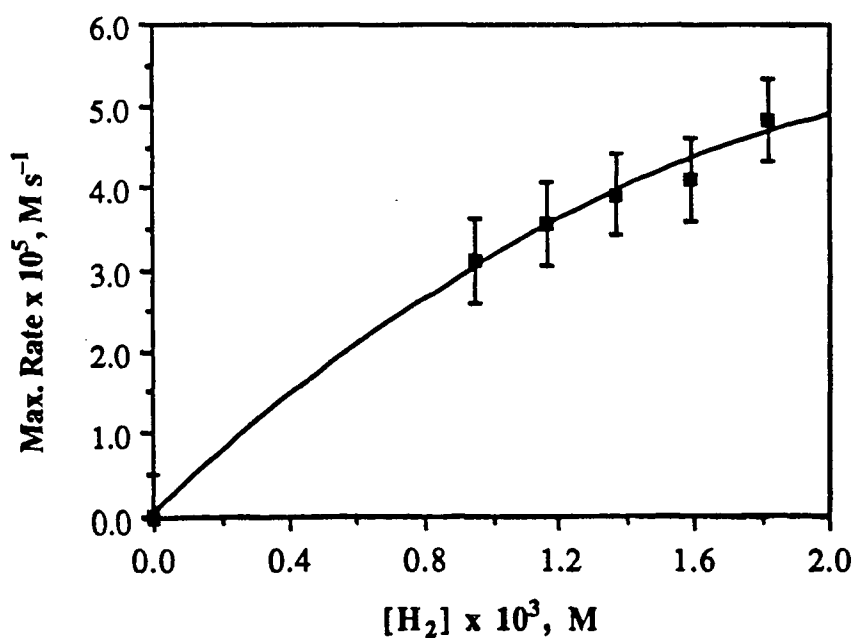
Figure 7.6: Dependence of the maximum hydrogenation rate on [H₂] at 30 °C.
$[Ru]_T = 1.58 \times 10^{-3}$ M, [styrene] = 0.043 M.

264

7.2.3 Analysis of the Kinetic Data and Discussion

The 100–200 s induction period observed during hydrogenation of styrene catalysed by [RuCl(DPPB)(μ-Cl)]$_2$, **14**, as monitored by H$_2$-uptake measurements, is attributed to the time taken for the catalyst (precursor) to dissolve in DMA. The complex **14** remained unchanged at the end of the catalytic runs. Attempts at detecting the possible catalytic intermediate(s) by examination of the hydrogenating solution using ^{31}P NMR spectroscopy were unsuccessful because of the relatively high hydrogenation activity of **14** (typical turnover frequencies ~8–10 min^{-1} M^{-1} of **14**) as the dissolved H$_2$ was quickly depleted. However, as noted in Section 5.3, **14** forms the trichloro-bridged dihydrogen complex [(L)(DPPB)Ru(μ-Cl)$_3$RuCl(DPPB)], **31a** (L = η^2-H$_2$), under H$_2$ atmosphere in benzene,[8] while the DMA analogue (L = DMA), **14h**, is obtained in DMA solution in the absence of H$_2$ (Chapter 3, Section 3.6.5). Furthermore, DMA solutions of **14** absorb a small amount of H$_2$ even in the absence of an alkene substrate, with the final uptake corresponding to ~0.4 mole equivalents per dimer at 30 °C under 785 Torr of H$_2$ pressure (Section 5.3.2). These observations suggest that the binding of H$_2$ to Ru is considerably stronger than that of DMA, which is present in large excess. Therefore, the formation of some of the dihydrogen complex **31a** under the catalytic hydrogenation conditions seems plausible. The slight broadening (~3–4 Hz) of the ^{31}P resonances of **14** in the presence of a ~50-fold excess of added styrene suggests a relatively weak interaction between the catalyst precursor and the substrate.

To explain the first-order dependence on [Ru]$_T$, the first- to zero-order dependence on [styrene], and the less than first-order dependence on H$_2$ pressure, the following mechanism is suggested:

$$[RuCl(DPPB)(\mu\text{-}Cl)]_2 + H_2 \underset{k_{-1}}{\overset{k_1}{\rightleftharpoons}} [(\eta^2\text{-}H_2)(DPPB)Ru(\mu\text{-}Cl)_3RuCl(DPPB)] \quad (7.1)$$

<div style="text-align:center">(K₁)</div>

$$\mathbf{14} \qquad\qquad\qquad\qquad\qquad \mathbf{31a}$$

$$[(\eta^2\text{-}H_2)(DPPB)Ru(\mu\text{-}Cl)_3RuCl(DPPB)] \xrightarrow{k_2} [RuCl(DPPB)(\mu\text{-}Cl)]_2 \quad (7.2)$$

$$+ \qquad\qquad\qquad\qquad +$$

$$C_6H_5CH\!=\!CH_2 \qquad\qquad\qquad C_6H_5CH_2CH_3$$
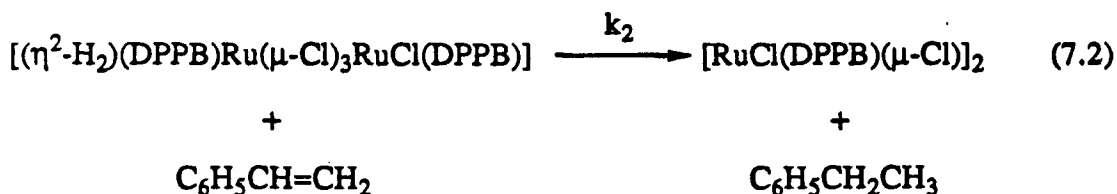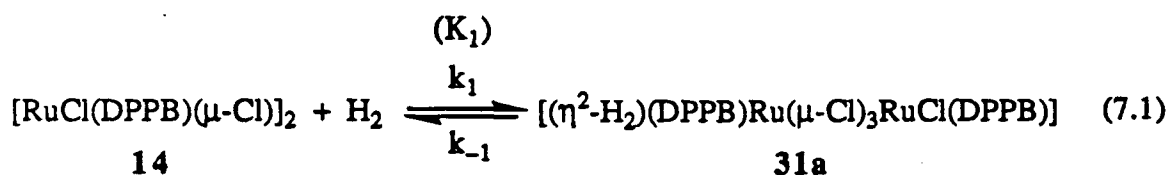
where k_1, k_{-1}, and k_2 are the rate constants of the individual steps, and K_1 represents the equilibrium constant for reaction 7.1.

Applying the steady-state treatment to the intermediate, $[(\eta^2\text{-}H_2)(DPPB)Ru\text{-}(\mu\text{-}Cl)_3RuCl(DPPB)]$, **31a**, the following rate law is obtained:

$$\text{Rate} = -\frac{d[H_2]}{dt} = \frac{k_1 k_2 [Ru_2]_T \cdot [\text{styrene}] \cdot [H_2]}{k_{-1} + k_1[H_2] + k_2[\text{styrene}]} \qquad (7.3)$$

where

$$[Ru_2]_T = [\mathbf{14}] + [\mathbf{31a}] = 1/2\,[Ru]_T \qquad (7.4)$$

7.2.3.1 Dependence of the Rate on Catalyst Concentration

At constant $[H_2]$ and constant [styrene], the rate equation 7.3 reduces to:

$$\text{Rate} = k_{obs}[Ru]_T$$

where

$$k_{obs} = \frac{1/2\,k_1 k_2 [\text{styrene}] \cdot [H_2]}{k_{-1} + k_1[H_2] + k_2[\text{styrene}]} \qquad (7.5)$$

The first-order dependence of the maximum rate on $[Ru]_T$, as predicted by Equation 7.5, is evident from the straight-line plot shown in Figure 7.4. A value of $6.7 \times 10^{-2}\ s^{-1}$ is obtained from the slope of the plot of maximum rate vs. $[Ru]_T$. The plot of maximum rate vs. $[Ru_2]_T$ (not shown; $[Ru_2]_T$ = concentration in terms of the dimer) is linear as expected

with the corresponding doubling of the k_{obs} value to 0.13 s^{-1}. Thus, these kinetic data do not distinguish between a monomeric and a dimeric catalyst species.

7.2.3.2 Dependence of the Rate on Styrene Concentration

At sufficiently lower styrene concentrations, the k_2[styrene] term in the denominator of Equation 7.3 could become negligible compared to $(k_{-1} + k_1[H_2])$ term, the rate equation then approximates to Equation 7.6, and a first-order dependence on [styrene] is expected. Such is indeed the case at [styrene] < 0.025 M, and the plot of maximum rate against [styrene] is linear (see Figure 7.5, INSET).

$$\text{Rate} = \frac{1/2\ k_1 k_2 [\text{styrene}] \cdot [\text{Ru}]_T}{k_{-1} + k_1[H_2]} \qquad (7.6)$$

On the contrary, at higher styrene concentrations the k_2[styrene] term in the denominator of Equation 7.4 may become predominant, and the rate equation (Equation 7.4) is expected to approximate to:

$$\text{Rate} = 1/2\ k_1 [\text{Ru}]_T \cdot [H_2] \qquad (7.7)$$

which is independent of styrene concentration. Whether the k_2[styrene] >> $(k_{-1} + k_1[H_2])$ condition is fulfilled at the maximum styrene concentration of 0.415 used in this study is not clear.

Further, the rate equation 7.4 can be rearranged to give:

$$\frac{1}{\text{Rate}} = \frac{k_{-1} + k_1[H_2]}{1/2\ k_1 k_2 [\text{Ru}]_T \cdot [H_2]} \times \frac{1}{[\text{styrene}]} + \frac{1}{1/2\ k_1 [\text{Ru}]_T \cdot [H_2]} \qquad (7.8)$$

267

At constant $[Ru]_T$ and $[H_2]$, therefore, the plot of 1/rate vs. 1/[styrene] should be a straight line, and the rate constant k_1 can then be calculated from the intercept. Such a plot (Figure 7.7) gives a straight line with slope = 583 s and intercept = 7521 s M^{-1}, and the k_1 value of 93 M^{-1} s^{-1} is obtained from the intercept for conditions when $[Ru]_T = 1.58 \times 10^{-3}$ M and $[H_2] = 1.82 \times 10^{-3}$ M, at 30 °C.
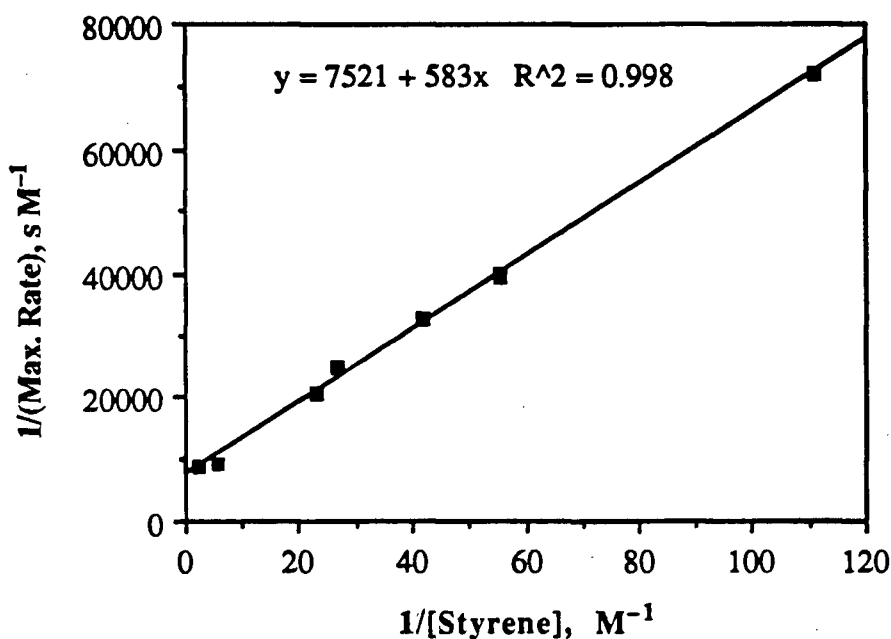
Figure 7.7: Plot of 1/(Maximum Rate) against 1/[Styrene]. $[Ru]_T = 1.58 \times 10^{-3}$ M, $[H_2] = 1.82 \times 10^{-3}$ M, at 30 °C.

7.2.3.3 Dependence of the Maximum Rate on Hydrogen Concentration

At high alkene concentrations where the rate equation 7.3 reduces to Equation 7.7 because k_2[styrene] >> $(k_{-1} + k_1[H_2])$, i.e. under conditions when the [styrene] dependence of the maximum rate is of zero-order, the H_2 dependence is expected to be first-order over the entire range of hydrogen concentrations. At lower alkene concentrations, however, a transition from first- to zero-order dependence is expected in accordance with Equation 7.6.

268

In this study, the $[H_2]$ dependence of the maximum rate was investigated at [styrene] = 0.043 M, which is not high enough to show a strictly first-order dependence, and a less than first-order dependence is observed (Figure 7.6); also, it can be shown that a plot of log(Maximum Rate) vs. log($[H_2]$) yields n = 0.67, where n is the order of the reaction in $[H_2]$. However, Equation 7.3 can be reorganised to give:

$$\frac{1}{\text{Rate}} = \frac{k_{-1} + k_2[\text{styrene}]}{1/2 \ k_1 k_2 [\text{Ru}]_T [\text{styrene}]} \times \frac{1}{[H_2]} + \frac{1}{1/2 \ k_2 [\text{Ru}]_T [\text{styrene}]} \quad (7.9)$$

The plot of 1/Rate vs. $1/[H_2]$ should be linear, and value of the rate constant k_2 can be calculated from the intercept. In fact, such a graph (Figure 7.8) yields a good straight-line, with slope = 20.9 s and an intercept of 10130 s M^{-1}, from which a k_2 value of 2.9 M^{-1} s^{-1} is obtained for $[\text{Ru}]_T = 1.58 \times 10^{-3}$ M and [styrene] = 0.043 M, at 30 °C.
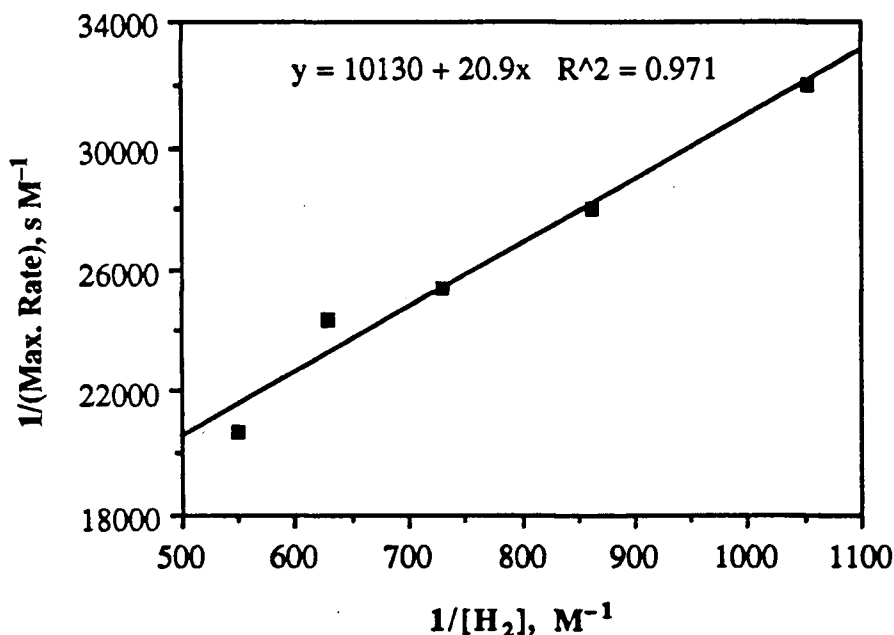
Figure 7.8: Plot of 1/(Maximum Rate) against $1/[H_2]$. $[\text{Ru}]_T = 1.58 \times 10^{-3}$ M, [styrene] = 0.043 M at 30 °C.

These values of k_1 (93 M^{-1} s^{-1}) and k_2 (2.9 M^{-1} s^{-1}) can be used to derive the value of k_{-1} (see Equations 7.1 and 7.2) from the slope of one of the lines plotted

according to Equations 7.8 or 7.9. Thus, values of 0.056 s^{-1} and 0.066 s^{-1} for k_{-1}, at 30 °C, are calculated from the slope of the lines shown in Figures 7.8 and 7.9, respectively, for the conditions specified earlier. This yields a value of 1.5 x 10^3 ± 150 M^{-1} for the equilibrium constant $K_1 = k_1/k_{-1}$, at 30 °C (see Equation 7.1), and a value of 48 ± 5 M^{-1} for the relative magnitudes of k_2 and k_{-1} (*i.e.* k_2/k_{-1}). Further, the equilibrium constant K_1 for the formation of the dihydrogen complex **31a** can be obtained directly from H_2-uptake measurements on the dimeric precursor **14** in the absence of styrene substrate. The observed H_2-uptake of *ca.* 0.4 mole equivalent per dimer (**14**) in DMA solution at 785 torr of H_2 pressure and 30 °C, from which a K_1 value of 3.7-x-10^2 M^{-1} is calculated, does not take into account any uptake by **14** in the solid state, and the K_1 value is likely an underestimate. Therefore, the K_1 values of 3.7 x 10^2 and 1.5 x 10^3 M^{-1} obtained respectively from the direct H_2-uptake measurements and by analysis of the rate data for styrene hydrogenation, although a factor of four different, can be considered in acceptable agreement.

The k_{-1} values of 0.056 and 0.066 s^{-1} obtained from the [styrene]- and the [H_2]-dependences, respectively, of the maximum rate of styrene hydrogenation catalysed by the dimeric [RuCl(DPPB)(μ-Cl)]$_2$ complex, **14**, are in reasonable agreement and show that the data are internally consistent.

The values of the rate constants k_1, k_{-1}, k_2, and the equilibrium constant K_1 (*cf.* Equations 7.1 and 7.2) are comparable to the corresponding values obtained in an earlier study from this laboratory on a similar hydrogenation system.[3, 9] Hydrogenation of 1-hexene catalysed by the dinuclear Ru-(PPh$_3$) complex [(η^2-H$_2$)(PPh$_3$)$_2$Ru(μ-H)-(μ-Cl)$_2$RuH(PPh$_3$)$_2$], containing a dihydrogen ligand (analogous to **31a** in the current study), has been suggested to proceed via a mechanism similar to that outlined in Equations 7.1 and 7.2.[9] The values of k_1 = 156 M^{-1} s^{-1}, k_{-1} = 0.028 s^{-1}, k_2 = 0.57 M^{-1} s^{-1}, and K_1 = 5.6 x 10^3 M^{-1} at 30 °C have been calculated.[9]

It should be noted that the rate data for the hydrogenation of styrene catalysed by **14** may well be analysed for a reaction sequence in which formation of a catalyst-substrate adduct ([(styrene)Ru_2]) precedes the hydrogen transfer step (*cf.* Equations 7.1 and 7.2). The steady-state approximation is then applied to the intermediate [(styrene)Ru_2] (instead of the dihydrogen complex **31a**), with the equilibrium constant K_1 and the rate constants k_1 and k_{-1} now refering to the formation of the [(styrene)Ru_2] adduct. The relatively large K_1-value of ~1500 M^{-1} is consistent with the experimental observation (and characterisation, see Chapter 5) of the η^2-H_2 complex **31a**, whereas there is no detectable formation of the corresponding styrene adduct, [(styrene)Ru_2].

Intermediate(s) similar to the ones suggested for the **14**-catalysed H_2/D_2 exchange reaction to give HD (see Section 5.3.1, Scheme 5-I), but with one of the dihydrogen molecules replaced by a π-bonded alkene, may be involved in the alkene hydrogenation (k_2-step, Equation 7.2).

7.3 Hydrogenation of Ketones and Imines Catalysed by [RuCl(P–P)(μ-Cl)]$_2$ and [RuHCl(P–P)]$_3$ Complexes

Various aspects of catalytic homogeneous hydrogenation of unsaturated organic substrates have been discussed previously in Chapter 1. The dinuclear dichloro-, and the trinuclear hydridochloro ruthenium complexes were found to catalyse hydrogenation of a variety of unsaturated substrates including ketones, imines and nitriles, as well as alkenes (Section 7.2).[8, 10–12] A short summary of the preliminary results from these studies is presented below.

7.3.1 Transfer Hydrogenation of Acetophenone

The dinuclear ruthenium complexes [RuCl(P–P)(μ-Cl)]$_2$, P–P = DPPB, **14** or

S,S-CHIRAPHOS, **16**, are extremely effective catalyst precursors for transfer

hydrogenation of ketone substrates using 2-propanol/KOH as the source of hydrogen

(Equation 7.10).

$$C_6H_5\!-\!\overset{O}{\overset{\|}{C}}\!-\!CH_3 + CH_3\!-\!\overset{OH}{\overset{|}{C(H)}}\!-\!CH_3 \underset{\overrightarrow{}}{\overset{Ru_2/KOH}{\rightleftharpoons}} C_6H_5\!-\!\overset{OH}{\overset{|}{C(H)}}\!-\!CH_3 + CH_3\!-\!\overset{O}{\overset{\|}{C}}\!-\!CH_3 \quad (7.10)$$

$$Ru_2 = [RuCl(P\!-\!P)(\mu\text{-}Cl)]_2;\ \ P\!-\!P = DPPB,\ \mathbf{14}\ \text{or}\ S,S\text{-CHIRAPHOS},\ \mathbf{16}$$
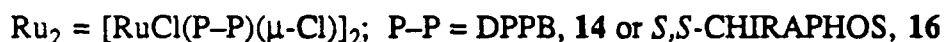
All reactions were carried out in thick-walled glass bombs under an argon

atmosphere. Typically, acetophenone followed by 2-propanol were added to the solid

catalyst and KOH mixture under a flow of argon. The system was then closed and the

mixture heated in a constant temperature oil-bath maintained at the specified temperature

(± 1 °C). The products were separated from the catalyst residue by distillation, and

analysed by GC to determine the % conversion and the enantiomeric excess where

appropriate (see Chapter 2, Sections 2.3 and 2.4 for details). The results are summarised

in Table 7.3.

The initially orange suspension turned dark red within a couple of minutes in the

heating bath. Turnover frequencies of > 500 h^{-1} [Ru$_2$]$_T$$^{-1}$ at equilibrium conversions (*ca.*

80% under typical conditions, see Table 7.3) are realised for transfer hydrogenation of

acetophenone to 1-phenylethanol in refluxing 2-propanol (boiling point: 83 °C); however,

the CHIRAPHOS system gives only 2% e.e. Of interest, **14** and **16** catalyse, albeit

slowly, the hydrogen transfer from 2-propanol to acetophenone even in the absence of the

KOH base (see for example, Run # 7 in Table 7.3). In the absence of the Ru catalyst,

KOH alone is also capable of catalysing the transfer hydrogenation of acetophenone at a

much slower rate compared to the Ru catalysed reaction (Table 7.3, Run # 5, 6), which is consistent with some earlier reports.[13] The KOH-catalysed hydrogen transfer to acetophenone probably contributes in part to the observed low e.e. for the CHIRAPHOS system.

Table 7.3: Data for Transfer Hydrogenation of Acetophenone in 2-Propanol/KOH
Catalysed by [RuCl(P–P)(μ-Cl)]$_2$ Complexes.[a, b]

Run #[c]	Time, h	% Conversion[d]	Comments
1.	48	81	
2.	4	82	Acetone detected in the distillate by GC.
3.	1	82	Turnover Frequency ≥ 520 h^{-1}[Ru$_2$]$^{-1}$.
4.	46	82	P–P = S,S-CHIRAPHOS; e.e.= 0.4% (R).
5.	48	31	Blank run with KOH; no Ru$_2$ catalyst added.
6.	7.5	7	Blank run with KOH; no Ru$_2$ catalyst added.
7.	48	6	No KOH; Ru$_2$ catalyst present.
8.	4	77	At 50 °C.
9.	1.5	78	At 50 °C; P–P = S,S-CHIRAPHOS; e.e.= 2% (R).
10.	48	17[e]	At 50 °C; reverse reaction (cf. Equation 7.10).[e]

[a] General conditions:

  5.0 mL 2-propanol   [acetophenone] = 1.43 M   [Ru$_2$] = 2.25 x 10^{-3} M
  [KOH]/[Ru$_2$] = 4   [acetophenone]/[Ru$_2$] = 630.

[b] P–P = DPPB, unless stated otherwise.

[c] Run # 1–7 were carried out at 100 °C (bath temperature; refluxing solution).

[d] Conversion to 1-phenylethanol.

[e] Using 1.43 M 1-phenylethanol in 5.0 mL acetone; the conversion refers to % acetophenone.

The *ca.* 82% conversions seen in Runs # 1–4 represent the equilibrium yields under the specified conditions. The reversibility of the transfer hydrogenation reaction (see Equation 7.10) and catalysis of the reverse reaction by the Ru catalyst are clearly demonstrated by the result of Run # 10 in which acetophenone is formed by transfer hydrogenation of acetone from 1-phenylethanol.

The ^{1}H NMR spectrum (hydride region) of the dark red residue recovered at the end of a typical run, with the CHIRAPHOS complex **16** as the catalyst precursor, is shown in Figure 7.9. The three resonances of equal intensity, and centred at δ –17.0 (dd, $^2J_{PH}$ = 36.6, 26.4 Hz), –19.4 (m, $^2J_{PH}$ ~8–21 Hz) and –24.8 ppm (dd, $^2J_{PH}$ = 36.3, 31.8 Hz) are readily assigned to the trinuclear hydridochloro species [RuHCl(CHIRAPHOS)]$_3$, **30**, described earlier (see Chapter 5, Sections 5.4 and 5.5). The remaining hydride resonance at –12.6 ppm, belonging to an as yet unidentified complex and constituting ~33% of the total intensity, also exhibits a doublet of doublet pattern with $^2J_{PH}$ = 37.2 and 25.2 Hz. The magnitudes of the coupling constants indicate a mutually *cis* arrangement of the hydride and two inequivalent phosphorus nuclei in the new hydride species.

Figure 7.9: ^{1}H NMR spectrum (hydride region, 300 MHz, 20 °C, toluene-d_8) of the residue obtained from transfer hydrogenation of acetophenone using the CHIRAPHOS system (Run # 4, Table 7.3).

The chemical shift of -12.6 ppm for the hydride is in the region found for other known *trans*–hydridochloro-Ru(II) species.[1, 14] A mononuclear species of the type "*trans*-RuHCl(CHIRAPHOS)(L)$_2$", with ketone or alcohol molecules (L) from the transfer hydrogenation system occupying the available coordination sites, seems plausible. Alternatively, the -12.6 ppm resonance could belong to a dinuclear complex containing only a single hydride ligand: [(P–P)HRu(μ-Cl)$_2$RuCl(P–P)] (*cf.* Intermediate I in Scheme 5-III, Section 5.7), or a related trichloro-bridged complex with a coordinated ketone or alcohol (L): [(P–P)HRu(μ-Cl)$_3$Ru(L)(P–P)] (*cf.* Figures 3.16, 3.17 in Section 3.7.1).

The ^{31}P NMR spectrum of the same residue consists of an AB quartet pattern centred at 84.0 ppm (Δv_{AB} = 0.5 ppm, $^2J_{PP}$ = 34.0 Hz, ~27% integral intensity) along with the signals assignable to the CHIRAPHOS trimer **30** (73% integral intensity; see Section 5.5 for chemical shifts). The new 84.0 ppm resonance is assigned to the species which exhibits the high-field ^{1}H NMR resonance at -12.6 ppm (see above). The observed integral intensity ratios for the new hydride species with respect to the resonances of [RuHCl(CHIRAPHOS)]$_3$ support the mononuclear "*trans*–RuHCl(CHIRAPHOS)(L)$_2$" formulation. Moreover, two sets of ^{31}P NMR AB quartet patterns will be expected for a "[(P–P)HRu(μ-Cl)$_3$Ru(L)(P–P)]" species, whereas only one exists in the actual spectrum.

Of particular note, the ^{1}H NMR spectrum of the residue obtained from the corresponding DPPB system also showed a similar, unassigned hydride signal as a triplet centred at -11.5 ppm ($^2J_{PH}$ = 34.4 Hz). Again, the chemical shift and the P–H coupling constant point to a species of the type "*trans*–RuHCl(P–P)". In addition, several other broad signals were apparent in the -7 to -20 ppm region, none of which could be assigned to the DPPB trimer analogue, **29**, described earlier (see Sections 5.4 and 5.5).

Formation of the trinuclear hydride complex [RuHCl(CHIRAPHOS)]$_3$, **30**, from the dimeric precursor **16** under transfer hydrogenation conditions (2-propanol/KOH) is not surprising, and probably proceeds by a mechanism similar to that proposed for its

formation under H_2 in the presence of NEt_3 base (*cf.* Scheme 5-III in Section 5.7), but with 2-propanol and KOH respectively acting as the hydrogen source and the base.

Further studies are necessary in order to establish the nature of the new hydride species formed from $[RuCl(P–P)(\mu-Cl)]_2$ precursors under the transfer hydrogenation conditions. Which of the major species, the dimeric precursor $[RuCl(P–P)(\mu-Cl)]_2$, the trinuclear hydride complex $[RuHCl(P–P)]_3$, or the tentatively formulated "*trans*–RuHCl(P–P)" species, is (are) the principal catalyst(s) remains to be seen.

7.3.2 H_2-Hydrogenation of Ketones and Imines

The $[RuCl(P–P)(\mu-Cl)]_2$ and $[RuHCl(P–P)]_3$ complexes catalysed the H_2-hydrogenation of ketones and imines under relatively mild conditions (1–12 atm H_2, 30–100 °C) with turnover frequencies in the 1–10 h^{-1} $[Ru]^{-1}$ range. In general, the trimeric hydridochloro ruthenium(II) complexes **29** and **30** exhibited hydrogenation activity which was an order of magnitude higher than their dimeric dichloro analogues (**14** and **16**). As exemplified by the data for acetophenone hydrogenation (Table 7.4), the best results for ketone hydrogenation were obtained in the relatively nonpolar toluene solvent.

Preliminary data using $[RuHCl(S,S\text{-CHIRAPHOS}]_3$, **30**, as catalyst (1.5 mM Ru_3 and 1.4 M acetophenone in toluene, 80 °C, 12 atm of H_2, 7 days) revealed asymmetric hydrogenation of acetophenone to the *R*-alcohol in *ca.* 55% e.e at 30% conversion. The use of $[RuCl(CHIRAPHOS)(\mu-Cl)]_2$, **16**, in the presence of 2 equivalents of NEt_3 also gave similar results; the dimeric NEt_3-adduct **16b** and the trimeric hydridochloro complex **30** were identified in the catalyst residue (~1:1 ratio) at the end of the runs by ^{31}P NMR spectroscopy (Section 5.4). In the absence of added NEt_3, however, the complex **16** showed poor hydrogenation activity (only ~3% conversion and ~17% e.e. under identical conditions). The hydridochloro derivative **30** is clearly the more effective precursor.

Table 7.4: Data for H_2-Hydrogenation of Acetophenone Catalysed by [RuCl(DPPB)(μ-Cl)]$_2$ and Related Complexes.[a]

Run #	Catalyst[b]	Solvent	Time, h	% Conversion	T.O.F.,[c] h^{-1} [Ru]$^{-1}$
1.	14	DMA	24	1.0	0.13
2.	14	Toluene	24	2.6	0.34
3.	14b	Toluene	24	1.1	0.14
4.	29	DMA	24	0.8	0.10
5.	29	THF	24	1.3	0.17
6.	29	Toluene	24	14.6	1.9
7.	29[d]	Toluene	24	13.6	3.2
8.	29[d]	Toluene	13	8.5	3.7
9.	29[d]	—[e]	18	4.4	2.8

[a] General conditions:

Solvent: 5.0 mL; temperature: 100±2 °C; 1 atm of H_2;

Acetophenone = 8.6 x 10^{-3} mols; Ru catalyst (monomer) = 2.7 x 10^{-5} mols.

[b] Catalyst precursors:

[RuCl(DPPB)(μ-Cl)]$_2$, 14; [Ru$_2$Cl$_4$(DPPB)$_2$(NEt$_3$)], 14b; [RuHCl(DPPB)]$_3$, 29.

[c] Turnover frequency.

[d] [Ru] = 1.5 x 10^{-5} mols.

[e] Neat acetophenone, 17.2 x 10^{-3} mols.

Results of hydrogenation of imines using the hydride trimer 30 as catalyst were less encouraging. For example, the imine shown in Figure 7.10 was hydrogenated with only 2% e.e. (R) and 4% conversion under conditions employed for acetophenone hydrogenation (see above).

Figure 7.10: An imine substrate tested for asymmetric H_2-hydrogenation using [RuHCl(S,S-CHIRAPHOS)]$_3$ as catalyst.

7.3.3 Hydrogenation of Nitriles

Homogeneous hydrogenation of nitriles has been little studied, from either synthetic or mechanistic viewpoints; the required use of relatively severe conditions has been a major drawback.[15] Very few catalytic systems capable of hydrogenating nitriles under relatively mild conditions have been reported.[10, 15–18]

The trimeric hydride complex [RuHCl(DPPB)]$_3$, **29**, catalyses hydrogenation of nitriles at 1 atm of H_2. N,N-Dimethylacetamide solutions containing 1mM **29**, and typically 2 M PhC≡N, give measurable rates even at 50 °C; under such conditions, the intermediate imine PhCH$_2$N=CHPh is seen en route to the final product dibenzylamine, (PhCH$_2$)$_2$NH. At 150 °C complete selectivity to the amine (and NH$_3$) is observed (Equation 7.11):

$$PhC\equiv N + 4\,H_2 \longrightarrow (PhCH_2)_2NH \qquad (7.11)$$

A catalytic reaction sequence at a Ru-phosphine centre for production of secondary from primary amines, with elimination of NH$_3$ and intermediacy of a coordinated imine, has been reported in the literature.[19] A plausible reaction sequence is shown in Equations 7.12–7.14.

278

$$PhC\equiv N \xrightarrow{+H_2} PhCH=NH \xrightarrow{+H_2} PhCH_2NH_2 \qquad (7.12)$$

$$PhCH_2NH_2 + PhCH=NH \longrightarrow PhCH_2N=CHPh + NH_3 \qquad (7.13)$$

$$PhCH_2N=CHPh \xrightarrow{+H_2} (PhCH_2)_2NH \qquad (7.14)$$
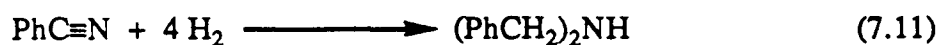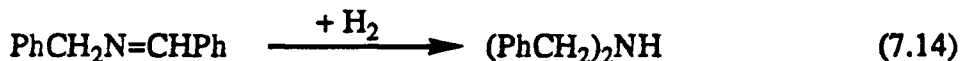
Turnover frequency for loss of PhCN is only about 1 h^{-1} $[Ru_3]^{-1}$ at 70 °C and 1 atm of H_2, but at higher temperatures and pressures, effective conversions are realised. For example, at 100 °C, about 70% of the PhCN is converted to $(PhCH_2)_2NH$ and the imine $PhCH_2N=CHPh$ (in a 4:1 ratio) in 24 h at 35 atm H_2. At 110 atm H_2, 85% of PhCN converts to the amine and imine (7:1). The use of toluene or THF as solvent, or precursor complexes such as $[RuCl(DPPB)(\mu-Cl)]_2$, with or without added base to promote *in situ* formation of **29**, give much less effective catalytic systems.

Kinetic studies on the hydrogenation of nitriles catalysed by $[RuHCl(DPPB)]_3$ are of particular interest because of the possibility of catalysis at a Ru_3 cluster site. Preliminary kinetic studies on the hydrogenation of MeCN catalysed by **29** (50 °C, 1 atm of H_2, 2 M MeCN in DMA) show increasing turnover numbers per Ru_3 with increasing concentration of the trimer (for $[Ru_3]$ = 0.60–3.5 mM, T.O. frequency = 0.5–4.8 h^{-1} $[Ru_3]^{-1}$),[12] implying catalysis at an aggregated site.[20] Stoichiometric hydrogenation of MeCN at Fe_3 cluster sites is well-documented by structural data,[21] but to our knowledge, there is no previous kinetic evidence to substantiate nitrile hydrogenation at a polynuclear site. Kinetic studies on the hydrogenation of PhCN have also been conducted,[12] but will not be discussed here.

7.4   References – Chapter 7

1.   Wang, D. K. W., Ph.D. Dissertation, The University of British Columbia, Vancouver, Canada, 1978.

2.   Chan, C. -Y., Ph.D. Dissertation, The University of British Columbia, Vancouver, Canada, 1974.

3.   Thorburn, I. S., M.Sc. Dissertation, The University of British Columbia, Vancouver, Canada, 1980.

4.   Hui, B. C., Ph.D. Dissertation, The University of British Columbia, Vancouver, Canada, 1969.

5.   Gamage, S. N., Ph.D. Dissertation, The University of British Columbia, Vancouver, Canada, 1985.

6.   Joshi, A. M., M.Sc. Dissertation, The University of British Columbia, Vancouver, Canada, 1986.

7.   DMA General Information Bulletin, Industrial and Biochemicals Department, E. I. Du Pont de Nemours and Co., Wilmington, Delaware, USA, 1962.

8.   Joshi, A. M.; James, B. R. *J. Chem. Soc., Chem. Commun.* **1989**, 1785.

9.   Hampton, C., Ph.D. Dissertation, The University of British Columbia, Vancouver, Canada, 1989.

10.   James, B. R.; Pacheco, A.; Rettig, S. J.; Thorburn, I. S.; Ball, R. G.; Ibers, J. A. *J. Mol. Catal.* **1987**, *41*, 147.

11.   James, B. R.; Joshi, A. M.; Kvintovics, P.; Morris, R. H.; Thorburn, I. S. in *Catalysis of Organic reactions*; Blackburn, D. W., Ed.; Marcel Dekker: New York, 1990; Chapter 2.

12.   (a) Joshi, A. M.; Frediani, P.; James, B. R. "Vth IUPAC Symposium on Organometallic Chemistry Directed Towards Organic Synthesis (OMCOS V)", Florence, Italy, October 1989; Abstract # PS2-13.
(b) Joshi, A. M.; James, B. R. "72nd Canadian Chemical Conference and Exhibition, Symposium on Bimetallic and Polymetallic Complexes", Victoria, B. C., Canada, June 1989; Abstract # 301.
(c) Joshi, A. M.; Thorburn, I. S.; James, B. R. "VIth International Symposium on Homogeneous Catalysis (ISHC-6)", Vancouver, B. C., Canada, August 1988; Abstract # P-146.

13.   (a) Spogliarich, R.; Kaspar, J.; Graziani, M. *J. Catal.* **1985**, *94*, 292.
(b) Sasson, Y.; Blum, J. *J. Org. Chem.* **1975**, *40*, 1887.

14.   Dekleva, T. W.; Joshi, A. M.; Thorburn, I. S.; James, B. R.; Evans, S. V.; Trotter, J. *Isr. J. Chem.* **1990**, *30(4)*; *in press*.

15.   James, B. R. *Homogeneous Hydrogenation*; Wiley: New York, 1973; see 'Nitriles' in Index.

16.   Grey, R. A.; Pez, G. P.; Wallo, A. *J. Am. Chem. Soc.* **1981**, *103*, 7536.

17.   Yoshida, T.; Okano, T.; Otsuka, S. *J. Chem. Soc., Chem. Commun.* **1979**, 870.

18.   Thorburn, I. S.; Rettig, S. J.; James, B. R. *J. Organomet. Chem.* **1985**, *296*, 103.

19.   Jung, C. W.; Fellman, J. D.; Garrou, P. E. *Organometallics* **1983**, *2*, 1042.

20.   Laine, R. M. *J. Mol. Catal.* **1982**, *14*, 137; and references therein.

21.   Andrews, M. A.; Kaesz, H. D. *J. Am. Chem. Soc.* **1977**, *99*, 6763.

CHAPTER 8

General Conclusions and Suggestions for Future Work

The objective of the work described in this thesis was to develop general synthetic routes to ruthenium complexes containing one chelating ligand per ruthenium centre. Incorporation of chiral diphosphines in such complexes would then allow these species to be tested as potential catalysts for asymmetric hydrogenation of unsaturated substrates.

The complexes of general formula $[RuCl(P–P)(\mu-Cl)]_2$ (P–P = DPPP, DPPB, DIOP, CHIRAPHOS, or NORPHOS) were previously synthesised in this laboratory via H_2-reduction of the corresponding mixed-valence precursors, $Ru_2Cl_5(P–P)_2$. The synthesis of mixed-valence dimers was extended to include the diphosphines: P–P = DPPN, DPPH, *rac*-DPPCP, *rac*-DPCYCP, *S,S*-BDPP, *R*- and *S*-BINAP, and *S*-PHENOP. The $Ru_2^{II,\,II}$ dimers were characterised only for DPPN, BDPP, and BINAP

Much of the chemistry was conducted on the DPPB derivative. The dichloro-bridged complex $[RuCl(DPPB)(\mu-Cl)]_2$ reacted readily with a variety of coordinating ligands to give the corresponding trichloro-bridged dinuclear species containing one coordinated ligand. The coordinative unsaturation at the two Ru(II) centres (C.N. = 5) and the availability of non-bonding electron pairs on the chloride are perhaps responsible for the observed propensity to form such trichloro-bridged complexes. Several new complexes of the type $[(L)(DPPB)Ru(\mu-Cl)_3RuCl(DPPB)]$ (L = CO, DMSO, NEt$_3$, NHBu$_2$, MeI, η^2-H$_2$, σ-N$_2$) were isolated or characterised *in situ* by NMR spectroscopy. A single crystal X-ray diffraction study of the DMSO analogue confirmed the trichloro-bridged structure with an unsymmetrical arrangement of the two diphosphine ligands; the DMSO ligand was found to be coordinated through the sulphur atom.

Of the trichloro-bridged species characterised during this work, the ones containing the η^2-H_2, σ-N_2 and MeI are perhaps the most intersting. The presence of the η^2-H_2 moiety was demonstrated by the typically short ^{1}H NMR T_1 relaxation time ($T_{1(min)}$ = 12 ms at 277 K and 300 MHz) and the relatively large H-D coupling for the η^2-HD isotopomer ($^1J_{HD}$ = 29.4 Hz). The H–H distance was estimated to be 0.86 ± 0.02 Å from the T_1 data. Hydrogen (and nitrogen!) uptake measurements on the DPPB system will allow determination of equilibrium constants for the formation of the η^2-H_2 (σ-N_2) complex, from which relevant thermodynamic parameters can be obtained. Studies should also be extended to Ru(II) dimers containing other diphosphines.

Reaction of [RuCl(P–P)(μ-Cl)]$_2$ complexes (P–P = DPPB or CHIRAPHOS) with H_2 in the presence of NEt$_3$ base afforded in much improved yields the trinuclear hydridochloro complexes of the formula [RuHCl(P–P)]$_3$, which have been characterised by NMR spectroscopy. The reaction likely proceeds via deprotonation of the η^2-H_2 complex. Interestingly, more than half the molecular hydrogen complexes reported to date contain Ru, and given the reluctance of a Ru(II) centre to undergo oxidative addition reactions (to Ru^{IV}), such deprotonation of a bound H_2 by an appropriate base may be a general mechanism for hydride formation in Ru systems. Reactions of other dimeric Ru(II) complexes with H_2 with or without NEt$_3$ should be investigated further. Reactions of the dimers with H_2S and silanes (R_3SiH or R_2SiH_2) may lead to some interesting chemistry and possible applications to hydrodesulphurisation and hydrosilylation processes, respectively.

Possible involvement of molecular hydrogen complexes in important catalytic processes such as hydrogenation and dehydrogenation of organic substrates had been suggested earlier; however, conclusive evidence was lacking. The kinetic study on hydrogenation of styrene catalysed by [RuCl(DPPB)(μ-Cl)]$_2$ showed strong evidence for the involvement of molecular hydrogen species in the catalytic cycle. Temperature dependence of the various rate constants and the equilibrium constant of the reaction steps

in the proposed mechanism should be carried out to obtain the corresponding activation and thermodynamic parameters. Such data, as well as solvent dependence studies, may provide an insight into the possible mode of hydrogen transfer to the substrate.

Preliminary studies showed that the hydridochloro trimers [RuHCl(P–P)]$_3$ were indeed effective catalyst precursors for the hydrogenation of ketones and nitriles under relatively mild conditions (30–100 °C, 1–12 atm H$_2$, typical turnover frequencies 1–10 h^{-1} [Ru]$^{-1}$ at 1 atm H$_2$ and 100 °C) Detailed kinetic studies are needed in order to establish a plausible mechanism.

A comparative solid-state ^{31}P NMR study of the complexes RuCl$_2$(DPPB)(PPh$_3$) and RuCl$_2$(PPh$_3$)$_3$ established the close similarity between the structures of the two species. Very few such studies on organometallic compounds have been reported to date. The current work serves to highlight the potential applications of the solid-state NMR techniques to structural problems in organometallic chemistry. Reactions of the mixed-phosphine complex RuCl$_2$(DPPB)(PPh$_3$) toward monodentate and bidentate ligands were explored in an attempt to develop an alternative route to the DPPB dimer, and indeed the reactivity was found to parallel that observed for the corresponding dichloro-bridged dimer.

Reactions of the complexes cis-RuCl$_2$(DMSO)$_4$ and [RuCl(p-cymene)(μ-Cl)]$_2$ with one equivalent of a bidentate phosphine demonstrated the influence of the chelate ring size on the nature of products obtained. No complexes of the stoichiometry "RuCl$_2$(P–P)" could be isolated for diphosphines with a chelate size of less than six, indicating that steric factors play a key role in determining the outcome of the reaction.

The norbornadiene complex, trans–RuHCl(nbd)(DPPB), containing a chelating phosphine was synthesised and characterised spectroscopically. Unlike its PPh$_3$ analogue, however, the dppb derivative did not react with H$_2$ or CO. Thus the 'minor' change of substituting two cis–PPh$_3$ ligands by a flexible chelating DPPB within a similar precursor (trans–RuHCl(nbd)(PPh$_3$)$_2$) induces for the DPPB species relative non-reactivity with H$_2$ or CO.

APPENDIX

APPENDIX A-1

Temperature and Concentration Dependence of the Optical Rotation of (R)-(+)-1-Phenylethanol

<u>Table A-1.1</u>: Data for the Effect of Temperature on the Optical Rotation of Pure (R)-(+)-1-Phenylethanol.

Temperature (°C)[a]	Observed Rotation (°)[b]	Density (g/mL)[c]	Absolute Rotation (°)
	(α)		$[\alpha]_D$
12.4	44.215	1.0196	43.366
14.3	44.158	1.0180	43.376
17.3	44.060	1.0156	43.383
17.8	44.040	1.0152	43.380
19.9	43.972	1.0135	43.386
22.1	43.895	1.0117	43.386
24.4	43.821	1.0099	43.393
25.0	43.798	1.0094	43.391
27.6	43.715	1.0073	43.399
29.2	43.661	1.0060	43.401
29.3	43.661	1.0059	43.404
31.8	43.579	1.0039	43.410
35.9	43.444	1.0006	43.419
39.4	43.324	0.9978	43.42
39.8	43.308	0.9974	43.42

(a) error in readings is ± 0.1°C.

(b) error from instrument is ± 0.2% of the reading, while the reproducibility is ± 0.002°; measured at the sodium D line.

(c) relative density.

Figure A-1.1: Plot of Observed Rotation (α) of Pure (*R*)-(+)-1-Phenylethanol vs. Temperature.
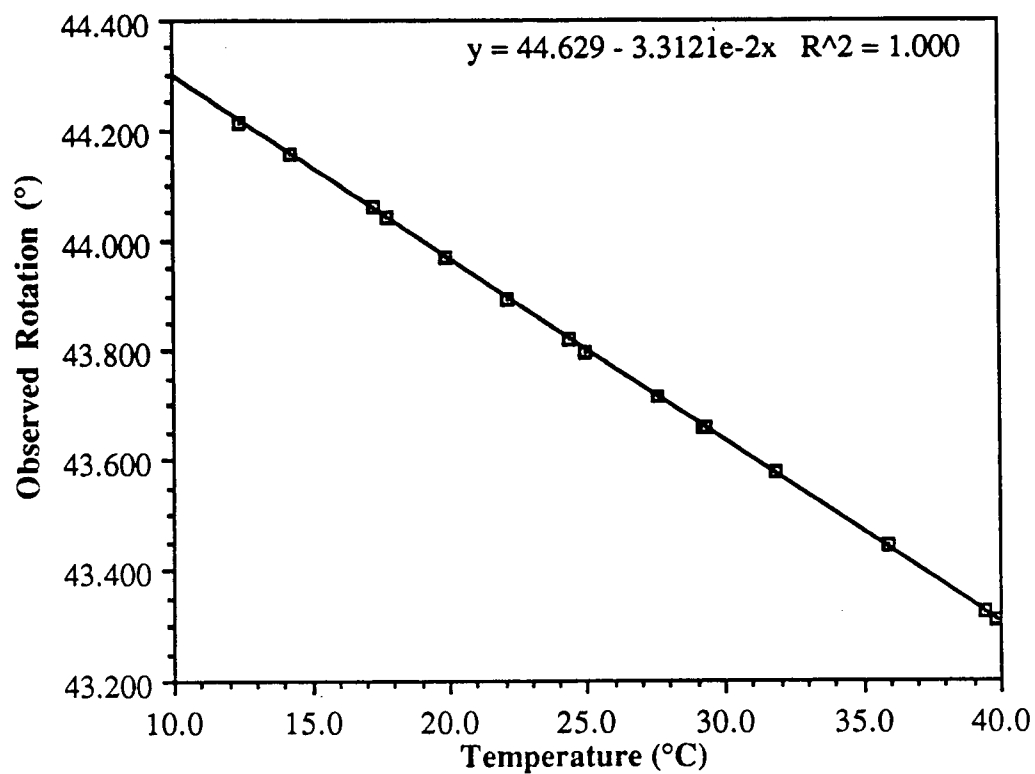
Table A-1.2: Data for the Effect of Concentration on the Optical Rotation of
(R)-(+)-1-Phenylethanol at 25°C.

Conc. (g/mL)[a] $[\alpha]_D^{25}$ (°)[a]		Conversion (%)[b]	Observed Rotation (°)[c]	Absolute Rotation	
(A)	(B)		(α)	(A)	(B)
pure	pure	100	43.798	43.4	43.4
0.908	0.877	86.85	40.301	44.4	46.0
0.609	0.584	56.95	28.656	47.1	49.1
0.493	0.472	46.70	23.545	47.8	49.9
0.399	0.353	35.01	19.220	48.2	54.5
0.322	0.319	31.59	15.675	48.7	49.1
0.261	0.220	21.76	12.729	48.8	57.9
0.211	0.214	19.77	10.223	48.5	47.8
0.163	0.171	16.84	7.827	48.0	45.9
0.119	0.095	9.31	5.623	47	59.1
0.086	0.086	8.53	4.006	47	47
0.070	0.057	7.17	3.008	43	53
0	0	0	0	0	0

(a) A – calculated from the amounts of acetophenone and 1-phenylethanol added;
B – calculated from the integration of the peaks in the gas chromatograms of the
mixtures.

(b) the conversion (or %-(R)-(+)-1-phenylethanol) was calculated from the integration of
the peaks in the gas chromatograms of the mixtures.

(c) error from instrument is ± 0.2% of the reading, while the reproducibility is ± 0.002°;
measured at the sodium D line.

Figure A-1.2: Plot of Observed Rotation of (R)-(+)-1-Phenylethanol vs.
% of (R)-(+)-1-Phenylethanol at a Temperature of 25°C.
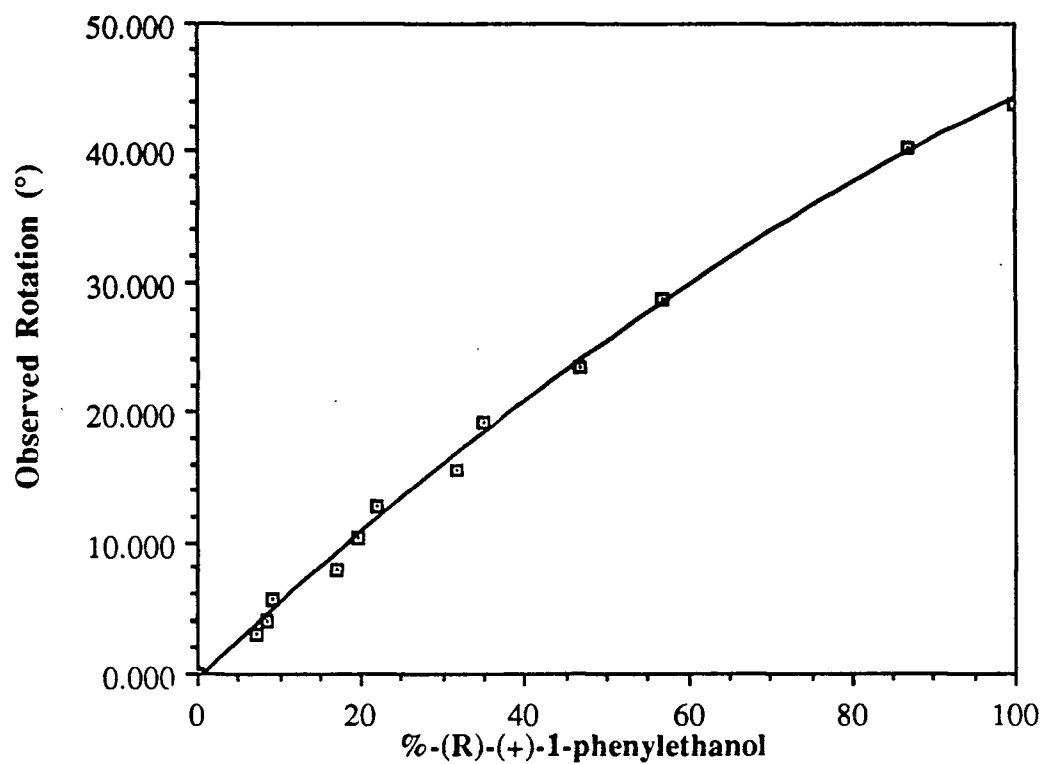
A-2.1:   X-ray Crystallographic Analysis of
mer–RuCl₃(PPh₃)(DMA)₂.DMA solvate
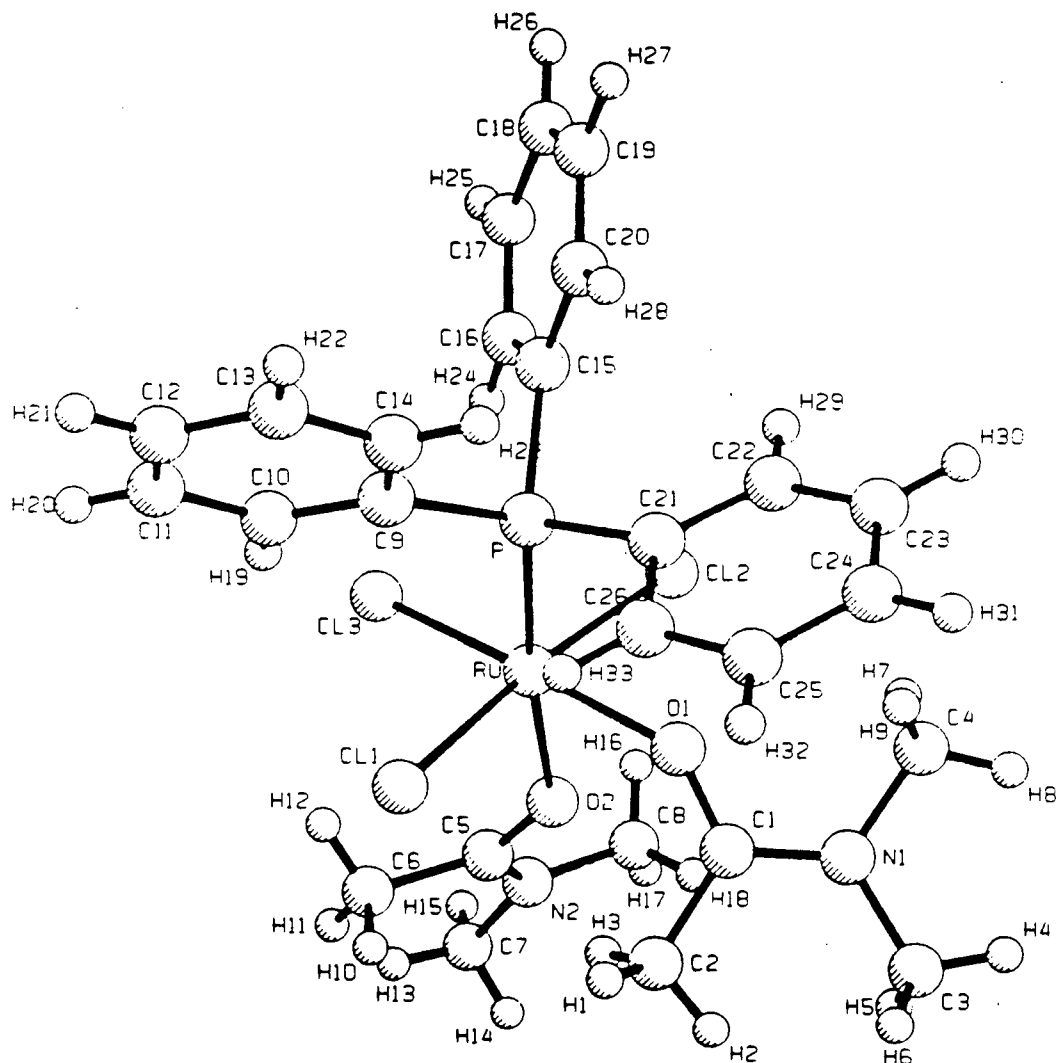
Molecular Structure

Experimental Details

Empirical Formula	$C_{30}H_{42}Cl_3N_3O_3PRu$
Formula Weight	731.08
Crystal System	Orthorhombic
Lattice Parameters:	
	a = 9.839 (3)Å
	b = 10.252 (2)Å
	c = 33.568 (7)Å
	V = 3386 (2)Å^3
Space Group	$P2_12_12_1$ (#19)
Z value	4
D_{calc}	1.43 g/cm^3
F_{000}	1508
$\mu_{(MoK\alpha)}$	7.72 cm^{-1}
Diffractometer	Rigaku AFC6
Radiation	MoKα(λ = 0.71069 Å) Graphite-monochromated
Temperature	21°C
$2\theta_{max}$	59.9°
No. Observations (I>3σ(I))	3861
No. Variables	388
Residuals: R; R_w	0.034; 0.043
Goodness of Fit Indicator	1.54
Maximum Shift in Final Cycle	0.21
Largest Peak in Final Diff. Map	0.78 e$^-$/Å^3

atom	atom	distance	atom	atom	distance
Ru	O(1)	2.064(3)	O(2)	C(5)	1.259(6)
Ru	O(2)	2.200(3)	N(1)	C(1)	1.314(6)
Ru	P	2.273(1)	N(1)	C(4)	1.463(7)
Ru	Cl(3)	2.311(1)	N(1)	C(3)	1.463(6)
Ru	Cl(1)	2.345(1)	N(2)	C(5)	1.336(7)
Ru	Cl(2)	2.350(1)	N(2)	C(8)	1.44(1)
P	C(21)	1.828(5)	N(2)	C(7)	1.467(7)
P	C(9)	1.831(5)	C(1)	C(2)	1.498(8)
P	C(15)	1.839(6)	C(5)	C(6)	1.506(9)
O(1)	C(1)	1.265(5)			

Table A-2.1.2: Bond Angles (deg) with estimated standard deviations in parentheses.

atom	atom	atom	angle	atom	atom	atom	angle
O(1)	Ru	O(2)	85.9(1)	C(9)	P	C(15)	98.7(2)
O(1)	Ru	P	90.91(8)	C(9)	P	Ru	118.7(2)
O(1)	Ru	Cl(3)	175.15(9)	C(15)	P	Ru	119.5(2)
O(1)	Ru	Cl(1)	88.5(1)	C(1)	O(1)	Ru	133.6(3)
O(1)	Ru	Cl(2)	84.7(1)	C(5)	O(2)	Ru	136.4(3)
O(2)	Ru	P	173.9(1)	C(1)	N(1)	C(4)	120.3(4)
O(2)	Ru	Cl(3)	89.3(1)	C(1)	N(1)	C(3)	123.4(4)
O(2)	Ru	Cl(1)	95.1(1)	C(4)	N(1)	C(3)	116.2(4)
O(2)	Ru	Cl(2)	84.1(1)	C(5)	N(2)	C(8)	120.9(5)
P	Ru	Cl(3)	93.69(4)	C(5)	N(2)	C(7)	124.2(6)
P	Ru	Cl(1)	90.09(5)	C(8)	N(2)	C(7)	114.9(6)
P	Ru	Cl(2)	90.43(5)	O(1)	C(1)	N(1)	117.9(5)
Cl(3)	Ru	Cl(1)	93.01(5)	O(1)	C(1)	C(2)	123.1(5)
Cl(3)	Ru	Cl(2)	93.73(5)	N(1)	C(1)	C(2)	119.0(4)
Cl(1)	Ru	Cl(2)	173.19(5)	O(2)	C(5)	N(2)	118.8(5)
C(21)	P	C(9)	104.0(2)	O(2)	C(5)	C(6)	121.5(5)
C(21)	P	C(15)	105.3(3)	N(2)	C(5)	C(6)	119.7(5)
C(21)	P	Ru	108.8(1)				

Table A-2.1.3: Final Atomic Coordinates (Fractional) and B(eq).

atom	x	y	z	B(eq)
Ru	0.22211(3)	0.52583(4)	0.17512(1)	2.76(1)
Cl(1)	0.2244(1)	0.7545(1)	0.17305(4)	3.95(5)
Cl(2)	0.2477(1)	0.2982(1)	0.17872(4)	4.09(6)
Cl(3)	-0.0123(1)	0.5158(1)	0.17215(4)	4.22(5)
P	0.2473(1)	0.5187(1)	0.10785(3)	2.78(4)
O(1)	0.4302(3)	0.5299(4)	0.18274(8)	3.5(1)
O(2)	0.2105(4)	0.5133(4)	0.2404(1)	4.6(2)
O(3)	-0.1859(7)	-0.0122(8)	0.5905(3)	12.5(5)
N(1)	0.6178(4)	0.4877(4)	0.2166(1)	3.6(2)
N(2)	0.1166(5)	0.4822(6)	0.3003(1)	4.8(2)
N(3)	0.030(2)	-0.012(1)	0.5826(5)	5.7(7)
N(4)	0.026(2)	-0.028(1)	0.6062(4)	5.5(6)
C(1)	0.5066(5)	0.5572(5)	0.2119(1)	3.4(2)
C(2)	0.4774(6)	0.6656(7)	0.2405(2)	5.4(3)
C(3)	0.7184(5)	0.5136(6)	0.2477(1)	4.4(2)
C(4)	0.6498(6)	0.3821(6)	0.1888(2)	4.2(2)
C(5)	0.1310(5)	0.5533(6)	0.2672(1)	3.7(2)
C(6)	0.0561(6)	0.6806(7)	0.2632(2)	5.0(3)
C(7)	0.0357(8)	0.522(1)	0.3349(2)	7.2(4)
C(8)	0.1808(9)	0.3568(8)	0.3040(2)	6.6(4)
C(9)	0.1796(5)	0.6553(5)	0.0780(1)	3.4(2)
C(10)	0.0573(6)	0.7117(6)	0.0875(2)	4.3(3)
C(11)	0.0005(7)	0.8048(7)	0.0617(2)	5.8(3)
C(12)	0.0638(9)	0.8368(7)	0.0267(2)	6.5(4)

Table   (cont.)

atom	x	y	z	B(eq)
C(13)	0.1813(8)	0.7782(7)	0.0166(2)	5.9(4)
C(14)	0.2399(7)	0.6866(6)	0.0421(1)	4.8(3)
C(15)	0.1742(6)	0.3819(5)	0.0797(2)	3.8(2)
C(16)	0.0639(6)	0.3134(6)	0.0935(2)	4.4(3)
C(17)	0.0010(7)	0.2195(6)	0.0684(2)	5.3(3)
C(18)	0.054(1)	0.1933(7)	0.0313(2)	6.6(4)
C(19)	0.164(1)	0.2614(7)	0.0180(2)	6.5(4)
C(20)	0.2250(8)	0.3557(6)	0.0412(2)	5.0(3)
C(21)	0.4287(5)	0.5174(6)	0.0961(1)	3.5(2)
C(22)	0.4987(6)	0.4019(6)	0.0893(2)	4.3(3)
C(23)	0.6377(7)	0.4026(8)	0.0831(2)	5.5(3)
C(24)	0.7084(6)	0.517(1)	0.0850(2)	6.3(3)
C(25)	0.6408(6)	0.6335(8)	0.0928(2)	5.5(3)
C(26)	0.5014(6)	0.6332(7)	0.0983(2)	4.6(3)
C(27)	−0.065(3)	−0.009(2)	0.577(1)	12(2)
C(28)	−0.071(4)	−0.032(3)	0.612(1)	14(3)
C(29)	0.001(1)	0.016(1)	0.5369(3)	9.6(6)
C(30)	−0.022(1)	−0.047(1)	0.6507(3)	10.9(7)
C(31)	0.1765(7)	−0.0210(8)	0.5972(2)	6.7(4)
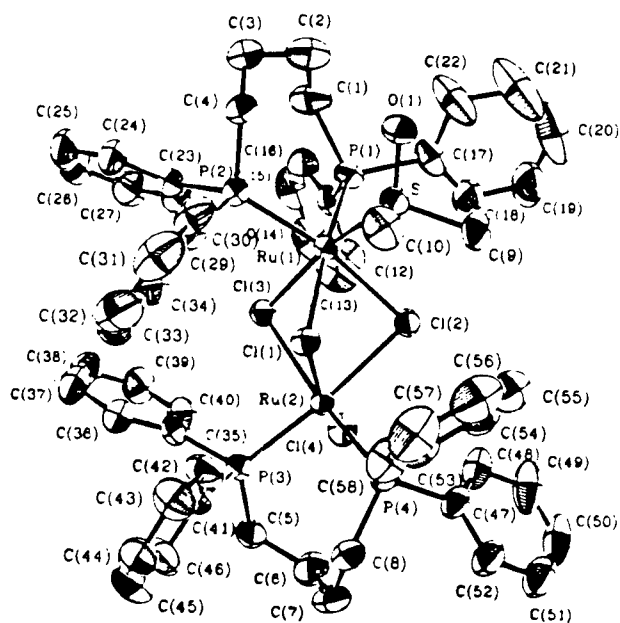
Molecular Structure

Experimental Details

compound	$Ru_2Cl_4(dppb)_2(dmso) \cdot 0.67\ Et_2O \cdot 0.33\ CH_2Cl_2$
formula	$C_{58}H_{62}Cl_4OP_4Ru_2S \cdot 0.67\ C_4H_{10}O \cdot 0.33\ CH_2Cl_2$
fw	1352.60
color, habit	yellow-orange prism
crystal size , mm	0.20 x 0.30 x 0.55
crystal system	triclinic
space group	$P\bar{1}$
a, Å	12.796(1)
b, Å	14.559(1)
c, Å	18.429(1)
α, deg	103.983(5)
β, deg	95.036(6)
γ, deg	99.634(6)
V, Å^3	3255.0(4)
Z	2
ρ_c, g/cm^3	1.380
$F(000)$	1383.88
radiation	Mo
wavelength (Å)	0.71073
μ, cm^{-1}	8.13
transmission factors	0.761-0.872
scan type	ω-2θ
scan range, deg in ω	$0.85 + 0.35\ \tan \theta$
scan rate, deg/min	2.0-20.0
data collected	$-h$, $\pm k$, $\pm l$
$2\theta_{max}$, deg	55
cryst decay	negligible

no. of unique reflections	14845
no. of reflcns with $I \geq 3\sigma(I)$	9088
no. of variables	663
R	0.037
R_w	0.046
gof	1.45
max Δ/σ (final cycle)	0.41
residual density $e/\text{Å}^3$	1.30 (near Ru)

[a] Temperature 294 K, Enraf-Nonius CAD4-F diffractometer, Mo-Kα radiation ($\lambda K_{\alpha 1}$ = 0.70930, $\lambda K_{\alpha 2}$ = 0.71359 Å), graphite monochromator, takeoff angle 2.7°, aperture (2.0 + tan θ) x 4.0 mm at a distance of 173 mm from the crystal, scan range extended by 25% on both sides for background measurement, $\sigma^2(I) = C + 2B + [0.04(C - B)]^2$ (S = scan rate, C = scan count, B = normalized background count), function minimized $\Sigma w(|F_o|-|F_c|)^2$ where w = $4F_o^2/\sigma^2(F_o^2)$, $R = \Sigma||F_o|-|F_c||/\Sigma|F_o|$, $R_w = (\Sigma w(|F_o|-|F_c|)^2/\Sigma w|F_o|^2)^{1/2}$, and gof = $[\Sigma(|F_o|-|F_c|)^2/(m-n)]^{1/2}$. Values given for R, R_w, and gof are based on those reflections with $I \geq 3\sigma(I)$.

Table A-2.2.1: Bond Lengths (Å) with estimated standard deviations in parentheses.

Bond	Length(Å)	Bond	Length(Å)
Ru(1)-Cl(1)	2.469(1)	C(21)-C(22)	1.41(1)
Ru(1)-Cl(2)	2.495(1)	C(23)-C(24)	1.396(6)
Ru(1)-Cl(3)	2.429(1)	C(23)-C(28)	1.373(7)
Ru(1)-P(1)	2.305(1)	C(24)-C(25)	1.367(7)
Ru(1)-P(2)	2.305(1)	C(25)-C(26)	1.348(9)
Ru(1)-S	2.244(1)	C(26)-C(27)	1.388(9)
Ru(2)-Cl(1)	2.418(1)	C(27)-C(28)	1.388(7)
Ru(2)-Cl(2)	2.517(1)	C(29)-C(30)	1.396(7)
Ru(2)-Cl(3)	2.492(1)	C(29)-C(34)	1.380(7)
Ru(2)-Cl(4)	2.399(1)	C(30)-C(31)	1.402(8)
Ru(2)-P(3)	2.261(1)	C(31)-C(32)	1.36(1)
Ru(2)-P(4)	2.257(1)	C(32)-C(33)	1.36(1)
P(1)-C(1)	1.849(6)	C(33)-C(34)	1.378(7)
P(1)-C(11)	1.831(5)	C(35)-C(36)	1.379(6)
P(1)-C(17)	1.851(5)	C(35)-C(40)	1.402(6)
P(2)-C(4)	1.842(4)	C(36)-C(37)	1.384(7)
P(2)-C(23)	1.839(5)	C(37)-C(38)	1.375(8)
P(2)-C(29)	1.836(5)	C(38)-C(39)	1.375(8)
P(3)-C(5)	1.840(4)	C(39)-C(40)	1.373(7)
P(3)-C(35)	1.836(4)	C(41)-C(42)	1.367(7)
P(3)-C(41)	1.847(4)	C(41)-C(46)	1.397(6)
P(4)-C(8)	1.847(5)	C(42)-C(43)	1.387(7)
P(4)-C(47)	1.832(5)	C(43)-C(44)	1.351(8)
P(4)-C(53)	1.846(5)	C(44)-C(45)	1.347(9)
S -O(1)	1.474(3)	C(45)-C(46)	1.371(8)
S -C(9)	1.788(5)	C(47)-C(48)	1.360(7)
S -C(10)	1.792(5)	C(47)-C(52)	1.396(7)
C(1)-C(2)	1.508(8)	C(48)-C(49)	1.403(7)
C(2)-C(3)	1.524(8)	C(49)-C(50)	1.36(1)
C(3)-C(4)	1.527(7)	C(50)-C(51)	1.37(1)
C(5)-C(6)	1.531(7)	C(51)-C(52)	1.370(8)
C(6)-C(7)	1.491(8)	C(53)-C(54)	1.381(7)
C(7)-C(8)	1.537(7)	C(53)-C(58)	1.389(7)
C(11)-C(12)	1.381(7)	C(54)-C(55)	1.383(7)
C(11)-C(16)	1.391(7)	C(55)-C(56)	1.355(9)
C(12)-C(13)	1.386(7)	C(56)-C(57)	1.358(10)
C(13)-C(14)	1.359(9)	C(57)-C(58)	1.362(8)
C(14)-C(15)	1.359(9)	O(2)-C(59)	1.26(5)
C(15)-C(16)	1.399(8)	O(2)-C(61)	1.31(6)
C(17)-C(18)	1.358(8)	Cl(6)-C(63)	1.62(8)
C(17)-C(22)	1.385(8)	Cl(5)-C(63)	1.49(7)
C(18)-C(19)	1.381(8)	C(59)-C(60)	1.72(4)
C(19)-C(20)	1.30(1)	C(61)-C(62)	1.18(5)
C(20)-C(21)	1.36(1)		

Bonds	Angle(deg)	Bonds	Angle(deg)
Cl(1)-Ru(1)-Cl(2)	78.25(3)	P(4)-C(8)-C(7)	117.2(4)
Cl(1)-Ru(1)-Cl(3)	78.46(3)	P(1)-C(11)-C(12)	119.4(4)
Cl(1)-Ru(1)-P(1)	172.23(4)	P(1)-C(11)-C(16)	124.1(4)
Cl(1)-Ru(1)-P(2)	93.62(4)	C(12)-C(11)-C(16)	116.5(5)
Cl(1)-Ru(1)-S	91.86(4)	C(11)-C(12)-C(13)	121.9(5)
Cl(2)-Ru(1)-Cl(3)	80.80(3)	C(12)-C(13)-C(14)	120.3(6)
Cl(2)-Ru(1)-P(1)	94.73(4)	C(13)-C(14)-C(15)	119.8(6)
Cl(2)-Ru(1)-P(2)	169.35(4)	C(14)-C(15)-C(16)	120.2(5)
Cl(2)-Ru(1)-S	91.94(4)	C(11)-C(16)-C(15)	121.2(6)
Cl(3)-Ru(1)-P(1)	97.29(4)	P(1)-C(17)-C(18)	120.9(4)
Cl(3)-Ru(1)-P(2)	90.90(4)	P(1)-C(17)-C(22)	120.7(5)
Cl(3)-Ru(1)-S	168.87(4)	C(18)-C(17)-C(22)	118.4(5)
P(1)-Ru(1)-P(2)	92.93(4)	C(17)-C(18)-C(19)	120.6(7)
P(1)-Ru(1)-S	91.68(4)	C(18)-C(19)-C(20)	122.3(8)
P(2)-Ru(1)-S	95.23(4)	C(19)-C(20)-C(21)	118.9(7)
Cl(1)-Ru(2)-Cl(2)	78.78(3)	C(20)-C(21)-C(22)	121.4(8)
Cl(1)-Ru(2)-Cl(3)	78.23(3)	C(17)-C(22)-C(21)	118.3(8)
Cl(1)-Ru(2)-Cl(4)	163.48(4)	P(2)-C(23)-C(24)	118.3(4)
Cl(1)-Ru(2)-P(3)	102.24(4)	P(2)-C(23)-C(28)	123.7(4)
Cl(1)-Ru(2)-P(4)	94.23(4)	C(24)-C(23)-C(28)	117.9(4)
Cl(2)-Ru(2)-Cl(3)	79.18(3)	C(23)-C(24)-C(25)	121.4(5)
Cl(2)-Ru(2)-Cl(4)	88.45(4)	C(24)-C(25)-C(26)	119.7(5)
Cl(2)-Ru(2)-P(3)	172.71(4)	C(25)-C(26)-C(27)	121.2(5)
Cl(2)-Ru(2)-P(4)	95.12(4)	C(26)-C(27)-C(28)	118.6(6)
Cl(3)-Ru(2)-Cl(4)	89.18(4)	C(23)-C(28)-C(27)	121.1(5)
Cl(3)-Ru(2)-P(3)	93.92(4)	P(2)-C(29)-C(30)	121.7(4)
Cl(3)-Ru(2)-P(4)	171.26(4)	P(2)-C(29)-C(34)	119.2(4)
Cl(4)-Ru(2)-P(3)	89.13(4)	C(30)-C(29)-C(34)	119.1(5)
Cl(4)-Ru(2)-P(4)	97.34(4)	C(29)-C(30)-C(31)	119.3(6)
P(3)-Ru(2)-P(4)	92.00(4)	C(30)-C(31)-C(32)	120.0(6)
Ru(1)-Cl(1)-Ru(2)	86.69(3)	C(31)-C(32)-C(33)	120.7(6)
Ru(1)-Cl(2)-Ru(2)	84.01(3)	C(32)-C(33)-C(34)	120.4(6)
Ru(1)-Cl(3)-Ru(2)	85.93(3)	C(29)-C(34)-C(33)	120.5(6)
Ru(1)-P(1)-C(1)	120.6(2)	P(3)-C(35)-C(36)	123.1(4)
Ru(1)-P(1)-C(11)	114.2(1)	P(3)-C(35)-C(40)	118.1(3)
Ru(1)-P(1)-C(17)	115.1(2)	C(36)-C(35)-C(40)	118.7(4)
C(1)-P(1)-C(11)	99.7(3)	C(35)-C(36)-C(37)	120.5(5)
C(1)-P(1)-C(17)	103.9(3)	C(36)-C(37)-C(38)	120.5(5)
C(11)-P(1)-C(17)	100.5(2)	C(37)-C(38)-C(39)	119.4(5)
Ru(1)-P(2)-C(4)	120.4(2)	C(38)-C(39)-C(40)	120.8(5)
Ru(1)-P(2)-C(23)	120.3(2)	C(35)-C(40)-C(39)	120.1(5)
Ru(1)-P(2)-C(29)	111.0(1)	P(3)-C(41)-C(42)	121.1(3)
C(4)-P(2)-C(23)	101.2(2)	P(3)-C(41)-C(46)	122.1(4)
C(4)-P(2)-C(29)	101.6(2)	C(42)-C(41)-C(46)	116.8(4)

C(23)-P(2)-C(29)	98.9(2)	C(41)-C(42)-C(43)	121.5(5)
Ru(2)-P(3)-C(5)	114.5(1)	C(42)-C(43)-C(44)	120.1(5)
Ru(2)-P(3)-C(35)	112.5(1)	C(43)-C(44)-C(45)	119.6(5)
Ru(2)-P(3)-C(41)	122.0(2)	C(44)-C(45)-C(46)	121.2(5)
C(5)-P(3)-C(35)	100.9(2)	C(41)-C(46)-C(45)	120.6(5)
C(5)-P(3)-C(41)	103.6(2)	P(4)-C(47)-C(48)	121.7(4)
C(35)-P(3)-C(41)	100.6(2)	P(4)-C(47)-C(52)	121.3(4)
Ru(2)-P(4)-C(8)	118.8(2)	C(48)-C(47)-C(52)	117.0(5)
Ru(2)-P(4)-C(47)	119.6(2)	C(47)-C(48)-C(49)	121.4(6)
Ru(2)-P(4)-C(53)	111.6(1)	C(48)-C(49)-C(50)	119.6(7)
C(8)-P(4)-C(47)	102.3(2)	C(49)-C(50)-C(51)	120.5(6)
C(8)-P(4)-C(53)	100.4(2)	C(50)-C(51)-C(52)	119.0(6)
C(47)-P(4)-C(53)	101.0(2)	C(47)-C(52)-C(51)	122.5(6)
Ru(1)-S -O(1)	120.8(1)	P(4)-C(53)-C(54)	120.4(4)
Ru(1)-S -C(9)	112.6(2)	P(4)-C(53)-C(58)	121.4(4)
Ru(1)-S -C(10)	112.7(2)	C(54)-C(53)-C(58)	117.9(5)
O(1)-S -C(9)	105.6(2)	C(53)-C(54)-C(55)	120.7(5)
O(1)-S -C(10)	104.9(2)	C(54)-C(55)-C(56)	119.4(6)
C(9)-S -C(10)	97.5(3)	C(55)-C(56)-C(57)	121.2(6)
P(1)-C(1)-C(2)	122.6(4)	C(56)-C(57)-C(58)	119.9(6)
C(1)-C(2)-C(3)	115.4(5)	C(53)-C(58)-C(57)	120.9(6)
C(2)-C(3)-C(4)	113.6(4)	C(59)-O(2)-C(61)	162(6)
P(2)-C(4)-C(3)	117.1(3)	O(2)-C(59)-C(60)	171(4)
P(3)-C(5)-C(6)	117.3(3)	O(2)-C(61)-C(62)	78(4)
C(5)-C(6)-C(7)	120.5(5)	Cl(6)-C(63)-Cl(5)	104(5)
C(6)-C(7)-C(8)	118.0(4)		

Table A-2.2.3: Final Atomic Coordinates (Fractional x 10^4; Ru, Cl, P, S x 10^5)

and

Isotropic Thermal Parameters (U x 10^3 Å^2) with estimated standard deviations in

parentheses.

Atom	x	y	z	U_{eq}/U_{iso}
Ru(1)	23098(2)	39241(2)	24199(2)	31
Ru(2)	44051(2)	28214(2)	21969(2)	30
Cl(1)	27687(8)	24681(7)	27268(6)	37
Cl(2)	42465(8)	44823(7)	29259(5)	36
Cl(3)	30744(8)	32144(7)	13065(5)	38
Cl(4)	58139(9)	35609(8)	16247(6)	47
P(1)	21230(10)	53395(8)	21172(7)	43
P(2)	6141(9)	31461(8)	18432(6)	38
P(3)	44571(9)	13776(8)	14110(6)	37
P(4)	54493(9)	25354(8)	31382(6)	40
S	18208(8)	44453(8)	35647(6)	41
O(1)	960(2)	5005(2)	3667(2)	56
C(1)	792(5)	5525(4)	1774(4)	71
C(2)	-167(5)	5365(4)	2181(4)	78
C(3)	-919(4)	4389(4)	1876(3)	62
C(4)	-567(3)	3589(3)	2183(3)	50
C(5)	5798(4)	1231(3)	1175(3)	50
C(6)	6723(4)	1556(4)	1823(3)	67
C(7)	6692(4)	1136(4)	2484(3)	70
C(8)	5629(4)	1341(4)	2998(3)	58
C(9)	2924(4)	5129(4)	4253(3)	57
C(10)	1461(5)	3489(4)	4006(3)	64
C(11)	2856(4)	5577(3)	1351(3)	48
C(12)	3904(4)	5455(4)	1355(3)	58
C(13)	4508(5)	5653(4)	803(4)	77
C(14)	4070(7)	5954(4)	224(4)	84
C(15)	3034(6)	6063(4)	188(3)	79
C(16)	2429(5)	5892(4)	755(3)	68
C(17)	2681(5)	6454(3)	2871(3)	57
C(18)	3755(5)	6773(4)	3051(4)	77
C(19)	4165(7)	7604(5)	3617(5)	108
C(20)	3555(10)	8111(6)	4004(5)	128
C(21)	2479(10)	7817(6)	3843(6)	148
C(22)	2012(6)	6989(4)	3262(5)	110
C(23)	269(4)	2914(3)	817(2)	47
C(24)	-707(4)	2316(4)	476(3)	60
C(25)	-1023(5)	2128(4)	-282(4)	74
C(26)	-375(6)	2514(5)	-715(3)	81
C(27)	595(5)	3128(4)	-403(3)	69
C(28)	902(4)	3324(4)	369(3)	53
C(29)	336(3)	1897(3)	1919(3)	48
C(30)	-253(4)	1636(4)	2466(3)	65

C(31)	-402(5)	679(5)	2519(4)	86
C(32)	8(5)	13(5)	2033(5)	96
C(33)	567(5)	264(4)	1492(4)	82
C(34)	742(4)	1203(4)	1437(3)	64
C(35)	3729(3)	1201(3)	469(2)	42
C(36)	2803(4)	522(4)	188(3)	55
C(37)	2239(4)	477(4)	-500(3)	71
C(38)	2600(5)	1102(5)	-917(3)	73
C(39)	3528(5)	1774(4)	-645(3)	64
C(40)	4094(4)	1833(4)	39(3)	54
C(41)	3908(4)	226(3)	1617(3)	.44
C(42)	3150(4)	175(3)	2092(3)	.58
C(43)	2771(5)	-675(4)	2280(3)	67
C(44)	3124(5)	-1488(4)	1973(4)	70
C(45)	3846(5)	-1467(4)	1485(4)	82
C(46)	4240(5)	-632(4)	1298(3)	68
C(47)	6723(3)	3362(4)	3542(3)	50
C(48)	6959(4)	4250(4)	3412(3)	62
C(49)	7940(5)	4877(5)	3717(3)	87
C(50)	8682(5)	4589(6)	4145(4)	94
C(51)	8471(5)	3699(6)	4285(4)	92
C(52)	7502(4)	3103(5)	3992(3)	73
C(53)	4773(3)	2579(4)	3987(3)	47
C(54)	4862(4)	3441(4)	4528(3)	57
C(55)	4298(5)	3491(5)	5138(3)	69
C(56)	3647(5)	2686(6)	5200(4)	86
C(57)	3542(5)	1830(6)	4677(4)	87
C(58)	4094(5)	1773(4)	4073(3)	69
Cl(5)[1]	8466(31)	7633(26)	3285(21)	432(17)
Cl(6)[1]	9634(30)	8202(27)	4493(23)	591(22)
O(2)[2]	7206(34)	7482(35)	2695(25)	477(23)
C(59)[2]	7161(25)	8293(28)	3114(19)	271(14)
C(60)[2]	7305(31)	9451(31)	3672(23)	387(19)
C(61)[2]	7511(42)	6803(41)	2205(30)	437(31)
C(62)[2]	6785(24)	6370(22)	2408(18)	257(13)
C(63)[1]	9241(66)	8508(56)	3744(48)	335(35)

[1]Occupancy factor 0.35.

[2]Occupancy factor 0.67.

303
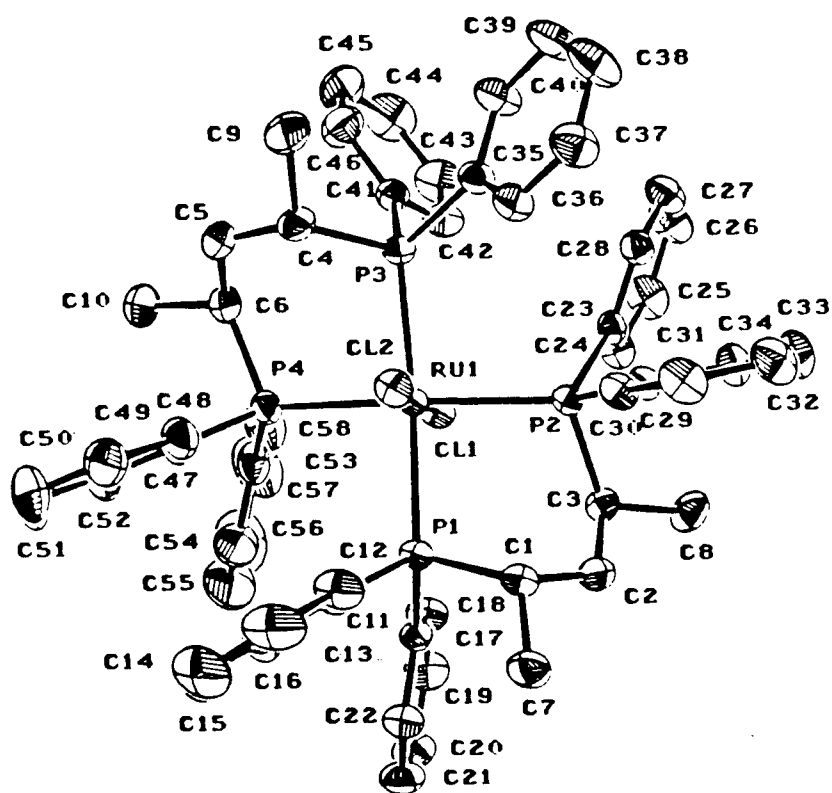
Molecular Structure

Experimental Details

A. Crystal Data

Empirical Formula	$C_{58}H_{60}Cl_2P_4Ru$
Formula Weight	1052.98
Crystal Color, Habit	red, prism
Crystal Dimensions (mm)	0.300 X 0.400 X 0.500
Crystal System	orthorhombic
No. Reflections Used for Unit Cell Determination (2θ range)	25 (40.0 - 43.0°)
Omega Scan Peak Width at Half-height	0.36

Lattice Parameters:

$$a = 18.961 \ (3) Å$$
$$b = 20.826 \ (4) Å$$
$$c = 12.998 \ (3) Å$$

$$V = 5133 \ (2) Å^3$$

Space Group	$P2_12_12_1$ (#19)
Z value	4
D_{calc}	1.362 g/cm^3
F_{000}	2184
$\mu_{(MoK\alpha)}$	5.63 cm^{-1}

B. Intensity Measurements

Diffractometer	Rigaku AFC6S
Radiation	MoKα (λ = 0.71069 Å)
Temperature	21°C
Take-off Angle	6.0°
Detector Aperture	6.0 mm horizontal 6.0 mm vertical
Crystal to Detector Distance	285 mm

Scan Type	$\omega-2\theta$
Scan Rate	16.0°/min (in omega) (8 rescans)
Scan Width	$(1.31 + 0.35 \tan\theta)°$
$2\theta_{max}$	70.1°
No. of Reflections Measured	Total: 12224 Unique: 12217 ($R_{int} = .074$)
Corrections	Lorentz-polarization Absorption (trans. factors: 0.93 - 1.00)

C.   Structure Solution and Refinement

Structure Solution	Patterson Method
Refinement	Full-matrix least-squares
Function Minimized	$\Sigma\, w\,(|Fo| - |Fc|)^2$
Least-squares Weights	$4Fo^2/\sigma^2(Fo^2)$
p-factor	0.04
Anomalous Dispersion	All non-hydrogen atoms
No. Observations (I>3.00σ(I))	7751
No. Variables	586
Reflection/Parameter Ratio	13.23
Residuals: R; R_w	0.035; 0.038
Goodness of Fit Indicator	1.32
Max Shift/Error in Final Cycle	0.00
Maximum Peak in Final Diff. Map	0.69 $e^-/\text{Å}^3$
Minimum Peak in Final Diff. Map	-0.59 $e^-/\text{Å}^3$

atom	atom	distance	atom	atom	distance
Ru(1)	Cl(1)	2.4036(9)	C(11)	C(12)	1.391(5)
Ru(1)	Cl(2)	2.4265(9)	C(11)	C(16)	1.396(6)
Ru(1)	P(1)	2.459(1)	C(12)	C(13)	1.386(6)
Ru(1)	P(2)	2.441(1)	C(13)	C(14)	1.369(8)
Ru(1)	P(3)	2.423(1)	C(14)	C(15)	1.375(8)
Ru(1)	P(4)	2.432(1)	C(15)	C(16)	1.380(6)
P(1)	C(1)	1.866(4)	C(17)	C(18)	1.393(5)
P(1)	C(11)	1.847(3)	C(17)	C(22)	1.400(5)
P(1)	C(17)	1.839(3)	C(18)	C(19)	1.378(5)
P(2)	C(3)	1.869(4)	C(19)	C(20)	1.384(6)
P(2)	C(23)	1.843(3)	C(20)	C(21)	1.369(6)
P(2)	C(29)	1.855(4)	C(21)	C(22)	1.383(5)
P(3)	C(4)	1.873(4)	C(23)	C(24)	1.397(5)
P(3)	C(35)	1.854(4)	C(23)	C(28)	1.397(5)
P(3)	C(41)	1.842(4)	C(24)	C(25)	1.390(6)
P(4)	C(6)	1.870(4)	C(25)	C(26)	1.369(7)
P(4)	C(47)	1.841(4)	C(26)	C(27)	1.384(7)
P(4)	C(53)	1.848(5)	C(27)	C(28)	1.378(5)
C(1)	C(2)	1.550(5)	C(29)	C(30)	1.400(5)
C(1)	C(7)	1.533(5)	C(29)	C(34)	1.406(5)
C(2)	C(3)	1.522(5)	C(30)	C(31)	1.390(5)
C(3)	C(8)	1.536(5)	C(31)	C(32)	1.373(6)
C(4)	C(5)	1.531(6)	C(32)	C(33)	1.388(6)
C(4)	C(9)	1.537(6)	C(33)	C(34)	1.372(5)
C(5)	C(6)	1.521(6)	C(35)	C(36)	1.384(6)
C(6)	C(10)	1.540(6)	C(35)	C(40)	1.398(5)

atom	atom	distance
C(36)	C(37)	1.392(6)
C(37)	C(38)	1.378(7)
C(38)	C(39)	1.373(7)
C(39)	C(40)	1.380(6)
C(41)	C(42)	1.401(5)
C(41)	C(46)	1.396(6)
C(42)	C(43)	1.381(6)
C(43)	C(44)	1.381(7)
C(44)	C(45)	1.358(8)
C(45)	C(46)	1.379(7)
C(47)	C(48)	1.385(6)
C(47)	C(52)	1.402(6)
C(48)	C(49)	1.398(6)
C(49)	C(50)	1.363(7)
C(50)	C(51)	1.384(8)
C(51)	C(52)	1.378(7)
C(53)	C(54)	1.387(7)
C(53)	C(58)	1.375(7)
C(54)	C(55)	1.395(7)
C(55)	C(56)	1.37(1)
C(56)	C(57)	1.34(1)
C(57)	C(58)	1.402(7)

Table A-2.3.2: Bond Angles (deg) with estimated standard deviations in parentheses.

atom	atom	atom	angle	atom	atom	atom	angle
Cl(1)	Ru(1)	Cl(2)	177.03(3)	C(23)	P(2)	C(29)	100.1(2)
Cl(1)	Ru(1)	P(1)	98.57(3)	Ru(1)	P(3)	C(4)	105.0(1)
Cl(1)	Ru(1)	P(2)	81.48(3)	Ru(1)	P(3)	C(35)	120.7(1)
Cl(1)	Ru(1)	P(3)	94.25(3)	Ru(1)	P(3)	C(41)	122.2(1)
Cl(1)	Ru(1)	P(4)	84.00(3)	C(4)	P(3)	C(35)	100.8(2)
Cl(2)	Ru(1)	P(1)	82.03(3)	C(4)	P(3)	C(41)	105.8(2)
Cl(2)	Ru(1)	P(2)	95.63(3)	C(35)	P(3)	C(41)	99.6(2)
Cl(2)	Ru(1)	P(3)	85.24(3)	Ru(1)	P(4)	C(6)	112.6(1)
Cl(2)	Ru(1)	P(4)	98.89(3)	Ru(1)	P(4)	C(47)	124.1(1)
P(1)	Ru(1)	P(2)	89.02(3)	Ru(1)	P(4)	C(53)	113.4(1)
P(1)	Ru(1)	P(3)	167.08(3)	C(6)	P(4)	C(47)	99.7(2)
P(1)	Ru(1)	P(4)	92.57(3)	C(6)	P(4)	C(53)	100.6(2)
P(2)	Ru(1)	P(3)	94.46(3)	C(47)	P(4)	C(53)	103.2(2)
P(2)	Ru(1)	P(4)	165.47(3)	P(1)	C(1)	C(2)	111.3(2)
P(3)	Ru(1)	P(4)	87.19(3)	P(1)	C(1)	C(7)	118.7(3)
Ru(1)	P(1)	C(1)	108.3(1)	C(2)	C(1)	C(7)	106.6(3)
Ru(1)	P(1)	C(11)	116.7(1)	C(1)	C(2)	C(3)	122.6(3)
Ru(1)	P(1)	C(17)	125.1(1)	P(2)	C(3)	C(2)	111.0(2)
C(1)	P(1)	C(11)	101.4(2)	P(2)	C(3)	C(8)	118.5(3)
C(1)	P(1)	C(17)	101.6(2)	C(2)	C(3)	C(8)	106.9(3)
C(11)	P(1)	C(17)	100.5(2)	P(3)	C(4)	C(5)	113.6(3)
Ru(1)	P(2)	C(3)	107.3(1)	P(3)	C(4)	C(9)	117.9(3)
Ru(1)	P(2)	C(23)	114.5(1)	C(5)	C(4)	C(9)	109.8(3)
Ru(1)	P(2)	C(29)	127.6(1)	C(4)	C(5)	C(6)	119.5(3)
C(3)	P(2)	C(23)	103.6(2)	P(4)	C(6)	C(5)	113.3(3)
C(3)	P(2)	C(29)	100.7(2)	P(4)	C(6)	C(10)	115.6(3)

atom	atom	atom	angle	atom	atom	atom	angle
C(5)	C(6)	C(10)	107.8(4)	P(2)	C(29)	C(34)	120.8(3)
P(1)	C(11)	C(12)	121.5(3)	C(30)	C(29)	C(34)	117.2(3)
P(1)	C(11)	C(16)	121.4(3)	C(29)	C(30)	C(31)	120.8(3)
C(12)	C(11)	C(16)	117.1(3)	C(30)	C(31)	C(32)	120.9(4)
C(11)	C(12)	C(13)	121.5(4)	C(31)	C(32)	C(33)	119.1(4)
C(12)	C(13)	C(14)	120.0(4)	C(32)	C(33)	C(34)	120.6(4)
C(13)	C(14)	C(15)	119.8(4)	C(29)	C(34)	C(33)	121.4(4)
C(14)	C(15)	C(16)	120.4(5)	P(3)	C(35)	C(36)	119.8(3)
C(11)	C(16)	C(15)	121.1(4)	P(3)	C(35)	C(40)	121.9(3)
P(1)	C(17)	C(18)	120.7(3)	C(36)	C(35)	C(40)	118.3(4)
P(1)	C(17)	C(22)	122.2(3)	C(35)	C(36)	C(37)	120.7(4)
C(18)	C(17)	C(22)	117.2(3)	C(36)	C(37)	C(38)	120.3(4)
C(17)	C(18)	C(19)	121.6(3)	C(37)	C(38)	C(39)	119.2(4)
C(18)	C(19)	C(20)	119.8(4)	C(38)	C(39)	C(40)	121.1(4)
C(19)	C(20)	C(21)	120.1(4)	C(35)	C(40)	C(39)	120.3(4)
C(20)	C(21)	C(22)	120.0(4)	P(3)	C(41)	C(42)	119.4(3)
C(17)	C(22)	C(21)	121.3(4)	P(3)	C(41)	C(46)	123.4(3)
P(2)	C(23)	C(24)	121.5(3)	C(42)	C(41)	C(46)	117.1(4)
P(2)	C(23)	C(28)	120.5(3)	C(41)	C(42)	C(43)	120.4(4)
C(24)	C(23)	C(28)	118.0(3)	C(42)	C(43)	C(44)	120.5(5)
C(23)	C(24)	C(25)	120.5(4)	C(43)	C(44)	C(45)	120.3(5)
C(24)	C(25)	C(26)	120.5(4)	C(44)	C(45)	C(46)	119.7(5)
C(25)	C(26)	C(27)	119.8(4)	C(41)	C(46)	C(45)	122.0(5)
C(26)	C(27)	C(28)	120.2(4)	P(4)	C(47)	C(48)	118.7(3)
C(23)	C(28)	C(27)	121.0(4)	P(4)	C(47)	C(52)	123.1(4)
P(2)	C(29)	C(30)	121.9(3)	C(48)	C(47)	C(52)	118.0(4)

atom	atom	atom	angle
C(47)	C(48)	C(49)	120.8(4)
C(48)	C(49)	C(50)	120.2(5)
C(49)	C(50)	C(51)	120.0(5)
C(50)	C(51)	C(52)	120.2(5)
C(47)	C(52)	C(51)	120.8(5)
P(4)	C(53)	C(54)	120.5(4)
P(4)	C(53)	C(58)	121.6(4)
C(54)	C(53)	C(58)	117.8(4)
C(53)	C(54)	C(55)	120.7(6)
C(54)	C(55)	C(56)	119.7(6)
C(55)	C(56)	C(57)	120.6(6)
C(56)	C(57)	C(58)	120.1(6)
C(53)	C(58)	C(57)	121.1(5)

Table A-2.3.3: Final Atomic Coordinates (Fractional) and B(eq).

atom	x	y	z	B_{eq}
Ru(1)	0.29874(1)	0.25916(1)	0.18194(2)	1.659(8)
Cl(1)	0.17328(4)	0.25183(4)	0.20561(6)	2.34(3)
Cl(2)	0.42523(4)	0.27196(4)	0.16235(7)	2.36(3)
P(1)	0.29994(5)	0.28933(4)	-0.00099(6)	1.92(3)
P(2)	0.27547(4)	0.37116(4)	0.22574(7)	1.79(3)
P(3)	0.32605(5)	0.22775(4)	0.35694(7)	2.07(3)
P(4)	0.28971(5)	0.14534(5)	0.14227(8)	2.37(4)
C(1)	0.3269(2)	0.3753(2)	-0.0107(3)	2.3(1)
C(2)	0.2670(2)	0.4206(2)	0.0257(3)	2.8(2)
C(3)	0.2214(2)	0.4061(2)	0.1193(3)	2.3(1)
C(4)	0.3936(2)	0.1626(2)	0.3443(3)	2.8(2)
C(5)	0.3623(2)	0.0971(2)	0.3169(3)	3.3(2)
C(6)	0.2924(2)	0.0937(2)	0.2600(3)	3.0(2)
C(7)	0.3521(2)	0.4010(2)	-0.1149(3)	3.5(2)
C(8)	0.1779(2)	0.4667(2)	0.1413(3)	3.4(2)
C(9)	0.4479(2)	0.1550(2)	0.4313(4)	4.0(2)
C(10)	0.2744(3)	0.0224(2)	0.2430(4)	4.5(2)
C(11)	0.3670(2)	0.2501(2)	-0.0826(2)	2.6(1)
C(12)	0.4371(2)	0.2697(2)	-0.0815(3)	3.4(2)
C(13)	0.4869(2)	0.2419(3)	-0.1455(4)	5.0(2)
C(14)	0.4679(3)	0.1930(3)	-0.2102(4)	5.8(3)
C(15)	0.3993(3)	0.1718(3)	-0.2116(4)	5.0(3)
C(16)	0.3493(2)	0.1999(2)	-0.1490(3)	3.4(2)
C(17)	0.2231(2)	0.2869(2)	-0.0872(3)	2.0(1)

atom	x	y	z	B_{eq}
C(18)	0.1555(2)	0.2775(2)	-0.0481(3)	2.7(2)
C(19)	0.0973(2)	0.2752(2)	-0.1114(3)	3.4(2)
C(20)	0.1055(2)	0.2815(2)	-0.2168(3)	3.5(2)
C(21)	0.1713(2)	0.2907(2)	-0.2577(3)	3.5(2)
C(22)	0.2296(2)	0.2935(2)	-0.1940(3)	2.8(2)
C(23)	0.2198(2)	0.3826(2)	0.3405(3)	2.1(1)
C(24)	0.1463(2)	0.3783(2)	0.3352(3)	2.8(2)
C(25)	0.1055(2)	0.3859(2)	0.4231(4)	3.6(2)
C(26)	0.1366(3)	0.3961(2)	0.5166(3)	3.9(2)
C(27)	0.2094(2)	0.3992(2)	0.5238(3)	3.2(2)
C(28)	0.2504(2)	0.3935(2)	0.4367(3)	2.5(1)
C(29)	0.3408(2)	0.4363(2)	0.2456(3)	2.1(1)
C(30)	0.4106(2)	0.4309(2)	0.2117(3)	2.4(1)
C(31)	0.4579(2)	0.4813(2)	0.2244(3)	3.2(2)
C(32)	0.4374(2)	0.5375(2)	0.2708(3)	3.6(2)
C(33)	0.3682(2)	0.5438(2)	0.3044(3)	3.5(2)
C(34)	0.3210(2)	0.4945(2)	0.2922(3)	2.8(2)
C(35)	0.3721(2)	0.2838(2)	0.4450(3)	2.5(1)
C(36)	0.4219(2)	0.3261(2)	0.4063(3)	2.9(2)
C(37)	0.4572(2)	0.3684(2)	0.4712(4)	3.8(2)
C(38)	0.4454(3)	0.3669(3)	0.5758(4)	4.7(3)
C(39)	0.3976(3)	0.3239(3)	0.6149(3)	4.7(2)
C(40)	0.3600(2)	0.2835(2)	0.5511(3)	3.6(2)
C(41)	0.2585(2)	0.1962(2)	0.4454(3)	2.5(1)
C(42)	0.1916(2)	0.2247(2)	0.4475(3)	3.1(2)

atom	x	y	z	B_{eq}
C(43)	0.1405(2)	0.2027(3)	0.5146(4)	4.3(2)
C(44)	0.1553(3)	0.1533(3)	0.5822(4)	5.0(3)
C(45)	0.2202(3)	0.1258(2)	0.5833(4)	5.0(3)
C(46)	0.2713(3)	0.1469(2)	0.5157(4)	4.0(2)
C(47)	0.3527(2)	0.1014(2)	0.0607(3)	3.0(2)
C(48)	0.4220(2)	0.1224(2)	0.0568(3)	3.3(2)
C(49)	0.4730(3)	0.0879(2)	0.0023(4)	4.3(2)
C(50)	0.4550(3)	0.0329(3)	-0.0483(5)	5.3(3)
C(51)	0.3861(4)	0.0110(2)	-0.0453(5)	5.5(3)
C(52)	0.3356(3)	0.0444(2)	0.0090(4)	4.0(2)
C(53)	0.2032(2)	0.1222(2)	0.0884(3)	3.3(2)
C(54)	0.1927(3)	0.1210(2)	-0.0171(4)	4.6(2)
C(55)	0.1269(4)	0.1053(3)	-0.0580(5)	6.5(4)
C(56)	0.0719(3)	0.0913(3)	0.0068(7)	7.3(4)
C(57)	0.0806(3)	0.0929(3)	0.1090(6)	6.5(3)
C(58)	0.1464(3)	0.1088(3)	0.1508(4)	4.5(2)